Small molecule Activation by Lanthanide Oxo Clusters and Proligand Approach Towards Assembling Heterometallic Architectures

A Thesis Submitted for the degree of DOCTOR OF PHILOSOPHY

By

Smruti Prangya Behera



School of Chemistry
University of Hyderabad
Hyderabad 500046

Telangana

India

♂ solemnly dedicate my work to

THE LORD GOD ALMIGHTY

&

MY LOVING PARENTS

To is a profound and necessary truth that the deep things in science are not found because they are useful, they were found because it was possible to find them.

I. Robert Oppenheimer

DECLARATION

I hereby declare that the matter embodied in the thesis entitled "Small molecule Activation by Lanthanide Oxo Clusters and Proligand Approach Towards Assembling Heterometallic Architectures" is the result of investigations carried out by me in the School of Chemistry, University of Hyderabad, India under the supervision of Prof. Viswanathan Baskar.

In keeping with the general practice of reporting scientific investigations, the acknowledgements have been made wherever the work described is based on the findings of other investigators. Any omission or error that might have crept in is regretted. This work is also free from plagiarism. I hereby agree that my thesis can be submitted in Shodhganga/INFLIBNET.

Prof. Viswanathan Baskar

V. Kah.

Smruti Prangya Behera

(17CHPH25)

University of Hyderabad

March, 2024

V. BASKAR
Professor
School of Chemistry
University of Hyderabad
Hyderabad - 500 046.



CERTIFICATE

This is to certify that the thesis entitled "Small molecule Activation by Lanthanide Oxo Clusters and Proligand Approach Towards Assembling Heterometallic Architectures" submitted by Miss. Smruti Prangya Behera bearing registration number 17CHPH25 in partial fulfilment of the requirements for the award of Doctor of Philosophy in the School of Chemistry is a bonafide work carried out by her under my supervision and guidance.

This thesis is free from plagiarism and has not been submitted previously in part or in full to this or any other University or Institution for award of any degree or diploma.

Parts of the thesis have been:

A. Communicated in the following publications:

"Activation of Small Molecules via Lewis acidic La6 Oxo Cluster."

Smruti Prangya Behera, Renuka Pradhan, Upakarasamy Lourderaj, Viswanathan Baskar.

Inorg. Chem. (Manuscript ID: ic-2023-04411z). (Communicated).

B. Presented in the following conferences:

Chemfest- 2022, Chemfest- 2023

Further the student has passed the following courses towards fulfilment of course work requirement for Ph.D.

	Course. No	Title	Credits	Pass/Fail
1.	CY-801	Research Proposal	4	Pass
2.	CY-805	Instrumental Methods A	4	Pass
3.	CY-806	Instrumental Methods B	4	Pass

Prof Viswanathan Baskar

hesis Supervisor) abad yderabad - 500 046 School of Chemistry

University of Hyderabad

SCHOOL OF CHEMISTRY University of Hyderabad Hyderabad-500 046

ACKNOWLEDGEMENTS

LORD Mighty God heavenly Father I thank you for your abounding love and forgiveness. LORD I am thanking you for your beautiful gift of salvation and I bow down unto Your mercy.

I express my sincere gratitude and profound regard to my supervisor Prof. Viswanathan Baskar, for his able guidance, encouragement, valuable suggestions, and constructive discussions at every stage of my research work. Not only chemistry, he also helped me in understanding the philosophy of life, taught how to handle a tuff situation, and overcome it. Such an approach has been instrumental in nurturing positive growth in me, both personally and professionally. Thus, his supervision is incomparable and it has been a great privilege and honour to be associated with him.

I would like to express my sincere thanks to my doctoral committee members, Prof. R. Nagarajan and Prof. K. Muralidharan for their timely support and help during my entire course.

I would like to thank Prof. Ashwini Nangia, Dean, School of Chemistry for providing the research facilities and the former Dean Prof. K. C. Kumara Swamy, for their kind help on various instances. I would also like to thank all the faculty members of School of Chemistry for their kind help on many occasions.

I would like to express my sincere thanks to Dr. Upakarasamy Lourderaj and Miss. Renuka Pradhan for their help in DFT calculation to understand the mechanistic procedures of the synthesized small molecules in presence of catalyst.

I wish to express my deep sense of appreciation to the technical staff working in NMR, Single crystal X-ray Diffraction, PXRD, and FESEM facilities of the school, especially SC-XRD operators Ramana Kumar Sir and Mahesh for their help whenever the time is required to collect the data

I am thankful to all my lab mates and senior researchers specially Dr. Amaleswari Rasamsetty, Dr. Junaid Ali, Dr. Uppara Ugandhar, Dr. Suman Mondal, Dr. Tokala Navaneetha Goud, Dr. Gujju Narsimulu and my juniors Mr. Calvin Samuel, Mrs. K. Gangajala, Mr. Vepula Pramod, Miss. Maheshwaram Prasuna, and Miss. Swandana for creating a cordial environment during my stay in Lab. Their assistance during the tenure of my work is gratefully acknowledged.

My special thanks to my friends, seniors and juniors Rina, Sneha, Kamala, Intzar, Praveen, Saroj, Asif, Irfan, Dr. Mamina, Dr. Gorachand, Dr. Samita, Dr. Shipra, Dr. Jayakrushna, Dr. Tanmaya, Prachuritha, Prasanatha, Hemant, Ranadeep, Santhosh, Ramanaidu, Aradhana,

Shivanee, Shyam, Arati, Sarbani, Florance, Bhubana, Rani, Seema, Dr. Chandrahash, Dr.

Shivalal, Shivram, Janardhan, Dr. Cherish Sheeba Nura for their camaraderie, constant support

and helping me whenever necessary.

I will not be sincere in my acknowledgements if I will not extend it to my GTC family members

Jyoti and Raju anna, Jose anna and Keren akka, Mary didi and Jash anna, Shabeena didi and

Franky anna, Neyesha, Areta, Blessy, Shyam anna and Priya akka, Manno aunty and

Seenivasan uncle, Nandana, Janet, Elsheeba, Angelin, Rufas anna, Jaya and Dama bhai, Renu

and Asher anna, Sandhya aunty, Niru, Keertana akka and Sharath anna, Anita akka and John

anna, Ruth didi and Suman anna, Priya akka and Ebez anna, Kranthi, Divya, Priyanka, Alma,

Jenny, Baby akka, Mercy akka, Charan, Asish, RK, Vinay and Suresh each of them for their

continuous and fervent prayers.

Finally, I find no way to express my deep gratitude and profound reverence to my most precious

and loving parents, Mr. Tikan Chandra Behera and Sakuntala Behera, brother and sister in law

Prayag Ranjan Behera and Manisha Behera, my maternal grandparents Mr. Anakula Behera

and Mrs. Sita Behera and a huge support from my loving uncles and aunts who treats me not

less than their own daughters Mr Maguni Behera, Mr Prabhat Behera and Mrs. Namita Behera,

Mr. Prakash Behera and Mrs. Sonali Behera. I would extend my heartfelt gratitude to my cousin

Mrs. Madhusmita Behera. I convey thankfulness to all my cousins for their support and love to

my dearest Ishar and Ishani for their unconditional love. Lastly but not the least my one-year

old Neace my dearest Dudu. I hope I can fulfil their wishes someday and bring as much joy to

them as they do to me by being my family.

Smruti Prangya Behera

University of Hyderabad

March, 2024

11

Name of the Student	Smruti Prangya Behera
Roll Number	17CHPH25
School	School of Chemistry
Name of Thesis Supervisor	Prof. V. Baskar
Thesis Title	Small molecule Activation by Lanthanide Oxo Clusters and Proligand Approach Towards Assembling Heterometallic Architectures.

SYNOPSIS

The thesis entitled "Small molecule Activation by Lanthanide Oxo Clusters and Proligand Approach Towards Assembling Heterometallic Architectures". It is divided into four chapters and details of each chapter are given below.

Chapter 1

Introduction

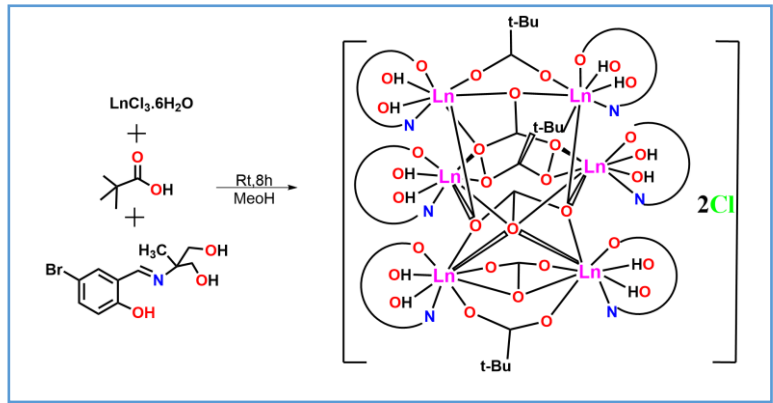
Introduction to various catalysts, their properties and mechanistic ways to enhance the catalytic properties has been explained. The potential of Lanthanide oxo clusters as catalysts have been explained to catalyse C-H bond activation of organic compounds, cycloaddition of epoxides and CO₂, catalytic reduction of CO₂, homogenous and heterogenous water oxidation with their respective proposed catalytic mechanisms and also for the production of Hydrogen. In other part of work a brief introduction has been given on various mixed stanoxane complexes formed via organo protic ligands. For paramagnetic mixed organo stanoxane complexes with transition metal and lanthanides, a brief explanation on SMM its operating principle and relaxation mechanisms have been included.

Chapter 2

Trigonal prismatic Ln₆ cluster encapsulating μ_4 -CO₃²- ion showing catalytic properties for cycloaddition reaction of epoxide and CO₂

This chapter deals with the synthesis, characterization and catalytic application of atmospheric CO₂ incorporated Lanthanum oxo clusters (LOC). The synthesis of the LOCs have been carried out by reacting respective hydrated salts, bromine based schiff base ligand, pivalic acid as coligand and triethyel amine as base in room temperature condition. Each of the lanthanide clusters have been keenly studied by single crystal X-Ray diffraction; revealed to the formation of [Ln₆(μ₄-CO₃)₃²-(piv)₃(LH₂)₆Cl₂] where Ln= La (2.1), Pr (2.2), Nd (2.3). The catalytic studies of compound 2.1 have been examined and the studies revealed that compound 2.1 is able to catalyze the cycloaddition reaction of CO₂ and different oragno substituted epoxides to

form cyclic carbonates. Each of the cyclic carbonates have been characterized by spectroscopic studies such as NMR and mass spectrometry.



Scheme -1; Synthetic scheme of compound 2.1-2.3

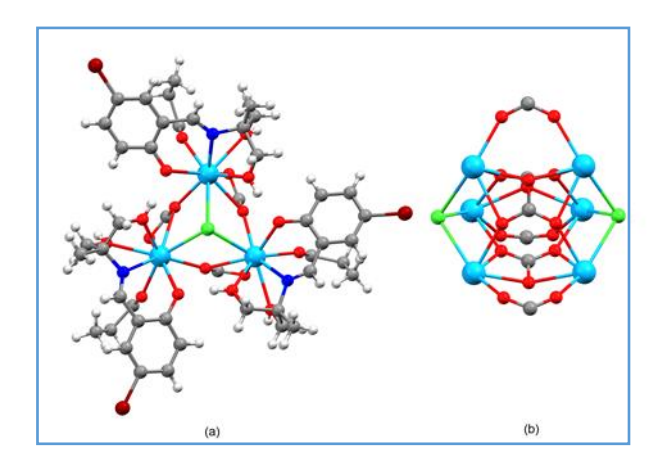
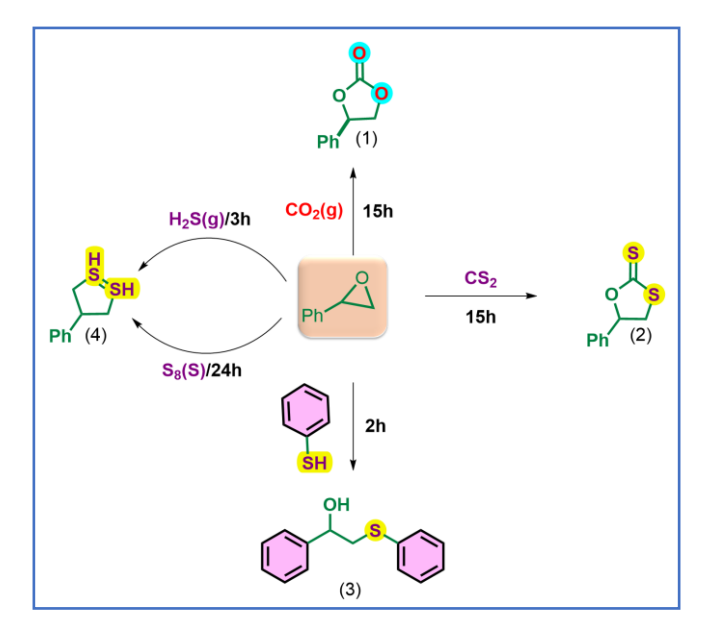


Figure 1. (a) Ball and stick diagram of $La_6(\mu_4\text{-CO}_3)_3(\text{piv})_3(LH_2)_6Cl_2$ (b) Core structure of La_6 cluster. Color legend; La; dodger blue, O; red, N; royal blue, Cl; green, Br; maroon, C; grey, H; white.

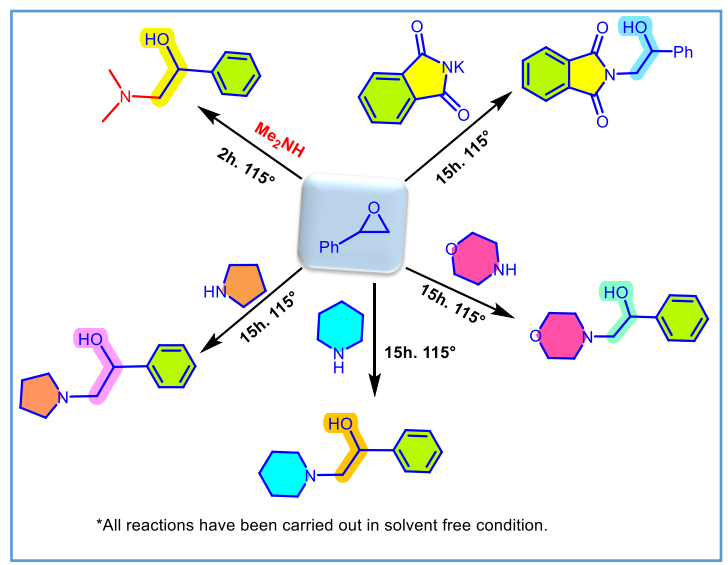
Chapter 3

Activation of small molecules via Lewis acidic La₆ oxo clusters

Activation of small molecules such as CO_2 , CS_2 , S_8 , H_2S , C_6H_5SH , and n-tosylaziridine to synthesize value-added products is an area of topical research. Herein, by employing a Ln_6 oxo cluster as a catalytic system, the conversion of the above-mentioned molecules in the presence of phenyl ethylene oxide has been carried out in neat reaction conditions. The versatility of the enhanced Lewis acidic La_6 cluster is established by the activation of ring-opening reaction of phenyl ethylene oxide in the presence of different substituted amines. The high Lewis acidic nature of our catalytic system has also resulted in activating other less reactive molecules the S_8 and H_2S leads to the formation of 5-phenyl-4,5-dihydro-1,2 λ^4 ,3 λ^4 -oxadithiole. Moreover, the versatility of the catalyst has been shown by the activation of suitable substrates to form β -amino alcohols, oxazolidinones and β -hydroxy sulphides in excellent yields. DFT studies has been performed to understand the cycloaddition reaction of CO_2 and CS_2 to styrene oxide in presence of our catalyst to understand the nature of the interaction of the substrate with the small molecules at a molecular level.



Scheme: 2 Activation of Sulphur based small molecules.



Scheme: 3 Activation of substituted amines to form β amino hydroxy alcohols.

Chapter 4

Proligand approach towards assembling heteromolecular architecture

This chapter deals with the synthesis and structural characterization of a series of mixed 3d-maingroup and 4f-main group metal-based oxo clusters. The clusters are synthesized by reaction of organo stanoxane phophonate based proligand with different hydrated transition metal precursors and hydrated lanthanide salts in a solvothermal. Single crystal X-ray diffraction confirms the formation of $[(n-BuSn)_3(\mu_2-O)_3(\mu_3-O)(RPO_3)_4Co.Py]$ (4.1) $[(n-BuSn)_3(\mu_2-O)_3(\mu_3-O)(RPO_3)_4Zn.Py]$ (4.2) $[(n-BuSn)_3(\mu_2-O)_3(\mu_3-O)(RPO_3)_4Dy.Py]_2$ (4.3) $[(n-BuSn)_3(\mu_2-O)_3(\mu_3-O)(RPO_3)_4Er.Py]_2$ (4.4) $[(n-BuSn)_3(\mu_2-O)_3(\mu_3-O)(RPO_3)_4Gd.Py]_2$ (4.5) $[(n-BuSn)_3(\mu_2-O)_3(\mu_3-O)(RPO_3)_4Y.Py]_2$ (4.6). The structural architecture for mixed 4f-main group clusters are dimers of mixed 3d-main group complexes. Electrocatalytic studies and molecular magnetic studies of the complexes have been carried out.

$$[(n-BuSn)_4(RPO_3H)_8O_2] + M(OAc)_2.4H_2O \xrightarrow{MeOH,Py} [(n-BuSn)_3(\mu_2-O)_3(\mu_3-O)(RPO_3)_4M.Py]$$

$$M = Co \text{ and } Zn$$
Solvothermal

Scheme:4 Synthesis of compound 4.1 and 4.2

$$[(n-BuSn)_4(RPO_3H)_8O_2] + LnCl_3.6H_2O \xrightarrow{MeOH,Py} [(n-BuSn)_3(\mu_2-O)_3(\mu_3-O)(RPO_3)_4Ln.Py]_2$$

$$Ln = Dy, Er,Gd \text{ and } Y$$
Solvothermal

Scheme: 5 Synthesis of compound 4.3 - 4.6

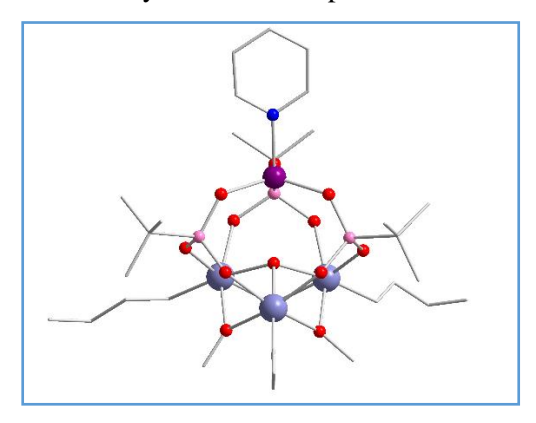


Figure 2: Ball and stick model of compound 4.1 and 4.2

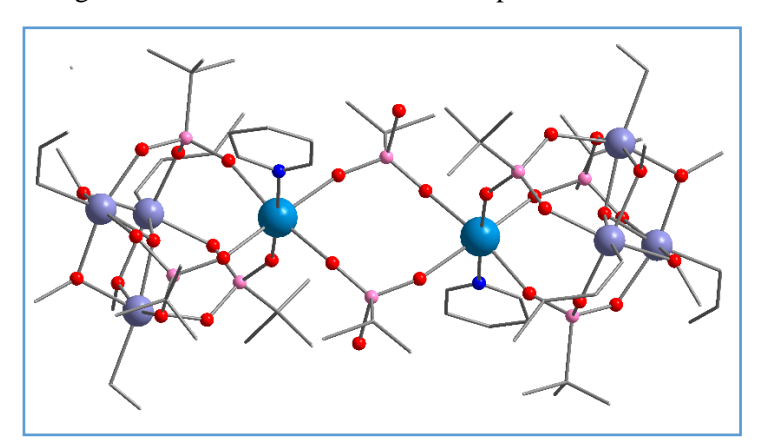


Figure 3: Ball and stick model of compound 4.3-4.6

List of Abbreviations

RNA Ribonucleic acid

DNA Deoxyribonucleic acid

API Active pharmaceutical ingredient

Ea Activation energy

T Temperature

LOC Lanthanide oxo cluster

Ln Lanthanide

Cp Coordination polymer

Cp* Cyclopentadienyl

MOF Metalo organic framework

IPA - Iso propynyl alcohol

MB Methylene blue

DSSC Dye sensitized solar cell

TBAB Tetra butyl ammonium bromide

TON Turnover number

TOF Turnover frequency

SMM Single molecule magnet

SIM Single Ion Magnet

MCE Magneto caloric effect

MQT Quantum tunneling magnetism

T_B Blocking temperature

SCXRD Single crystal x-ray diffraction

ⁱOPr Iso propoxide

DCM Dichloromethane

DMF Dimethylformamide

EtOH Ethanol

MeOH Methanol

Py Pyridine

TM Transition Metal

IR Infrared

HRMS High resolution mass spectrometry

NMR Nuclear Magnetic Resonance

ORTEP Oak Ridge Thermal Ellipsoid Plot

EADX Energy Dispersive X-Ray Analysis

HER Hydrogen evolution reaction

THF Tetrahydro furan

DFT Density Functional Theory

TLC Thin layer chromatography

PMA Phosphomolybdic acid

UV Ultraviolet

TMS Tetra methyl silane

Contents

Declaration

Certificate

Acknowledgements

Synopsis

List of abbreviations

Chapter 1	1-31	
Introduction		
1. General Introduction	Page no.	
1.1: Catalysis	26	
I. Homogeneous Catalyst:	26-27	
II. Heterogeneous Catalyst:	27	
III. Heterogenized homogeneous Catalysts:	28	
IV. Biocatalysts:	28	
V. How to rate constant enhances the catalytic properties	29	
by lowering the activation energy:		
1.2 Lanthanides as various catalysts:	29	
1.2.1 C-H bond activation of organic substrates in the presence	30	
of Lanthanide complexes:		
1.2.2 Lanthanide coordination polymer as green photocatalyst:	30-31	
1.2.3 Lanthanide organic frameworks as advanced catalysts:	31-32	
1.2.4 Lanthanide-based double perovskites as catalysts:	33	
1.2.5 Lanthanide-based double perovskites as photocatalysis:	33	
1.2.6 Lanthanide-based double perovskite as electrocatalyst:	34	
1.2.7 Lanthanide-based nanoparticles as a catalyst:	34	

1.2.8 Lanthanide photochemistry	34-35
1.2.9 Lanthanide oxo clusters as various catalysts:	35
1.2.10 LOC for catalytic cycloaddition of CO ₂ and epoxides:	35
1.2.11 Catalytic Reduction of CO ₂	36
1.2.12 LOCs as Homogeneous Water Oxidation Catalysts:	37
1.2.13 LOC as heterogeneous catalysts for water oxidation:	38
1.2.14 LOCs as Hydrogen Production Catalysts	39
1.3 Brief Introduction to Magnetism	40
 Diamagnetism: Paramagnetism: Ferromagnetism: Antiferromagnetism: 	
5. Ferrimagnetism:1.3.1 Fundamentals of Magnetism	41
1.3.2 Magnetisation curve: Hysteresis	41-43
1.3.3 Quantum Tunnelling of Magnetism:	44
1.3.4 First examples of lanthanide SMM	45
1.3.5 Breakthrough examples of lanthanide SMM	45-50 50 - 56
1.4 Briefing on various organo-stannoxane clusters	
formed by organic protic acids:	
Thesis overview	57
Chapter 2	62-83
Trigonal prismatic Ln_6 cluster encapsulating $\mu_4\text{-CO}_3^2\text{-ion}$ showing	
catalytic properties for cycloaddition reaction of epoxide and CO ₂	
2.1 Introduction	63

2.2 Experimental Section	64
2.2.1 General methods and Procedures:	64
2.2.2 Instrumentation	64
2.2.3 General Synthetic procedure:	65
2.3 Results and Discussion:	65
2.3.1 Description of crystal structure:	65
2.4. Catalytic activity of La ₆ cluster for the cycloaddition	66
reaction of epoxides:	
2.4.1 Synthetic procedure for cyclic carbonates from	68
epoxides catalysing by compound-1:	
2.4.2 Cycloaddition reaction of epoxide with CO ₂	69-70
2.4.3 Catalytic activity through absorption spectra:	71
2.5 Conclusion	71
References:	71-73
Supporting Information	74-83
Chapter 3	84-104
Activation of Small Molecules via Lewis acidic Hexanuclear	
La ₆ Oxo Cluster	
3.1 Introduction:	85
3.2 Experimental Section	86
3.2.1 General Information	86
3.2.2 General Synthetic procedure:	86
3.2.3 Spectral Data	87
3.3 Results and discussion	88

3.4 Conclusion:	93	
References:	93-95 96-104	
Supporting Information		
Chapter 4	104- 132	
Proligand approach towards assembling		
heteromolecular architecture		
4.1 Introduction	106	
4.2 Experimental	107	
4.2.1 Instrumentation:	109	
4.2.2 Reagents and general procedures	110	
4.2.3 General Synthetic procedures for compound 1 to 6	110	
4.3 Results and discussion	111	
4.4 Conclusion:	111	
References	112	
Supporting Information	113-132	

Future Scope of Thesis

List of publications

Poster / Oral presentations/ workshops

Plagiarism Report

Introduction

1

1. General Introduction

1.1: Catalysis

The Swedish chemist Berzelius invented the term "*catalysis*" in 1835 by, but Ostwald established a suitable interpretation significantly delayed, in 1894 he noted:

"Catalysis is the acceleration of a slow chemical process by the presence of a foreign material."

Catalysts, by binding and interacting with reactant molecules, facilitates a reaction through decreasing its activation energy. Catalyst convert many reactants to products, participates in a reaction but is not eaten up. Since it can consume in huge quantity, it should only be added in catalytic amounts. A series of stoichiometric rudimentary reactions makes up catalysis, which is kinetic.

Catalyst lifetimes have switched by the development of surface science, where many experimental methods have enabled the study of interactions of adsorbed molecules on the plane of single crystal. Although this is an important advancement, it has limited relevance for catalysis based on facts such as: (1) Under high temperatures, vacuum conditions, where motion is frozen and chemical reactions do not occur most surface technologies have worked well, therefore, the research group has made great efforts to close the pressure gap with practical conditions towards applications. (2) Gradually, research groups realised that rough defected surfaces within crystal facets, corners along with edges leads to significantly better catalytic activity than the smooth single-crystal facets.²

Scientists categorizes catalysts into four different types such as (i) Homogeneous catalyst, (ii) Heterogeneous (solid) catalyst, (iii) Heterogenized homogeneous catalysts, and (iv) Bio-catalysts.

Homogeneous Catalyst: In case of homogeneous catalysts, the catalyst is present with the reactants in the same phase of the reaction and demonstrates maximum uniformity, leading to excessive interaction with each other, high reactivity and selectivity in the reaction condition under ambient temperature and pressure. Transition metals,

organocatalysts, organometallic complexes and Bronsted-Lewis acids are few instances for homogeneous catalysts. In homogeneous catalysis few prominent chemical processes occur such as hydrogenation, carbonylation, hydrocyanation, metathesis, and oxidation.

By using kinetics to estimate the starting rate R_0 of a reaction for various reactant accumulations in homogeneous catalytic reaction systems, it is simple to determine the nature of a reaction mechanism. If the concentration of reactant A, [A], is proportional to R_0 , then A is directly involved in the process of calculating rate. R_0 relies on [A] even though [A] remains unaffected over duration of the reaction (and [A] is not available to certain excess therefore the alternative concentration is simply not evidient). In this case, we can say that A serves as a catalyst because R_0 depends on [A].²

I.Heterogeneous Catalyst: In this system, catalysts subsist in a separate system from reaction mixture. The Fischer-Tropsch process, which creates a range of hydrocarbons, and the Haber-Bosch method of ammonia synthesis are two examples of processes that utilise heterogeneous catalysts. Major industrial processes are dominated in heterogeneous catalysts because of the simplicity of product separation and catalyst repossession. Heterogeneous catalysts are described by scientific communities as tiny particles, powders, and granules. These catalysts can either be utilized in bulk form (unsupported catalysts) or can be placed on a solid support. Catalysts with support were essential to the industrial revolution

The heterogeneous catalysts performed on an exposed surface area, since it is a surface phenomenon. While exposed surface area rises as particle size decreases, smaller particles tend to accumulate and cause the catalyst to become inactive. By preventing catalytic particle aggregation and increasing catalytic efficiency, the catalytic active site is tethered to a solid support. Solid supports provide a high degree of chemical, mechanical, and thermal resilience for industrial applications. It must also have a high surface-to-volume ratio and be inert. Polymers (like polystyrene), copolymers (like inorganic supports such as graphene, activated carbon, alumina, zeolites, titanium dioxide, styrene-divinylbenzene, and silica, are also used. examples of commonly used organic solid supports. Unsupported catalysts dominate a significant portion of industrial catalysis which contains zeolites, metals, metal oxides, metal alloys, and metal sulphides.²

II.Heterogenized homogeneous Catalysts: In practice heterogenous catalysts are more challenging than homogenous catalysts. One factor is the intricacy, which prevents investigation in molecular level along with the evolution by means of structure reactivity correlations. In addition, less activity than modern selectivity and reactivity of heterogeneous catalysts (metal oxides or supported metals). Those problems have overcome by grafting the homogeneous catalyst upon the solid supports to create their heterogenic analogous. In both academic and industrial research, Homogeneous catalysts with strong support are well-recognized and often utilized. This method combines the advantageous properties involves immobilizing catalysts, such as metal complexes and organometallic compounds on the solid surface through physisorption or chemisorption, of both homogeneous (selectivity and reactivity) and heterogeneous (reproducibility) catalysts. The most preferred method for creating heterogenized homogeneous catalysts is revealed to be covalent grafting of active catalytic species on concrete surfaces. ²

III.Biocatalysts: Biocatalysis is the use of naturally occurring proteins (enzymes), nucleic acids (RNA or ribozymes), or DNAs to catalyse particular chemical activities outside of alive cells. Plants, animal tissues and microorganisms (such as fungi, bacteria, or yeast) all contain enzymes. Biocatalysts are an alternative to traditional industrial catalysts due to their great selectivity, environmental friendliness, moderate reaction conditions and efficiency. Significant progress has been made in the field of biocatalysis for the industrialscale synthesis of active ingredients (APIs) in the production of biodiesel from vegetable oil, fine chemicals, the dairy industry (such as lipase for lactose removal, protease, and renin for cheese preparation), and the baking industry (such as amylase for bread softness and volume, glucose oxidase for dough strengthening). Different enzymes that make detergents, such as proteinase, amylase, and lipase, separately remove protein, fat, and starch stains. Amylase is used in the paper and textile industries to extract starch from woven materials, and protease is used in the leather industry for unhairing and tannings. Enzymes immobilized on solid substrates become heterogeneous solid catalysts with improved activity, stability, and longevity that can be recycled numerous times. Protein, fat, and starch marks are each removed by different enzymes that produce detergents, such as proteinase, lipase, and amylase. Paper, textile, and leather industries (for example, protease for unhairing and bating) all use enzymes to remove starch from woven materials. Enzymes immobilized on solid substrates become heterogeneous solid catalysts with improved activity, stability, and longevity that can be recycled numerous times.²

How to rate constant enhances the catalytic properties by lowering the activation energy:

Activation energy: The activation energy is the least quantity for energy in a certain amount required to convert atoms or molecules into a condition that allows for chemical reactions. Arrhenius' equation is referred to as activation energy.

$$k = A \cdot \exp\left(-\frac{E_a}{RT}\right) \tag{1) 'A'}$$

denotes the pre-exponential factor of high-temperature limit of constant 'k', where

R' = gas constant,

'T' = temperature k = rate constant of reaction

The equation has been frequently plotted in the logarithmic form in which

ln(k/unit) = ln(A/unit) - Ea/RT, as the function of 1/T

The plot draws a straight line with ln(A/unit) as the intercept –Ea/R as its slope.¹

1.2 Lanthanides as various catalysts:

The systematic and reproducible synthesis of LOCs is still a major obstacle, which has prevented lanthanide oxo clusters from being widely used in catalysis. Second, very little is known about how LOCs behave in solutions or how stable they are; this knowledge is crucial for both the uses of LOCs as catalysts and, more importantly, for understanding the catalytic mechanism. Finally, the presence of many metal sites inside a LOC makes it difficult to correlate the catalytic activity of these materials with their molecular structures.

The affluent redox chemistry of several Ln ions (Ce⁴⁺/Ce³⁺, Sm³⁺/Sm²⁺, and Eu³⁺/Eu²⁺), as well as their adaptable coordination attributes owing to the solely ionic interactions that occur between an Ln ion and a ligand, contribute to their qualities favourable to catalysis.³ In addition, due to the existence of more than one abutting metallic positions allows the possibility for catalysis known as synergistic catalysis; finally, Ln ions exhibit special electronic characteristics which ensure LOCs as an excellent catalytic property.

Primarily because of the Lewis acidic nature of Ln ions, research groups have established multiple catalytic domains, including metal-organic frameworks, nanoparticles, coordination polymers (CPs), perovskites and metal-organic frameworks.

1.2.1 C-H bond activation of organic substrates in the presence of Lanthanide complexes:

Most homogeneous catalysis uses metal complexes to capture tiny molecules and transform them into higher-value products. When bis (permethylcyclopentadienyl) lanthanide methyl [(5-C₅Me₅)₂Ln(CH₃)] complexes of organometallic lanthanide compounds selectively cleaved the one C-H bond present in methane, they provided, the tantalizing sight of their promising for catalysed C-H bond conversions.

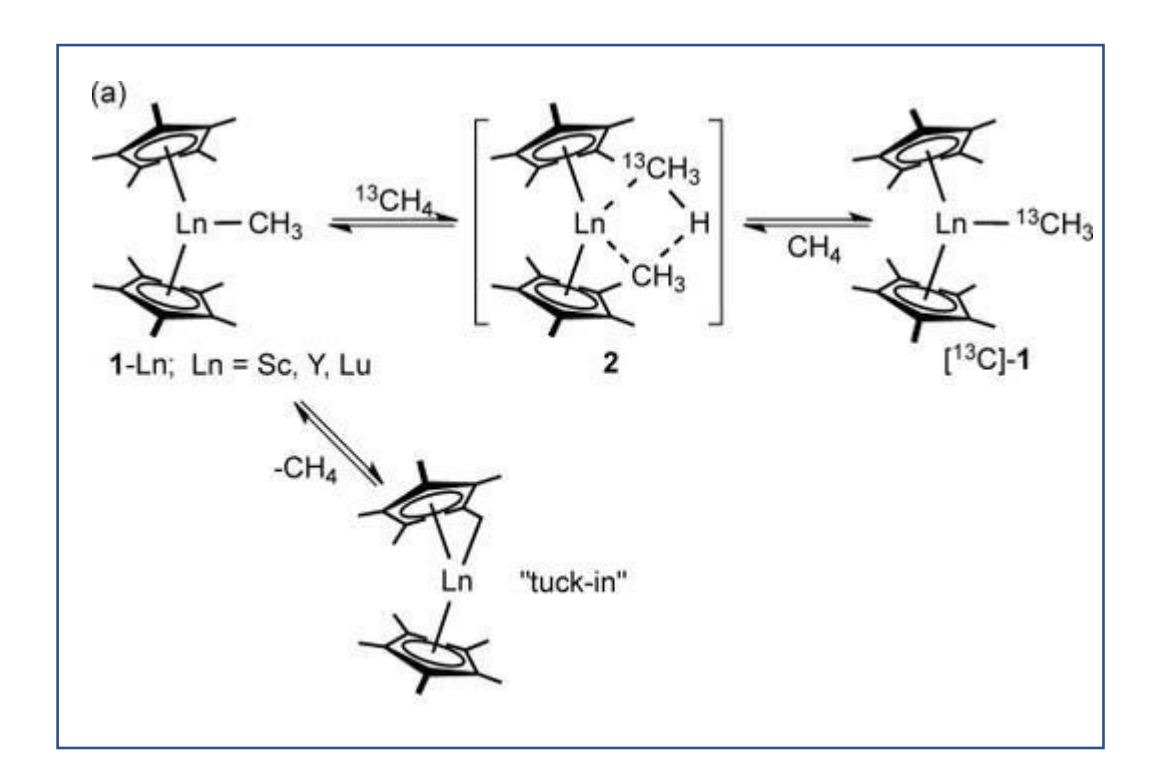


Fig 1.1 Catalyst-mediated activation of methane in the presence of Ln catalysts

It has also seen that ethane and propane to react with the aforementioned reported Ln complex, no isolable substance was, and the metal products are presumed to decompose through hydrogen elimination in the reaction in which [(Cp*)₂Ln(CH₃)] was exhibited to trigger methane. The strong M-C bond, the tight binding and steric protection of Cp* ligands, and the metal centre is not redox reactive make bond metathesis an easy reaction for lanthanide metal complexes.⁴

1.2.2 Lanthanide coordination polymer as green photocatalyst:

Dáz et al. developed an array of LOC coordination polymers to offer an excellent platform for assembling light antennas and dynamic catalytic centres that carry out solar-energy transformation as green replacements in the synthesis of imines. It is crucial to bring to light the advantages of employing CPs in photocatalytic processes since in day-to-day life this

procedure can integrate light harvesting and catalytic active regions on just one stable platform, enabling solar energy conversion to chemical energy. Lanthanide cyclopentadienyls (LnCP(s)) are attractive candidates in this situation due to their long-term stability inside the water, strong Lewis acidic properties, and excellent firmness related to their transition-metal-based counterpart. Using the relatively inflexible dipodal ligand 9,9'-spirobi[9H-fluorene]-2,2'dicarboxylic acid and metal sources La, Nd, Sm, Ho, and Er combined through comparatively unbending dipodal ligand 9,9'-spirobi[9H-fluorene]-2,2'-dicarboxylic acid, a few examples of Ln-CP materials were produced.⁵

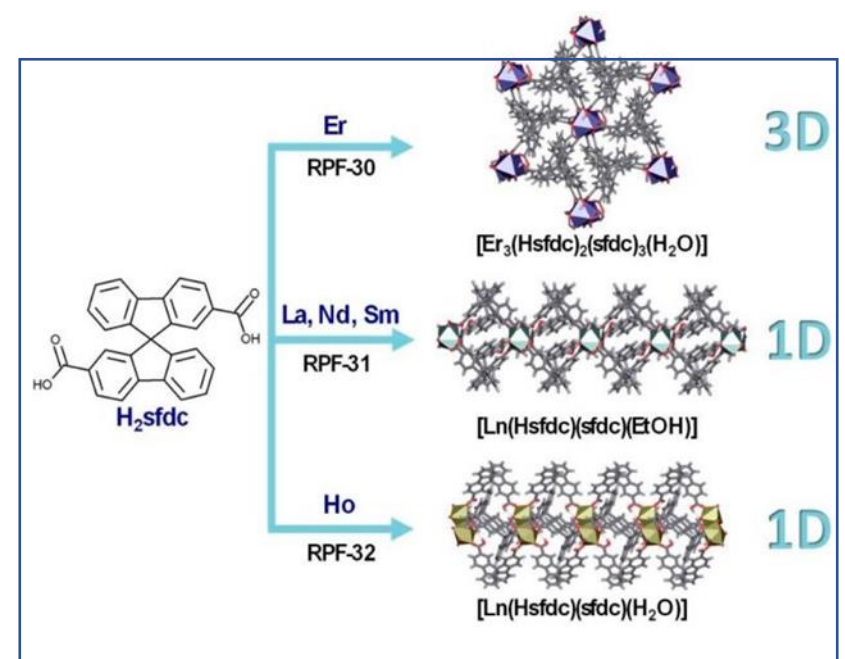


Fig 1.2 Organic Ligand H₂sfdc Reacting with Several Lanthanide Metals to Form a Series of New Ln-CPs.

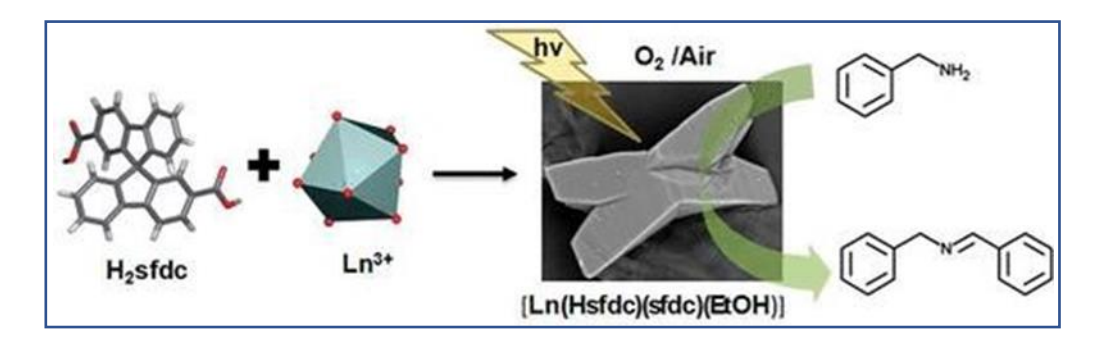


Fig 1.3 Photocatalysis of amines in the presence of Ln-CPs to form imines.

1.2.3 Lanthanide organic frameworks as advanced catalysts:

The unique qualities of MOFs include their predominant porosity, limited pore architectures, locations of active sites resulting from the initially stated synthesis or post-synthetic changes, and flexible chemical structures. Due to their qualities, they are good competitors for various

implementations involving gas storage, catalysis, separation, sensing, etc. The advantages of MOFs for catalysis depend on two key features: first, their substantial internal surface area, which offers scope for reactions, and second, their catalytic functionality for organic processes, which results in both active organic and metal properties. Other traits include the originality of the distinct pore environments acting as catalysts. The particular characteristics of MOF chemistry are found in rare-earth metal-organic frameworks (REMOFs), a subtype of MOFs.⁶

The first thermally stable dynamic heterogeneous catalyst, formed as Sc₂(C₄H₄O₄)_{2.5}(OH), was reported by Ruiz-Valero et al. It was produced via the solvothermal reaction of Sc3+ with succinic acid, which catalyses the acetalization of benzaldehyde.⁷ The same group subsequently created two 3D succinate-based **MOFs** with the formulas $[Y_2(C_4H_4O_4)3(H_2O)_2]H_2O$ and $[La_2(C_4H_4O_4)3(H_2O)_2]H_2O$. By carrying out the acetalization of aldehydes under comparable circumstances, these two MOFs demonstrated similar catalytic characteristics to those of Sc₂(C₄H₄O₄)_{2.5}(OH).⁸ Together with their ability to absorb guest molecules and their ability to release them thermally, the coordination environment of these three MOFs was a key element in determining their catalytic activities. The process is made possible by the unbound water molecules in reversible manner. The advantages of MOFs for catalysis are based on two key features: first, their substantial internal surface area, which offers scope for reactions, and second, their catalytic activity for organic processes, which results in both active organic and metal properties. Other traits include the originality of the distinct pore environments acting as catalysts. The particular characteristics of MOF chemistry are found in rare-earth metal-organic frameworks (RE-MOFs), a subtype of MOFs.⁹

Amghouz et al. successfully synthesized two new chiral heteronuclear MOFs by using two different linkers, namely the flexibly chiral tartaric acid (H_2 Tart) and the rigid terephthalic acid (H_2 BDC). ¹⁰ Chiral MOFs with various topologies are useful for chiral separation, asymmetrical catalysis, and nonlinear optical activity. The electronic-donating ability of H_2 Tart and its variety of chiral centres, including D(-), L(+), racemic mixture, and meso isomers, led to its selection. NaY(Tart)(BDC)(H_2 O₂) (Y-(BDC)-MOF) and NaY(Tart)(biBDC)(H_2 O₂) Y(biBDC)-MOF are a couple of Y³⁺ based catalysts. NaY(Tart)(BDC)(H_2 O₂) (Y-(BDC)-MOF) and NaY(Tart)(biBDC)(H_2 O₂) (Y-(biBDC)-MOF) are a couple of Y³⁺ based catalysts. ¹¹

1.2.4 Lanthanide-based double perovskites as catalysts:

It has been shown that "Perovskite oxides" are suitable catalysts with excellent thermal stability and exertion, and particularly that double perovskites based on lanthanides have shown

to be superior catalysts than simple perovskites. 12 La₂CuNiO₆ with LaNiO₃ and LaCuO₃ has demonstrated the catalytic performance for methane combustion by Hu et al. The results show that La₂CuNiO₆ has a higher catalytic activity than LaNiO₃ or a mixture of LaNiO₃ and LaCuO₃. La₂CuNiO₆'s 90% conversion temperature to LaNiO₃ dropped by 63.2 °C. Later, it was demonstrated using infrared spectroscopic analysis that the M-O bond firmness diminishes the cation measurements are of sequence Co is more than Ni is more than Cu, ensuring more reactive O during catalytic combustion of propane on La₂MMnO₆ (M = Co, Ni, and Cu). 13

Compared to other materials, La₂MMnO₆ exhibits the highest conversion. Double perovskites containing Cu and Co transition metal ions show the highest catalytic ability for removing volatile organic compounds and excellent activity for removing toluene at gas space velocities as high as 30,000 h⁻¹. They are also resistant to water and carbon dioxide. 'Microwave-induced catalytic oxidation' is a potential method for eliminating organic contaminants from wastewater because of its capacity for selective heating, greater heating tariffs, and enhanced energy effectiveness. An advantage of microwave irradiation is that conductive materials like activated carbon can absorb electromagnetic wave energy, creating "hot spots" around surface-supported catalysts. La₂NiMnO₆-cellulose carbon xerogel composite was recently created by Wang et al. using a "one-step sol-gel" technique, which, owing to better La₂NiMnO₆ dispersion within a hierarchical porous structure and more active adsorption sites, displays greater activities than pure La₂NiMnO₆.¹⁴

1.2.5 Lanthanide-based double perovskites as photocatalysis:

Hu et al.'s discovered that in presence of visible light the photocatalytic activity of LaFeO₃ and La₂FeTiO₆ in the degradation of p-chlorophenol demonstrates the latter exhibits substantially higher performances in next five hours of irradiation and that the rate of degradation is 62.1% as opposed to the former's 49%. La₂FeTiO₆ has a greater photocatalytic activity due to UV absorption spectroscopy. ¹⁵ Another example involves the photocatalytic destruction of iso propanol (IPA) in gaseous form and methylene blue (MB) Ba₂REBiO₆ (RE = Gd, Dy, La, Nd, Sm, Ce, Eu) when exposed to visible light. In the valency state four the condition of Ce and Pr is probably what caused the remarkable photocatalytic activity of Ba₂CeBiO₆ and Ba₂PrBiO₆ that were previously reported. ¹⁶

1.2.6 Lanthanide-based double perovskite as electrocatalyst:

Ba₂LnMoO₆ (Ln = Pr, Nd) has good morphological steadiness with greater temperatures and chemically similar to the electrolytic solution, making it an excellent solid oxide fuel cell anode

material. Due to the deposited carbon's blocking of the methane diffusion path, the conductivities of Ba₂PrMoO₆ and Ba₂NdMoO₆ are as great as 348.5 and 146 Sm⁻¹ under moistened CH₄ at 800 °C, respectively, guaranteeing stronger hydrogen electrocatalysts oxidation reaction than the oxidation process for methane.¹⁷ Aiming for increment ongoing productiveness of dye-sensitized solar cells (DSSCs) as a counter electrode, a graphene-La₂CuNiO₆-ZnSe composite was recently created.¹⁸ One among the greatest transformation productivities revealed for ternary oxide likewise graphene DSSCs is 11.05%, which is possible with DSSCs. The composite shows remarkable catalytic performance toward the I³-/I⁻ redox pair.

1.2.7 Lanthanide-based nanoparticles as a catalyst:

Cerium oxide and substances containing cerium dioxide have undergone substantial research as structural and catalytic electrical factors that support heterogeneous catalytic processes. The analysis of ceria and CeO²⁻ containing catalysts has recently attracted much attention due to their potential for interacting with molecules like oxygen, nitric oxide, hydrogen, carbon and monoxide. Critical direct and reverse spill over phenomena, as well as the creation of intermetallic Ir/Ce clusters, have all been tentatively linked to the Ir/ CeO catalyst. Supported Pt/Ce/AlO, Pd/Ce/AlO, and Rh/Ce/SiO were used to show the level of surface ceria decrease and the distribution of sustained CeO in cold conditions. ¹⁹ The metal speeds up the synthesis of cerium aluminate in the case of CeO, /AlO. When metal is present, cerium aluminate CeAlO forms faster. This synergistic interaction among the support and the metal is lost if Pt, Rh, and CeO is doped with other lanthanide elements such as La and Nd. ²⁰

1.2.8 Lanthanide photochemistry

A deeper knowledge for the emission-related photo-physics of molecular lanthanide photocatalysts colours and brightness is established by establishing the physical foundation to modify the photocatalytic capabilities. For example, in the investigation of the photochemistry of Ce(III) guanidine-amide complexes, he potential for excited-state reduction (E1/2*), and the photocatalytic activity of a Ce(III) complex is mainly dependent on the settling rate for organic substrates.²¹

The conversion was improved by adding groups that provide the aryl bromides electrons. This is consistent with a SET pathway in the inner sphere in which the Ce(III) cation interacts more favourably with the electron-rich substrates than the electron-poor ones. Only Ce(III) photocatalysts with narrower steric profiles can involve a Ce^{IV}-Br intermediate. Gradually, it

becomes more and more critical to fully realize the applications of Ce(III) photocatalysts in photocatalysis by better grasping the structural property correlations. The more powerful Ce(III) photocatalysts with possibly superior with innovative uses in organic synthesis have been investigated in light of this photophysical basis and successes in C-C bond-formation. To create the [NEt₄]₃[Ce^{III}Cl₆] complex, either [NEt₄]₂[Ce^{IV}Cl₆] can be photo reduced under visible light, or CeCl₃ can be dissolved in an excess base solution, such as NEt₄Cl. The same team has also photocatalyzed the reduction of aryl chlorides by including ten equivalents of toluene as a atoning reducing agent for renewing the Ce(III) catalyst, adding to the list of accomplishments for lanthanide photocatalysts. Radical trapping experiments were used to support the aryl radical mechanism that was intended to drive these events. To produce aryl radicals, the [CeIIICl₆]³⁻ may therefore mediate the homolytic breakage of sp² C-Cl bonds. The synthesized aryl radicals were capable of building sp² carbon-heteroatom bonds.²²

1.2.9 Lanthanide oxo clusters as various catalysts:

Synergistic catalysis may be possible when numerous neighbouring metal sites are present; this structural property is not present in mononuclear or low nuclear rare-earth metal complexes or Ln MOFs. Only some groups have studied the catalytic properties of LOCs since their distinctive electrical and structural characteristics emerged.²³

1.2.10 LOC for catalytic cycloaddition of CO₂ and epoxides:

It is crucial to mention that although creating polycarbonates often requires lower activation energy, it is thermodynamically less advantageous than synthesizing cyclic carbonates. It should be feasible to selectively manufacture one or the other type of carbonate by choosing an appropriate catalytic system and adjusting the reaction conditions. The strength of the metaloxygen bond can be reduced by electron-donating ligands and the groups on the ligands themselves, which favours the back-biting process and increases the selectivity for the synthesis of cyclic carbonate. For instance, zeolites, one of the primary porous substances, are extensively utilized in ion exchange, catalysis, and sorbents. On the other hand, because of their extreme stability and Lewis-acidic strong nature, multidimensional lanthanide-zeolites made only of lanthanide ions and oxygen linkers have been applied as catalysts. Pair of electron-donors and electron-withdrawing last epoxides could be turned for respective cyclic carbonates with excellent yields using n-Bu₄NBr (TBAB) as a cocatalyst and Ln₆₀ nanocages (Ln = Gd, Tb, Dy) zeolite as a catalyst (Fig. 1.4). After 12 hours, 70% of the sought-after

compound, 4-phenyl-1,3-dioxolan-2-one, was produced. However, the product could only be made with a pitiful 23% yield without lanthanide.²⁴

Scheme 1.1 Mediating epoxide to cyclic carbonate in the presence of catalyst and cocatalyst

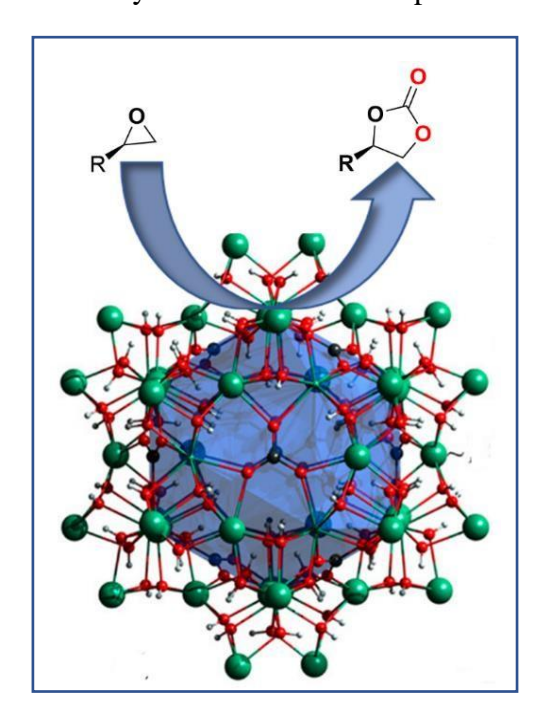


Fig 1.4 Ultra-strong Ln zeolite complex mediating epoxide to cyclic carbonate.

1.2.11 Catalytic Reduction of CO₂

Through the catalytic reduction of CO₂, a series of value-added products can be obtained, such as CO, HCHO, HCOOH, CH₃OH, and CH₄.²⁵ There are many promising photocatalytic and electrocatalytic catalysts, including bare Ni-based catalysts that have more affinity towards CO.²⁶ Hence lanthanide oxo clusters with Ni metal centres have been proven to be promising catalysts for the production of CO.

From the research group of Zheng and others, they have reported 138 numbered metal gigantic lanthanide oxo cluster $Ni_{36}Gd_{102}$. This gigantic structure is known as the 'Star of David-like structure' (Fig 1.5). It shows an exceptional turnover number = 29,700 and turnover frequency = 1.2 s^{-1} Characteristically, from various studies, it has been confirmed that CO₂-Ni binding is in the preliminary stage of the reaction. In the structure's core, many μ 3 bridged hydroxide

groups are available, which form a hydrogen bond with the O atom of CO₂. So, the presence of multiple hydroxide groups helps stabilize the intermediate and initiate the catalytic process by breaking the C-O bond. The structural integrity of the LOC in the solution state remains unchanged even after five consecutive catalytic reactions. Not only catalytic properties, but this gigantic Ni₃₆Gd₁₀₂ cluster also shows an efficient magnetocaloric effect.²⁷

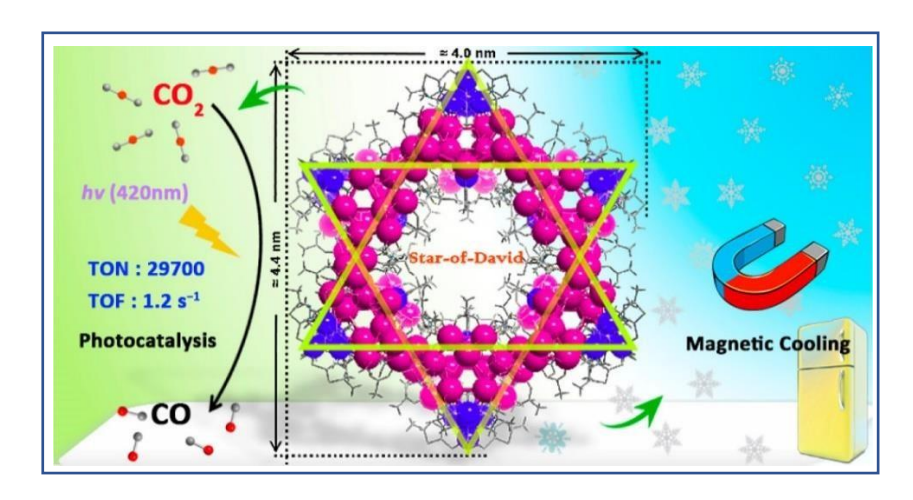


Fig 1.5 Ni₃₆Gd₁₀₂ LOC being used as a catalyst and magnetic coolant

1.2.12 LOCs as Homogeneous Water Oxidation Catalysts:

An oxidation and reduction half-cell reaction make up the water-splitting reaction. Therefore, water molecules will divide into four protons and four electrons during an oxidation half-cell reaction. Numerous lanthanide and transition metal catalysts have been investigated to mediate this reaction. A few Ru-based catalysts successfully catalysed the oxidation half-cell process.²⁸

The Yao group has reported another instance of a water oxidation reaction; after examining the cuboidal CaMn₄O₅ structure, it was determined that the oxygen-evolving centre of photosystem II was a powerful catalyst. By improving the Lewis acidic characteristics of the lanthanum oxo cluster, Lanthanide ions can be used to replace Ca²⁺ ions, offering a reliable model for structure-function correlation investigations in the oxygen-evolving core. Structure-function interaction and the Lewis acidic effect of Ln³⁺ ions on Mn redox potential have been thoroughly investigated.²⁹ By examining the characteristics of isomorphous LOCs bearing various catalysis indulging qualities, such as Lewis acidity, redox properties and ionic size, capacities to achieve great lanthanide oxo homogeneous catalysts, LOCs give an analytical platform for structure function correlation.

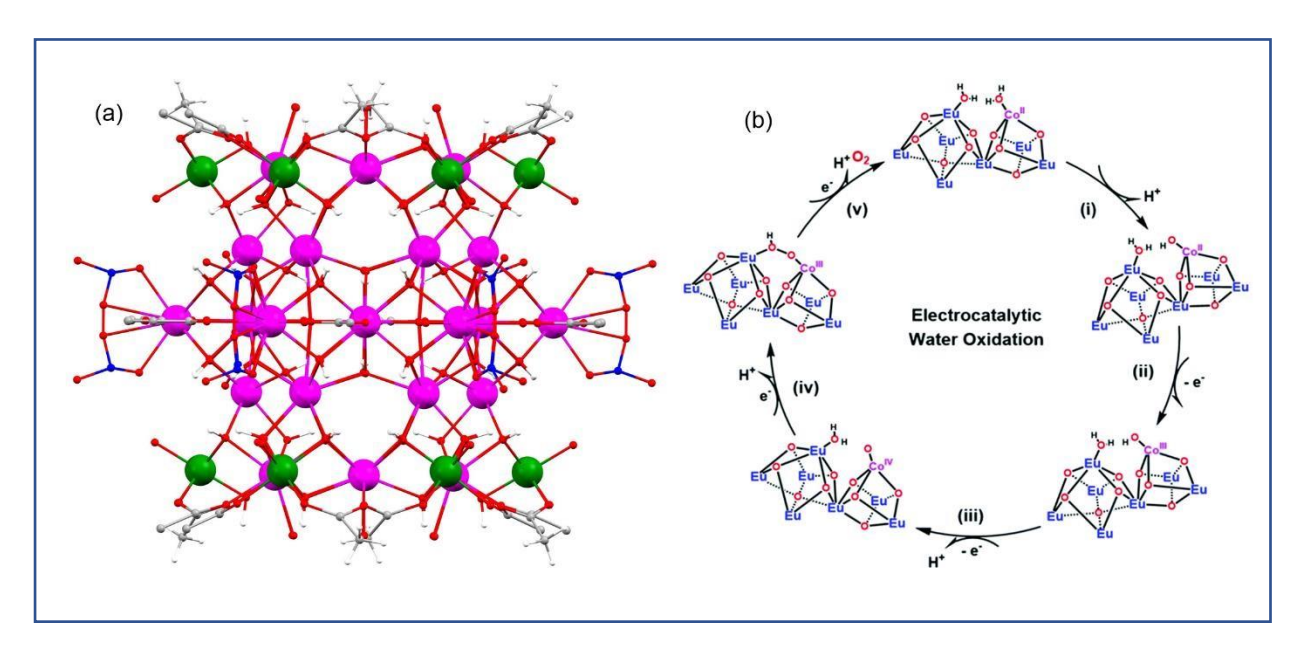


Fig 1.6 (a)Ball and stick model of Eu₃₆Co₁₂ structure and (b) Proposed mechanism for the water oxidation reaction.³⁰

1.2.13 LOC as heterogeneous catalysts for water oxidation:

In contrast to metalorganic frameworks, which have demonstrated substantial catalytic characteristics, direct solar energy conversion to valued chemical fuels in the presence of photocatalysts is a potential agent. As an illustration, different metalorganic frameworks such as Ti complexes Zr complexes, have drawn much attention in case of photocatalytic process, as a result of similarity to the widely used photocatalyst (TiO₂) and good stability. A significant development in the creation of Ti based photocatalysts is using metalorganic frameworks (MOFs). Ti-based MOFs are similar to the semiconducting titanium oxide in zeolites with titanium grafting that Ti-O clusters can be considered isolated titanium oxide quantum dots.

For the photoelectrochemical oxidation of heterogeneous water, Kong, and co-workers have reported three isomorphous Ti-containing LOC with the standard formula $[Ln_8Ti_{10}(\mu_3O)_{14}(L_4)_{34}(OAc)_2(H_2O)_4(THF)_2].2HL$ (Ln = Eu, Sm, Gd). The best outcomes with Eu_8Ti_{10} are noticeably superior to those of anatase, one of the traditional photoelectrochemical catalysts of Ti complexes (a TON of 7581. and a TOF of 2527.0 h⁻¹) for oxidizing water.³¹

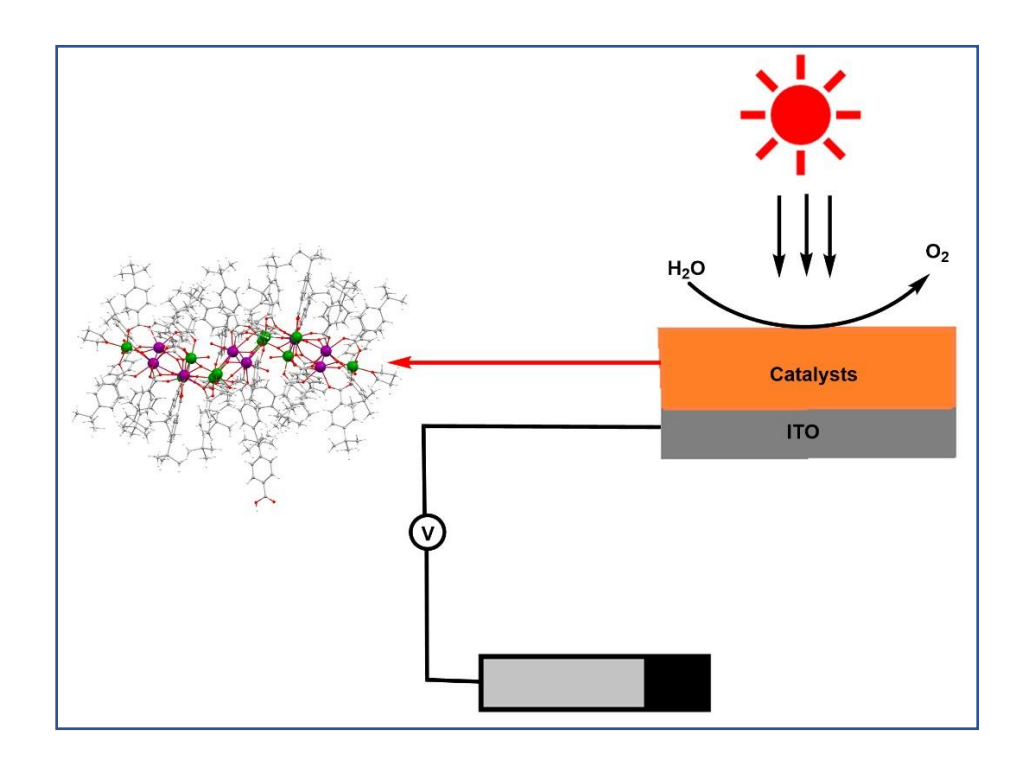


Fig 1.6 (a)Ball and stick model of Eu₃₆Co₁₂ structure and (b) Proposed mechanism for the water oxidation reaction.

1.2.14 LOCs as Hydrogen Production Catalysts

The second half of the water-splitting reaction is hydrogen evolution. Different semiconductors have been produced investigated for the photocatalytic synthesis of H2, but CdS has received the most attention because of its ideal electronic structure for the absorption of visible light, ideal bandgap, and ideal electronic charge transfer.

In 2018, Chen et al. created many high nuclear LOCs generally formulating as $[Ln_{52}Ni_{56x}Cd_x(L^5)_{48}(\mu_3\text{-OH})(H_2O)_{38}]^{18+}$ ($Ln_{52}Ni_{56-x}Cd_x$, where Ln = Eu, Pr, Nd, and Gd, and $H_2L^5 = Iminodiacetic acid$). Under hydrothermal circumstances, $Ln_{52}Ni_{56}$ and $Cd(NO_3)_2$ were reacted to achieve this synthetic aim, and the resulting $Ln_{52}Ni_{56-x}Cd_x$ has the identical fourshell core construction resembling a nesting doll as its parent $Ln_{52}Ni_{56-x}Cd_x$ has the identical fourshell core construction resembling a nesting doll as its parent $Ln_{52}Ni_{56}$. It is simple to load these Cd-doped heterometallic lanthanide -oxo-cluster onto the surface of CdS producing the appropriate $Ln_{52}Ni_{56-x}Cd_x/CdS$ nanocomposites. The author concluded that the difference in catalytic activity between $Eu_{52}Ni_{56-x}Cd_x$ and it's akin of Pr, Nd and Gd is caused by charge separation. In particular, electrons that have been photoexcited CdS surface particles that fall into the correct LUMO energy level of $Ln_{52}Ni_{56-x}Cd_x$ by reducing protons into hydrogen along a known path to all $Ln_{52}Ni_{56-x}Cd_x$ cocatalysts. In the case of $Eu_{52}Ni_{56-x}Cd_x$, however, a secondary catalytic site and Eu^{2+} are produced when photoinduced electrons move from the reaching an acceptable electrical level in the conduction band of CdS Eu^{3+} . This method is only viable for $Eu^{52}Ni^{56-x}Cd^x$ since the CdS conduction band's energy coincides with the reduction potential of Eu^{3+} .

1.3 Brief Introduction to Magnetism

Continuous research on magnetochemistry commenced dealing with the everyday use of appliances in our day-to-day life. Contemplating these basic needs, the research on magnetism started accelerating with magnetic properties of inorganic, transition, or lanthanide metal oxides reacting with various ligand systems in different synthesis procedures. Hence, the typical applications of medical instruments, loudspeakers, microphones, sensors, data storage devices, switches, etc., started evolving in our daily life. The magnetic properties of all materials are determined when external magnetic field is present. In the electronic configuration of atoms and ions in the case of a diamagnetic material, electrons are arranged in a spin-paired manner. For paramagnetic materials, electrons are arranged in a spin unpaired mode. Some types of magnetic interactions involve cases where the metal centres play essential roles in forming Ferro-, anti-ferro- and ferrimagnetic magnets.

(1) Diamagnetism

All spin states are paired in this magnetism section, which cancels the spin contribution. Then applying an external magnetic field causes the magnetic moment to be opposed by the applied magnetic field, resulting in a poor magnetic susceptibility where retention does not occur without a magnetic field.

(2) Paramagnetism

The presence of unpaired electrons gives rise to its magnetic moment. Because it amplifies the external magnetic field, it loses a small positive susceptibility when the external magnetic field is removed.

(3) Ferromagnetism

Ferromagnets, like paramagnets, contain unpaired electrons; in addition to this intrinsic magnetic moment of unpaired electrons being parallel to an applied magnetic field, the situated magnetic moments are parallel to one another, exhibiting a net magnetic moment, which also exhibits a magnetic field even when there is no external magnetic field. A magnetic material's Curie point, sometimes called Curie temperature, is the temperature at which its magnetic characteristics abruptly change.

(4) Antiferromagnetism: In antiferromagnetism, adjacent electrons show intrinsic properties, and the spin of the electrons directs in a direction antiparallel to each other, which cancels out the net magnetic momentum. This happens at a considerably low temperature above a specific temperature called Neel temperature.

(5) **Ferrimagnetism:** The electron spins directly in opposite directions making the magnetic properties go through a prolonged relaxation even after removing the external magnetic field. In this case, all adjacent electrons are aligned antiparallelly, and the nearest electrons do not carry the same magnetic strength, which results in a nonzero residual.

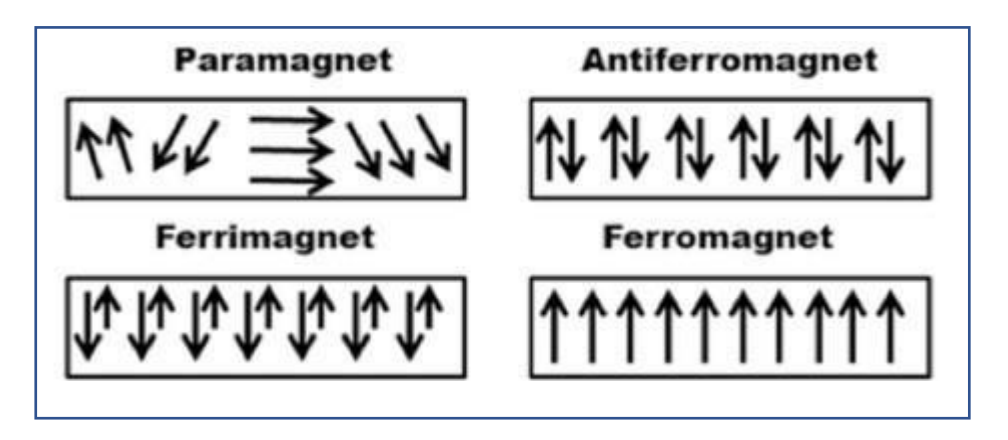


Fig 1.8 Types of magnetic behaviours through the electronic spin

1.3.1 Fundamentals of Magnetism

Magnetism results from individual magnetic moments of spinning electrons in magnetic materials by combining the orbital and intrinsic angular momentum. According to electrodynamics laws, spinning charged particles or electrons around the nucleus generates an orbital magnetic moment.

1.3.2 Magnetisation curve: Hysteresis

Under the Curie temperature, spontaneous magnetization and the presence of a ferromagnetic phase are explained by the molecular field theory. Contrary to the Curie-Weiss theory, the relationship between magnetization and the external field is more complex. The domains of these species align parallel to the area when these materials are exposed to an external magnetic field, which causes the substance to become magnetized and reach a saturation point of its magnetization.

Remanence: The retention of magnetization in zero-field conditions is known as remanence. When H = 0, the magnetic field represents the residual flux density.

Coercivity: An area that needs to be applied to bring about magnetization in the reverse direction back to zero is called a coercive field or coercivity.

Hysteresis: One can increase magnetization by applying an opposite field, and after passing through a point where there is no magnetization, the loop is completed by decreasing the field and applying it again in the opposite direction. Hysteresis is the name given to this spontaneous magnetization that occurs when a magnetic field is introduced and removed.

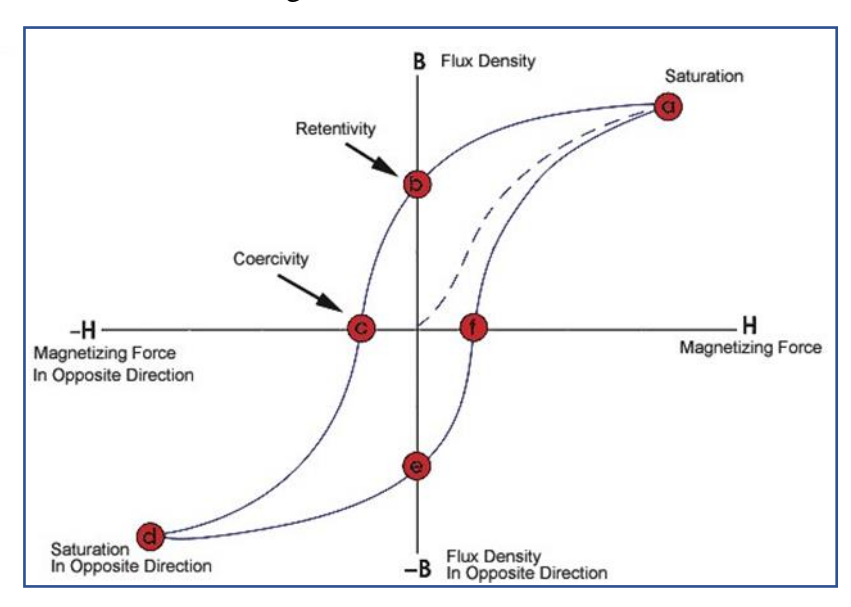


Fig 1.9 Hysteresis loop explaining remanence, coercivity, and hysteresis.

Ion-based magnets were developed from molecule-based magnets in 1990 by research teams. The latest discovery that molecules consisting multiple transition-metal ions display characteristics like tiny magnetic particles (nanomagnets) represents an appealing possible answer to different needs.³³ These polynuclear metal complexes with characteristics like superparamagnetic materials are known as single-molecule magnets (SMMs) for this reason. The first mesoscopic magnet was found by R. Sessolli and his team in 1993. The bulk magnets are to be broken up for the creation of this mesoscopic magnet; however, a more manageable strategy is to start from the bottom up and use chemistry to create distinct clusters of metal ions.

Several groups have reported twelve-membered manganese cluster ions with eight Mn ions in the +3-oxidation state (spin S= I) and four in the +4 state (S= 3/l). Mn12 cluster magnetization is very anisotropic., and at temperatures below 4 K, the magnetization relaxation time becomes exceptionally long, leading to significant hysteresis. These ions are magnetically coupled to the S=10 ground state, exhibiting anomalous magnetic relaxation properties. The significant anisotropy in the susceptibility, which is supported by the anisotropy measurements, is

compatible with these relaxation effects. The M=10 levels are the lowest in energy and the M=9 levels are at $10\,\mathrm{cm}^{-1}$ in electron paramagnetic resonance spectra, which showed a significant zero-field splitting. The lowest levels are inhabited only with low temperatures, and these are what cause the significant ising magnetic anisotropy visible. The single-ion anisotropy of the Jahn-Teller distorted manganese (III) ions are linked by the reason of substantial zero-field splitting. The parallel alignment of each individual S=2 spin with ground spin state S=10 provides the significant zero-field splitting consequent.

One method for creating these magnetic building blocks uses tiny complexes with two, three, or four metal ions as building blocks. Due course of time, using a reagent opens up one edge for the relatively small multi-block complex by eliminating part of the organic ligands. Another method involves adding polydentate ligands of the constituent complexes trigger accumulation to produce bigger results. These ligands can create multiple binds with multiple metal ions.

With compositions of Mn₃, Mn₄, Mn₆, Mn₇, Mn₈, Mn₁₀, Mn₁₂, Mn₁₈, and Mn₃₀, polynuclear Mn complexes have been made. Sadly, bigger does not always imply better. The ground spin state must be elevated for SMMs to function properly. The ground spin state must be elevated for SMMs to function properly. An antiferromagnetic pairwise interaction between a Mn ^{III} (S=2) ion and a Mn ^{IV} (S=3/2) ion can pair up electrons to produce a net spin of S=1/2 or a ferromagnetic pairwise interaction can produce S=7/2. Magnetic exchange interactions are generated via the crossing over O₂, OH, RO, or RCO₂ ligands. Consequently, in order to provide polynuclear complexes with giant ground spin state, metal ions, along with bridging ligands (i.e., to take advantage of the complex's architecture to obtain an excessive spin ground must be arranged suitably.

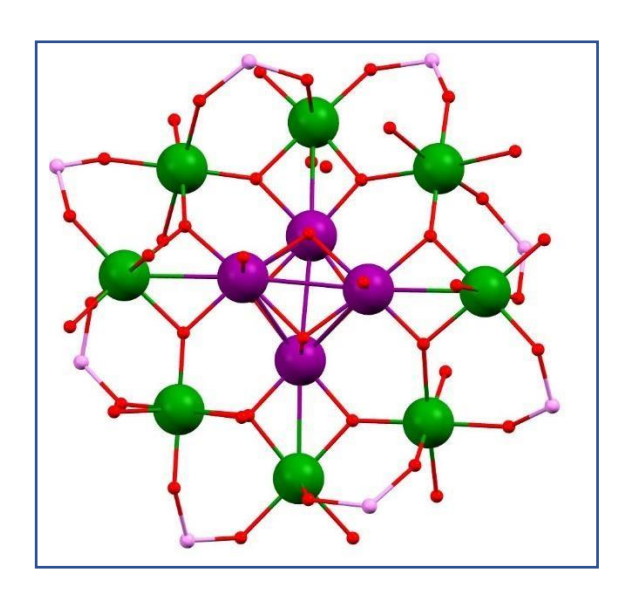


Fig2.0 Colour legend Purple Mn^{IV} green Mn^{III} ; $[Mn_{12}O_{12}(O_2CCH_3)_{16}(H_2O)_4].4H_2O.2CH_3CO_2H$ complex.

A polynuclear complex will function as a powerful single-molecule magnet with reachable blocking temperature, though, if its spin state is more relevant. For instance, $(Mn^{III})_6$ complexes with a S=12 ground state has been produced. However, the zero-field splitting of these complexes is insignificant (D=0) because the six Mn^{III} ions are grouped in a high-symmetry octahedron. As a result, the energy barrier " U_{eff} " depends on S and D which is very tiny, for complexes to operate as SMMs.

A search for single molecule magnet with spin standards that span a wide scope is proving to be a task for which chemistry is well suited. For instance, the results of changing a complex's spin from a bit of value, like S=3, to a significant discount, like S=30. Quantum mechanics best describes an S=3 complex, whereas an S=30 complex would have several spin states. The ground spin state S=9/2 is present in the compound $[Mn^{IV}Mn^{III}_3]$. It may be feasible to produce thin layers of single molecule magnets by altering ligands on a complex's perimeter to make it more or less soluble.

1.3.3 Quantum Tunnelling of Magnetism:

In theory, a process known as macroscopic quantum tunnelling, which involves mixing "up" and "down" quantum states, can cause the magnetization of nanoscale particles to relax. In 1996, the first instance of macroscopic quantum tunnelling was reported. However, according to prevailing wisdom, MQT must be an extremely unusual occurrence because a visible particle is a system large enough to be detected.³⁶ The corresponding magnet's hysteresis loop was not uniform. The graph of magnetization vs. magnetic field shows series of regular intervals. The phases in the hysteresis loop correlate to a faster speed, at which magnetization changes when energy coincidentally exists at levels on the opposing sides of a double-well potential.

If there is some admixing for two states, tunnelling between the two levels happens with the same energy. The transverse interaction that combines the states and results in the feigned "tunnel splitting" could be produced through little less symmetry crystal field components or by a magnetic field generated through magnetic nuclei or nearby molecules. Mixing of two wave functions is minor, and the tunnelling rate is lower, the more significant the m_s value. The rate of burrowing is not always increased by applying a field along the hard axis. In contrast, it causes oscillations and quenches tunnelling for critical field values where destructive interference exists between the tunnelling routes. The zero-field splitting parameter(s) is/are

connected to the period of the tunnelling rate oscillation. As a result, by supplying a transverse magnetic field, one may regulate the lengthways magnetization's rate of tunnelling and, in turn, the coercivity in hysteresis loops. These happenings, which is specific to single molecules magnets and reflects their underlying quantum nature, may have scientific advantages.

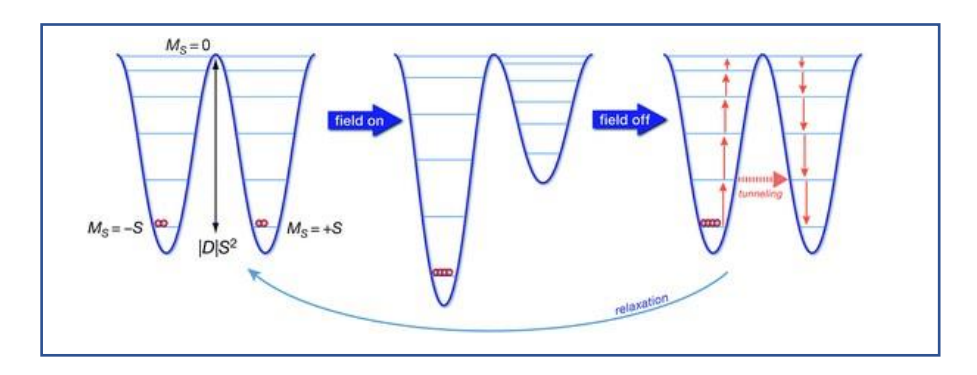


Fig 2.1 Explains the magnetization and magnetic relaxation processes in an SMM.

1.3.4 First examples of lanthanide SMM

In the year of 2003, Ishikawa and group reported a double-decker phthalocyanine complex (Fig 2.2) with different Ln^{3+} metal ions, and very prominently, the research group discovered the temperature range in the case of lanthanide clusters as SMM is far higher than transition metal single-molecule magnet clusters, which confirms the mechanism in case of lanthanide clusters for the formation of SMM is different in case of transition metal complexes.³⁷ The group measured the AC susceptibilities on double-decker lanthanide complexes (Ln = Tb, Dy, Ho, Er, Tm, and Yb). Doping in diamagnetic [Pc₂Y]-TBA+ with an approximate molar ratio of [Pc₂Tb]-/[Pc₂Y]-= 1/4 was used to conduct the measurement (Figure 1). In the diluted sample, the peaks for the χ_M "/ χ_M curves and the χ_M "T dispersion migrated to higher temperatures. This suggests that the flip of the magnetic dipole is slowed by reducing intermolecular contact from a nearby [Pc₂Tb]- complex. The results of the studies unambiguously demonstrate that [Pc₂Tb]'s slow magnetization relaxation is a single-molecular characteristic rather than the product of intermolecular interactions and long-range order. The first lanthanide cluster exhibiting SMM characteristics and a peak temperature of χ_M " above 8 K has been documented by this group.³⁸

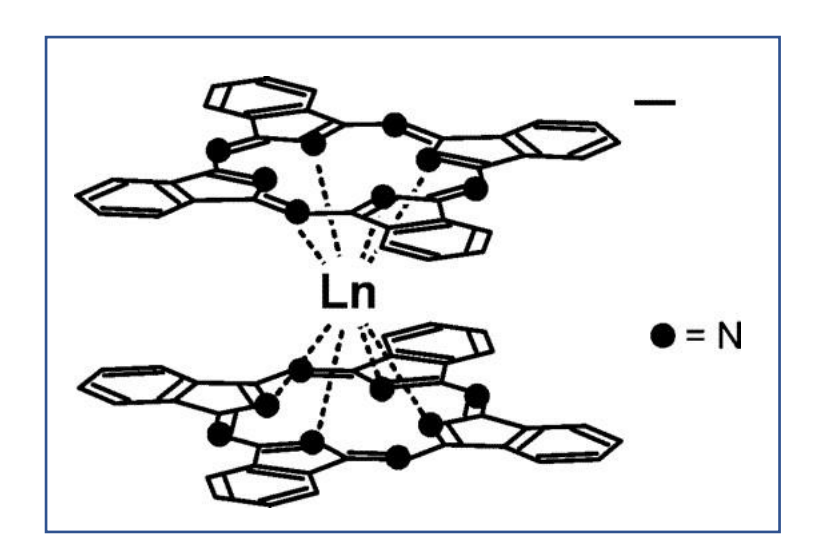


Fig 2.2 Phthalocyanine lanthanide complex where Ln = Tb, Dy, Ho, Er, Tm, and Yb

1.3.5 Breakthrough examples of lanthanide SMM

[Dy₃(μ_3 -OH)₂L₃Cl(H₂O)₅]Cl and [Dy₃(μ_3 -OH)₂L₃Cl(H₂O)₅]Cl₅ are Powell, and research groups have reported two prototype lanthanide clusters.³⁹ All Dy metal ions are octacoordinated distorted geometry bridged by two μ_3 -hydroxo groups in one side pentagonal plane site above and below the plane. The unprecedented nonmagnetic ground state was observed, which is not observed for an odd number of paramagnetic centres with a J value of half-integer and slow magnetic relaxation. Oxo bridges are bridging to each Dy centre antiferromagnetically. Sessoli and the research group discovered that due to single ion easy axes magnetization, the metal ions arranged themselves noncolinear 120 degree to the plane of the Dy3 triangular system, which caused a nonmagnetic ground state. These results show the remarkable phenomena known as 'toroidal magnetic moment' or 'vortex spin chirality.'

Lanthanide clusters show that spin-orbit solid coupling is essential to building prominent single-molecule magnets with lanthanide-based polynuclear systems. By reducing the fast quantum tunnelling of the magnetization of lanthanide metal ions and overlapping bridging ligand orbitals, which together can increase the magneto anisotropy energy barriers in SMMs, it is possible to increase the interaction between lanthanide ions in lanthanide-only systems. Murugesu and the study team have mentioned that using the right ligand system in combination with dysprosium (III) ions results in high blocking temperatures for lanthanide-only SMMs by taking advantage of the significant intrinsic magnetic anisotropy, high spin, and lowered QTM.⁴⁰ As a result of their successful tactics, a highly anisotropic barrier polynuclear lanthanide single molecule magnet has been created. They created a tetra-nuclear dysprosium (III) single molecule magnet with the most significant relaxation barrier yet observed in a

polynuclear single molecule magnet. Another Dy₄ core cluster was reported by Zang et al., who reported that an ac susceptibility shows the presence of two maxima at the 9 K and 30 K peaks, suggesting two types of relaxation processes in the molecular system at low and high temperatures. They have calculated two anisotropic energy barriers from Arrhenius analysis, i.e., $U_{eff} = 9.7 \text{ K}$ ($\tau_0 = 3.2 \times 10^{-5} \text{s}$) and $U_{eff} = 170 \text{ K}$ ($\tau_0 = 4 \times 10^{-7} \text{s}$).

In 2011one, the largest observed U_{eff} among the d and f block complexes is a square-based pyramid pentanuclear cluster [Dy₅O(OⁱPr)₁₃], which shows slow magnetic relaxation at temperature 40 K and U_{eff} =530K. It was discovered by Winpenny et al., and their SCXRD explains that all the Dy (III)-ions are six-coordinated, and the cluster's centre comprises the μ_5 -oxo bridge.⁴¹

Polynuclear lanthanides show high anisotropic energy barriers, yet it is lagging in the case of fast quantum tunnelling of magnetism, which causes them to form a narrow hysteresis loop. Hence to avoid fast QTM, researchers have been searching for new synthetic methodologies where QTM can be reduced by using radical ligands. For example, Demir and the research team have synthesized dinuclear complex [K(crypt-222)][(CpMe₄H $_2$ Tb)₂(μ -N₂)]; it shows high coercive field Hc = 7.9 T at 10 K is higher than the permanent commercial magnet that shows U_{eff} = 276 cm⁻¹ and 100 s magnetic blocking temperature T_B =20 K.

Two examples of mononuclear lanthanide complexes, SIMs (Single Ion Magnet), were discovered. The research groups have been strategically designed according to molecular symmetry, enhancing the single molecule magnetic properties. A pentagonal-bipyramidal (PB), pseudo-D_{5h} symmetry containing complex [L₂Dy(H₂O)₅]³⁺ (L= ¹BuPO(NHⁱPr)₂) was reported by Murugavel et al., through single crystal x-ray analysis they have disclosed that five water molecules and axial positions have occupied all equatorial positions are occupied by phosphoryl oxygen(P=O). It shows a high anisotropic barrier (U_{eff}) 735.4 K with magnetization-blocking (T_B) previous to 12 K and magnetic-hysteresis up to 12 K (30 K) with a greater coercivity 0.9 T (1.5-T) at a field-sweep rate of 0.0018 Ts⁻¹ (0.02 Ts⁻¹).⁴²

A different impressive SIM, exhibiting a nearly flawless pentagonal bipyramidal structure, $[Dy(O^tBu)_2(py)_5][BPh_4]$ (depicted in Figure 2.3 a), was documented. This SIM displays the most considerable effective magnetic moment, $U_{eff} = 1815(1)$ K, and a blocking temperature T_B of 14 K. Although it possesses high magnetic anisotropy, its T_B value is lower than that reported by Murugavel et al., previously, it was considered the only instance of the highest

anisotropic energy barrier until 2016. At that point, this compound was the most noteworthy air-stable SIM/SMM that had been documented.

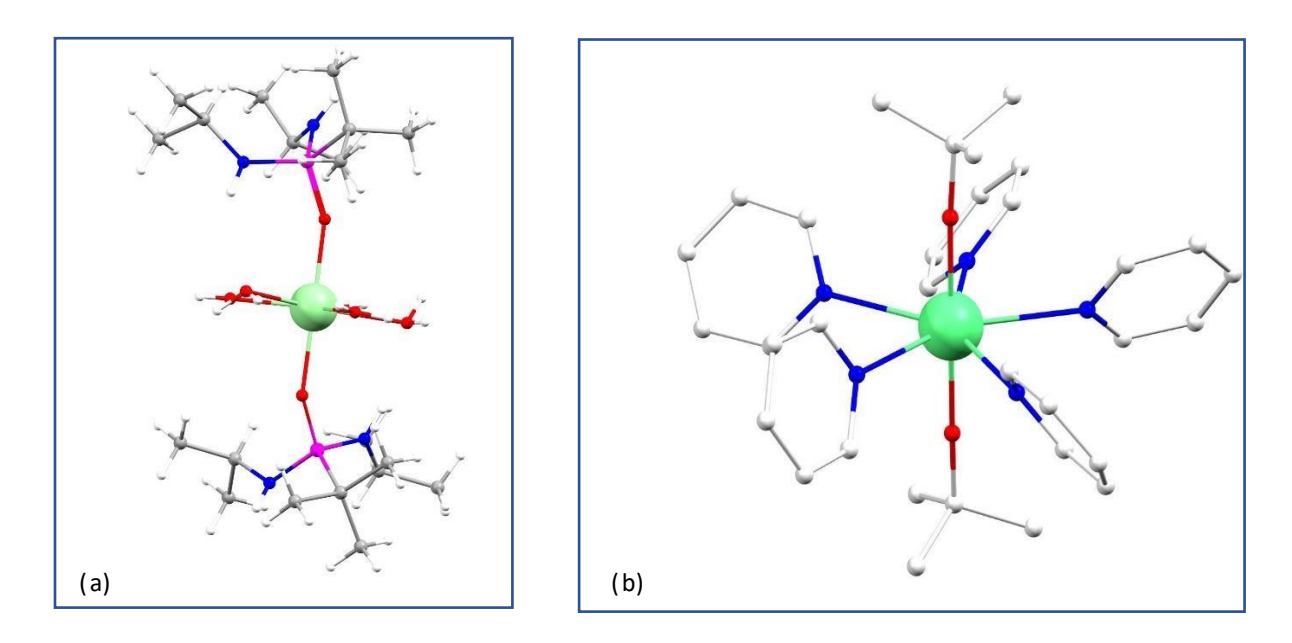


Fig 2.3 (a)An air-stable single ion magnet, the counter ions have been deleted color legend Dy: light green, pink: phosphorus, red: oxygen, blue: nitrogen, light grey: carbon (b) Pentagonal Bipyramidal Dysprosium(III) Single-Molecule Magnet; light green: Dy, blue: N, red: O, light grey: C.

In 2018, Layfield, Tong, and research group reported an extraordinary example of an organometallic lanthanide SMM [(CpiPr₅)Dy(Cp*)][B(C6F₅)4] (CpiPr₅=penta-isopropyl cyclopentadienyl; Cp*=pentamethylcyclopentadienyl) in which the exceptionally high anisotropic energy barrier (U_{eff}) was 1541 cm⁻¹ and the highest blocking temperature (T_B) was 80K (Figure 2.3 b).⁴³This molecule represents a significant breakthrough in the field of SMM as it overcomes the present limitation that all SMM molecules require liquid helium refrigerating to exhibit magnetocaloric effects by reaching above the boiling point temperature of liquid nitrogen. Additionally, this molecule emits a golden light in the dark night, further adding to its uniqueness in the realm of SMM.

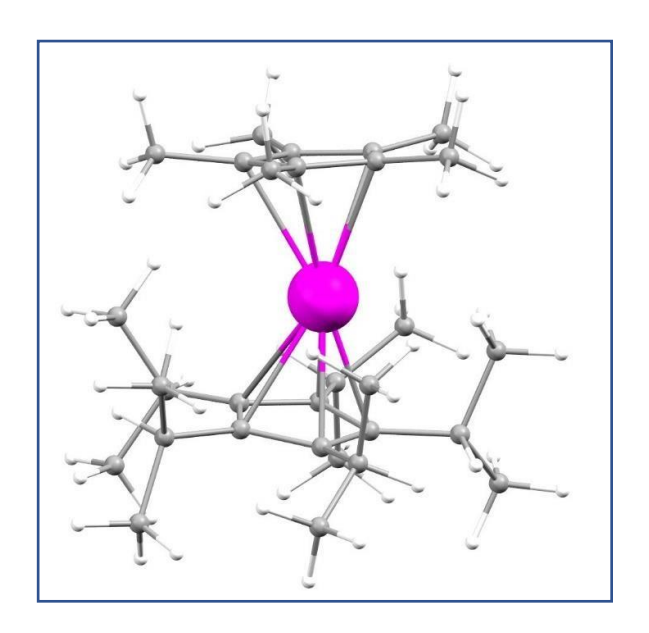


Fig 2.4 Ball and stick model for $[Dy(\eta^5-Cp^iPr_5)(BH_4)_2(THF)]$ complex; color legend: purple Dy, white H, Light grey C.

Gould and the research group recently announced the discovery of a lanthanide complex $(Cp^iPr_5)_2Dy_2I_3$ (Figure 2.4), which exhibits mixed valence lanthanide complex. This complex displays a significant coercive magnetic field, with a minimum value of 14 T at 60 K. Its coercivity at liquid nitrogen temperatures surpasses that of even commercial magnets such as $SmCo_5$ (4.3 T at 4.2 K) and $Nd_2Fe_{14}B$ (5.0 T at 80 K). Due to its exceptional properties, it has been named the Ultrahard magnet.⁴⁴

Using potassium graphite in hexane, $(Cp^iPr_5)_2Dy_2I_4$ was reduced to $(Cp^iPr_5)_2Dy_2I_3$, as shown in (Figure 2.5). The solid-state structure, determined by SCXRD, revealed that three iodine anions act as bridges between the two dysprosium centres, resulting in a Dy_2I_3 core. All metal centres are capped with (Cp^iPr_5) ligands, resulting in trigonal symmetry. The Dy...Dy bond measures 3.713Å, which falls within the sum of the covalent radii of the Dy-metal atom, indicating the presence of Dy...Dy metal bonding. The $(Cp^iPr_5)_2Dy_2I_3$ complex was reported to have $U_{eff} = 1631(25)$ cm⁻¹ and blocking temperature = 72 K through the AC and DC magnetic data, surpassing the previous record set by Layfield et al., the strong magnetic conjoin between the two lanthanide ions reduces Raman and QTM processes, resulting in a considerable H_c value. This is the first example where the exchange interaction and the large magnetic anisotropy induced by the crystal field are collinear.

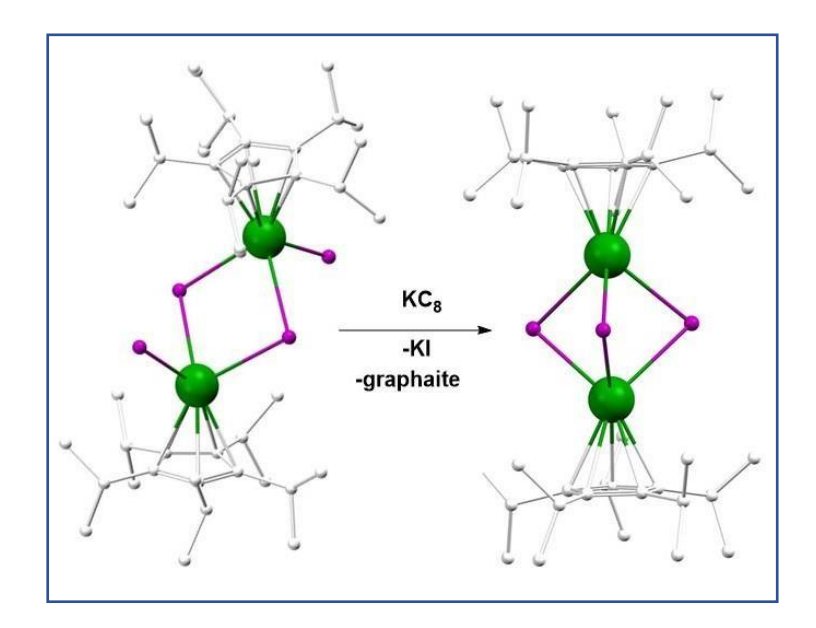


Fig 2.5 Single-electron reduction of $(Cp^{iPr5})_2Ln_2I_4$ (left) with potassium graphite in *n*-hexane affords the compounds $(Cp^iPr_5)_2Ln_2I_3$ (Ln = Dy)

1.4 Briefing on various organo-stannoxane clusters formed by organic protic acids:

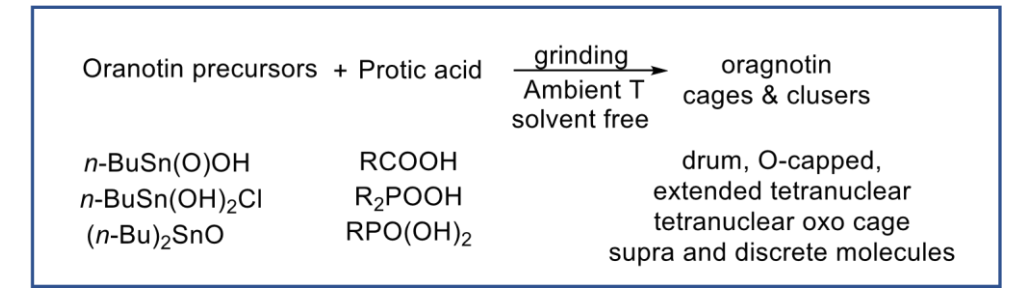
Organotin compounds have drawn much attention recently due to their use in biologically active substances. Aquatic species like fish, molluscs, crabs, and algae are susceptible to trinbutyl tin, triphenyl tin, and tri-cyclohexyl tin compounds. Several tri-oregano and di-organic tin compounds have been tested for in vitro activity against various tumour lines and found to be as practical or more effective than conventional heavy metal anticancer agents such as cisplatin. It exhibits particular activity in mitochondrial oxidative phosphorylation for incorporation into antifouling paints for shipping vessels. Compounds containing organotin function as catalysts or reagents in organic processes. The versatility of organostanoxanes as catalysts for transesterification processes has been demonstrated. The stabilization of PVC is a commercial use for organotin chemicals. The potential of organotin compounds to engineer multiple structural diversities by assembling various heteronuclear clusters has also attracted interest.

Robert R. Holmes and his research teams introduced an affluent cluster chemistry in the early 1990s that explains the different new structural forms of ligand-coordinated monoorgano oxo tin compounds that come from employing phosphorus-based acids. Nuclearities range from two to seven coordinated in tin compounds and derivatives. Some geometrical structures include prismanes or drums, cubes, oxygen-capped clusters and related sulphurcapped products, butterfly forms, crowns, double cubes, and extended groups.⁴⁵

The kind of phosphorus ligand and the groups affixed to it dictate these structures. The condensation reaction of organostannic acids with phosphoric (Fig. 2.6), phosphinic, or phosphoric acids was the result of the leading reactions (Scheme 1.2). Earlier, in some other reaction processes, created clusters moved forward with a previously described cluster unit before reacting with a phosphorus-based acid. The unique tetranuclear clusters

 $[Me_2Sn_2(OH)(O_2P(Ph)_2)_3(O_3POPh)]_2$ (1) and $[(n-Bu)_2Sn_2O(O_2P(OH)t-Bu)_4]_2$ (2), which constitute yet another new structural class that may be referred to as "cage" formulations, were specifically created by this group.

According to Vadapalli et al., stanonic acids and other substituted phosphonic acids can be combined to create organotin molecules. Different research teams have used synthetic approaches, like refluxed, high-boiling solvents. These reactions are incredibly intricate and implement numerous bond-forming and bond-breaking mechanisms. Their synthesis protocols have used solventless techniques to create various structural shapes, such as the drum, O capped cluster, tetranuclear oxo cage, and discrete and polymeric molecules with quantifiable yields. The property of the pr



Scheme 1.2

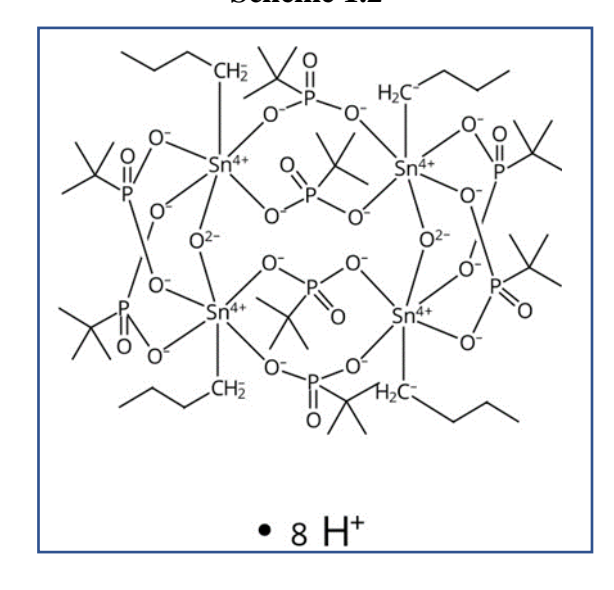


Fig 2.6 Chemdraw diagram for $[(n-Bu-Sn)_4(RPO_3H)_8O_2]$

A first-ever hydrated mono organotin cation, which is also denoted as PhSn(H₂O)₃(-OH)₂, was reported by Puja et al.[{1,5-C₁₀H₆-(SO₃)₂}₂] (**Fig. 2.7**); the Ph₂SnO reaction with the naphthalene-1,5-sulfonic acid tetrahydrate (Scheme1.3) results in the formation of the mono organotin mentioned above complex via the breaking of the Sn-aryl link.⁴⁸ According to the structural explanation, the complex consists of a tetra-cationic di-nuclear unit with two hydroxide ligands as a bridge between the two tin atoms. Each tin has three water molecules. To form organo sulfonic stannoxane complexes the interaction between water molecules and disulfonates develops the hydrogen bonding interaction within molecules create a stack of network three dimensionally. The same group has reported the formation of organo stanonic acid-based clusters such as [*n*-BuSn(O)O₂C-C₆H₄-4-OR]₆ and [*n*-BuSn(O)O₂C-C₆H₃-3,5(OR)₂]₆ by reacting various alkyl groups butyl tin oxide hydroxide with appropriate carboxylic acid in 1:1 stochiometry. When the synthesis procedure is switched to solventless mode, these compounds show gelation behaviour in aromatic solvents.

Scheme: 1.3

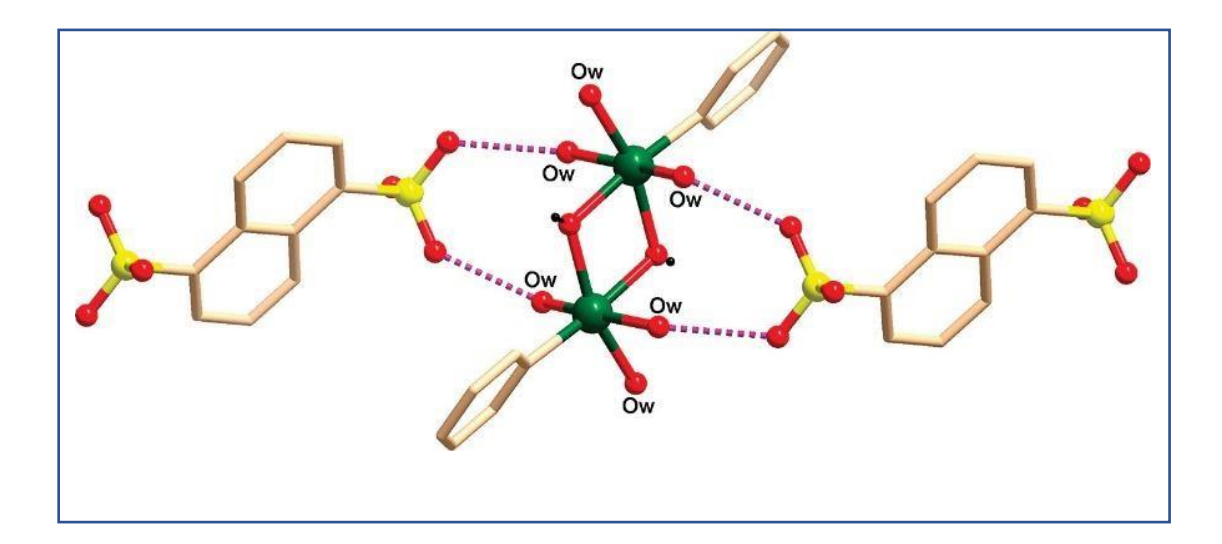
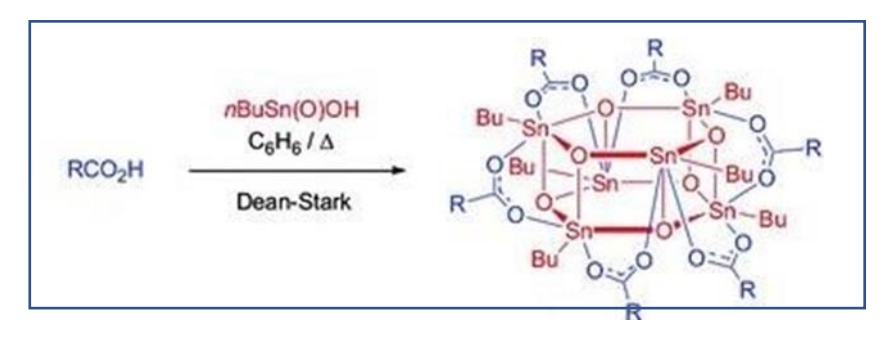


Fig 2.7 Hydrated mono organostanoxane drum; colour legend S yellow, O red, Sn green.

According to Smith et al., a reaction with n-butylstannoic acid with the appropriate carboxylic acids produces a well-defined 'tin-drum' nanocluster that constitutes modular gelation in organic solvents and supports the hierarchical construction of nanostructured fibers. Because a straightforward one-pot assembly procedure can produce structurally varied products, creating organo-oxo-tin clusters (Fig. 2.8) is particularly interesting. Around the "tin" Drum "Nanocore," ferrocene, porphyrin, and fullerene all form. The team has shown how to make organic oxo tin clusters by heating carboxylic acid and n-butylstannoic acid in benzene under Dean-Stark conditions. The clusters were then thoroughly analysed using several spectroscopic techniques.



Scheme 1.4

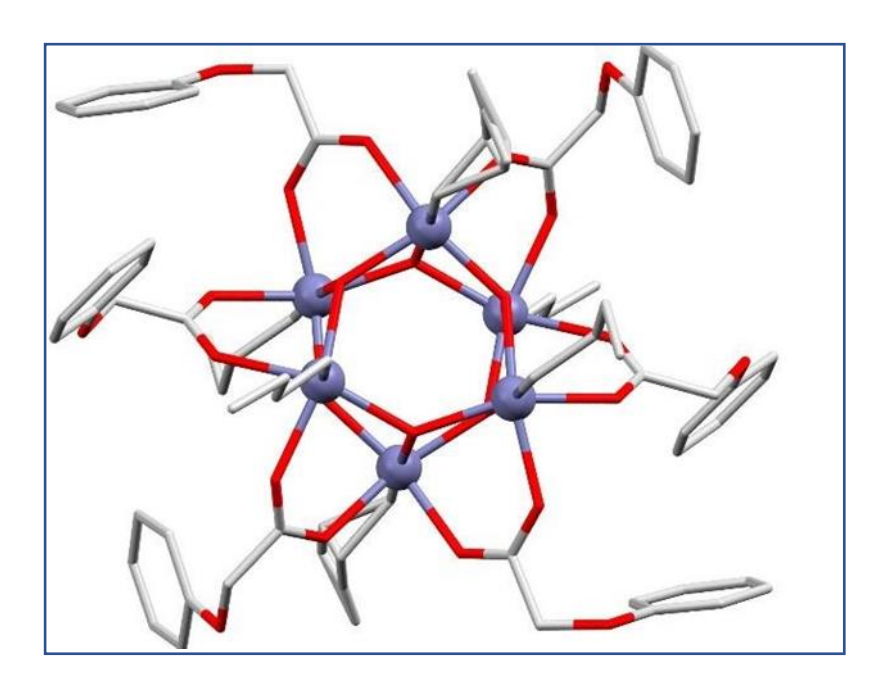


Fig 2.8 Ball stick model for tin drum nanocluster; color legend C grey, O red, Sn greyish navy blue.

Vadapalli et al. reported a hexa-ferrocene unit on a tin oxygen cluster and a unique assembly of a Fe wheel on a tin drum. Detailing the synthesis procedure of the wheel-shaped tin cluster, they have reacted n-butyl stannonic acid with ferrocene monocarboxylic acid (**Scheme 1.6**) in a 1:1 stoichiometry in benzene (**Scheme 1.5**) afforded a dark red compound in quantitative yield. The schematic representation of the reaction is given below.⁵⁰

6BuSn(O)OH + 6FcCOOH
$$\frac{C_6H_6}{80^{\circ}C}$$
 [{BuSn(O)OC(O)Fc}₆]+6H₂O

Scheme: 1.5

The ferrocenyl tin oxo clusters are thermally relatively stable; the structure contains six ferrocene units with a drum-like stannoxane central core serving as support to carry the giant wheel arrangement; it shows that the ferrocene carboxylate moiety is involved in binding to two alternate tin atoms of a distannoxane unit, there is a slight asymmetry in the Sn-O bond lengths arising from the carboxylate linkages. In contrast, the two C-O distances within a ferrocene carboxylate moiety are similar. The central stannoxane cluster in this wheel-shaped cluster comprises two hexameric Sn_3O_3 rings, each with a chair-like conformation that is puckered. Six Sn_2O_2 distannoxane units serve as the cluster's side faces thanks to the connection of these rings to one another. This is the distinguishing structural element of stannoxane clusters.

Zacchini et al. reported mono oregano oxo tin drums' architectures and aromatic substituents' influence on the supramolecular moiety (Fig 2.9). Hexanuclear organostannoxane drums with R groups ranging from 2,6-dimethyl acetophenone, para xylene, meta xylene are produced when n-BuSn(O)(OH) reacts with different substituted benzoic acids. These compounds share a stannoxane (Sn₆O₆) motif in the core, which surrounds six substituted benzoic acid groups. In the solid state, every drum demonstrates many supramolecular clusters.⁵¹

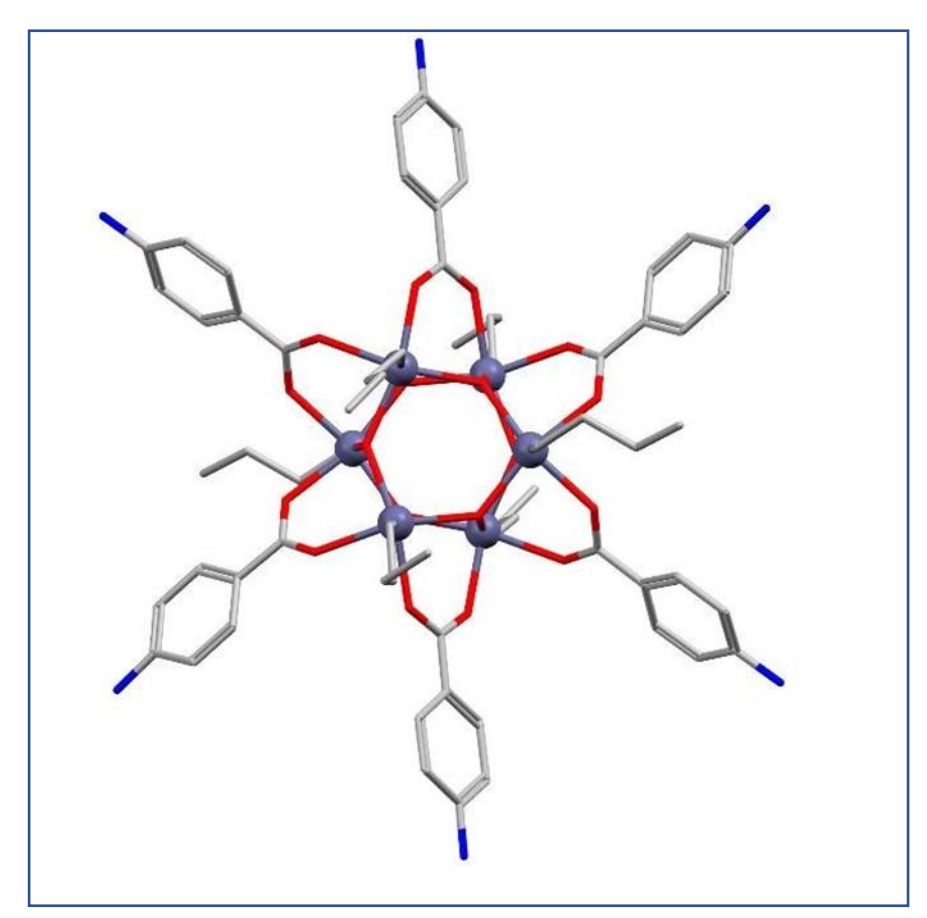


Fig 2.9 Ball-stick model Supramolecular monoorganooxotin; color legend N blue, O red, C light grey, Sn greyish blue.

The carboxylic acid functions along with C_{60} derivatives encounter self-build by combining n-butyl stannonic acid results a stannoxane cantered fullerene substantial nanostructure with an efficient yield according to research by Nierengarten et al. Butyl stannic acid was refluxed in benzene for 12 hours using a dean and stark. The reaction was then followed by a workup and produced a hexameric oragnostanoxane derivative. The crystallographic analysis describes the structural characteristics of the drum-shaped tin motif made up of six Sn metal ions coordinated by five oxygen and one carbon.⁵²

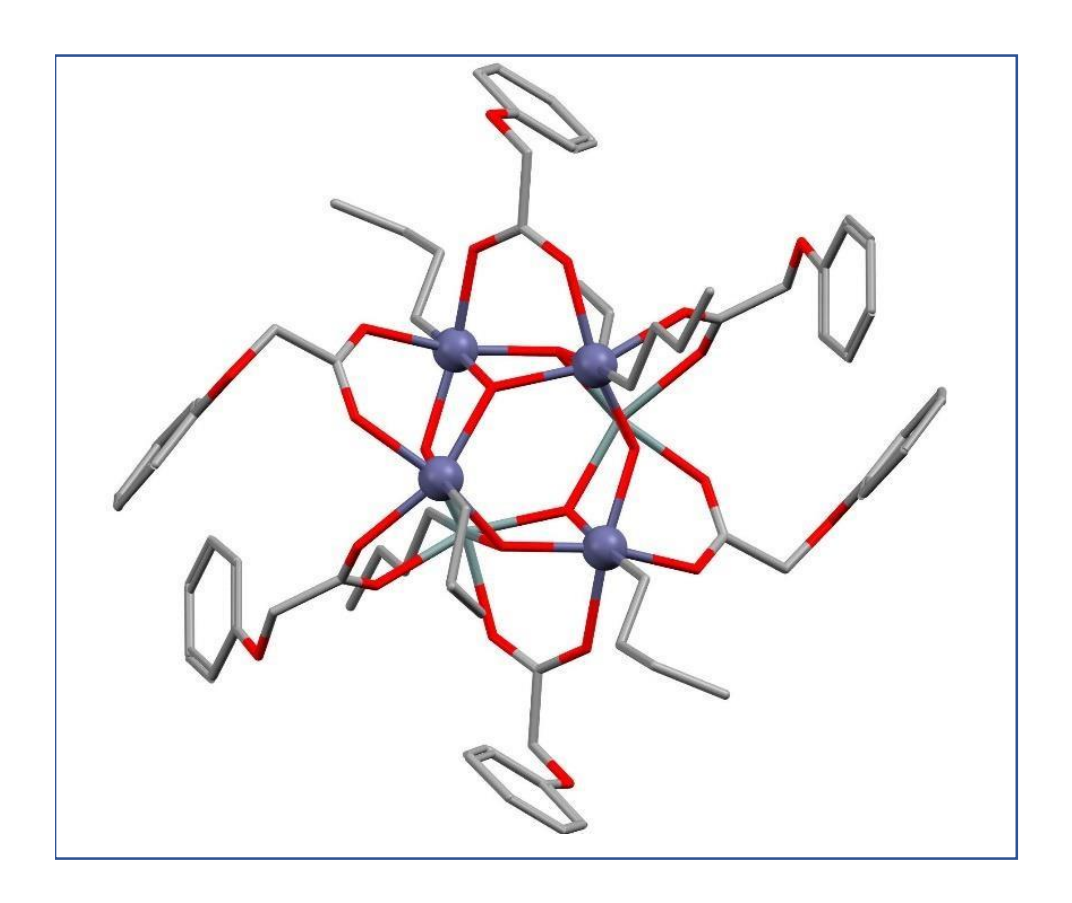


Fig 2.10 Fullerene-rich nanostructures with a stannoxane core; color legend C grey, O red, Sn bluish-grey

Thesis overview

The thesis work mainly consists of two parts; the first part deals with the design, synthesis characterization, and catalytic application of lanthanide oxo hydroxo clusters, whereas the second part of the thesis deals with the synthesis and characterization of organic phosphonic oregano siloxane proligand-based hetero nuclear transition metal and lanthanide clusters.

Chapter 2 deals with the reactivity and catalytic properties of lanthanide oxo hydroxo clusters synthesized by reacting Schiff base ligands and pivalic acid ligands in the presence of excess base at room temperature conditions. La has been vastly used as the catalyst among all three (La, Pr, Nd) isostructural hexa nuclear lanthanide oxo hydroxo clusters. The La₆ oxo cluster catalyzed the cycloaddition reaction of various substituted phenyl ethyl oxide and CO₂. To optimize the catalytic properties of the hexanuclear lanthanum oxo cluster, we have also carried out the same reactions by using ordinary lanthanide salts as catalysts, but the reactants did not consume within the stipulated time. The same reaction has also been carried out without a catalyst, but the reaction did not proceed properly. All substituted organic molecules have been purified through column chromatography and characterized via NMR and HRM spectroscopy.

Along with the activation of various epoxides and CO_2 , we have examined the versatility of our extranuclear lanthanum oxo hydroxo cluster in the presence of a cocatalyst that is tetra butyl ammonium bromide (TBAB), less reactive sulfur-based small molecules such as $CS_2(l)$, $H_2S(g)$, and elemental sulfur, also known as (S_8) . The extranuclear lanthanum oxo cluster has also activated some other sulfur-based small molecules as a thiol and substituted aziridines resulting in the related products in a good yield. All the characterizations and details have been reported in Chapter -3.

In Chapter 4, we investigated pro-ligand's reactivity toward the transition metals and lanthanides. We are planning to study the magnetic behavior of these metal clusters. In main group-3d clusters and main group-4f clusters, various studies have been reported with 3d-4f mixed valence clusters, but very few are there where the leading group -3d /4f clusters have been reported. Moreover, their magnetic studies will be value-added to magnetochemistry. SCXRD reveals fascinating structures. The carried work is presented in Chapter 4.

References

- 1. Roduner, E.; Chem. Soc. Rev., 2014, 1-34.
- 2. www.legaladvanatge.net, An overview of different types of catalysts, **2017**.
- 3. Qiao, Y.; Schelter, E. J. Acc. Chem. Res. 2018, 51, 2926–2936.
- 4. Arnold, P. L.; McMullon, M. W.; Rieb, J.; Kuhn, F. E. Angew. Chem. Int. Ed. 2015, 54, 82-100.
- 5. Díaz, L.M. A.; Snejko, N.; Iglesias, M.; Sánchez, F.; Puebla, E. G.; Monge, M. Á., *Inorg. Chem.* **2018**, 57, 12, 6883–6892.
- 6. Alzamly, A.; Bakiro, M.; Hussein Ahmed, S.; Alnaqbi, M.A.; Nguyen, H.L. *Coord. Chem. Rev.* **2020**, 425, 213543.
- 7. Perles, J.; Iglesias, M.; Martı´n-Luengo, M. Ä.; Valero, C. R.; Snejko, N., *Chem. Mater.* **2005**, 17, 5837-5842.
- 8a. Perles, J.; Iglesias, M.; Valero, C. R.; Snejko, N. J. Mater. Chem., 2004, 14, 2683–2689.
- b. Perles, J.; Snejko, N.; Iglesias, M.; Monge, M. A. J. Mater. Chem., 2009, 19, 6504–6511.
- 9. Saraci, F.; Novoa, V. Q.; Donnarumma, P. R.; Howarth, A. J., *Chem. Soc. Rev.*, **2020**, 49, 7949-7977.
- 10. Abdelbaky, M. S. M.; Amghouz, Z.; Granda, S. G.; García, J. R. *Polymers*, **2016**, 8, 86, 1-15.
- 11. Abdelbaky, M. S. M.; Amghouz, Z.; Granda, S. G.; Garcíaa, J. R. *Dalton Trans.*, **2014**, 43, 5739-5746.
- 12. Chen, X.; Xu, Jun.; Xu, Y.; Luob, F.; Du, Y.; *Inorg. Chem. Front.*, **2019**, 6, 2226–2238.
- 13. Tasca, J. E.; Lavat, A. E.; González, M. G. J. Asian Ceram. Soc. 2017, 5, 235–241.
- 14. Wang, Y.; Xiong, Y.; Wang, J.; Zhang, X. Catal. Commun. 2017, 90, 14-18.
- 15. Hu, R.; Li, C.; Wang, X.; Sun, Y.; Jia, H.; Su, H.; Zhang, Y.; Catal. Commun., 2012, 29, 35-39.

- 16. Hatakeyama, T.; Takeda S.; Ishikawa, F.; Ohmura, A.; Nakayama A.; Yamada Y.; Matushita A.; Yea, J. *J. Ceram. Soc. Jpn.***2010**, 118, 91-95.
- 17. Rath, M.; Lee, K. T.; J. Alloys Compd. 2018, 737, 152-159.
- 18.Oh, W. C.; Cho, K. Y.; Jung, C. H.; Areerob, Y. *Photochem. Photobiol. Sci.*, **2019**, 18, 1389–1397.
- 19. Jinyan, C.; Yutao, L.; Tianrun, S.; Qiulin, Z.; Ping, N.; Jianjun, C.; Guocai, T.; Liangtao, y.; Siyuan, X.; Rongbing, N. *Appl. Surf. Sci.* **2023**, 60, 156826.
- 20.Ma, L.; Ding, C.; Wang, J.; Xu, H.; Zhang, K. Int. J. Hydrog. Energy. **2023**,48, 19074-19086.
- 21.Qiao, Y.; Cheisson, T.; Manor, B. C.; Carroll, P. J.; Schelter, E. J. *Chem. Commun.*, **2019**, 55, 4067-4070.
- 22. a) Yin, H.; Yi, J.; Hertzog, J. E.; Mullane, K. C.; Carroll, P. J.; Manor; Brian C.; Schelter, Eric J. *J. Am. Chem. Soc.* **2016**, 138, 16266–1627. b) Wang, Y. H.; Yang, Q.; Walsh, P. J.; Schelter, E. *J. Org. Chem. Front.*, **2022**, 9, 2612–2620.
- 23. Huang, W.; Liu, Q.; Chen, W.; Feng, M.; Zheng, Z. Magnetochemistry, 2021, 7, 161.
- 24. Dong, J.; Cui, P.; Shi, P. F.; Cheng, P.; Zhao, B. *J. Am. Chem. Soc.* **2015**, 137, 51, 15988–15991.
- 25. Fukuzumi, S.; Lee, Y. M.; Ahn, H. S.; Nam, W. Chem. Sci., 2018, 9, 6017–6034.
- 26. Kojima, T.; Chem. Photo. Chem. 2021, 5, 512–520.
- 27. Jin, P.B.; Zhang, L.; Ling, B. K.; Wang, S. C.; Chan, Y. T.; Chen, X. M.; Zheng, Y. Z.
- *J. Am. Chem. Soc.* **2020**, 142, 10, 4663–4670.
- 28. Duan, L.; Wang, L.; Li, F.; Li, F.; Sun, L. Acc. Chem. Res. 2015, 48, 7, 2084–2096.
- 29. Li, P.; Zhao, R.; Chen, H.; Wang, H.; Wei, P.; Huang, H.; Liu, Q.; Li, T.; Shi, X.; Zhang, Y.; Liu, M.; Sun, X. Small. **2019**, 15, 1805103.
- 30. <u>Chen</u>, R.; <u>Chen</u>, C. L.; <u>Du</u>, M. H.; <u>Wang</u>, X.; <u>Wang</u>, C.; <u>Long</u>, L. S.; <u>Kong</u>, X. J.; <u>Zheng</u>, L. S. *Chem. Commun.*, **2021**, 57, 3611–3614.

- 31. <u>Lu</u>, D. F.; <u>Kong</u>, X. J.; <u>Lu</u>, T. B.; <u>Long</u>, L. S.; <u>Zheng</u>, L. S. *Inorg. Chem.* **2017**, 56, 3, 1057–1060.
- 32. Chen, R.; Yan, Z. H.; Kong, X. J.; Long, L. S.; Zheng, L. S. *Angew. Chem.* Int. Ed. **2018**, 57, 16796 –16800.
- 33. (a) Gatteschi, D.; Sessoli, R.; Villain, J. Molecular Nanomagnets, *Oxford University Press*. **2006**. (b) Christou, G.; Gatteschi, D.; Hendrickson, D. N.; Sessoli, R. *MRS Bull.* **2000**, 25, 66. (c) Gatteschi, D.; Sessoli. R. *Angew. Chem. Int. Ed.* **2003**, 43, 268. (d) Aromi, G.; Brechin, E.
- K. Struct. Bonding. 2006, 122, 1. (e) Bagai, R.; Christou, G. Chem. Soc. Rev. 2009, 38, 1011.
- 34. Lis, T. Acta Crystallogr., Sect. B: Struct. Crystallogr. Cryst. Chem. 1980, 36, 2042.
- 35. (a) Sessoli, R.; Gatteschi, D.; Caneschi, A.; Novak, M. A. *Nature* **1993**, 365, 141. (b) Sessoli, R.; Tsai, H. L.; Schake, A. R.; Wang, S. Y.; Vincent, J. B.; Folting, K.; Gatteschi, D.; Christou, G.; Hendrickson, D. N. *J. Am. Chem. Soc.* **1993**, 115, 1804.
- 36. Friedman, J. R.; M. P. Sarachik, J. R.; Tejada, J.; Ziolo, R. *Phys. Rev. Lett.*, **1996**, 76, 3830–3833.
- 37. Ishikawa, N.; Sugita, M.; Ishikawa, T.; Koshihara, S. Y.; Kaizu, Y. *J. Am. Chem. Soc.*, **2003**, 125, 8694–8695.
- 38. Koike, N.; Uekusa, H.; Ohashi, Y.; Harnoode, C.; Kitamura, F.; Ohsaka, T.; Tokuda, K. *Inorg. Chem.*, **1996**, 35, 5798–5804.
- 39. Powell. A. K.; Tang, J.; Hewitt, I.; Madhu, N. T.; Chastanet, G.; Wernsdorfer, W.; Anson, C. E.; Benelli, C.; Sessoli, R. *Angew. Chemie Int. Ed.*, **2006**, 45, 1729–1733.
- 40. Lin, M. M. Po-H.; Burchell, T. J.; Ungur, L.; Chibotaru, L. F.; Wernsdorfer, W.; *Angew. Chemie*, **2009**, 1221, 9653–9656.
- 41. Blagg, R. J.; Muryn, C. A.; McInnes, E. J. L.; Tuna, F.; Winpenny, R. E. P.; *Angew. Chemie Int. Ed.*, **2011**, 50, 6530–6533.
- 42. Gupta, S. K.; Rajeshkumar, T.; Rajaraman, G.; Murugavel, R. *Chem. Sci.*, **2016**, 7, 5181–5191.
- 43. Guo, F. S.; Day, B. M.; Chen, Y. C.; Tong, M. L.; Mansikkamäki, A.; Layfield, R. A. *Science*, **2018**, 362, 1400–1403

- 44. Gould, C. A.; McClain, K. R.; Reta, D.; Kragskow, J. G. C.; Marchiori; Lachman, D. A. E.; Choi, E. S.; Analytis, J. G.; Britt, Chilton, R. D.; Harvey, N. F. B. G.; Long, J. R. Science, **2022**, 375, 198–202.
- 45. Swamy, K. C. K.; Schmid, C. G.; Day, C. G.; Holmes, R. R. J. Am. Chem. Soc. **1990**, 112, 1, 223–228.
- 46. Chandrasekhar, V.; Nagendran, S.; Baskar, V. Coord. Chem. Rev., 2002, 235, 1-52.
- 47. <u>Day</u>, R. O.; <u>Holmes</u>, J. M.; <u>Chandrasekhar</u>, V.; <u>Holmes</u>, Robert R. *J. Am. Chem. Soc.* **1987**, 109, 3, 940–941
- 48. Chandrasekhar, V.; Gopal, K.; Singh, P.; Narayanan, R. S.; Duthie, A. *Organometallics* **2009**, 28, 15, 4593–4601.
- 49. Hahn, U.; Hirst, A. R.; Delgado, J. L.; Kaeser, A.; Nicot, B. D.; Nierengarten, J. F.; Smith, D. K. *Chem. Commun.*, **2007**, 4943-4945.
- 50. <u>Chandrasekhar.</u>, V.; <u>Nagendran</u>, S.; <u>Bansal</u>, S.; <u>Kozee</u>, M. A.; <u>Powell</u>, D. R.; *Angew. Chem. Int. Ed.***2000**,39,1833-1835.
- 51. Chandrasekhar, V.; Baskar, V.; Boomishankar, R.; Gopal, K.; Zacchini, S.; Bickley, J. F. Steiner A. *Organometallics*. **2003**, 22, 18, 3710–3716.
- 52. Chandrasekhar, V.; Gopal, K.; Singh, P.; Narayanan, R. S.; Duthie, A. *Organometallics* **2009**, 28, 15, 4593–4601.

Trigonal prismatic Ln₆ cluster encapsulating μ_4 -CO₃²ion showing catalytic properties for cycloaddition reaction of epoxide and CO₂

An array of new hexanuclear lanthanide complexes are isolated via a multicomponent reaction combining hydrated lanthanide salts with LH₂ [(E)-2-((5-bromo-2-hydroxybenzylidene) amino)-2-methylpropane-1,3-diol] in the presence of co-ligand and excess base. In the interior cavity of each lanthanide cluster encapsulated with CO_3^{2-} anions of the compound $La_6(\mu_4-CO_3)_3(\text{piv})_3(LH_2)_6Cl_2(2.1)$, $Pr_6(\mu_4-CO_3)_3(\text{piv})_3(LH_2)_6Cl_2(2.2)$ and $Nd_6(\mu_4-CO_3)_3(\text{piv})_3(LH_2)_6Cl_2$ (2.3) from the source of atmospheric CO_2 . All the structures have been characterized by single crystal X-ray diffraction and other spectral techniques. Out of all three Ln clusters, compound 2.1 has been successfully catalyzed the cycloaddition reaction of CO_2 to epoxide in solvent free condition to form cyclic carbonates.

2.1 Introduction

Much interest has been paid to high-nuclearity lanthanide clusters because of their unusual physical and chemical characteristics and their prospective applications. One of the most intriguing areas of inquiry is the chemistry of high-nuclearity lanthanide clusters. Due to their unique architecture, fascinating physical and chemical characteristics, and potential applications in a variety of fields, such as optics,¹ electronics,² catalysis³and magnetism,⁴ particularly in single-molecular magnets (SMMs) and magnetocaloric effects (MCEs),⁵ these clusters are currently generating a lot of interest.

The unique catalytic properties of these clusters, which are primarily caused by the Lewis acidic Lanthanide ions, have largely gone unrecognized despite the discovery of catalytically intriguing Ln-containing complexes,6 coordination polymers (CPs),⁷ metal-organic frameworks (MOFs), ⁸ perovskites, ⁹ and nanoparticles. ¹⁰ This is in contrast to the growing body of research on the magnetic properties of Lanthanide Oxo Clusters.

Metal salts, a ligand, and a coligand are all involved in a single pot, multi-component reaction that is well documented in the literature. ¹¹Cluster assembly is typically accomplished in lanthanide chemistry using one of two broad techniques. The first technique uses processes in an inert atmosphere to control the hydrolysis of anhydrous metal salts. According to reports in the literature, this investigation produced an intriguing molecular architecture. ¹² The reaction of hydrated Ln salt-bearing protic ligands when employing an excess base is another widely used technique. This aids in the construction of the metal oxo core, which is surrounded by ligands.

There has been long curiosity in the capture, activation and fixation, of carbon dioxide for the chemical conversion of CO₂ into various formic acids, carbonates, and other C1 feedstocks. of this work has been devoted to the introduction of ambient CO₂, most notably when a carbonate anion forms coordination complex. That reaction resulting in the various bridging modes of the CO₃²⁻ ion, is well known to be carried out by several ZnII, CuII, and NiII complexes.¹⁴

One of the primary contributors to global warming is CO₂, a stable combustion byproduct and greenhouse gas. Finding a CO₂ conversion technology that is both affordable and effective could reduce the CO₂ build-up in the environment. In this vein, the catalytic reaction of CO₂ with epoxides produces cyclic carbonates, a valuable resource for the creation of polymeric materials, and is undoubtedly one of the reactions garnering the most attention.¹⁵⁻¹⁷ An epoxide

and CO_2 are both activated in the widely accepted process. Multiple catalysts, including those based on Ln, have been developed for this purpose because Ln3+'s oxophilicity and harsh Lewis acidity are ideal for the activation of epoxide.¹⁸ Consequently, several catalysts, including those based on Ln, have been created for this reaction. This capability has also been investigated for LOCs. For example, Zhang et al. reported two series of heterometallic LOCs, namely $Ln_2Zn_2(\mu_3-OH)_2(L^1)_4(NO_3)_4$ (Ln_2Zn_2 , Ln = Eu, Tb, Er, Yb, Nd, $HL^1 = Methyl-3-methoxysalicylate$, and $Ln_2Zn_4(\mu_3-OH)_2(L^1)_4(OAc)_6(NO_3)_2$ (Ln_2Zn_4 , Ln = Tb, Nd), and studied their implementations for the CO_2 and epoxide.¹⁹

2.2 Experimental Section

2.2.1 General methods and Procedures:

All chemicals used were of analytical reagent grade and used as received without further purification. The ligand LH₂ was prepared according to the literature procedure. Lanthanum salts were prepared by neutralizing the corresponding lanthanum oxides with concentrated hydrochloric acid.

2.2.2 Instrumentation

A Nicolet iS5 FTIR spectrometer was used to record infrared spectra. An EA Series 1112 CHNS analyser from Flash was used for the elemental analysis. Compound 1 -3 single crystal X-ray data were collected at 100(2) K using a Bruker Smart Apex CCD area detector system with a graphite monochromator and (Mo-K α) = 0.71073 as the detector's metal-of-choice. For ALL the compounds, the data were reduced using CrysAlisPro 1.171.40.35a (Rigaku OD, 2018). In the Olex2 1.3-ac4 software, ²⁰ the structures were solved using SHELXT and refined using SHELXL-2018/3. Anisotropic refinement was performed on all non-hydrogen atoms. At a scan rate of 3.9° min⁻¹, X-ray diffraction patterns were gathered over the 2θ range of 5-80°. Using BaSO₄ powder as the reflectance reference, the JASCO-V-770 spectrophotometer was used to record solid-state UV-vis absorption spectra. Software called Shape v2.1 was used to calculate the shapes. Using Diamond (version 2), the crystal structure visuals were created. Anisotropic refinement was performed on all non-hydrogen atoms. A HyPix3000 diffractometer equipped with an XtaLAB Synergy, Single source at offset/far, was used to acquire the SCXRD data for 2.1 to 2.3 at 100K. With a mirror monochromator, the Rigaku Oxford HyPix3000 CCD plate detector system has (Mo K) = 0.71107. Using Olex228 as a starting point, the structure was solved using Intrinsic Phasing in the ShelXT29 structure solution program and refined using Least Squares minimization in the SHELXL 2018/3 refinement tool. The riding model was used to fix hydrogen atoms.

2.2.3 General Synthetic procedure:

Reaction of 1 equivalent of hydrated lanthanum halide and 1 equivalent of LH₂ [(E)-2-((5-bromo-2-hydroxybenzylidene) amino)-2-methylpropane-1,3-diol]²¹ in presence of excess triethylamine in methanol yielded a yellow clear solution which was evaporated and the product was collected. The solid was then dissolved in methanol and acetonitrile, left undisturbed for crystallization. Yellow block shaped crystals suitable for X-ray diffraction were formed after two days' time.

Scheme:1

Compound 2.1: LaCl₃.6H₂O (0.150 g, 0.424 mmol), LH₂ (0.120g, 0.424 mmol), pivalic acid(0.042g) Et₃N (0.156 mL, 1.696 mmol). Yield: 90%, IR: 3316, 2950, 2599, 2495, 2221 cm⁻¹.

Compound 2.2: PrCl₃.6H₂O (0.150g,0.422 mmol), LH₂ (0.121g,0.422mmol), pivalic acid (0.043g), NEt₃ 0.24ml,1.688mmol). Yield:80 %, IR:3364, 2964, 1631, 1461, 1279, 1061cm⁻¹.

Compound 2.3: NdCl₃.6H₂O (0.150g,0.598 mmol), LH₂ (0.173g,0.598mmol), pivalic acid (0.061g), NEt₃ (0.2ml, 2.392mmol). Yield: 78%, IR: 3365, 2981, 2697, 1651, 1509, 1453, 1376 and 1061 cm⁻¹.

2.3 Results and Discussion:

The synthetic process was taken from research in the literature. After the clear solution mixture evaporated, the hydrated lanthanum halides, (LH₂) ligand, pivalic acid coligand, and triethylamine interacted in methanol in a 1:1:1:4 ratio to produce the product as a yellow powder. Three iso-structured hexanuclear Ln clusters were synthesized using a controlled hydrolysis technique. The final product was examined using common spectroscopic and analytical methods. The infrared spectra of 2.1–2.3 exhibit a peak within (2850–2930) cm⁻¹ owing to weak C–H bond interaction stretching frequency and a distinctive band at around

3387 cm⁻¹ attributable to the phenolic O–H stretch after deprotonation. Additionally, a signal at 1452 cm⁻¹ in the IR spectra suggested the existence of carbonate ions in 2.1–2.3. A signal around 177 ppm is visible in the additional ¹³C NMR spectra of 2.1, which is comparable with the signal for carbonate ions seen in published publications indicating the existence of carbonate ions amid the synthetic cluster. Studying single crystal X-ray diffraction, hexanuclear lanthanide clusters [Ln₆(μ₄-CO₃)₃²-(piv)₃(LH₂)₆Cl₂] were formed. (Ln= La 2.1, Pr 2.2, Nd 2.3) demonstrating the existence of carbonate ions produced through atmospheric CO₂ fixation. Since CO₂ fixation from atmospheric moisture was serendipitous the first time around, controlled synthetic methods were adopted to incorporate CO₂ in the cluster. Hence the reaction and crystallization were carried out under a constant flow of CO₂ gas. The yield of the crystals was increased and more importantly, the crystallization time too were reduced leading to formation of hexagonal rod shape crystals in good yields.

2.3.1 Description of crystal structure:

The clusters 1-3 were defined by common analytical along with spectroscopic methods. SCXRD revealed the formation of a trigonal prismatic Ln_6 oxo cluster. Since the structure of the clusters obtained with all the three ions were isostructural, the lanthanum-based cluster is taken for structural description. In the hexanuclear cluster 1, the metal ion is present in a nine-coordinated geometry with each metal ion being bound terminally to a Schiff base ligand, three pivalate ions bound through oxygen's in a monodentate fashion and the remaining three coordination from oxygen of a carbonate ions encapsulated in the cluster by atmospheric fixation of CO_2 . It should be noted that the three such μ_4 - CO_3^{2-} are found encapsulated in the core of the hexanuclear cluster. SHAPE calculation revealed each nine coordinated La^{+3} ion is present in a coordination of 'Muffin' geometry with 'Cs' symmetry. Overall, the structure of the hexa-nuclear cluster can be explained in the following way. There are two of them Ln3 triangles capped by a μ_3 -Cl ion. The two Ln3 triangles are held together by three pivalates in [2.11] mode and three (CO_3)²⁻ ions binding in a [4.222] mode in terms of Harris notation. CO_3 A Schiff base binds to each of the CO_3 base are present in the molecular complexes.

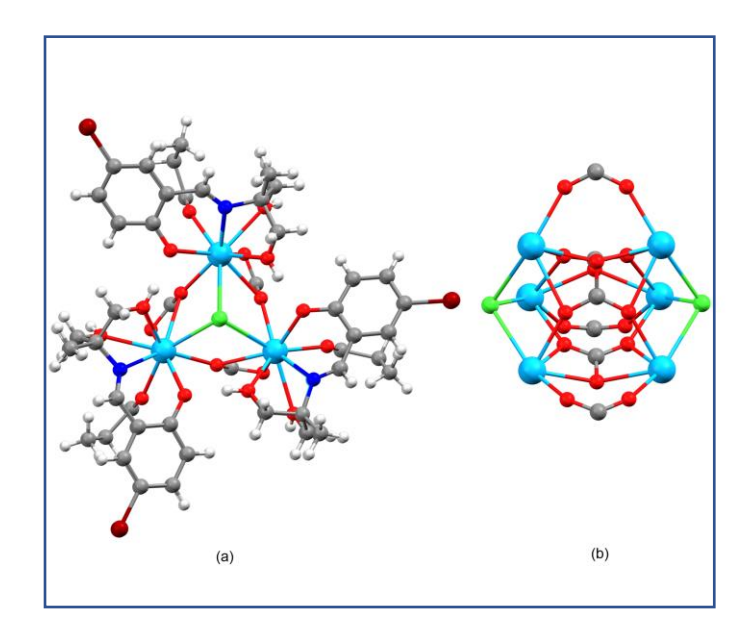


Figure 2.1. (a) Ball and stick diagram of $La_6(\mu_4\text{-CO}_3)_3(\text{piv})_3(LH_2)_6Cl_2$ (b) Core structure of La_6 cluster. Color legend; La; dodger blue, O; red, N; royal blue, Cl; green, Br; maroon, C; grey, H; white.

2.4. Catalytic activity of La₆ cluster for the cycloaddition reaction of epoxides:

Lanthanides have been previously shown to act as excellent catalysts for wide range of reactions ranging from photocatalytic reduction of CO_2 , 23 water oxidation, 24 and HER. 25 In few cases, lanthanides have also shown to serve as effective catalysts for activation of CO_2 . In all the cases, the stability of the Ln6 cluster was checked by measuring the IR spectra of the catalyst pre- and post-reaction conditions by isolating the cluster form the silica gel. In all the cases, the IR spectra revealed the structural stability of the Ln6 cluster. In this chapter we have mainly focused on Production of carbonates with cyclic rings by cyclo addition reaction of different substituted epoxides. Other small molecule activations have been discussed in the next chapter.

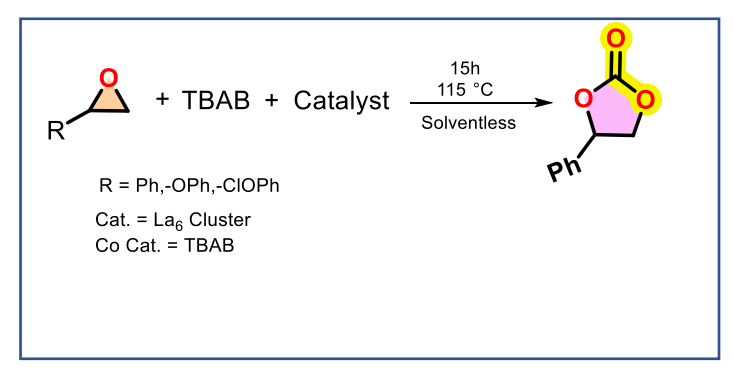
2.4. Catalytic activity of La6 cluster for the cycloaddition reaction of epoxides:

Lanthanides have been previously shown to act as excellent catalysts for wide range of reactions ranging from photocatalytic reduction of CO_2 , 23 water oxidation, 24 and HER. 25 In few cases, lanthanides have also shown to serve as effective catalysts for activation of CO_2 . In all the cases, the stability of the Ln6 cluster was checked by measuring the IR spectra of the catalyst pre- and post-reaction conditions by isolating the cluster form the silica gel. In all the cases, the IR spectra revealed the structural stability of the Ln6 cluster. In this chapter we have

mainly focused on Production of carbonates with cyclic rings by cyclo addition reaction of different substituted epoxides. Other small molecule activations have been discussed in the next chapter.

The catalytic reaction of formation of cyclic carbonate did not proceed in the absence of catalyst. The hydrated lanthanide chloride was also tested for catalytic activity under the reaction conditions employed in our reaction, no traceable product was formed in the reaction, which confirms the catalytic activity occurs only in the presence of La₆ cluster. Other two substituted epoxides have also been examined to confirm the catalytic properties of La₆ cluster.

2.4.1 Synthetic procedure for cyclic carbonates from epoxides catalysing by compound1:



Scheme: 2.2

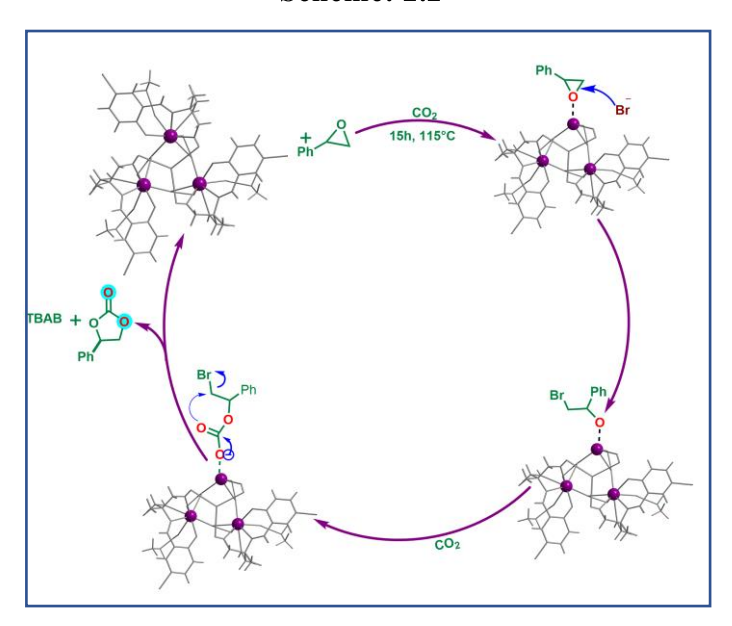


Fig 2.2 Plausible mechanism for the conversion of epoxide to cyclic carbonate in presence of La₆ catalyst.

2.4.2 Cycloaddition reaction of epoxide with CO₂

The phenyl ethylene oxide 0.5 mmol, tetra butyl ammonium bromide (TBAB) 0.025 mmol as cocatalyst, La complex 0.00136 mmol were taken in a 50 ml. round bottom flask well fitted with a two-way L- adaptor connecting CO₂ gas balloon. The CO₂ gas was in continuous flow to the reaction mixture till the completion of the reaction. The reaction mixture was heated at

(a) **4-phenyl-1,3-dioxolan-2-one**Isolated Yield: 78%, 1 H NMR (500 MHz, CDCl₃): δ 2.72 (S,1H), 3.05(t, J = 5Hz, 2H), 3.79 (s,1H), 7.26–7.31 (m, 5 H, Ph). 13 C NMR δ = 125.89, 129.25, 129.74, 135.84, 154.85 ppm. mass = 187.0373.

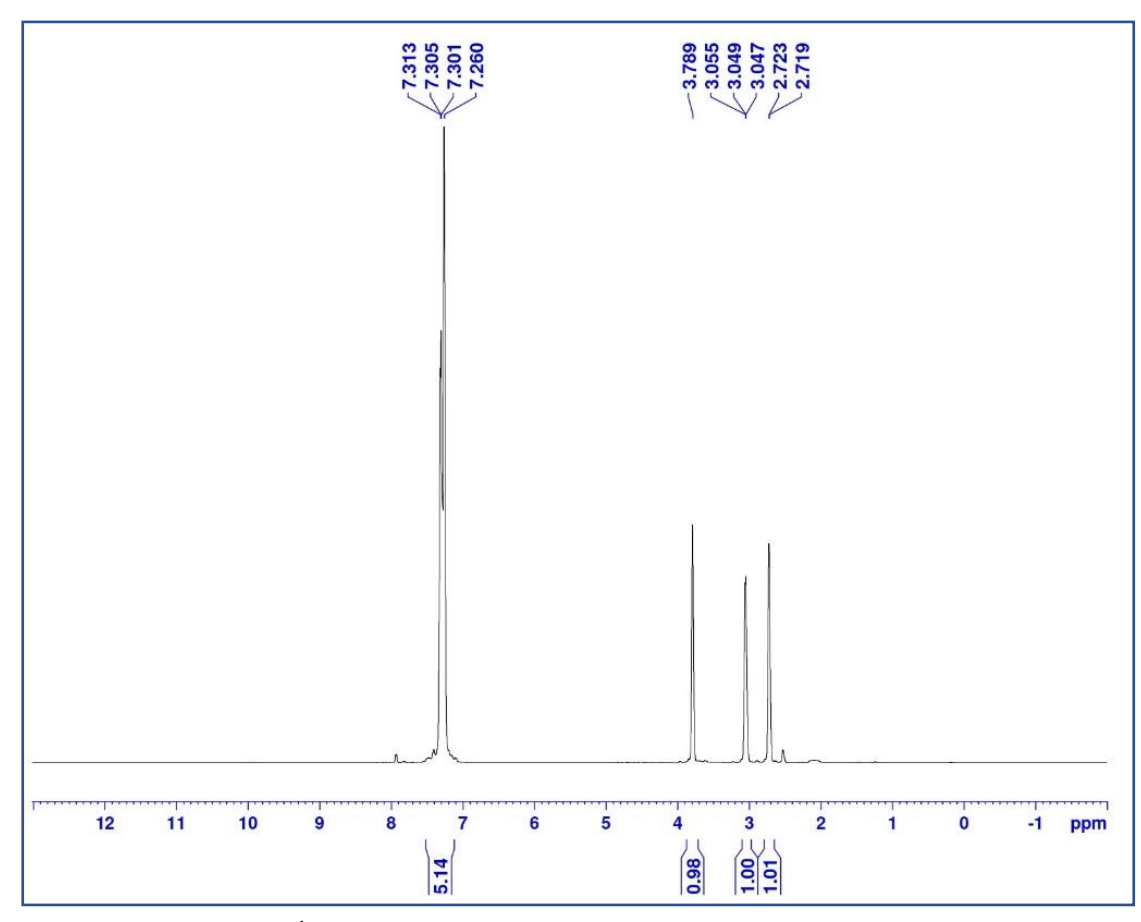


Fig 2.3 ¹H NMR spectra of 4-phenyl-1,3-dioxolan-2-one.

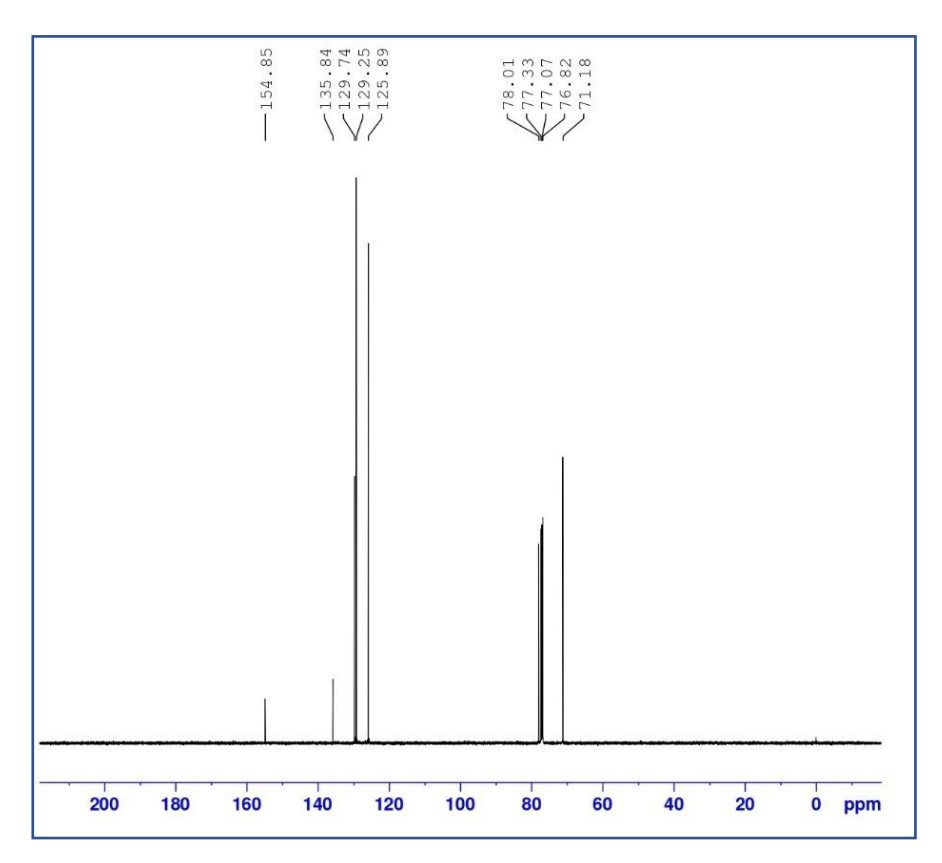


Fig 2.4 ¹³C NMR spectra of 4-phenyl-1,3-dioxolan-2-one.

2.4.3 Catalytic activity through absorption spectra:

In the below fig the absorption spectra have been recorded for the catalytic conversion of styrene oxide to cyclic carbonate in different time interval of 0h, 4h, 8h and 15h. So, at the initial it gives a sharp peak without any shoulder, then after 4h of reaction it gives one peak around 350 nm, after 8h the intensity of that particular shoulder has been decreased and finally after completion of the reaction the shoulder has been shifted towards 300 nm. Whereas carbonyl groups (C=O) shows absorption at 300 nm, which confirms the formation of cyclic carbonate since the catalyst La₆ cluster is present. Through this we can check the timely activity of the catalyst.

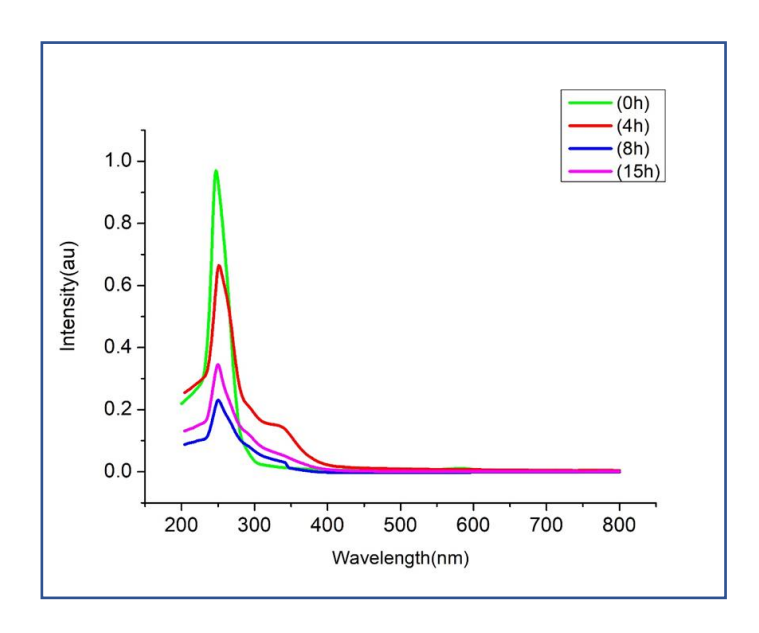


Fig 2.5 Absorption spectra for the catalytic conversion of styrene oxide to cyclic carbonate.

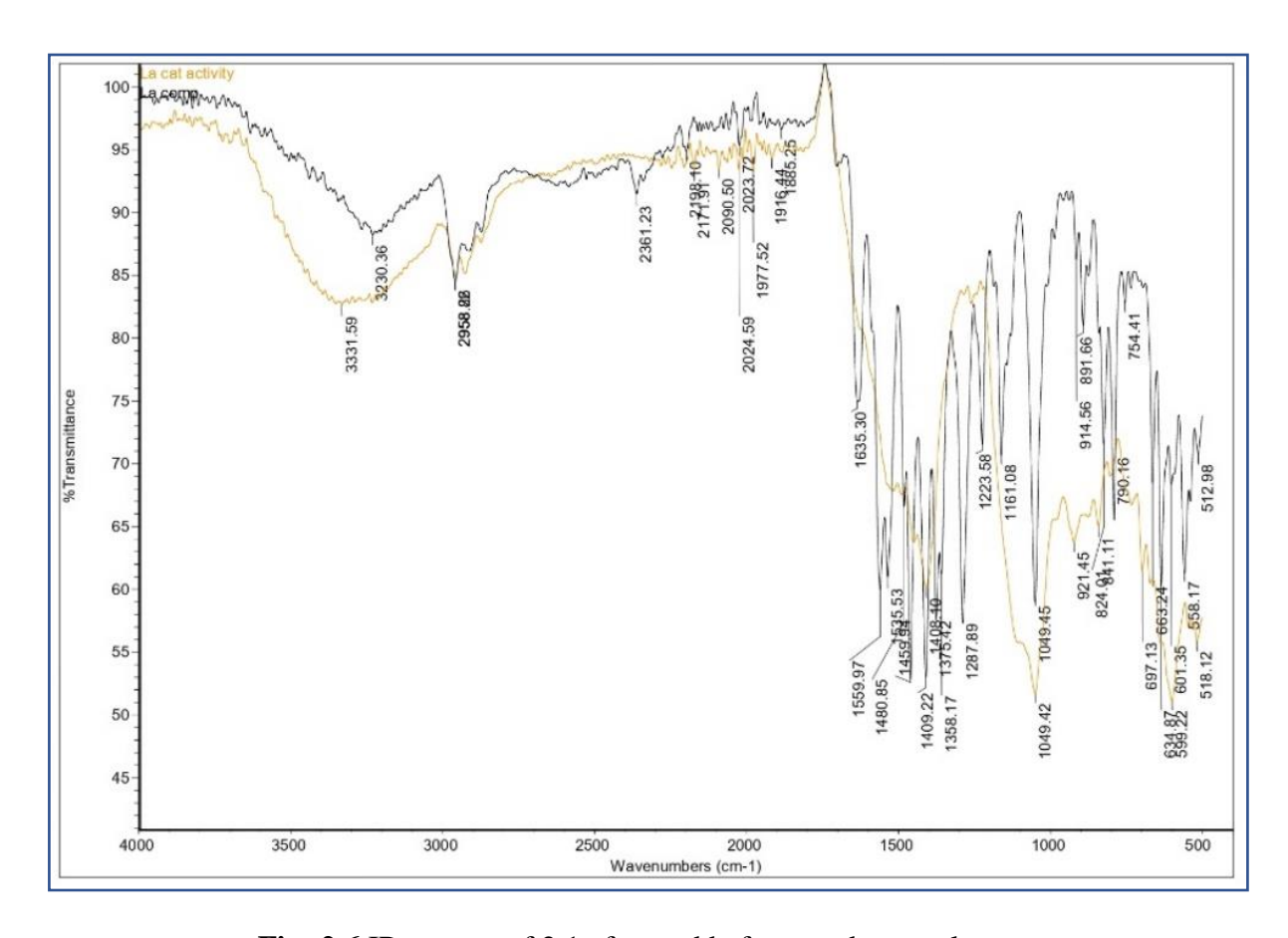


Fig: 2.6 IR spectra of 2.1 after and before used as catalyst.

2.5 Conclusion

We have synthesized three lanthanum oxo clusters Ln = La comp 2.1, Pr comp2.2, Nd comp 2.3 in room temperature condition in presence of ligand and coligand. The reaction results products of general formula [Ln₆(μ ₄-CO₃)₃²-(piv)₃(LH₂)₆Cl₂] clusters, in all these lanthanide clusters atmospheric carbon dioxide have been encapsulated serendipitously as three carbonate

ions. The carbonate anion adopts a novel bridging mode of. Out of all three lanthanide oxo clusters, we have used La₆ cluster as catalyst to activate the cycloaddition reaction of various substituted phenyl ethylene oxide and CO₂. In comparison to earlier reported works where complexes have been used as catalysts; the La₆ cluster is the novel hexa nuclear lanthanide complex for the very first time is being used as catalyst. This catalyst has efficiently inhibited the yield of the small organic molecule comparison to earlier reported transition metal complex catalysts.

References:

- (a) Tang, X. L.; Wang, W.H., Dou W.; Jiang, J., Liu, W. S.; Qin, W.W.; Zhang, G.; Zhang, H.R.; Yu K.B.; Zheng L.M. Angew. Chem. Int. Ed. 2009, 48, 3499–3502. (b) Rasamsetty, A.; Baskar, V.; Sañudo, C.E. ChemistrySelect 2016, 1, 3323–3327. (c) Arikawa, Y.; Nakamura, T.; Ogushi, S.; Eguchi, K.; Umakoshi, K. Dalton Trans., 2015, 44, 5303-5305. (d) (Gálico, D. A.; Calado, C. M. S.; Murugesu, M. Chem. Sci., 2023, 14, 5827-5841.
- (a) Dong, J.; Cui, P.; Shi, P.F.; Cheng, P.; Zhao, B. Ultrastrong alkali-resisting lanthanide-zeolites assembled by [Ln₆₀] nanocages. *J. Am. Chem. Soc.* 2015, 137, 51, 15988–15991. (b) Wang, L.; Xu, C.; Han, Q.; Tang, X.; Zhou, P.; Zhang, R.; Gao, G.; Xu, B.; Qin, W.; Liu, W. Chem. Commun. 2018, 54, 2212–2215. (c) Qin, J.; Xu, B.; Zhang, Y.; Yuan, D.; Yao, Y. Green Chem. 2016, 18, 4270–4275. (d). Fukuzumi, S.; Lee, Y.-M.; Ahn, H.S.; Nam, W. Chem. Sci. 2018, 9, 6017–6034. (e) Wu, J.; Huang, Y.; Ye, W.; Li, Y. CO₂ Adv. Sci. 2017, 4, 1700194. (f) Kojima, T. *Chem.Photo.Chem.* 2021, 5, 512–520. (g) Ouyang, T.; Huang, H.-H.; Wang, J.-W.; Zhong, D.-C.; Lu, T.-B. Angew. Chem. Int. Ed. 2017, 56, 738–743. (h) Hong, D.; Kawanishi, T.; Tsukakoshi, Y.; Kotani, H.; Ishizuka, T.; Kojima, T. J. Am. Chem. Soc. 2019, 141, 20309–20317. (i) Spennati, E.; Riani, P.; Garbarino, G. *Catalysis Today.* 2023, 418,114131.
- 3. (a)Rinehart, J. D.; Long, J. R. Exploiting single-ion anisotropy in the design of f-element single-molecule magnets. *Chem. Sci.*, 2011,2, 2078-2085. (b)Lis, T. Acta Crystallogr. Sect. B Struct. Crystallogr. Cryst. Chem. 1980, 36, 2042–2046. (c) Sessoli, R.; Tsai, H. L.; Schake, A. R.; Wang, S.; Vincent, J. B.; Foiling, K.; Gatteschi, D.; Christou, G.; Hendrickson, D. N. J. Am. Chem. Soc. 1993, 115, 1804–1816. (d) Caneschi, A.; Gatteschi, D; Sessoli, R.; Barra, A. L.; Brunel, L. C.; Guillot, M. J. Am. Chem. Soc. 1991, 113, 5873–5874. (e) Sessoli, R.; Gatteschi, D.; Caneschi, A.; Novak, M.A. Magnetic bistability in a metal ion cluster. Nature 1993, 365, 141-143. (f)Friedman, J. R.; Sarachik, M. P.; Tejada, J.; Ziolo, R. Phys. Rev. Lett. 1996, 76, 3830–3833. (g) Thomas, L.; Lionti, F.; Ballou, R.; Gatteschi, D.; Sessoli, R.; Barbara, B. Nature 1996, 383, 145-147. (h) Ishikawa, N.; Sugita, M.; Ishikawa, T.; Koshihara, S. Y.; Kaizu, Y. J. Am. Chem. Soc. 2003, 125, 8694–8695.
- (a) Warburg, E. Ann. Phys (Leipzig), 1881, 13, 141. (b) Pecharsky, V. K.; Gschneider, Jr. K. A. J. Magn. Magn. Mater. 1999, 200, 44. (c) Gschneider, Jr., K. A.; Pecharsky, V. K. J. Appl. Phys. 1999, 85, 5365

- 5. Arnold, P.L.; McMullon, M.W.; Rieb, J.; Kühn, F.E. *Angew. Chem. Int. Ed.* **2015**, 54, 82–100.
- 6. Aguirre-Díaz, L.M.; Snejko, N.; Iglesias, M.; Sánchez, F.; Gutiérrez-Puebla, E.; Monge, M.Á. *Inorg. Chem.* **2018**, 57, 6883–6892
- 7. Alzamly, A.; Bakiro, M.; Hussein Ahmed, S.; Alnaqbi, M.A.; Nguyen, H.L. Coord. *Chem. Rev.* **2020**, 425, 213543.
- 8. Chen, X.; Xu, J.; Xu, Y.; Luo, F.; Du, Y. *Inorg. Chem. Front.* **2019**, 6, 2226–2238.
- 9. Trovarelli, A. Catal. Rev. **1996**, 38, 439–520
- 10. Baghan, S.H.; Mirzaei, M.; Hosseini, H.E.; Zadsirjan, V.; Heravi, M.M.; Mague, J.T. *Appl. Organomet. Chem.* **2020**, 34, 1–23.
- 11. Petrus, R.; Chomiak, K.; Utko, J.; Bienko, A.; Lis, T.; Sobota, P. *Inorg. Chem.* **2020**, 59 16545–16556.
- (a) Palmer, D. A.; Eldik, R. V. *Chem. Rev.* 1983, 83, 651; (b) Leitner, W. *Coord. Chem. Rev.* 1996, 153, 257; (c) Yin, X. L.; Moss, J. R. *Coord. Chem. Rev.* 1999, 181, 27; (d) Amico, D. B. D.; Calderazzo, F.; Labella, L.; Marchetti, F.; Pampaloni, G. *Chem. Rev.* 2003, 103, 3857.
- 13. (a) Mulkapuri, S.; Kurapati, S. K.; Das, S. K. Carbonate encapsulation from dissolved atmospheric CO₂ into a polyoxovanadate capsule. *Dalton Trans.*, 2019, 48, 8773–8781.
 (b) Nath, J. K.; Ritupan B. A lanthanide cluster formed by fixing atmospheric CO₂ to carbonate: a molecular magnetic refrigerant and photoluminescent material. *J. Chem. Sci.* 2023,135, 58, 10.
- 14. Thammakan, S.; Kuwamura, N.; Chiangraeng, N.; Nimmanpipug, P.; Konno, T.; Rujiwatra, A. Highly disordering nanoporous frameworks of lanthanide-dicarboxylates for catalysis of CO₂ cycloaddition with epoxides. *J. Solid State Chem.*, **2021**, 303,122464.
- 15. Sodpiban, O.; Gobbo, S. D.; Barman, S.; Aomchad, V.; Kidkhunthod, P.; Chikh, S. O.; Poater, A.; D'Elia, V.; Basset, J. M. Synthesis of well-defined yttrium-based Lewis acids by capturing a reaction intermediate and catalytic application for cycloaddition of CO₂ to epoxides under atmospheric pressure. *Catal. Sci. Technol.*, **2019**, 9, 6152–6165.
- 16. Kathalikkattil, A. C.; Babu, R.; Tharun, J.; Roshan, R.; Park, D.W. Advancements in the Conversion of Carbon Dioxide to Cyclic Carbonates Using Metal Organic Frameworks as Catalysts. *Catal Surv Asia.*, **2015**, 19, 223–235.
- 17. (a) Chemical fixation and conversion of CO₂ into cyclic and cage-type metal carbonates. Brzostek, K. S.; Terlecki, M.; Sokołowski, K.; Lewinski, J. *Coord. Chem. Rev.*, **2017**, 334, 199–231. (b) Kim, H.; Moon, H. S.; Sohail, M.; Yoon, Y. N.; Shah, S. F. A.; Yim, K.; Moon, J. H.; Park, Y. C. Synthesis of cyclic carbonate by CO₂ fixation to epoxides using interpenetrated MOF-5/n-Bu₄NBr. *J Mater Sci.* **2019**, 54, 11796–11803.
- 18. Guo, L.; Lamb, K. J.; Nort, M. Recent developments in organocatalysed transformations of epoxides and carbon dioxide into cyclic carbonates. *Green Chem.*, **2021**, 23, 77.

Spectroscopic Data

 Table 2.1 Crystal data and structure refinement parameters for 2.1-2.3

	2.1	2.2	2.3
Formula	C ₈₁ H ₉₉ Br ₆ Cl ₂ La ₆ N ₆ O ₃₃	Br ₆ C ₈₁ Cl ₂ N ₆ O ₃₃ Pr ₆	C ₈₇ H ₉₉ Br ₆ Cl ₂ N ₆ Nd ₆ O ₃₃
Formula weight	3068.48	2980.69	3064.06
Temp (K)	100.0	297.89	300(1)
Crystal system	Hexagonal	hexagonal	hexagonal
Space group	P6 ₃ /m	P6 ₃ /m	P6 ₃ /m
Crystal size (mm)	0.8 × 0.6 × 0.4	0.8 × 0.6 × 0.4	0.6 × 0.4 × 0.2
a (Å)	17.745(3)	17.7938(3)	17.7781(4)
b (Å)	17.745(3)	17.7938(3)	17.7781(4)
c (Å)	25.834(5)	25.6079(6)	25.4527(6)
α (deg)	90	90	90
β (deg)	90	90	90
γ (deg)	120	120	120
V(ų)	7045(2)	7021.7(3)	6966.8(4)
Z	2	2	2
ρ _{calc} g/cm ³	1.447	1.430	1.461
μ/mm ⁻¹	3.576	3.843	3.986
F (000)	2954.0	2822.0	2858.0
Radiation	ΜοΚα (λ = 0.71073)	Μο Κα (λ = 0.71073)	Mo Kα (λ = 0.71073)
20 range for data collection/°	3.084 to 52.88	4.136 to 53.974	4.152 to 54.03
Reflections collected	243232	56287	55332
alndex ranges	-22 ≤ h ≤ 22, -22 ≤ k ≤ 22,	-22 ≤ h ≤ 22, -22 ≤ k ≤	-19 ≤ h ≤ 21, -22 ≤ k ≤ 22,
	-32 ≤ I ≤ 32	22, -32 ≤ l ≤ 31	-31 ≤ l ≤ 32
Independent reflections	4960	5078	5033
Data/restraints/parameters	4960/6/216	5078/0/214	5033/6/231
Goodness-of-fit on F2	1.047	1.053	1.126
R_1/wR_2 (I>2 σ (I))	R1 = 0.0389, wR2 = 0.1076	R1 = 0.0531, wR2 = 0.1804	R1 = 0.0374, wR2 = 0.1091

R ₁ /wR ₂ (all data)	R1 = 0.0418, wR2 =	R1 = 0.0788, wR2 =	R1 = 0.0556, wR2 =
	0.1105	0.1960	0.1144
largest diff peak/hole,e Å-3	1.94/-1.89	1.83/-0.69	1.15/-0.58

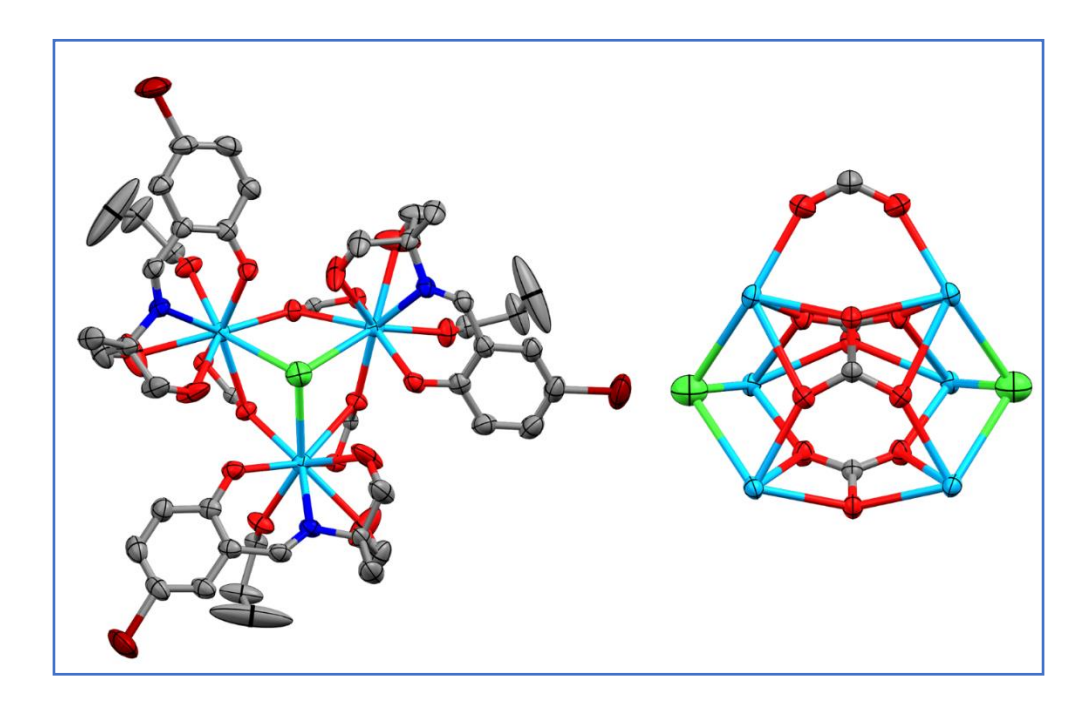


Fig 2.7 (a) ORTEP diagram of [$La_6(\mu_4\text{-CO}_3)_3(\text{piv})_3(LH_2)6\text{Cl}_2$] (b) Core structure of the same, showed with 50% probability; Color legend: dodger blue; La metal ion, grey; carbon, red; oxygen, royal blue; nitrogen, green; chlorine, maroon; bromine and hydrogen atoms have been omitted in this model for clarity purposes.

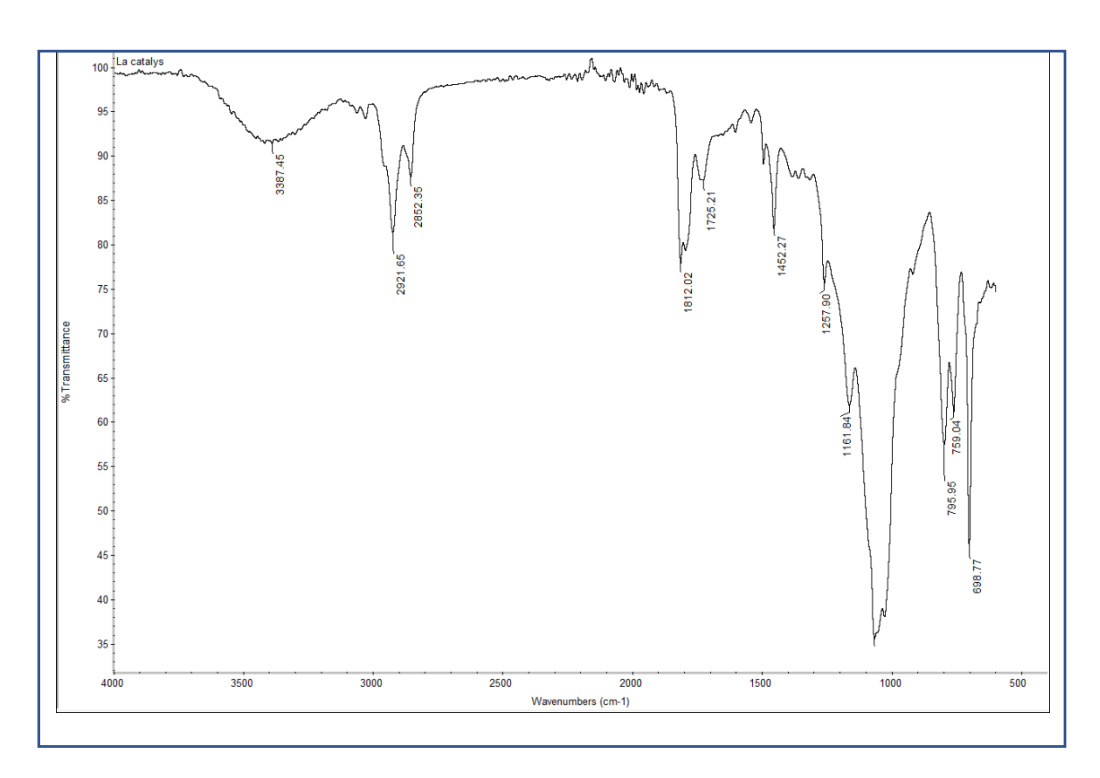


Fig 2.8 IR spectra of 2.1

 $\textbf{Table 2.2} \ \textbf{Important bond length (Å) and bond angle (deg) parameter of compound 2.1}$

O(2) La(1) Cl(1)	132.74(14)	La(1) Cl(1)	2.9690(14)
O(2) La(1) O(3)	90.51(14)	La(1) O(3)	2.683(3)
O(2) La(1) N(1)	60.45(11)	La(1) O(4)	2.428(3)
O(2) La(1) C(12)	83.07(13)	La(1) O(5)	2.5202(16)
O(4) La(1) O(2)	124.51(13)	La(1) O(6)	2.423(3)
O(6) La(1) O(2)	77.81(17)	La(1) O(2)	2.610(4)
O(5) La(1) O(2)	68.85(12)	La(1) C(12)	2.985(3)
O(1) La(1) O(2)	65.59(19)	La(1) N(1)	2.682(3)
O(1) La(1) N(1)	61.32(11)	La(1) O(1)	2.519(4)

Table 2.3 Data for shape analysis of 2.1

S.No.	Geometry	Cshm value for La1
1	Enneagon (D9h)	33.724
2	Octagonal pyramid (C8v)	23.120
3	Heptagonal bipyramid (D7h)	17.746
4	Johnson triangular cupola J3 (C3v)	13.553
5	Capped cube J8 (C4v)	10.870
6	Spherical-relaxed capped cube (C4v)	9.954
7	Capped square antiprism J10 (C4v)	2.982

8	Spherical capped square antiprism (C4v)	1.908
9	Tricapped trigonal prism J51 (D3h)	3.854
10	Spherical tricapped trigonal prism (D3h)	2.679
11	Tridiminished icosahedron J63 (C3v)	11.230
12	Hula-hoop (C2v)	9.611
13	Muffin (Cs)	1.571

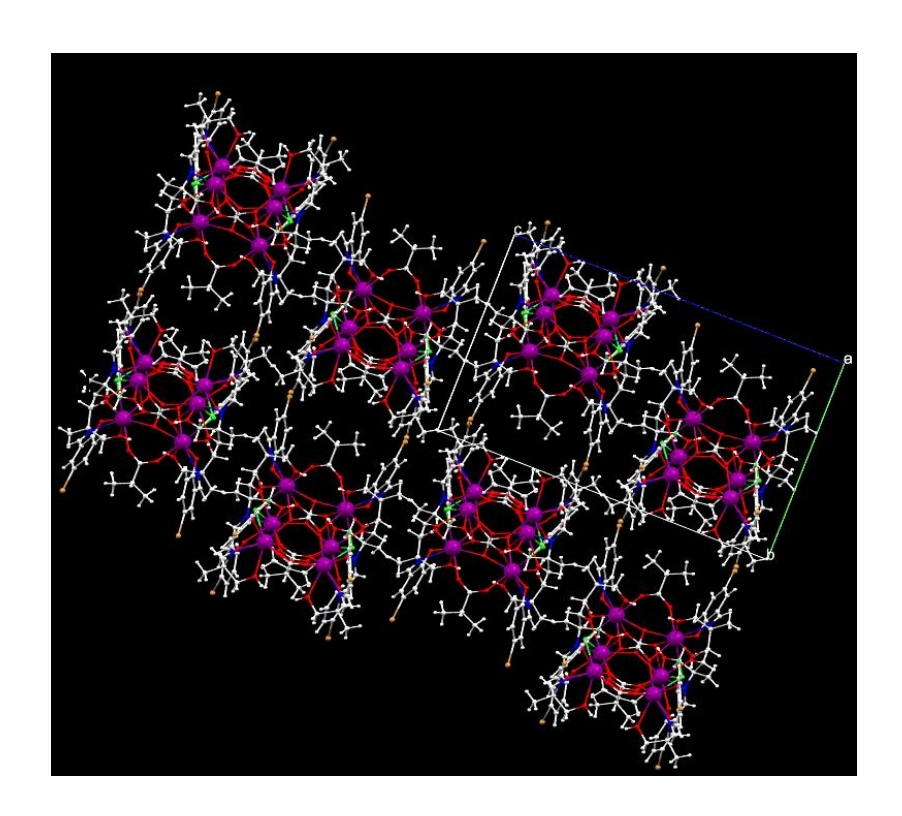


Fig 2.9 Packing diagram array of compound 2.1

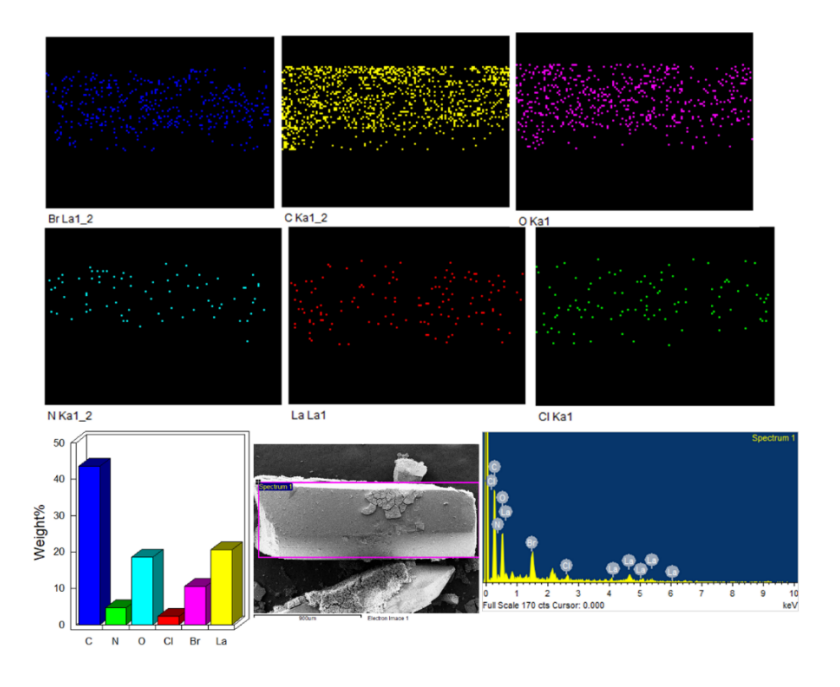


Fig 2.10 Elemental mapping of compound 2.1

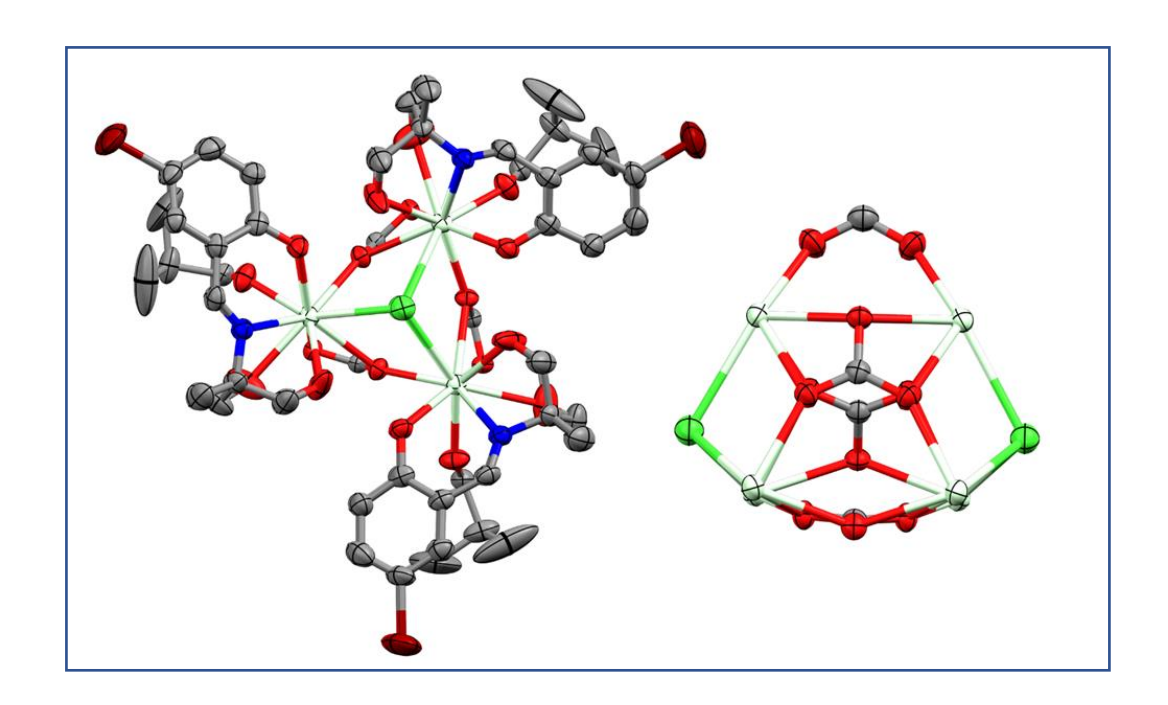


Fig 2.11 (a): ORTEP model of compound 2(Ln = Pr) (b) Core structure of complex 2.2. Color legend: red; oxygen, tea green; Pr, blue; nitrogen, green; chlorine, grey; carbon, maroon; bromine, hydrogen atoms have been omitted in OTEP model for clarity purpose.

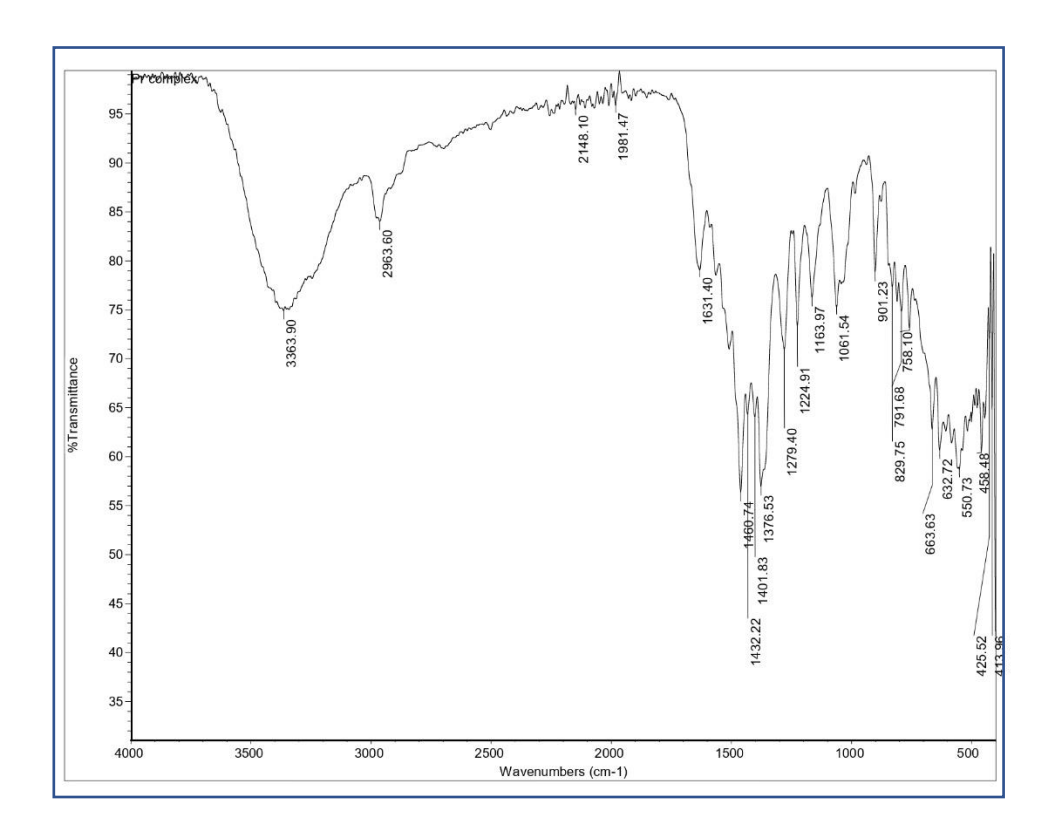


Fig 2.12 IR spectra of 2.2

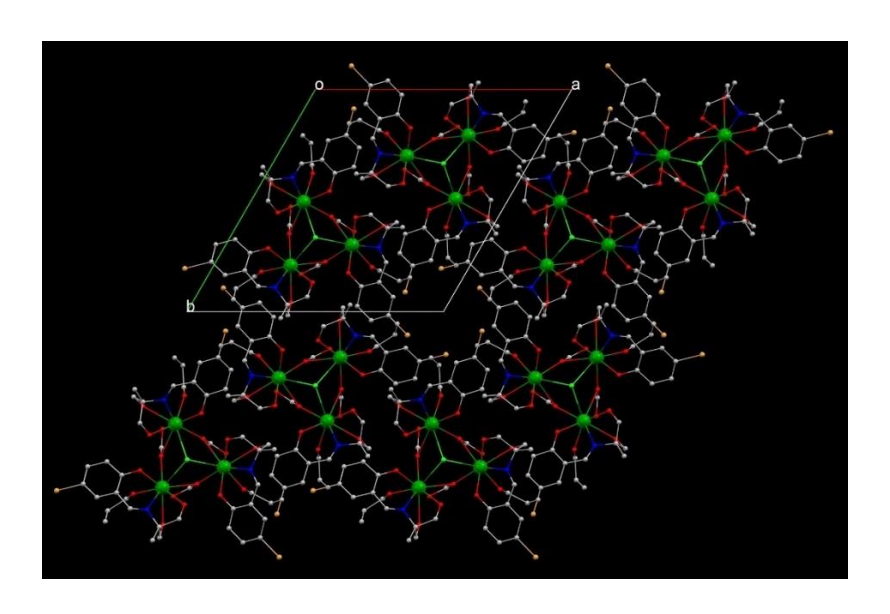


Fig 2.13 Packing diagram array of compound 2.2

 $\begin{tabular}{ll} \textbf{Table 2.4:} Important bond length (Å) and bond angle (deg) parameter of compound 2.2; Ln = \\ Pr \end{tabular}$

Pr1-Cl1	2.982(2)	O3-C15	1.301(13)
Pr1-O41	2.480(5)	O5-C4	1.325(10)
Pr1-O4	2.681(6)	O2-C14	1.251(8)
Pr1-O3	2.466(3)	O4-Pr1-Cl1	68.22(13)
Pr1-05	2.376(6)	O41-Pr1-Cl1	70.67(14)
Pr1-O2	2.385(6)	O41-Pr1-O4	75.5(3)
Pr1-C15	2.964(7)	O41-Pr1-	70.9(2)
Pr1-O1	2.581(8)	O4-Pr1-C15	25.5(2)
Pr1-N1	2.632(7)	041-Pr1-01	145.4(2)
Pr1-06	2.476(7)	O41-Pr1-N1	145.6(2)
Br1-C1	1.915(9)	O3-Pr1-Cl1	116.18(18)
O4-C15	1.275(7)	O3-Pr1-O41	78.3(2)
O3-C15	1.301(13)	O3-Pr1-O4	50.4(2)
O5-C4	1.325(10)	O3-Pr1-C15	25.7(2)
O2-C14	1.251(8)	O3-Pr1-O1	69.0(3)
O1-C10	1.445(13)	O3-Pr1-N1	129.3(2)
Pr1-Cl1	2.982(2)	O3-Pr1-O6	106.3(3
Pr1-O41	2.480(5)	O5-Pr1-Cl1	76.84(15)
Pr1-O4	2.681(6)	O5-Pr1-O41	78.0(2)
Pr1-O3	2.466(3)	O5-Pr1-O4	141.41(19)
Pr1-05	2.376(6)	O5-Pr1-O3	146.7(2)
Pr1-O2	2.385(6)	O5-Pr1-O2	79.3(2)
Pr1-C15	2.964(7)	O5-Pr1-C15	148.9(3)
Pr1-O1	2.581(8)	O5-Pr1-O1	125.5(2)
Pr1-N1	2.632(7)	O5-Pr1-N1	68.0(2)
Pr1-06	2.476(7)	O5-Pr1-O6	107.0(3)

Br1-C1	1.915(9)	O5-Pr1-Cl1	76.84(15)
O4-C15	1.275(7)	O5-Pr1-O41	78.0(2)
O5-Pr1-O2	79.3(2)	O5-Pr1-O4	141.41(19)
O5-Pr1-O3	146.7(2)		

Table 2.5: Shape analysis data for compound 2.2, Ln = Pr complex;

Sl.No.	Geometry	Cshm value for La
1	Enneagon (D9h)	34.330
2	Octagonal pyramid (C8v)	23.035
3	Heptagonal bipyramid (D7h)	17.999
4	Johnson triangular cupola J3 (C3v)	13.940
5	Capped cube J8 (C4v)	11.204
6	Spherical-relaxed capped cube (C4v)	10.430
7	Capped square antiprism J10 (C4v)	3.100
8	Spherical capped square antiprism (C4v)	1.951
9	Tricapped trigonal prism J51 (D3h)	4.083
10	Spherical tricapped trigonal prism (D3h)	2.463
11	Tridiminished icosahedron J63 (C3v)	11.239
12	Hula-hoop (C2v)	9.773
13	Muffin (Cs)	1.608

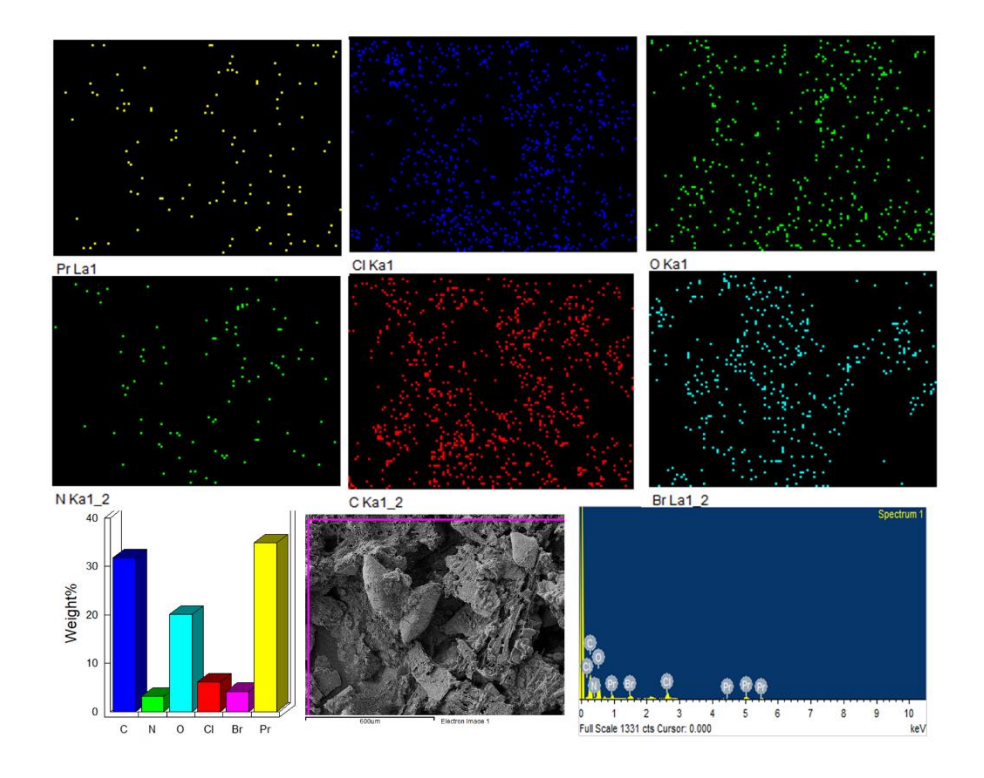


Fig 2.14 Elemental mapping of compound 2.2

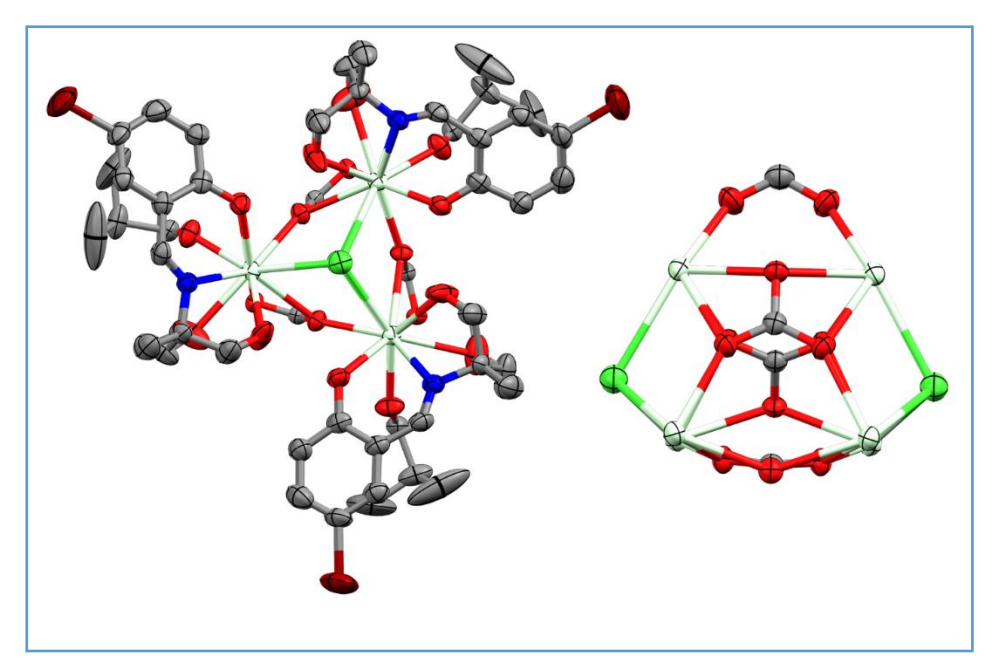


Fig 2.15 (a): Ortep model of compound 2.3(Ln = Nd) (b) Core structure of complex 2. Color legend: red; oxygen, tea green; Nd, blue; nitrogen, green; chlorine, grey; carbon, maroon; bromine, hydrogen atoms have been omitted in ortep model.

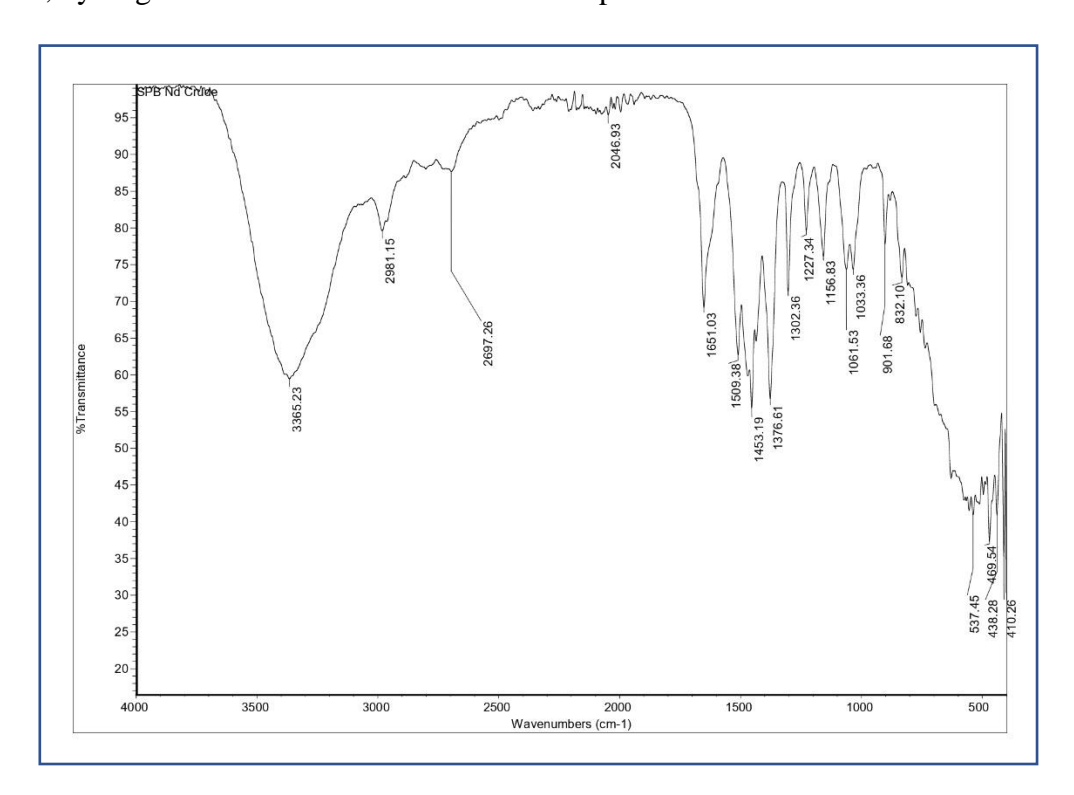


Fig 2.16 IR spectra 2.3

Table 2.6: Important bond length (Å) and bond angle (deg) parameter of compound 2.3; Ln = Nd;

Nd1-Cl1	2.9735(11)	O2-Nd1-Cl1	67.95(7)
Nd1-O2	2.666(3)	O21-Nd1-Cl1	70.36(8)
Nd1-O21	2.467(3)	O21-Nd1-O2	75.35(15)
Nd1-O3	2.4489(18)	O2-Nd1-C13	25.62(12)
Nd1-O1	2.371(3)	O21-Nd1-	70.92(14)
Nd1-O5	2.366(4)	O21-Nd1-O4	145.43(12)
Nd1-C13	2.948(4)	O21-Nd1-N1	145.52(12)
Nd1-O4	2.555(4)	O3-Nd1-Cl1	116.24(11)
Nd1-N1	2.620(4)	O3-Nd1-O21	78.44(13)
Nd1-O6	2.443(4)	O3-Nd1-O2	50.73(12)
Br1-C5	1.905(6)	O3-Nd1-C13	25.86(14)
O2-C13	1.275(4)	O2-Nd1-Cl1	67.95(7)
O3-C13	1.302(8)	O21-Nd1-Cl1	70.36(8)
O1-C2	1.315(6)	O21-Nd1-O2	75.35(15)
O5-C14	1.263(5)	O2-Nd1-C13	25.62(12)
O4-C11	1.413(7)	O21-Nd1-	70.92(14)
N1-C8	1.285(6)	O21-Nd1-O4	145.43(12)
O3-Nd1-O21	78.44(13)	O21-Nd1-N1	145.52(12)
O3-Nd1-O2	50.73(12)	O3-Nd1-Cl1	116.24(11)

Table 2.7 Shape analysis data for compound 3, Ln = Nd complex;

SI no	Geometry	Cshm value
1	Enneagon D9h	40.193
2	Octagonal pyramid C8v	32.341
3	Heptagonal bipyramid D7h	31.291
4	Johnson triangular cupola J3 C3v	22.091
5	Capped cube J8 C4v	27.665
6	Spherical-relaxed capped cube C4v	27.093
7	Capped square antiprism J10 C4v	22.263
8	Spherical capped square antiprism	21.806
9	Tricapped trigonal prism J51 D3h	20.936
10	Spherical tricapped trigonal prism	22.337
11	Tridiminished icosahedron J63	29.505
12	Hula-hoop C2v	26.753
13	Muffin Cs	21.603

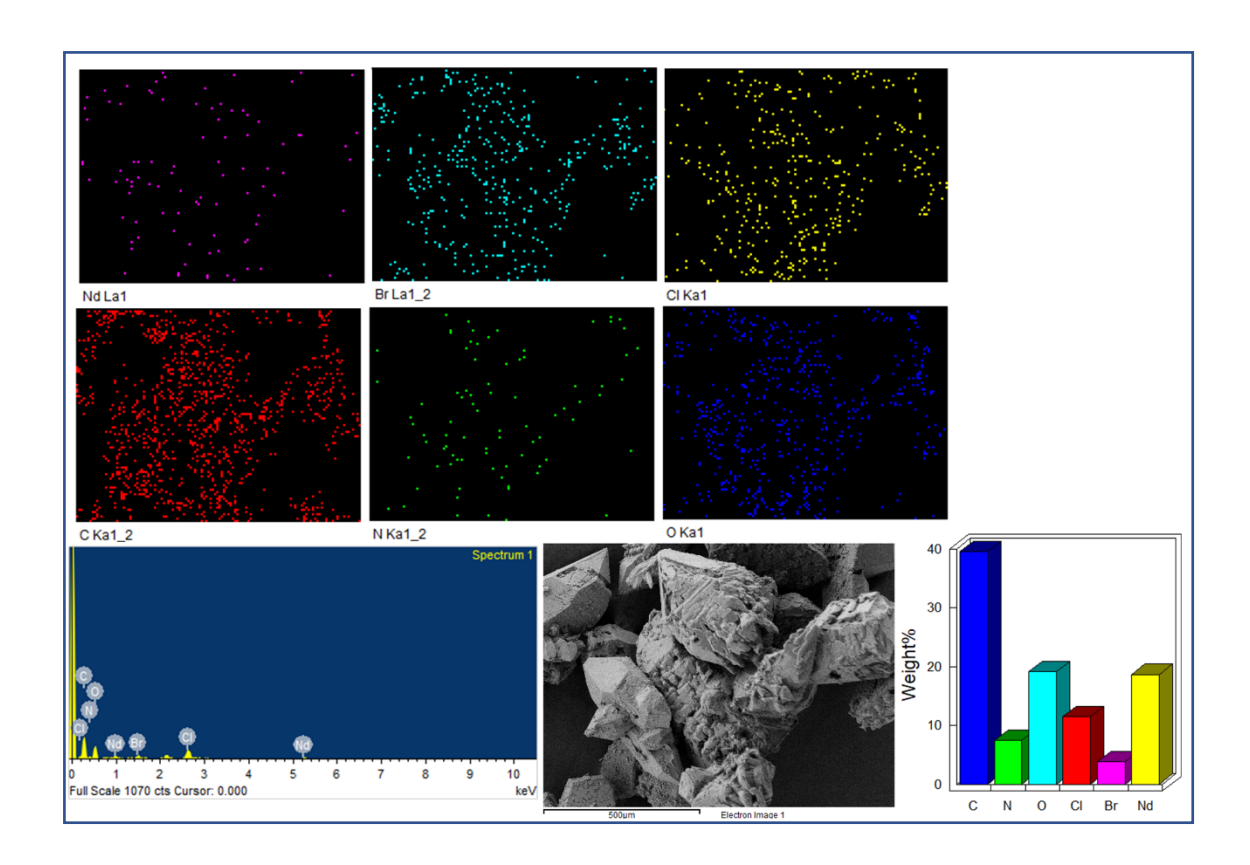


Fig 2.17: Elemental mapping of compound 2.3

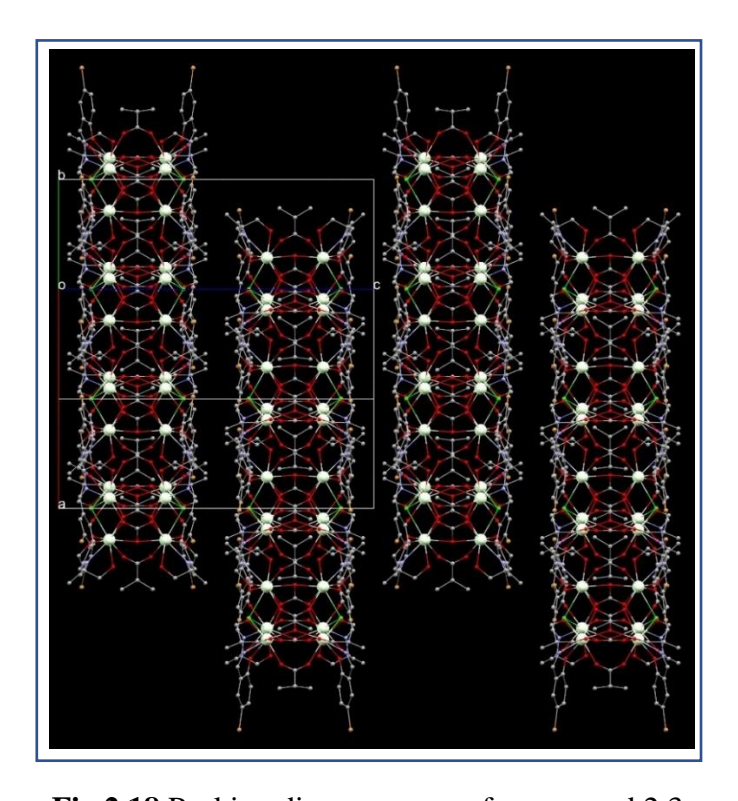


Fig 2.18 Packing diagram array of compound 2.3.

Activation of Small Molecules via Lewis acidic Hexanuclear La₆ Oxo

Topical research focuses on the activation of small molecules, including CO₂, CS₂, S₈, H₂S, C₆H₅SH and *n*-tosylaziridine to synthesize value added compounds. Here, the solitary conversion of the aforementioned molecule in the presence of phenylethylene oxide has been carried out under well-controlled reaction conditions using a Ln6 oxo cluster as a catalytic device. The activation of phenyl ethylene oxide ring opening reaction in the presence of various substituted amines establishes the improved Lewis acid and Ln₆ cluster's flexibility. Through the activation process involving H₂S and S₈ in the presence of phenyl ethylene oxide, a new cyclic phenyl-dihydro oxadithiole with a skeletal form inside the cyclic group has been isolated. It is interesting to note that the Lewis acidic cluster contains activated inert substituents that can be found in solid (S₈), liquid (CS₂), or gaseous (H₂S) form.

3.1 Introduction:

Activation of small molecules leading to the formation of value-added products has been an area of immense interest in recent years since they are important in converting environmentally toxic chemicals to useful molecules. The catalytic conversion of CO₂ to cyclic or polycarbonate, formic acid, and products of commercial interest has been investigated in detail, and several catalytic systems based on transition metals or lanthanides have been employed for this purpose. Particularly of interest is the report of Arikawa et al., who have isolated a Ru pincer complex encapsulating atmospheric CO₂ as a carbonate ion. By reacting the Ru complex with a methylating reagent, the absorbed carbonate has been released as products like carbonates, formic acid, and other C1 feedstock. Recently, using [Ln₆₀] nanocage, ring-opening of epoxides has been carried out. Parallelly, activation of other small molecules like CS₂, S₈, and H₂S has also been carried out, leading to the formation of functionalized molecular systems.1 It should be mentioned here that several metal complexes based on transition metals, lanthanide, and main group metal ions are well known for the activation of CO2.2 However, very few catalytic systems have been investigated for activation of small molecules like CS₂, S₈, and H₂S and in particular a single catalytic system activation of these small molecules is unknown. Organosulfur compounds are useful for a wide range of applications such as in agrochemistry, organo biochemistry, and also as components for rechargeable lithium batteries, and often CS₂ is a by-product in the manufacturing processes. For example, CS₂ is produced as a by-product while manufacturing viscose fibers and cellophane films.³ Since CS₂ has a low boiling point, it gets released in air, where it is converted to SO₂ and COS in the presence of oxygen. These two forms of sulfur are toxic to the environment. Hence, it is important to find methodologies to convert CS2 molecules to various value-added products like activation to form cyclic thiocarbonates.

The first example was reported in 1969 by Jones and coworkers using thiophosgene with lead (II) monoacetate with 2-mercaptoethanol to form thiocarbonate.⁴ Later, a few research groups explored the synthesis of cyclic thiocarbonate by using various sulfur sources in the presence of a base.⁵ Reactions of CS₂ with epoxides in the presence of bases have been investigated, and the cyclic products isolated were in relatively low yields. Recently, 2,3-epoxy alcohols have been synthesized from trans epoxy alcohols with the migration of xanthate group. Apart from all these stoichiometric approaches, Endo and coworkers developed the catalytic system based on alkali metal halides to selectively form 1,3-oxathiolane-2-thiones from epoxides and CS₂ in the presence of LiBr and THF.⁶ The group also explored the synthesis of

different functionalized thiocarbonates wherein protection/deprotection of the alkoxide group was involved as the direct reaction led to some failed experiments.⁷

Though there are several catalytic systems which catalyze the conversion of CO₂ to cyclic carbonates, conversion of CS₂ to cyclic thiocarbonates is less investigated. Herein, we report the synthesis and characterization of CO₂ inserted Ln₆ based molecular cluster and its versatile catalytic activity for activation of small molecules like CO₂, CS₂, ⁸ S₈, H₂S, and thiol. Further, the catalyst has also been examined for the formation of β-amino alcohols⁹ in solvent-free ring-opening reactions of phenyl ethylene oxide with various aliphatic and aromatic amines, including amino alcohol. Very recently, *N*-substituted aziridine¹⁰ was used for the synthesis of β-amino acids by the reaction with CO₂ in the presence of Nickel catalysts. Our catalyst was found to be versatile and can be used for several nucleophilic ring-opening and substitution reactions, and we demonstrated some of those applications. DFT studies were performed to understand the atomic-level mechanisms of the conversion.

3.2 Experimental Section

3.2.1 General Information

All the reactions were carried out in ambient condition and monitored by thin layer chromatography (TLC) using silica gel GF_{254} plates with detection by charring with 5% (v/v) H_2SO_4 in methanol or by phosphomolybdic acid (PMA) stain or by ultra violet (UV) detection.

Solvents used in the reactions were distilled over dehydrated agents. Silica-gel (100-200 mesh) was used for column chromatography. All NMR spectra were recorded on Bruker 400 MHz and 500 MHz spectrometer in CDCl₃. 1 H NMR chemical shifts were reported in ppm (δ) with TMS as internal standard (δ 0.00) and 13 C NMR were reported in chemical shifts with solvent reference (CDCl₃, δ 77.00).

3.2.2 General Synthetic procedure:

In a solvent-less condition the phenyl ethylene oxide 0.5 mmol, tetra butyl ammonium bromide 0.025 mmol which we are using as cocatalyst, La complex 0.00136 mmol as catalyst and 0.26 mmol starting material will be stirred together at various temperatures depending upon various starting materials. All the reactions carried out at 115°C using oil bath. After complete conversion of starting material crude product which was purified over basic alumina using hexane and ethyl acetate to obtain cyclic dihydro oxadithiole.

(a) Cycloaddition reaction of epoxide with CS2, H2S, S8, Thiophenol

The phenyl ethylene oxide 0.5 mmol, tetra butyl ammonium bromide 0.025 mmol, La complex 0.00136 mmol and 0.26 mmol of CS₂ were taken and stirred for 15 h at a temperature of 115 °C. After completion of the reaction, the temperature was brought down to room temperature. The product was purified by column chromatography.

In case of both H₂S and S₈ the reaction started with the same amount of phenyl ethylene oxide catalyst and cocatalyst but in case of S₈, 0.26 mmol of elemental Sulphur powder was added and the reaction was carried out for 24 hours at a temperature of 115 °C, and completion of the reaction was being monitored by thin layered chromatography. After cooling down to room temperature the crude product was purified by column chromatography in ethylactetate/hexane. The product was confirmed by NMR HRMS and IR spectroscopy.

In the case of H₂S after same amount of catalyst cocatalyst and styrene oxide was taken in a two-neck round bottom flask, H₂S gas was passed, and the reaction was carried out for 3 hours at 115 °C. After complete conversion of the reactant to product the product was purified through column chromatography in ethylactetate/hexane and spectroscopically characterized.

For thiophenol also same procedure has been followed as in the case of S_8 , but the reaction completed in a period of 15 h time.

(b) Cycloaddition reaction of amines:

Different kinds of amines, such as Primary amine, secondary amine, ethanol amine, potassium pthalamide, morpholine, pyrrolidine, piperidine, and aziridine all have been taken in 0.26 mmol along with the same amount of styrene oxide, catalyst, and cocatalyst as afore mentioned for other reactions. The completion of the reaction and purification has been done in same procedure as mentioned before for other reactions.

3.2.3 Spectral Data

(a) 5-phenyl-1,3-oxathiolane-2-thione

¹H NMR (500MHz, CDCl₃) δ = 4.03 (1 H, dd, ²J = 12.0 Hz, ³J = 5.7 Hz), 4.17 (1 H, dd, ²J = 12.0 Hz, ³J = 11.8 Hz), 5.65 (1 H, dd, ²J = 10.3 Hz, ³J = 5.7 Hz), 7.37–7.44 (3 H, m), 7.50 (2 H, d, ³J = 7.2 Hz). ¹³C NMR δ = 49.8, 64.2, 127.5, 129.2, 129.3, 135.3, 227.2 ppm

mass = 197.1169

(b) 4-phenyl-4,5-dihydro-3H- $1\lambda^4$,2 λ^4 -dithiole [H₂S/S₈]

¹H NMR (500MHz, CDCl₃): δ 1.79 (dd, 2H), 1.54(dd,2H), 2.8(1H, m), 7.28(m,5H)

¹³C NMR δ = 42.3, 52.0, 148.4, 126.1, 128.4, 125.9

mas = 187.2257

(c) (2-(phenylthiol)phenyl) methanol

¹H NMR (500MHz, CDCl₃) δ 7.15-7.33 (m, 10H) 4.6425(dd, J₁= 10, J₂ = 5), 3.2375 (dd, J₁= 10, J₂ = 15). ¹³C NMR δ = 125.91, 126.80, 18.02, 128.59, 129.17, 130.23,135.02, 142.23.

mass = 218.2132

(d) 2-(2-hydroxy-2-phenylethyl) isoindoline-1, 3-dione

¹H NMR (500MHz, CDCl₃) δ 5.075 (dd, J = 3.5 Hz, 1H), 4.76 (t, J= 3.5, 2H), 4.7(dd, J= 4, (2H)), 7.8(m, 2H), 7.7(m, 2H), 7.34(S, 5H). ¹³C NMR 168.7, 141.0, 134.1, 131.9, 128.6, 125.9, 123.5 ppm. mass = 290.0803

(e) 2-morpholino-1-phenylethan-1-ol

¹H NMR (500MHz, CDCl₃) δ 7.4 (m, 5H), 5.67(t, 1H), 5.9 (s, 1H), 4.12 (m, 4H), ¹³C NMR; 53.5, 67, 128.9, 127.6, 128.4, 141.9 ppm.

mass = 208.1326

(e) 1-phenyl-2-(pyrrolidin-1-yl) ethan-1-ol

¹H NMR (500MHz, CDCl₃) δ 1.26(m, 4H), 4.1 (m, 1H), 6.1(m, 1H), 7, 43 (m, 5H); ¹³C NMR 127.7, 128.9, 127.6, 64.2, 70.7, 56.8, 23.6

mass = 214.1215

(f) 2-(di-methyl amino)-1-phenylethan-1-ol

 1 H NMR (500MHz, CDCl₃) δ 2.62 (s, 3H), 3.36 (dd, J=1), 4.84 (dd, 1H, J₁=0.5, J₂ =0.5), 7.6 (m, 5H) 13 C NMR 36.1, 59.3, 71.5, 125.9, 127.7, 128.5, 142.6 ppm.

mass = 152.1075

(i) 3-tosyloxazolidin-2-one

¹H NMR (500MHz, CDCl₃) δ 2.37 (S, 3H), 7.25-7.71(m,5H), 3.36 (t, J = 10, 2H), 3.28 (t, J = 10, 2H). ¹³C NMR δ 143.36, 137.07,129.67, 129.07, 68.56, 43.00, 21.47 ppm.

mass = 242.2813

3.3 Results and discussion

By observing the structural integrity in solution state of our La₆ cluster, the catalytic activity has been investigated. Lanthanides have been previously shown to act as excellent catalysts for wide range of reactions ranging from catalytic reduction of CO₂ to form carbon

monoxide, formic acid, methanol and methane, photochemical and electrochemical reduction of CO₂, water oxidation and HER. In few cases, lanthanides have also shown to act as efficient catalysts for activation of CO₂. Freshly Oberdorf et. al. has reported insertion of CO₂ and CS₂ into Bi-N bonds which enables to catalyze C-H activation and light induced bismuthinidene transfer. We have investigated the catalytic activity of the Ln₆ cluster for activation of small molecules CO₂, CS₂, S₈, H₂S and different substituted organic amines. In all the cases, the stability of the Ln₆ cluster was checked by measuring the IR spectra of the catalyst pre- and post-reaction conditions by isolating the cluster form the silica gel. In all the cases, the IR spectra revealed the structural stability of the Ln₆ cluster.

Under n-Bu₄NBr (TBAB) as co-catalyst and La₆ cluster as catalyst both electron withdrawing and electron donating terminal epoxides can be converted to the corresponding cyclic carbonate in good yields under solvent-free conditions. The reaction mixture was heated at 115 °C and a continuous flow of CO₂ gas. The product 4-phenyl-1,3-dioxolan-2-one was isolated in 78% yield after 15 h. The catalytic reaction of formation of cyclic carbonate did not proceed in the absence of catalyst. The hydrated lanthanide chloride was also tested for catalytic activity under the reaction conditions employed in our reaction, and no traceable product was formed in the reaction, which confirms the catalytic activity occurs only in the presence of Ln₆ cluster. Few substituted derivatives of styrene oxide [R = phenoxy and Cl-phenoxy] also have been used as starting materials to check the formation of cyclic carbonates under standardized reaction condition. The expected products were isolated in good yields and the products were thoroughly characterized by standard spectroscopic and analytical methods. To further check the catalytic scope of the Ln₆ cluster, reaction with CS₂ in presence of TBAB as co-catalyst was carried out under standardized reaction conditions. The cyclic thio carbonate 5-phenyl-1,3-oxathiolane-2-thione was obtained in good yield. It is pertinent to mention here that very few catalytic systems have been reported in literature for activation of CS2. A multimetallic uranium complex has been reported for activation of CS₂ wherein the activated CS₂ is clapped inside the uranium complex as a part of the ligand system filling the coordination sphere of the metal atom.^{3e} In our study, we have been successful in incorporating the small molecules with styrene oxide resulting in the formation of interesting molecular systems with versatile catalytic applications. The Ln₆ cluster showed catalytic activity in not only activating CO₂ (g) but also in activating the other small molecule CS₂ (l) which is also an inert molecule as CO₂ (g). Since the Ln₆ cluster showed versatile catalytic activity, we were further interested in exploring activating other small molecules using our catalytic system. So, the next targeted small

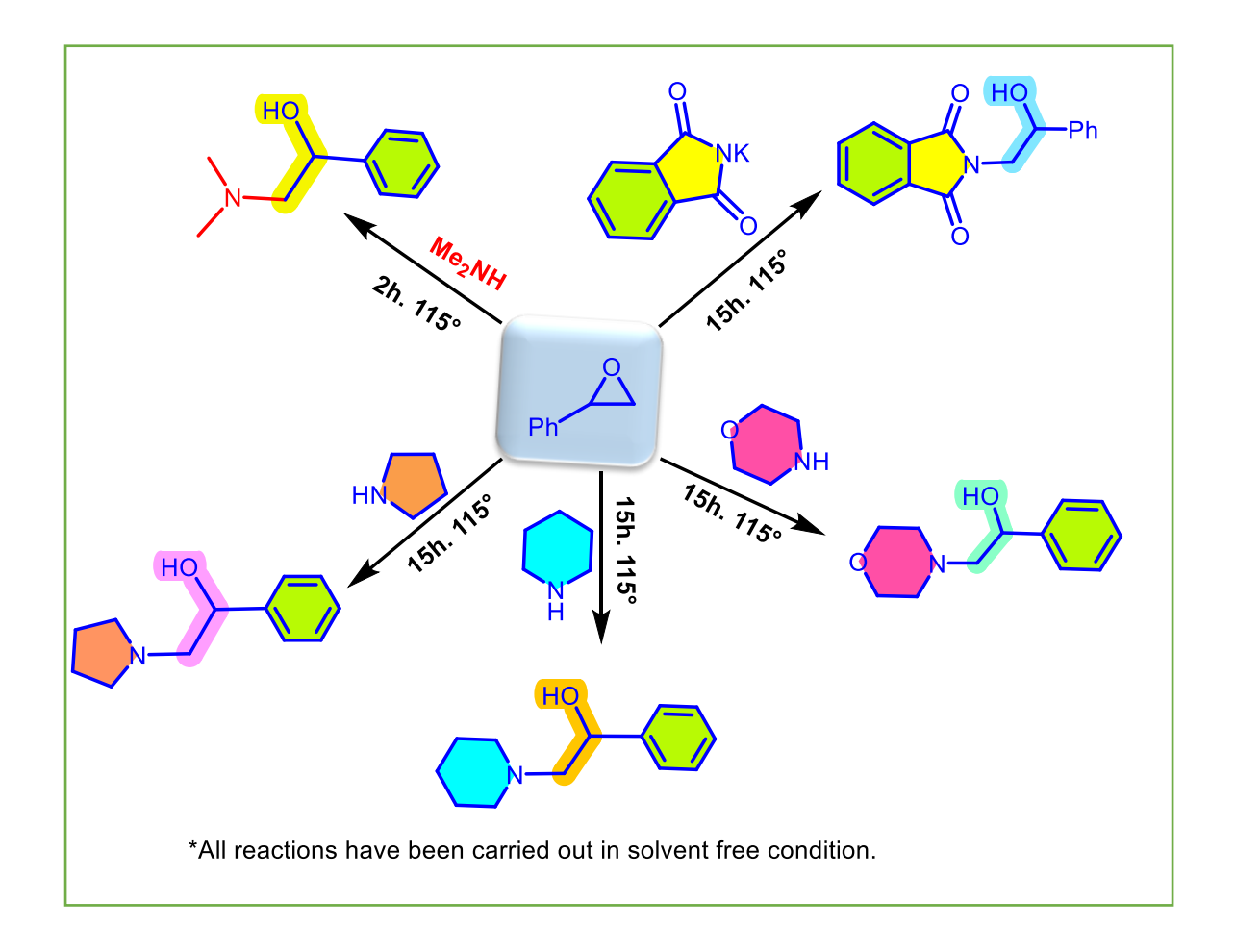
molecules were S₈ (s) and H₂S (g). The activation of H₂S gas and elemental Sulfur (S₈) in presence of styrene oxide in independent reactions following the standardized set of conditions followed in the earlier reactions were carried out. Remarkably, the spectroscopic and analytical data confirmed the formation of a novel molecule 5-phenyl-4,5-dihydro-1, $2\lambda^4$, $3\lambda^4$ -oxadithiole (60% and 67% yield) respectively. The product contains a cyclic dithiolate moiety which can be used as a potential ligand system in presence of transition metal ions. It is pertinent to mention here that in the case of activation of S₈, adventitious water also has played a role in the formation of the resultant S-H bonds seen in the product. The probable reaction pathway is as follows, S₈ when heated to temperatures above 115 °C breaks in to four molecules of S²which then in presence of water leads to the formation of [SH]⁻ and H⁺ ions. Two such [SH]⁻ ions probably combine to form [-SH=SH-] moiety in presence of styrene oxide and the Ln₆ catalyst to form the novel cyclic dihydro oxadithiole product in good yield. In the case of H₂S, the small molecule breaks in to [SH] and H ions in presence of Ln₆ catalysts and gets incorporated in to the three membered oxygen containing ring system. As has been in the case of CS₂, in earlier literature reports on activation of S₈ and H₂S as small molecules, the activated small molecules always have been found to be the part of the coordinated ligand system to the metal ions. When S₈ was activated using a uranium complex, it has been incorporated in to the molecular system in two parts, as $[S_2]^{n-}$ and bent $[S_3]^{m-}$ molecular fragments.^{3e} Similarly, activation of H_2S also lead to formation of uranium sulfur containing triple bonded systems. 3c Likewise, other examples of Sulphur compounds, for thiophenol also we have checked the catalytic property. According to earlier reported work in presence of 'Erbium triflate' as catalysts for ring opening reaction of epoxides with thiophenol has been carried out resulting regioselective hydroxy sulfide compound. The spectroscopic analysis has confirmed the ring opening of epoxides to thiophenol forming a β-hydroxy sulfide through the reported La cluster scheme 3.1.

$$\begin{array}{c} & & & & \\ & & & \\ & & & \\ & & & \\ & & & \\ & & & \\ & & & \\ & & & \\ & & & \\ & &$$

Scheme: 3.1

Activation of Sulphur based small molecules; Formation of cyclic-carbonates and cyclic thio-carbonates in presence of La₆ catalyst. Reaction condition: epoxides (0.5 mmol), La₆ catalyst (0.00136) and n-Bu₄NBr as co-catalyst (0.025), CO₂, CS₂ (0.26), H₂S (g), thiol (0.26), S₈ (0.26). All reactions have been carried out separately.

Ln₆ catalyst has also been examined for the formation of β -amino alcohols in solvent free ring opening reaction of styrene oxide with various aliphatic and aromatic amines. The scope of the reaction has been examined by using a variety of amines like primary amines, secondary amines and various functionalized amines including an β -amino alcohol (Scheme 3). In all the cases in the presence of La₆ cluster, the ring opening of the epoxides followed by addition of the amines has led to the formation of β -amino alcohols in good yields. Regioselective ring-opening of epoxides with various substituted amines are an area of topical interest. By employing mesoporous TiO₂-Fe₂O₃ or mesoporous chiral material based on iron, ring opening of various amines have been carried out in heterogenous conditions. To the best of our knowledge, this is the first instance in which a Ln based cluster has been used as a catalyst for such transformation.



Ring opening reactions of epoxides to form different substituted β -amino alcohols. Reaction conditions: epoxide (0.5 mmol), rare-earth metal cluster catalyst (0.00136), substituted amines (0.26) and n-Bu₄NBr as co-catalyst (0.025 mmol).

Finally, the La₆ cluster has been examined for cycloaddition of CO₂ with *n*-tosylaziridine at 120 °C for 24 h. in presence of co-catalyst TBAB and 1-butanol (as solvent) forming **3-tosylazolidin-2-one** with a very good yield (Scheme 3). From earlier reports Ni catalyzed carboxylation of aziridines enroute to β -amino acids have been set a mark to design alternative catalytic carboxylation techniques. Whereas some other reports are by Nayak *et.al*. cycloaddition of CO₂ with aziridine to form corresponding oxazolidinones by Zn-salen having B-N coordinated phenanthrol imidazole motif as a photocatalyst. ^{12c}

Schem: 3.3

3.4 Conclusion:

The Ln₆ cluster shows enhanced Lewis acidity and has been shown to act as a value-added catalyst for activating less active sulfur molecule like CS₂, S₈, and H₂S. Activation of S₈ and H₂S in the presence of styrene oxides has led to the isolation of novel cyclic sulfur ring systems, 5-phenyl-4,5-dihydro-1,2 λ^4 ,3 λ^4 -oxadithiole. In literature, the activated small molecule (S₈ and H₂S) happens to be present as part of a metal complex. Herein, the small molecule happens to form novel value-added products. Further, the versatility of the catalyst has been shown by its ability to catalyze the ring-opening reaction of epoxide in the presence of different substituted amines to form β - amino alcohols.

References:

(1)(a) Takenaka, Y.; Fukaya, N.; Chi, S. J.; Mori, G.; Kiyosu. T.; Yasuda, H.; Choi, J. C. Synthesis of cyclic thiocarbonates from thiiranes and CS₂ with silica-immobilized catalysts. *Ind. Eng. Chem. Res.* **2018**, 57, 3, 891–896. (b) Quintana, L. M. A.; Rajeshkumar, T.; Jiang, N.; Niklas, J. E.; Bacsa, J.; Maron, L.; Pierre, H.S.L. Elemental chalcogen reactions of a tetravalent uranium imidophosphorane complex: cleavage of dioxygen. *Chem. Commun.*, **2022**,58, 13242-13245. c) Rosenzweig, M.W.; Scheurer, A.; Lamsfus, C. A.; Heinemann, F.W.; Maron, L.; Andrez, j.; Mazzantib, M.; Meyer, K. Uranium (IV) terminal hydrosulfido and sulfido complexes: insights into the nature of the uranium–sulfur bond. *Chem. Sci.*, **2016**, 7, 5857–5866. (d) Clegg W., Harrington R.W., North M., Villuendas P., *J. Org. Chem.* **2010**, 75, 18, 6201–6207. (e) Barluzzi, L.; Falcone, M.; Mazzanti, M. Small molecule activation by multimetallic uranium complexes supported by siloxide ligands. *Chem. Commun.*, **2019**, 55, 13031-13047.

(2) (a) Wang, L.; Xu, C.; Han, Q.; Tang, X.; Zhou, P.; Zhang, R.; Gao, G.; Xu, B.; Qin, W.; Liu, W. Ambient chemical fixation of CO₂ using a highly efficient heterometallic helicate catalyst system. *Chem. Commun.*, **2018**, 54, 2212-2215. (b) Zhang, R.; Wang, L.; Xu, C.; Yang, H.; Chen, W.; Gao, G.; Liu, W. Anion-induced 3d–4f luminescent coordination clusters: structural characteristics and chemical fixation of CO₂ under mild conditions. *Dalton Trans.*, **2018**, 47, 7159-7165. (c) Sinchow, M.; Semakul, N.; Konno, T.; Rujiwatra, A. Lanthanide coordination polymers through design for exceptional catalytic performances in CO₂ cycloaddition reactions. *ACS Sustainable Chem. Eng.* **2021**,9, 8581–8591. (d) Chen, W. P.; Liao, P. Q.; Jin P. B.; Zhang L., Ling, B. K.; Wang, S. C.; Chan, Y. T.; Chen, X. M. The

gigantic {Ni₃₆Gd₁₀₂} hexagon: a sulfate-templated "star-of-David" for photocatalytic CO₂ reduction and magnetic cooling. J. Am. Chem. Soc. 2020, 142, 4663–4670. (e) España, E. G.; Gaviña, P.; Lattore, J.; Soriano, C.; Verdejo, B. CO₂ fixation by copper (ii) complexes of a terpyridinophane aza receptor. J. Am. Chem. Soc. 2004, 126, 5082–5083. (f) Dolai, M.; Biswas, S.; Pineda, E. M.; Wernsdorfer, W.; Ali, M.; Alshgari, R. A.; Wabaidur, S. M.; Ghosh, A. CO₂ fixation by dimeric Tb (III) complexes: synthesis, structure, and magnetism. Cryst. Growth Des. 2023, 23, 2, 801–810. (g) Velpuri, V. R.; Muralidharan, K. High yield room temperature conversion of carbon dioxide into cyclic carbonates catalyzed by mixed metal oxide (CuO-ZnO) nano-flakes/micro-flakes (Cozi-nmf). Appl. Organomet. Chem., 2021, 35, e6224. (g) Biswas T., Mahalingam V., New J. Chem., 2017, 41, 14839. (h) Thammakan, S.; Kuwamura, N.; Chiangraeng, N.; Nimmanpipug, P.; Konno, T.; Rujiwatra, A. Highly disordering nanoporous frameworks of lanthanide-dicarboxylates for catalysis of CO₂ cycloaddition with epoxides. J. Solid State Chem. 2021, 303, 122464. (i) Sodpiban, O.; Gobbo, S. D.; Barman, S.; Aomchad, V.; Kidkhunthod, P.; Chikh, S. C.; Poater, A.; D'Elia, V.; Basset, J. M. Synthesis of well-defined yttrium-based Lewis acids by capturing a reaction intermediate and catalytic application for cycloaddition of CO₂ to epoxides under atmospheric pressure. Catal. Sci. Technol., 2019, 9, 6152-6165. (j) Hua, L.; Li, B.; Han, C.; Gao, P.; Wang, Y.; Yuan, D.; Yao, Y. Synthesis of homo and heteronuclear rare-earth metal complexes stabilized by ethanolamine-bridged bis(phenolato) ligands and their application in catalyzing reactions of CO₂ and epoxides. *Inorg. Chem.* **2019**, 58, 8775–8786.

- (3) Majumadar, D.; Bhanarkar, A.; Rao, C.; Gouda, D. Atmos. Environ.: X, 2022, 13, 100157
- (4) Tomita, H.; Sanda, F.; Endo, T. *Macromolecules*, **2001**, 34, 727–733.
- (5) Jones, F. N.; Andreades, S. J. Org. Chem., 1969, 34, 3011–3014.
- (6)(a) Taguchi, Y.; Yanagiya, K.; Shibuya, I.; Suhara, Y.; *Bull. Chem. Soc. Jpn.*, **1988**, 61, 921–925. (b) Taguchi, Y.; Yasumoto, M.; Shibuya, I.; Suhara, Y. *Bull. Chem. Soc. Jpn.*, **1989**, 62, 474–478.
- (7)(a) Comba, M. B.; Suárez, A. G.; Sarotti, A. M.; Mangione, M. I.; Spanevello, R. A.; Giordano, E. D. *Org. Lett.*, **2016**, 18, 1748–1751. (b) Comba, M. B.; Mangione, M. I.; Suárez, A. G.; Sarotti, A. M.; Spanevello, R. A. *Eur. J. Org. Chem.*, **2018**, 6848–6856.
- (8)(a) Kihara, N.; Nakawaki, Y.; Endo, T. *J. Org. Chem.*, 1995, 60, 473–475. (b) Motokucho, S.; Takeuchi, D.; Sanda, F.; Endo, T.; *Tetrahedron*, **2001**, 57, 7149–7152.
- (9) Zolfigol, M. A.; Reza, A.; Zare, M.; Zarei, M.; Zare, A.; Noroozizadeh, E.; Karamiand, R.; Asadbegy, M. Synthesis of β-phthalimido-alcohols via regioselective ring opening of epoxide by using reusable basic magnetic nano particles and their biological investigation. *RSC Adv.*, **2016**, 6, 62460 (b) Yang, L. C.; Wang, Y. N.; Zhang, Y.; Zhao, Y. Acid assisted Ru-catalyzed enantioselective amination of 1,2-Diols through borrowing hydrogen. *ACS Catal.* **2017**, 7(1), 93–97 (c) Li, D.; Wang, J.; Yu, S.; Zou, W.; Zhang, H.; Chen, J. Highly regioselective ringopening of epoxides with amines: a metal- and solvent-free protocol for the synthesis of β-amino alcohols. *Chem. Commun.*, **2020**, 56, 2256. (d) Sousa, S. E.; O'Brien, P.; Pilgram, C.D. Optimisation of enantioselectivity for the chiral base-mediated rearrangement of bis-protected meso-4,5-dihydroxycyclohexene oxides: asymmetric synthesis of 4-deoxyconduritols and conduritol F. *Tetrahedron.* **2002**, 58, 4643-4654. (e) Zhang, Y.; Zhang, Y.; Yansong, R.; Olof,

- R. Synthesis of chiral oxazolidinone derivatives through lipase-catalyzed kinetic resolution. *J. Mol. Catal., B Enzym.* **2015,** 122, 29-34.
- (10) (a) Davies, J.; Müller, D. J.; Zimin, D. P.; Day, C. S.; Yanagi, T.; Elfert, J.; Martin, R. Nicatalyzed carboxylation of aziridines enroute to β-Amino acids. *J. Am. Chem. Soc.* **2021**, 143, 4949–4954. (b)Liu, H., Hua, R., *Tetrahedron*,**2016**, 72, 1200-1204. (c) Nayak, P.; Murali A. C.; Rao, V.; Chandrasekhar, V.; Venkatasubbaiaha, K. B–N coordinated phenanthroimidazole-based zinc-salen as a photocatalyst for the synthesis of oxazolidinones using carbon dioxide as a C1 source under mild reaction conditions. *Adv. Synth. Catal.* **2023**, 365, 230-237.

Spectroscopically Observed Data



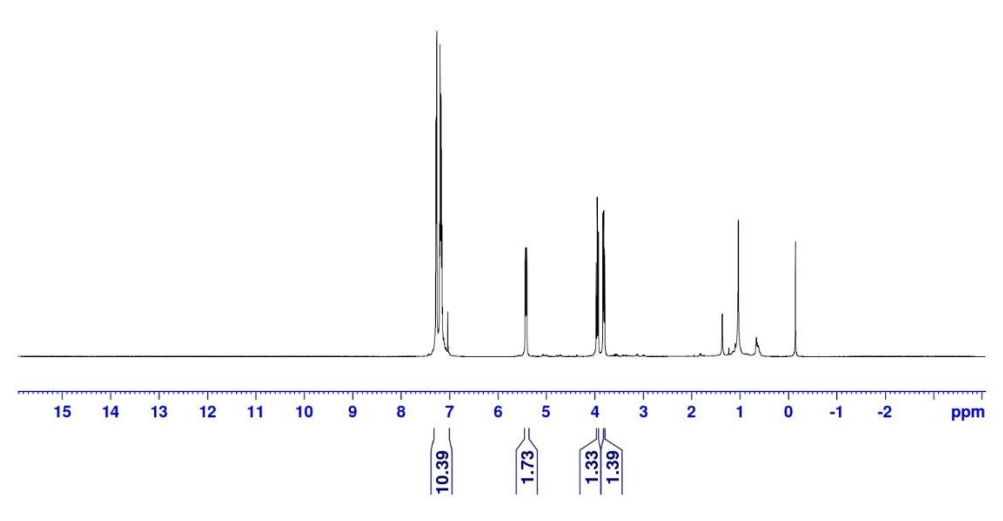


Fig 3.1 ¹H NMR spectra of 3a

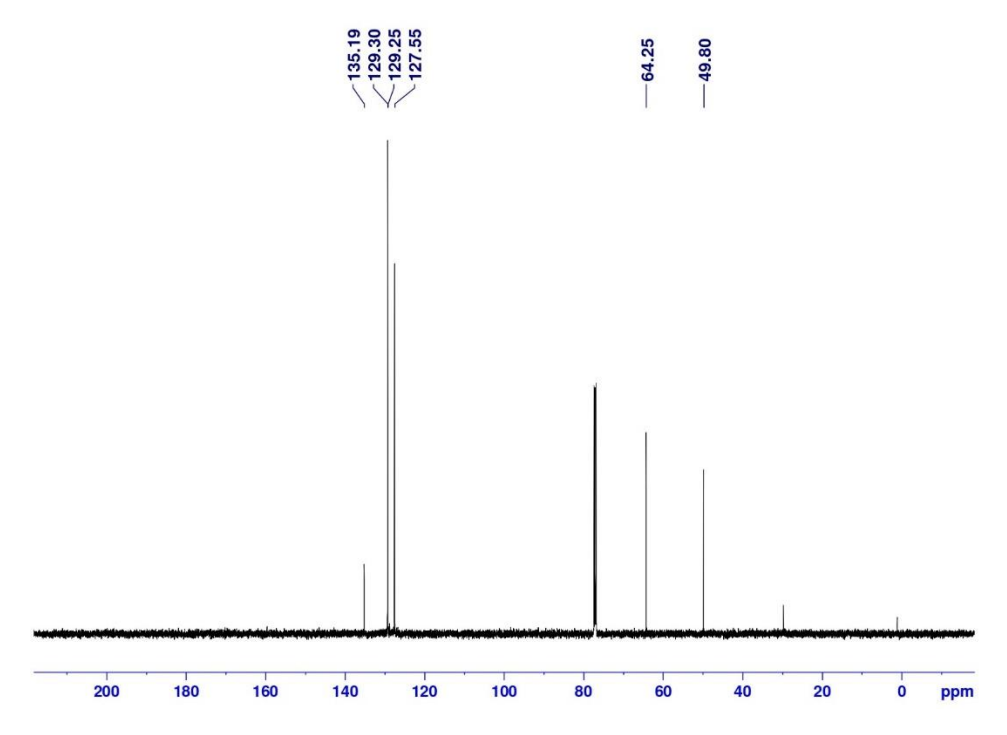


Fig 3.2 ¹³C NMR spectra of 3a

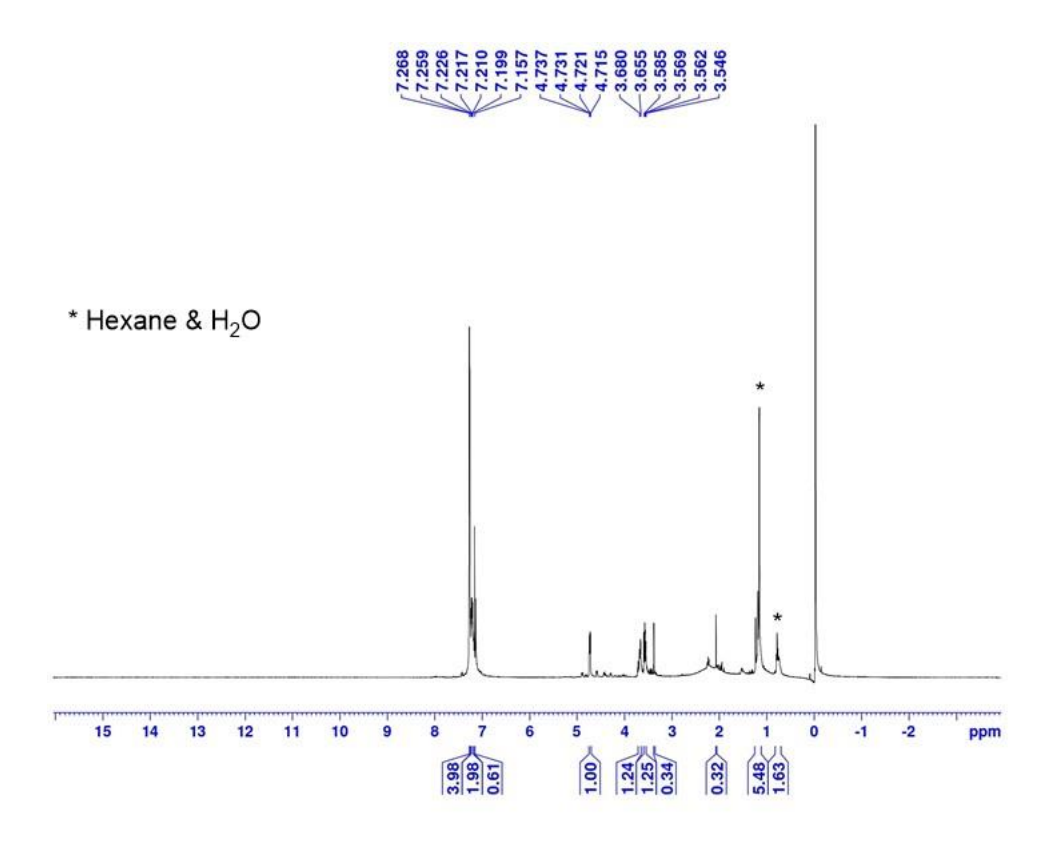


Fig 3.3 ¹H NMR spectra of 3b

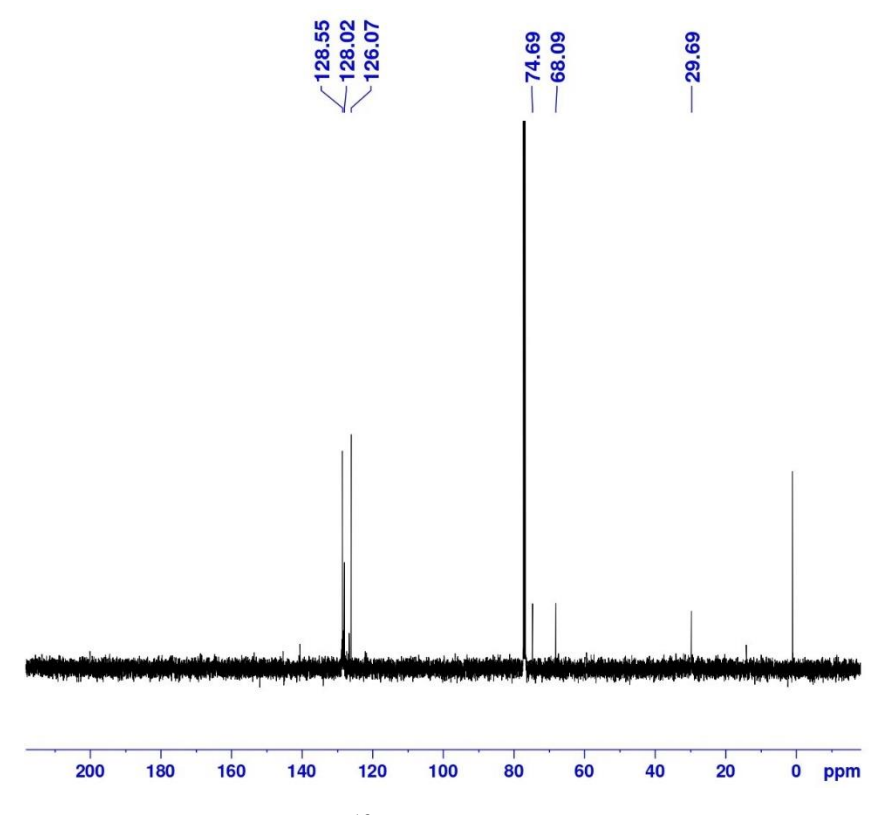


Fig 3.4 ¹³C NMR spectra of 3b

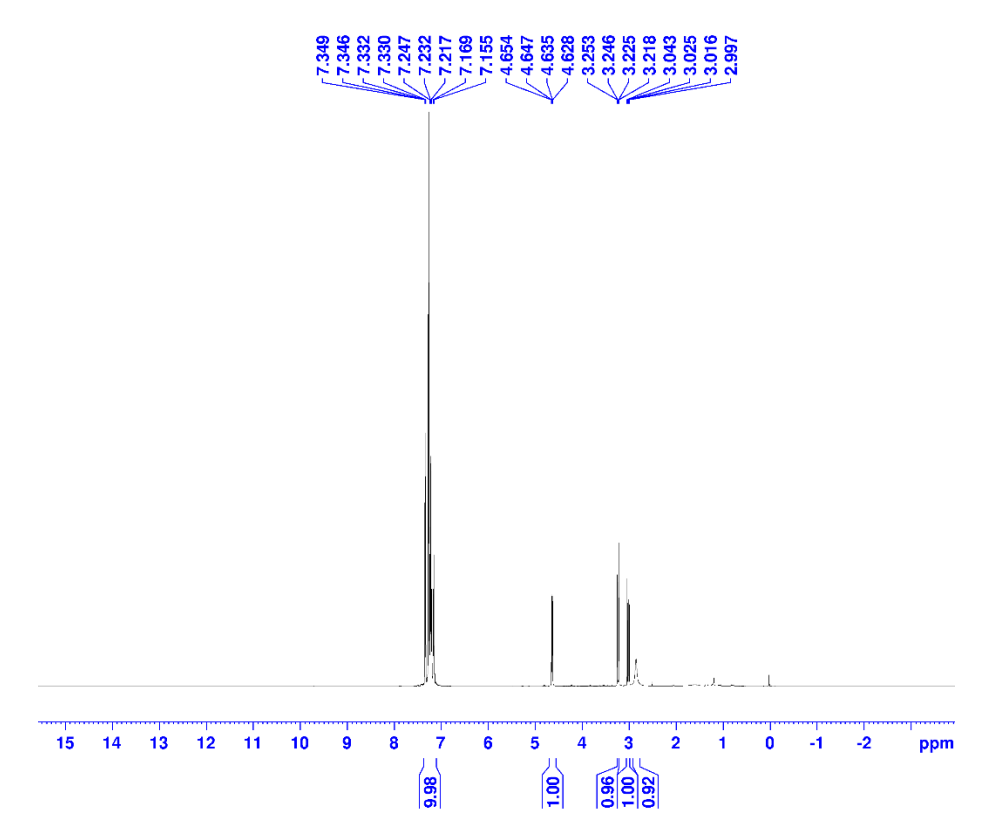


Fig 3.5 ¹H NMR of 3c.

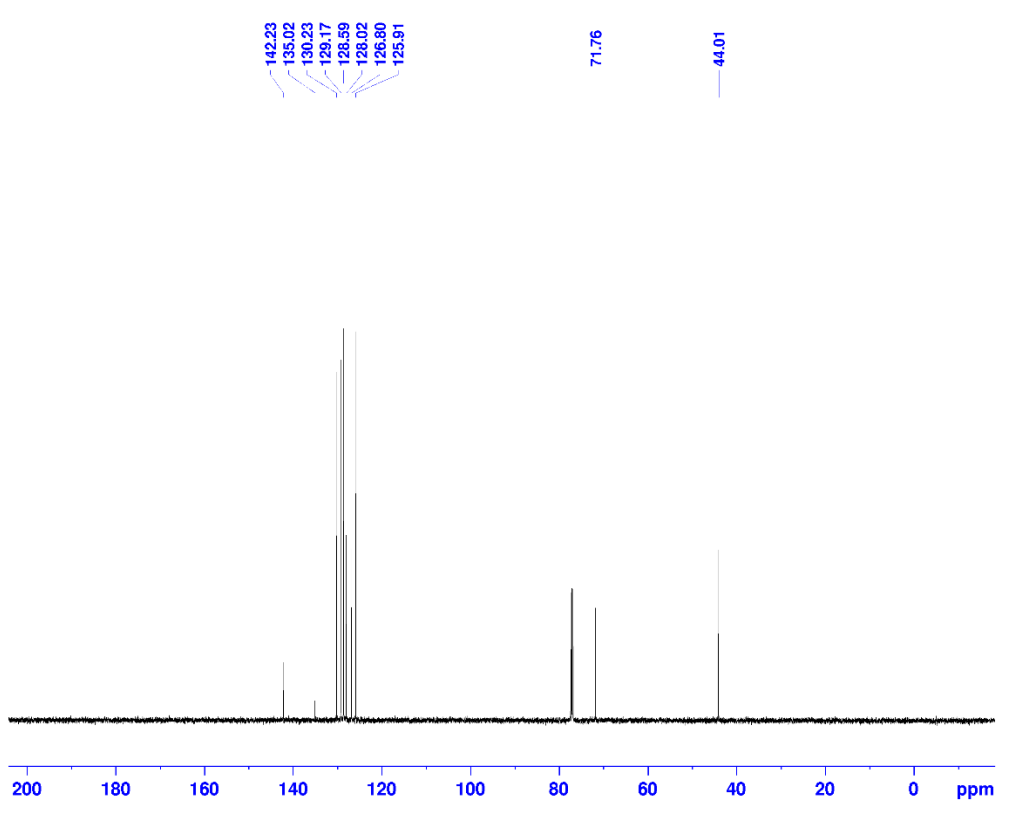


Fig 3.6 ¹³C NMR of 3c

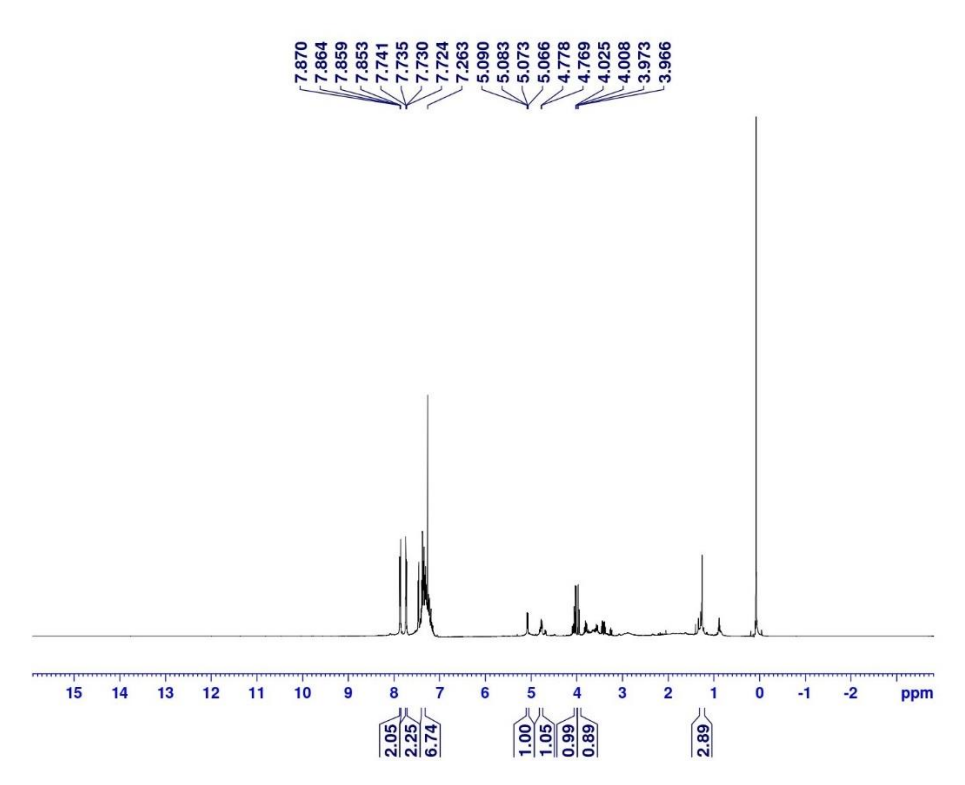


Fig 3.7 ¹H NMR spectra of 3d.

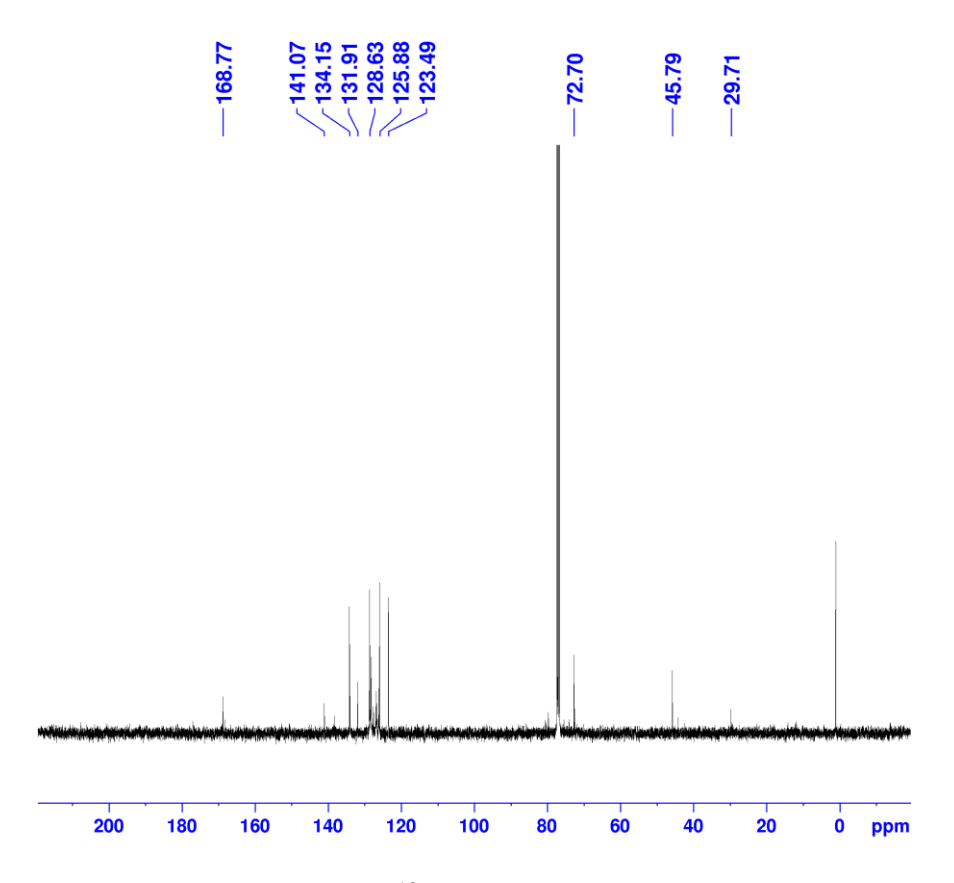


Fig 3.8 ¹³C NMR spectra of 3d.



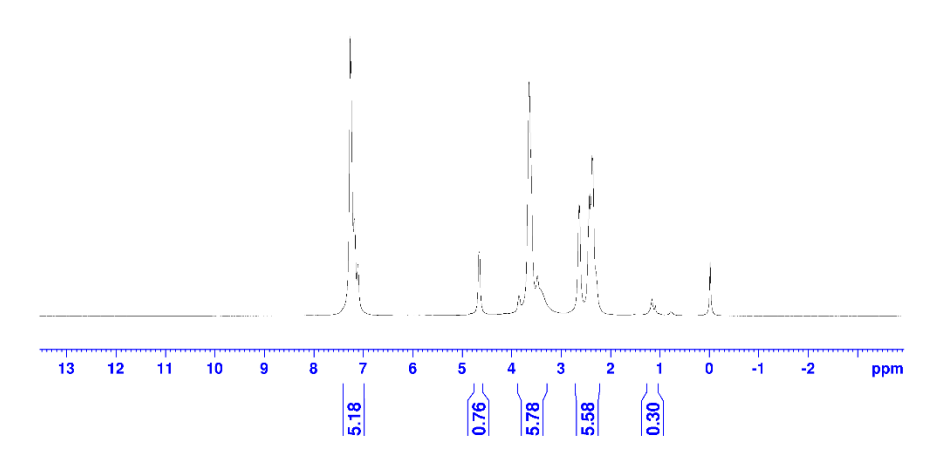


Fig 3.9 ¹H NMR of 3e

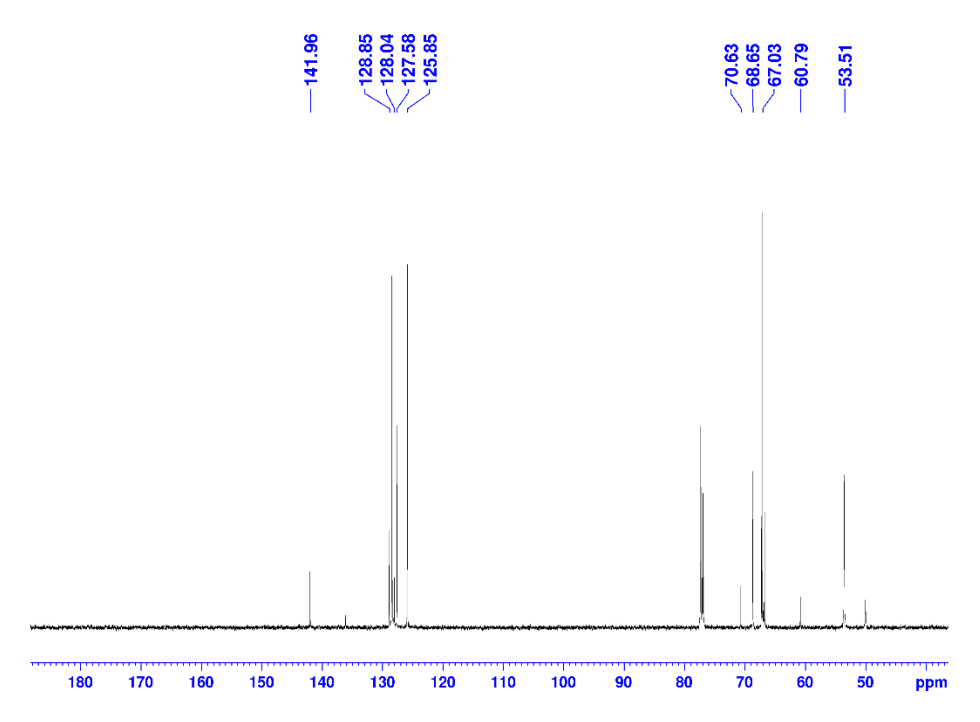


Fig 3.10 ¹³C NMR of 3e

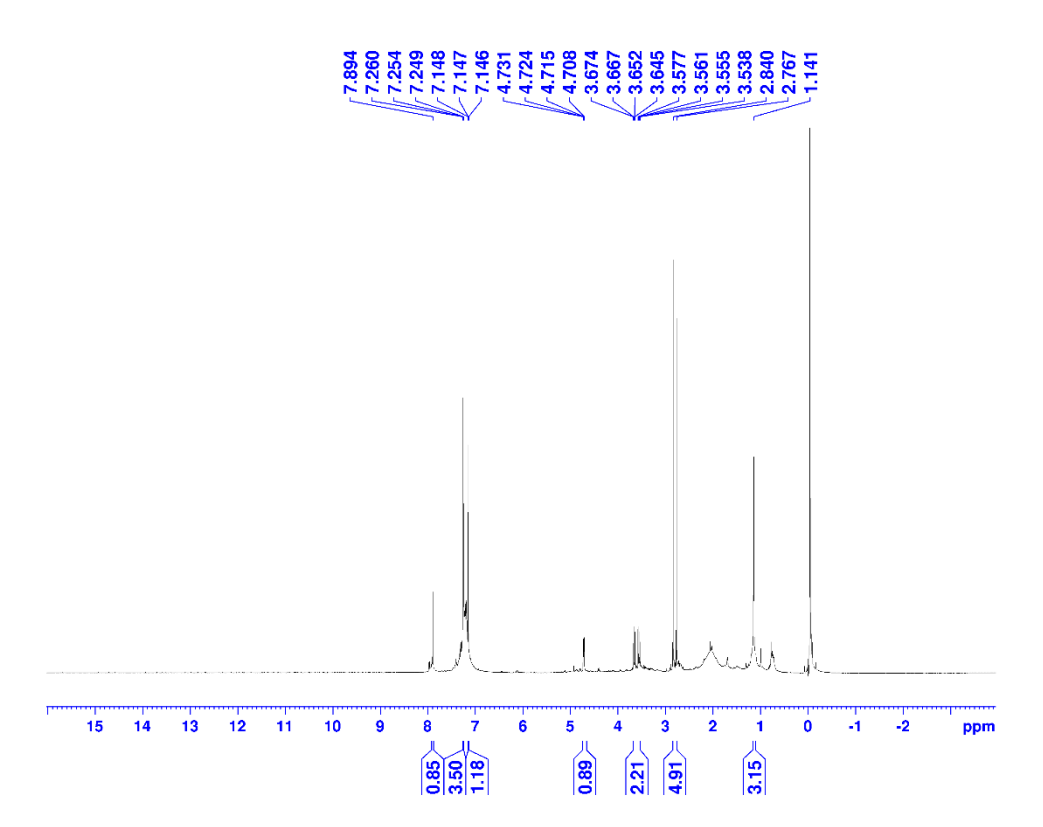


Fig 3.11 ¹H NMR of 3f.

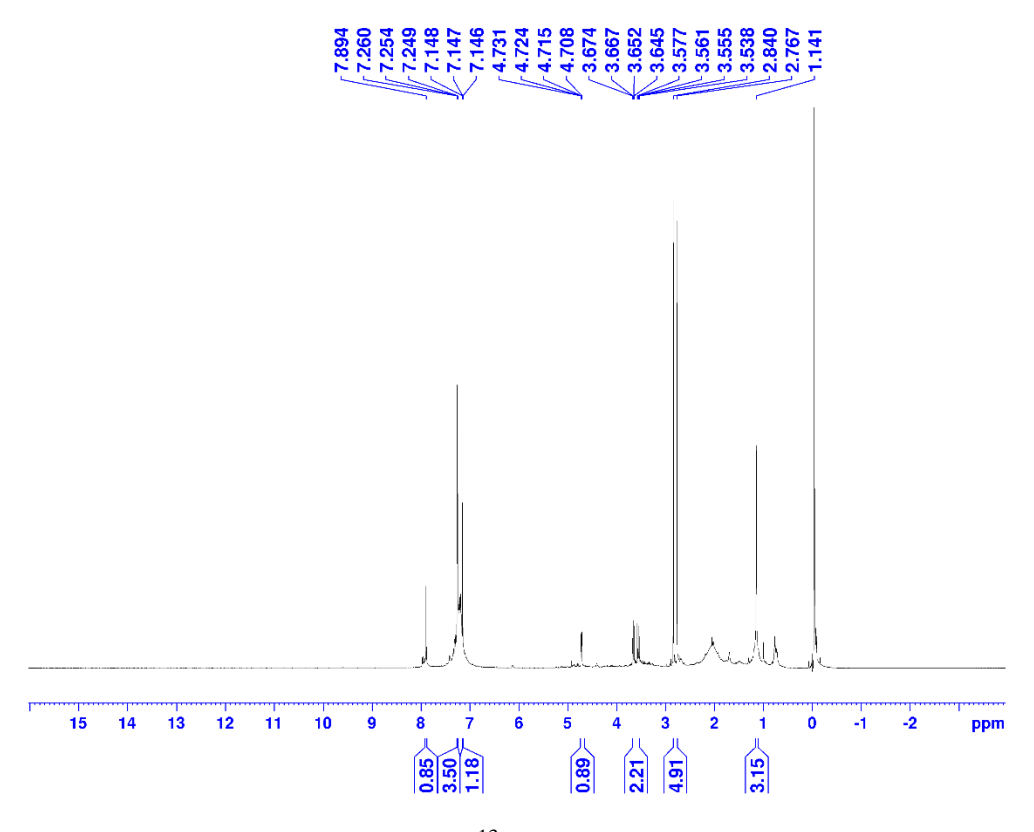


Fig 3.12 ¹³C NMR of 3f.



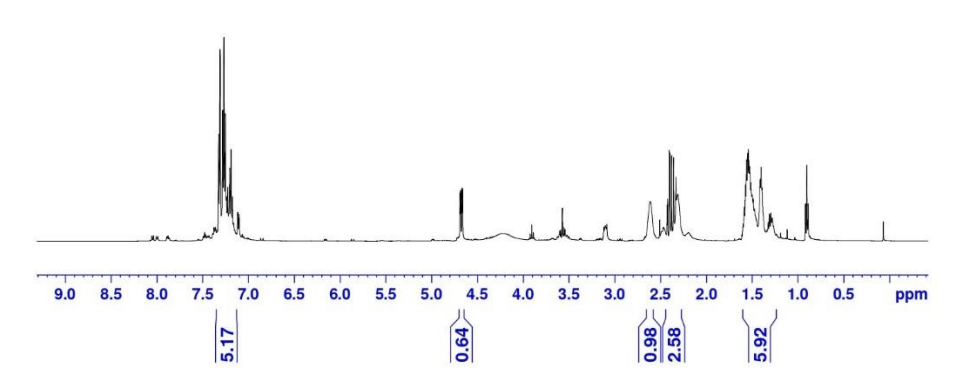


Fig 3.13 ¹H NMR of 3g

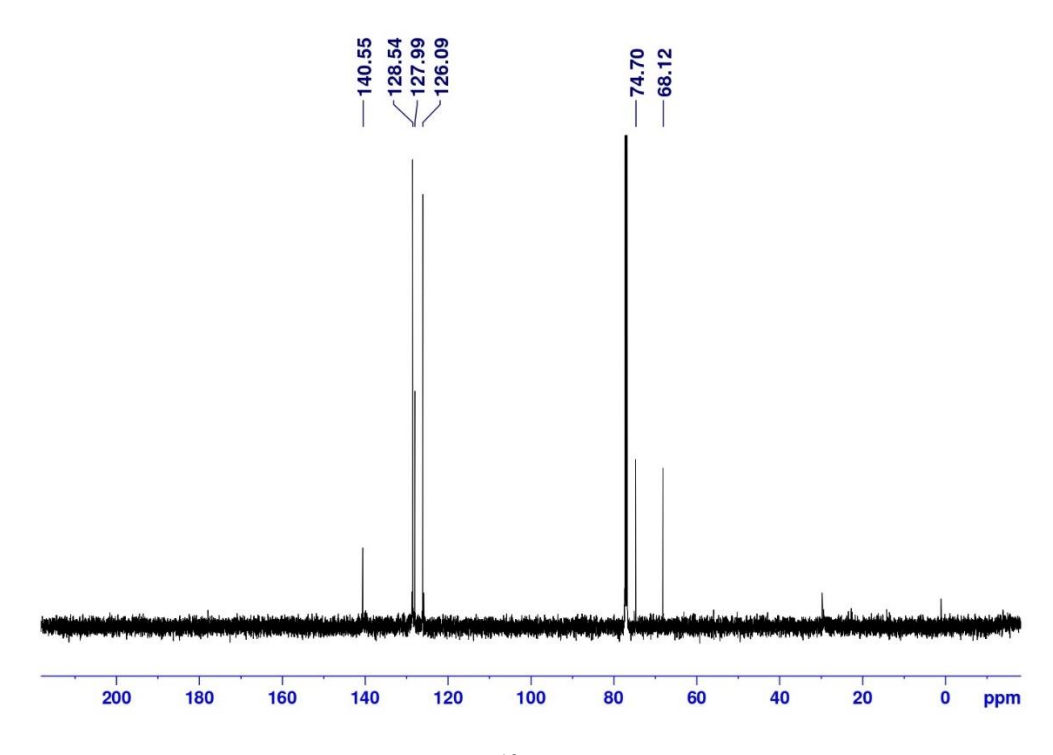


Fig 3.14 ¹³C NMR of 3g

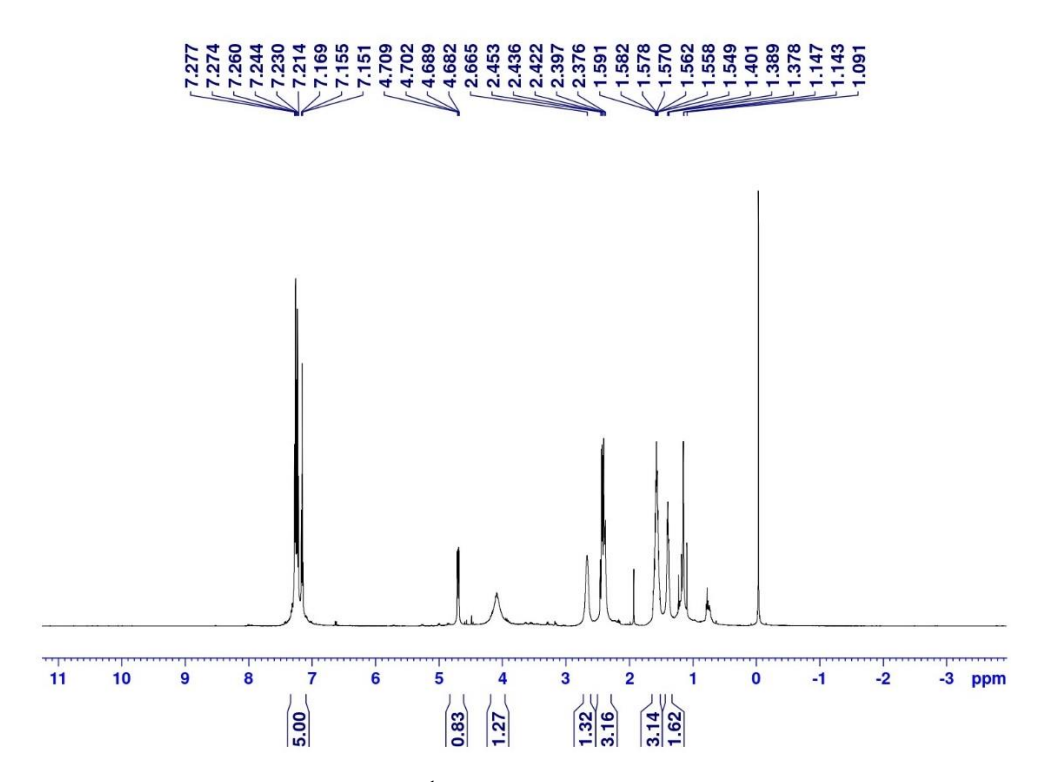


Fig 3.15 ¹H NMR spectra of 3h.

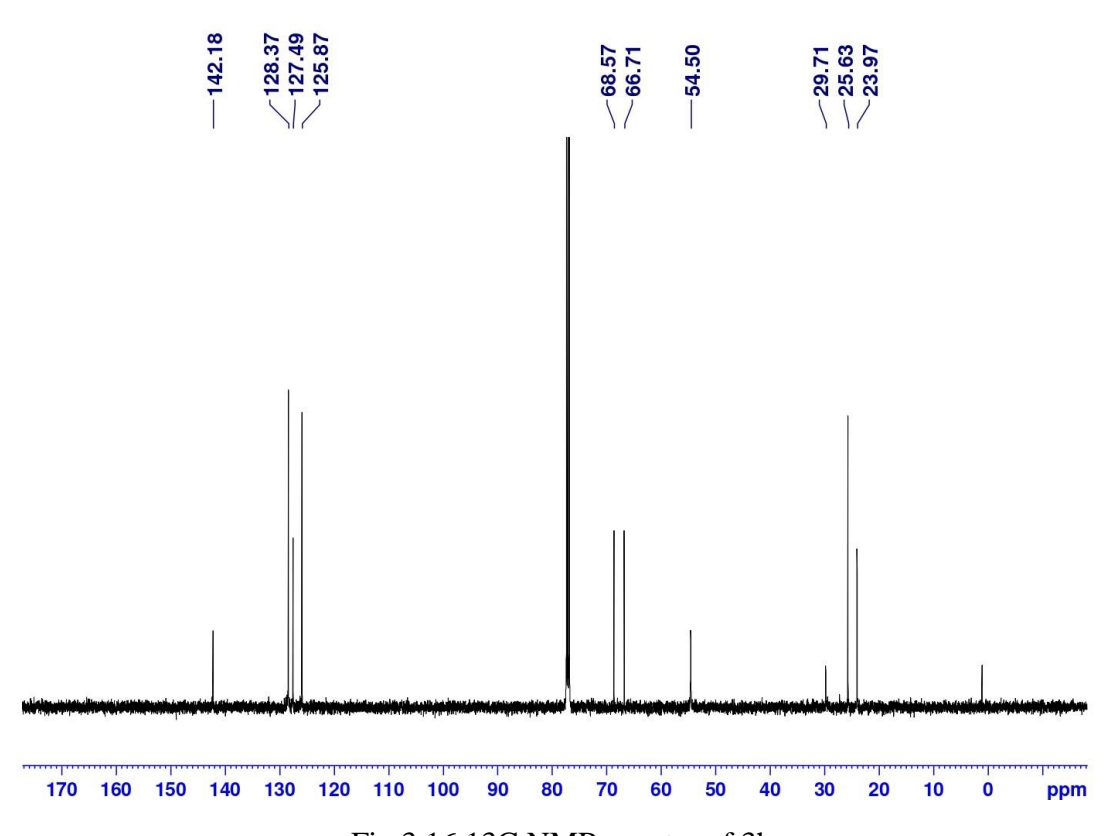


Fig 3.16 13C NMR spectra of 3h

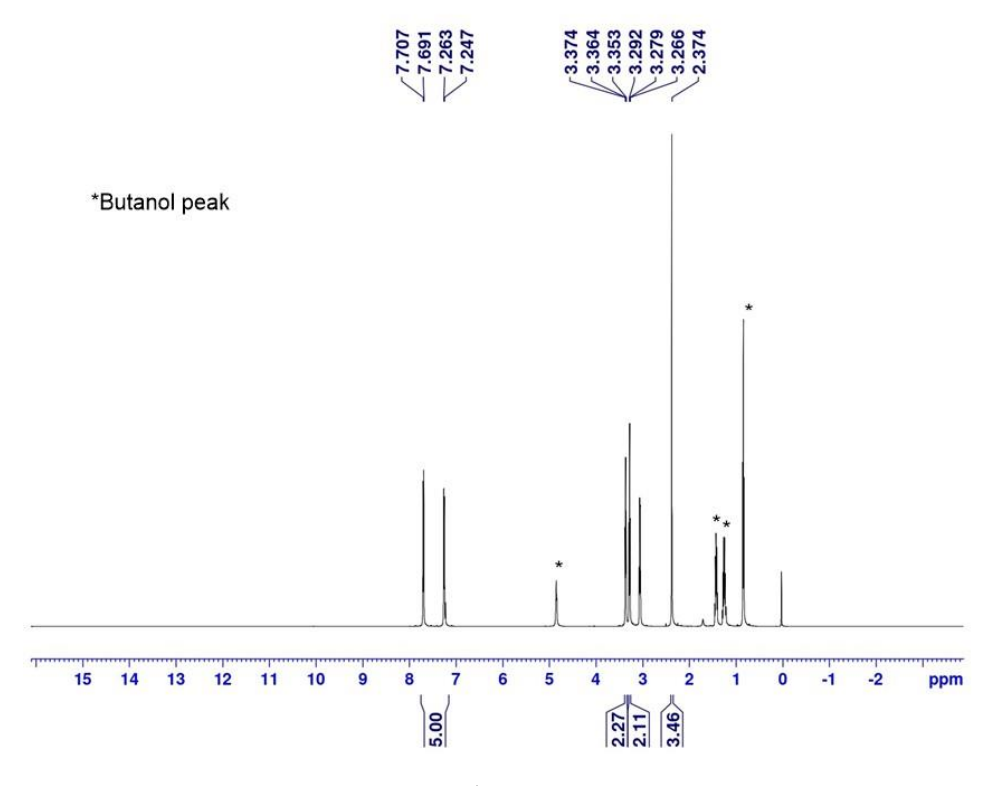


Fig 3.17 ¹H NMR of 3i



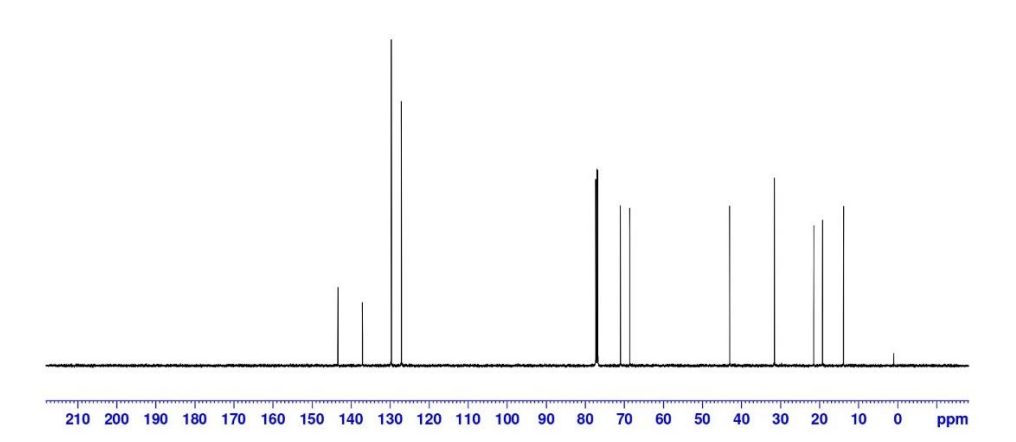


Fig 3.18 ¹³C NMR of 3i

Proligand approach towards assembling heteromolecular architecture

leads to the isolation of [(n-Bu-Sn)4(RPO3H)8O2], which we have used as proligand system and reacted with hydrated transition metal precursors as well as hydrated lanthanide salts in solovothermal condition in presence of Py. Studies using single crystal X-ray diffraction shows the development of $[(n-BuSn)_3(\mu_2-O)_3(\mu_3-O) (RPO_3)_4Co.Py]$ (4.1), $[(n-BuSn)_3(\mu_2-O)_3(\mu_3-$ O)(RPO₃)₄Zn.Py] (4.2), $[(n-BuSn)_3(\mu_2-O)_3(\mu_3-O)(RPO_3)_4Dy.Py]_2$ (4.3), $[(n-BuSn)_3(\mu_2-O)_3(\mu_3-O)(RPO_3)_4Dy.Py]_2$ (4.3), BuSn)₃(μ_2 -O)₃(μ_3 -O)(RPO₃)₄Er.Py]₂ (4.4), $[(n-BuSn)_3(\mu_2-O)_3(\mu_3-$ O)(RPO₃)₄Gd.Py]₂ (4.5), [(n-BuSn)₃(μ_2 -O)₃(μ_3 -O)(RPO₃)₄Y.Py]₂ (4.6) while R = t-Bu. A variety of structural forms ranging from dimeric to distorted tetrahedral structures-based clusters have been isolated. The magnetic and catalytic studies of the paramagnetic lanthanide clusters and transition metal complexes are under studies.

4.1 Introduction

For a number of motives, such as their biological and catalytic activities, organotin chemicals have proved vital. Numerous compounds containing organotins have exhibited significant potential as treatments against cancer. Researchers have used trialkyltin compounds, which were especially effective against mollusks, to create a variety of antifouling paints and tri-organotin compounds having biocidal action. However, the environmental issues surrounding organotin chemicals have partially diminished this utility in recent years. Tri-organotin hydrides have been used in organic synthesis, and this has been well-reported by research organizations. Organooxotin compounds have also been reported to be used as catalysts in several papers, especially in esterification processes.¹

The interaction of organotin hydroxides, oxides, and oxide hydroxides with hydrogen contained reagents such as carboxylic acids, phosphonic acids, sulfonic acids, and phosphinic acids is one of the specific members of this family of organotin compounds, namely organostannooxanes produced by controlled hydrolysis approach. With the vast structural diversity found in compounds, it has drawn special attention. The ability of a few of these substances to operate as scaffolds for a functional peripheral that is photochemically, electrochemically, or catalytically active is another intriguing feature. With the aid of non-covalent interactions such $\pi \cdots \pi$ interactions, $C-H\cdots \pi$, and H-bondingstudies have reported several supramolecular frameworks in the crystal structures of organostannoxane complexes.

Specifically, the interaction between phosphorus-based acids and mono organotin substrates like [n-BuSn(O)OH] has shown to be highly advantageous. Many of the structural variations of organo-oxotin assemblies have been achieved by very easy synthetic techniques, which mostly entail substituent change at the phosphorus center. Thus, structural preparations were made for a number of new cages, including drum, cubic, O-cap clusters, double O-cap, tetranuclear, butterfly clusters, and sucker cages. Research teams have already created the aforementioned oragnooxotin cages and clusters using solventless techniques. They have investigated the structural diversity of [n-BuSn(O)OH] by reacting it with phosphorus-based acids in matching reactions involving di- and triorganotin precursors.²

Prior research has demonstrated that organostibonic acids function as adaptable building blocks when creating distinct molecular structures. Our research group, as well as others, have demonstrated the ability of the distinct stibonate-phosphonate cluster to function as a tunable proligand.³ It is being utilized to assemble novel chemical compounds using transition-metal

ions and lanthanides. Very recently Baskar et. al has reported the reaction of different substituted oragno phsophonic with aryl substituted antimony metal precursors to form $(RSb)_2(O)(t-BuPO_3H)_6$. This they have used as proligand and again reacted with VCl₃ to form vanadyl-organoantimony(v) hexanuclear oxo cluster possessing the formula $[(RSb)_4V_2(O)_2(\mu_3-O)_2(\mu_2-O)_2(t-BuPO_3)_4(\mu_2-OCH_3)_4]$, where $R = p-ClC_6H_4$. The other reactions they have tried with other transition metals are Mn, Co, Ni and Cu. They have also studied the magnetic and optical properties of the organo stibonate clusters. Getting inspiration from this we thought of extending our work to organostannoxane complexes. Hence, we have reacted tertiary butyl phosphonic acid with oragnostanoxane metal precursor to give $[(n-Bu-Sn)_4(RPO_3H)_8O_2]$ which we are using as proligand and again carry forwarding the reaction in solvothermals condition with transition metal and hydrated lanthanide precursors to form $[[(n-BuSn)_3(\mu_2O_3)(\mu_3O)(RPO_3)_3]MPy]$ and the corresponding dimer in case of lanthanides.

4.2 Experimental

4.2.1 Instrumentation: FTIR spectrometer Nicolet iS5 was utilized to record infrared spectra. The X-ray data was obtained using a graphite monochromator and the Smart Apex CCD area detection system from Bruker at 293.9 K (λ (Mo-K α) = 0.71073 Å). APEX-2 was used to minimize the data. Olex2 1.3-ac4 software was used to solve the structures using SHELXT and refine them using SHELXL-2018/3. Every non-hydrogen atom underwent anisotropic refinement. At a scan rate of 3.9° min-1, X-ray diffraction patterns were obtained spanning the 20 range of 5–80°. The Shape v2.1 software was used to calculate shapes. The crystal structures have been graphicalized using Mercury 4.2.0 and Diamond (version 2).⁵ The disordered electron density was hidden using the OLEX2 Solvent Mask method, which is comparable to PLATON/SQUEEZE.

4.2.2 Reagents and general procedures

Tertiary-butyl phosphonic acid was prepared by earlier reported method. Common reagents and solvents were bought from businesses. All the resulted products were kept under vacuum for a longer period before it being characterised.

4.2.3 General Synthetic procedures for compound 1 to 6

The general synthetic methods for this preparation follow by taking mixedantimonate phosphonate proligand 1.33 equivalents to tin metal precursor and using as coligand reacting with n-butyl tin hydroxide oxide in presence of methanol as solvent. After stirring in room temperature condition for half an hour the reaction mixture was transferred to 23 ml teflon lined autoclave stainless steels not filling up to the brim of the vial.⁶ The reaction was carried out in solvothermal condition by properly sealing the bomb. The compound 1 and 2 were heated up to 100°C for 12h are then cooled for 48h slowly. After almost three days of heating -cooling conditions the vials are kept in room temperature conditions for two days, slowly X-ray quality coloured crystals were being obtained. Whereas for Compounds 3-6 the temperature was fixed to 150°C for same time span within similar reaction conditions.

Compound 1: $[((n-Bu) Sn)_4(RPO_3H_8) O_2]$ (0.050 g, 0.0545 mmol), tetrahydrate cobalt acetate (0.009 g, 0.0724mmol) and pyridine (0.05ml) were used. Dark blue coloured crystals formed upon slow evaporation of the cooled reaction mixture. I.R values in cm⁻¹ 2960 (s), 2926 (s), 2856 (s), 1451(s), 1259(s), 1080(s), 1015(s), 976(s), 795(s), 663(s) cm⁻¹.

Compound 2: $[((n-Bu) Sn)_4(RPO_3H_8) O_2]$ (0.050 g, 0.0545 mmol), dihydrate zinc acetate (0.015 g, 0.0724mmol) and pyridine (0.05ml) were used. White coloured crystals formed upon slow evaporation of the cooled reaction mixture. I.R values in cm⁻¹: 1545, 1202, 1043, 986, 752, 685 cm⁻¹. All of these peaks are sharp peaks.

Compound 3: [((*n*-Bu) Sn)₄(RPO₃H₈) O₂] (0.050 g, 0.0545 mmol), hexahydrate dysprosium nitrate (0.017, 0.0724mmol) and pyridine (0.05ml) were used. White coloured crystals formed upon slow evaporation of the cooled reaction mixture. I.R values in cm⁻¹: 2954(s), 1097(s), 1042(s), 972(s), 662(s).

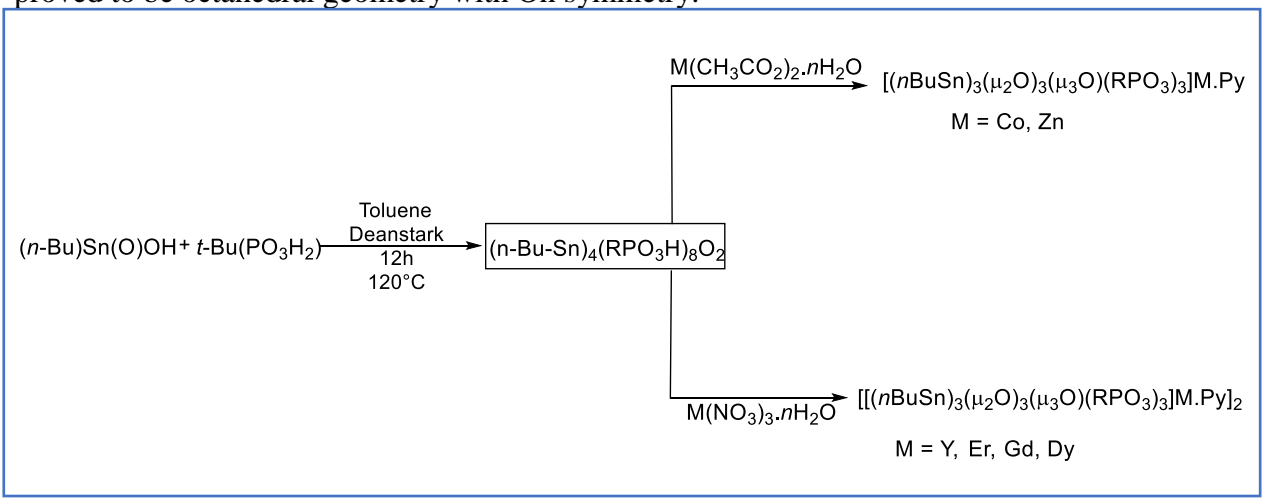
Compound 4: [((*n*-Bu) Sn)₄(RPO₃H₈) O₂] (0.050 g, 0.0545 mmol), hexahydrate Erbium nitrate (0.017 g, 0.0724mmol) and pyridine (0.05ml) were used. White coloured crystals formed upon slow evaporation of the cooled reaction mixture. I.R values in cm⁻¹: 2952(s), 1082(s), 947(s), 656(s).

Compound 5: [((*n*-Bu) Sn)₄(RPO₃H₈) O₂] (0.050 g, 0.0545 mmol), hexahydrate Gadolinium nitrate (0.016, 0.0724mmol) and pyridine (0.05ml) were used. White coloured crystals formed upon slow evaporation of the cooled reaction mixture. I.R values in cm⁻¹: 2956(s), 1114(s), 982(s), 660(s).

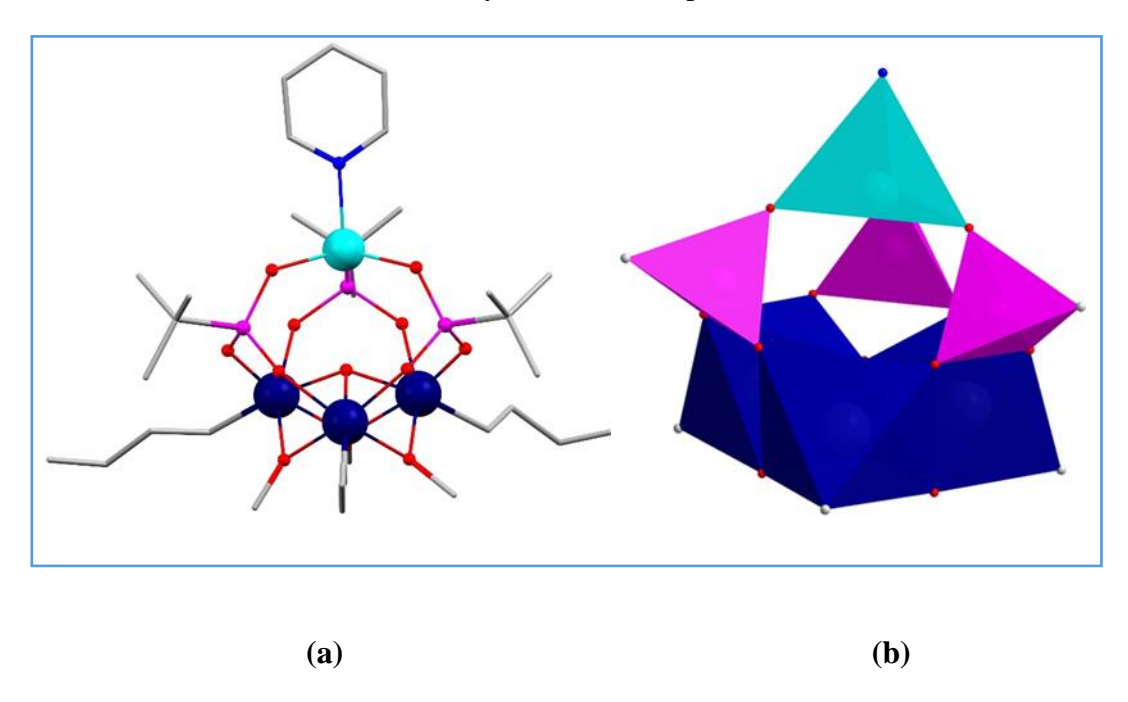
Compound 6: [((*n*-Bu) Sn)₄(RPO₃H₈) O₂] (0.050 g, 0.0545 mmol), hexahydrate Yttrium nitrate (0.011, 0.0724mmol) and pyridine (0.05ml) were used. White coloured crystals formed upon slow evaporation of the cooled reaction mixture. I.R values in cm⁻¹: 2952, 1477, 1067, 986, 831, 657, 553 cm⁻¹. All these reported peaks are sharp peaks.

4.3 Results and discussion

Compound 1 was synthesized by reaction of [(n-Bu-Sn)₄(RPO₃H)₈O₂] with Cobalt (II) acetate tetrahydrate in 1:1.33 ratios in presence of pyridine under solvothermal condition. Dark purple colour crystal was grown by cooling in room temperature condition for extra two days. Compound 1 crystallizes in $P2_1/n$ in monoclinic space group. Data from crystallography and the parameters of the bond metric of compound 4.1 to 4.3 are given in the table 4.1 and from compound 4.4 to 4.6 are given in table 4.2. Single crystal X-ray characterization reveals the formation of a cobalt-organostanoxane distorted tetrahedral oxo cluster having the formula $[(n-BuSn)_3(\mu_2O_3)(\mu_3O)(RPO_3)_3]CoPy]$. The molecular structure of compound 4.1 (Fig 4.1) reveals the formation of a heart shaped Sn₃Co core held together by three phosphonate and one Co metal ions. Interestingly, through the analysis of the crystal structure we have confirmed one oxo bridged crown shape Sn triangular motif coordinating to each other by μ_2 -O of methoxide ions most probable extracted from solvent (methanol). The structure has three different types of phosphonates: each phosphonate bound to two Sn metal ions through μ_2 oxo bridges from phosphonate O. All three phosphonate ions are binding to that only one transition metal, herein Co metal ion through μ_3 -O (1.222) and for Sn metal ion the coordination of different donor ligands is 3.1111. Out of all the compounds from 4.1 to 4.6 are paramagnetic metal except compound 4.2 the organostannoxane proligand with Zinc metal ion, which can show 119 isotope of Sn NMR and ³¹P NMR signals, ³¹P shows a sharp peak at 32.56 and 33.28 ppm; while ¹¹⁹Sn NMR gives a multiplet value around -512.08 ppm. Each Sn centre is hexa coordinated attributing to Oh symmetry. In each shape calculations, it has been concluded that in both Compound 4.1 and 4.3 all tin metals are of octahedron geometry. In case of compound 4.1 surrounding Co the geometry is vacant trigonal bipyramidal with C3V symmetry and in lanthanide mixed valence metal clusters surround all lanthanide metal ion the geometry is proved to be octahedral geometry with Oh symmetry.



Scheme 4.1 Synthesis of complex 1 to 6



4.1 Fig (a) Molecular structure of 1; colour code Sn Dark blue, Co cyan, P purple, N light blue, O red, C light grey. (b) Polyhedral representation of compound 1.

Compound 4.3 – 4.6 were synthesized by stannoxo phosphonate proligand [(n-Bu- $Sn)_4(RPO_3H)_8O_2$ with hydrated lanthanide nitrate salts (Ln (NO₃)₃. nH_2O) (Ln = Dy, Gd, Er, Y) applying solvothermal conditions to pyridine as a base in methanol (Scheme −1). Single crystals are formed after cooling the solvothermal heated reaction mixture for more days at room temperature conditions. Compound 4.3 - 4.6 crystallized with $P2_1/n$ in monoclinic space group, which is a dimer of Compound-1. The table 4.1-4.2 contains the bond metric parameters and crystallographic data for 4.3 - 4.6. Since each cluster is isostructural, compound - 4.3 will be described in detail. The structure in solid state of compound 4.3 shows that the development of three μ_2 oxo bridged two crown shaped tin triangular core motifs holding two Dy metal ions connecting via two organo phosphonate ligand core systems. Interestingly, these two triangular tin motifs are self-condensed connecting through one μ_3 oxo bridged oxygen atom. In each tin triangular motif each of the three tin metal ions are μ_2 oxo bridged from methoxy group might be from methanol solvent. Eight phosphonates have been coordinated to the metal ions in the structure, out of which six are coordinated to Sn metal ions three-three in each side of the two tin triangular motifs whereas other two are coordinated to the two lanthanide metal ions through tertiary butyl phosphonate µ2 oxo bridges. In each asymmetric unit two pyridine molecules have been coordinated to the lanthanide metal ions through N atom. The two phosphonate ions connected to the two lanthanide metal ions

through double bonded oxygen atom and both hydroxide groups are intact without being deprotonated. The same phosphonate groups while coordinated to two crown shaped triangular tin motif in each side of the two lanthanide metal ions the phosphonate ions have undergone deprotonation and one side coordinated to the tin metal ion and other side coordinated to the lanthanide metal ions.

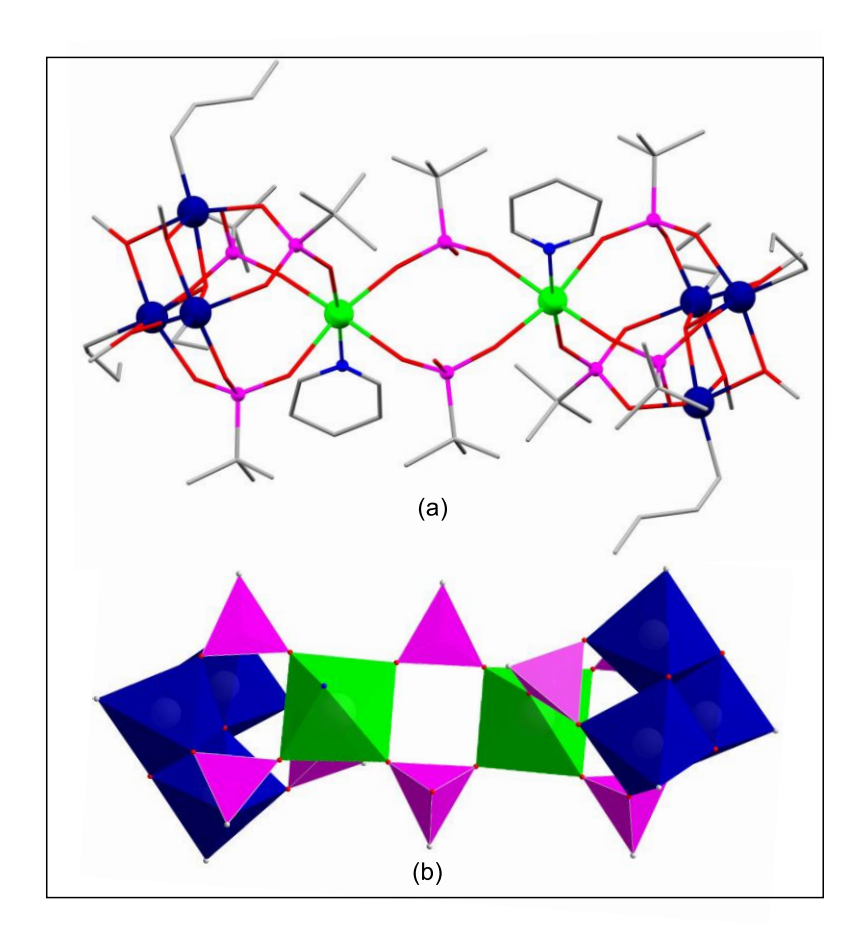


Fig 4.2 Molecular structure of compound 3 colour code Sn Dark blue, Dy light green, P purple, N light blue, O red, C light grey (Hydrogens have been omitted for clarity purpose). (b) Polyhedral representation of compound 3; green octahedra represents two DyNO₄ units, two dark blue octahedra represents SnCO₅, six purple tetrahedra unit represents CPO₃. The purity check of the complexes in the synthesized clusters has been done through EDAX also known as energy-dispersive X-ray spectroscopy, and it has been proved that all the structures are completely pure.

4.4 Conclusion:

In case of compound 1 and 2 one of the tin metal ions from cluster $[((n-Bu)Sn)_4(RPO_3H_8)O_2]$ is being substituted by one Co metal ion and Zn metal ion in compound

1 and 2 respectively, hence the reaction of hydrated transition metal salts with organo phosphonate organo-stannoxane as proligand have led to the isolation of a distorted tetrahedral structure. The cluster can be anticipated to show a good magnetic as well as optical properties. Again, in case of compound 3 - 6 the reaction of the tin proligand with hydrated lanthanide salts isolates a dimer of the distorted tetrahedral structure. The reported mixed valence dimers each metal ions are hexa coordinated. It has been noticed that the mixture of mixed valence coligand system lead to assembly of novel structural architecture.

References:

- (a)Chandrasekhar, V.; Kundu, S.; Kundu, S.; Kundu, S.; Kundu, S.; Kundu, S.;
 Subramaniam, K. Cryst. Growth Des. 2013, 13, 4, 1665–1675. (b) Jami, A. K.; Prabhu,
 M. S. R.; Baskar, V. Organometallics. 2010, 29, 5, 1137–1143.
- 2) Chandrasekhar, V.; Baskar, V.; Steiner, A.; Zacchini, S. *Organometallics*. 2004, 23, 6, 1390–1395.
- 3) Navaneetha, T.; Ali, A.; Ramana, C. V.; Ramana, C. V.; Baskar, V. *Inorg. Chem.* 2023, 62, 13, 5237–5247.
- 4) Ugandhar, U.; Navaneetha, T.; Ali, J.; Mondal, S.; Vaitheeswaran, G.; Baskar, V. *Inorg. Chem.* 2020, 59, 10, 6689–6696.
- 5) Navaneetha, T.; Ugandhar, U.; Samuel C.; Guizouarn, T.; Pointillart, F.; Raghunathan, R.; Baskar, V. *Dalton Trans.*, 2023,52, 9328-93365.
- 6) Sheldrick, G. M. Acta Crystallogr. Sect. A Found. Crystallogr. 2015, 71, 3–8.
- 7) Dolomanov, O. V.; Bourhis, L. J.; Gildea, R. J.; Howard, J. A. K.; Puschmann, H. *J. Appl. Crystallogr.* **2009**, *42*, 339–341,
- 8) Sheldrick, G. M. Crystal Structure Refinement with SHELXL. *Acta Crystallogr. Sect. C Struct. Chem.* **2015**, *71*, 3–8.

Spectroscopic Data

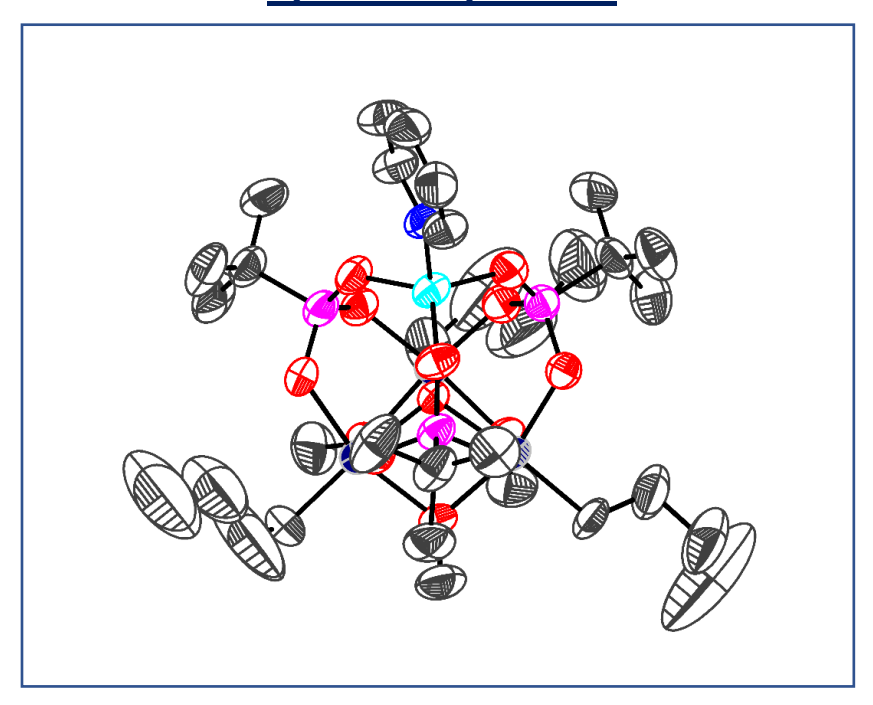


Figure 4.3 ORTEP view of 4.1 with thermal ellipsoid 30% probability.

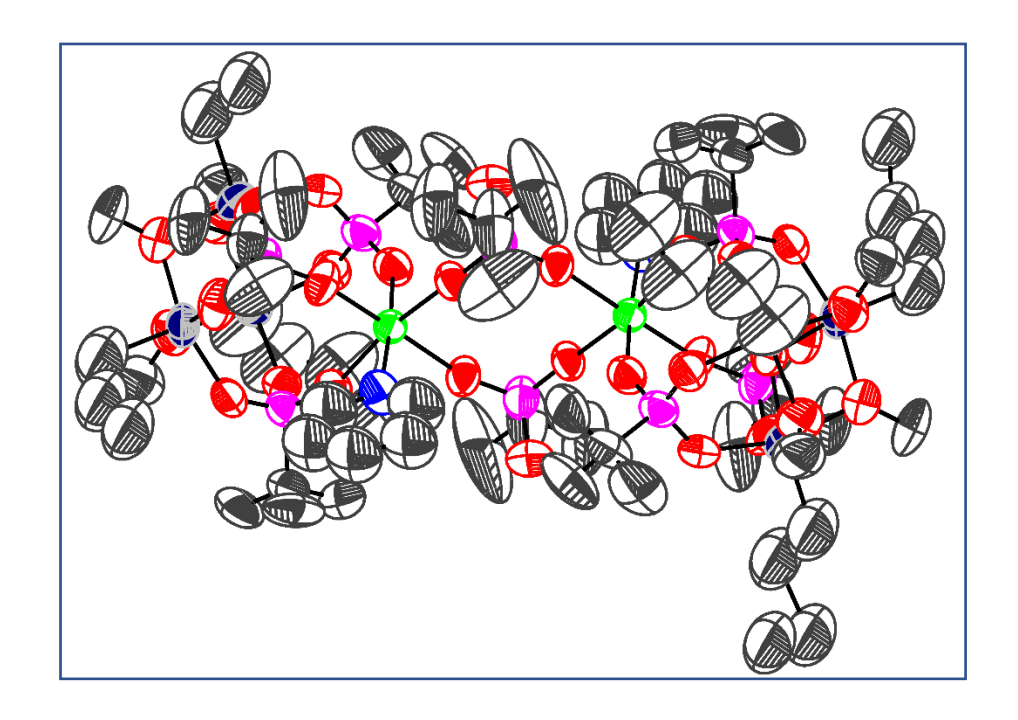


Figure 4.4 ORTEP view of 4.3 with thermal ellipsoid 30% probability.

 Table 4.1 Crystal data and structure refinement parameters for 4.1-4.3

Identification code	Compound 1	Compound 2	Compound 3
Empirical formula	C ₃₂ H ₇₁ CoNO ₁₃ P ₃ Sn ₃	C ₃₂ NO ₁₃ P ₃ Sn ₃ Zn	C ₇₂ H ₁₁₆ Dy ₂ N ₂ O ₃₂ P ₈ Sn ₆
Formula weight	1185.80	1120.68	2806.56
Temperature/K	299.01(10)	298.4(2)	293.9(9)
Crystal system	monoclinic	monoclinic	monoclinic
Space group	P2 ₁ /n	P2 ₁ /n	P2 ₁ /n
a/Å	10.7493(2)	11.7003(2)	13.1851(4)
b/Å	26.5144(5)	12.2355(2)	18.6821(7)
c/Å	17.1851(3)	35.0268(8)	22.9992(8)
α/°	90	90	90
β/°	95.072(2)	92.255(2)	91.520(4)
γ/°	90	90	90
Volume/ų	4878.77(16)	5010.52(16)	5663.3(3)
Z	4	4	2
$\rho_{calc}g/cm^3$	1.614	1.486	1.646
μ/mm ⁻¹	2.003	2.094	2.780
F(000)	2384.0	2112.0	2740.0
Crystal size/mm³	$0.4 \times 0.06 \times 0.02$	0.6 × 0.04 × 0.02	0.6 × 0.4 × 0.2
Radiation	Mo Kα (λ = 0.71073)	Μο Κα (λ = 0.71073)	Μο Κα (λ = 0.71073)
20 range for data collection/°	3.886 to 53.872	4.062 to 54.122	4.142 to 54.176
Index ranges	-13 ≤ h ≤ 13, -33 ≤ k ≤ 33, -20 ≤ l ≤ 21	-14 ≤ h ≤ 14, -15 ≤ k ≤ 14, -38 ≤ l ≤ 44	-16 ≤ h ≤ 16, -18 ≤ k ≤ 23, -28 ≤ l ≤ 28
Reflections collected	58348	60429	37947
Independent reflections	10189 [R _{int} = 0.0376, R _{sigma} = 0.0287]	10490 [R _{int} = 0.0603, R _{sigma} = 0.0537]	10603 [R _{int} = 0.0739, R _{sigma} = 0.0750]
Data/restraints/parameters	10189/9/502	10490/0/478	10603/0/481
Goodness-of-fit on F ²	1.054	1.040	1.043
Final R indexes [I>=2σ (I)]	R ₁ = 0.0419, wR ₂ = 0.0924	R ₁ = 0.0667, wR ₂ = 0.1645	R ₁ = 0.0696, wR ₂ = 0.1902
Final R indexes [all data]	R ₁ = 0.0722, wR ₂ = 0.1056	R ₁ = 0.1078, wR ₂ = 0.1904	R ₁ = 0.1257, wR ₂ = 0.2268

Largest diff. peak/hole / e Å ⁻³	0.57/-0.80	1.76/-0.91	1.36/-1.00

Table 4.2 Crystal data and structure refinement parameters for 4.4 - 4.6

Identification code	Compound 4	Compound 5	Compound 6
Empirical formula	C ₇₀ Gd ₂ N ₂ O ₃₄ P ₈ Sn ₆	$C_{66.58}Er_2N_2O_{32}P_8Sn_6$	C ₇₂ N ₄ O ₃₂ P ₈ Sn ₆ Y ₂
Formula weight	2687.328	2633.95	2570.48
Temperature/K	100.0(4)	298.7(2)	296(2)
Crystal system	monoclinic	monoclinic	monoclinic
Space group	P2 ₁ /n	P2₁/n	P2₁/n
a/Å	13.1690(2)	13.0976(5)	13.1951(16)
b/Å	19.6785(4)	18.0504(8)	18.681(2)
c/Å	21.8520(4)	23.4021(11)	23.034(3)
α/°	90	90	90
β/°	90.434(2)	90.964(4)	90
γ/°	90	90	90
Volume/ų	5662.70(18)	5531.9(4)	5677.9(13)
Z	2	2	2
$\rho_{calc}g/cm^3$	1.576	1.581	1.503
μ/mm ⁻¹	2.631	3.007	2.483
F(000)	2504.8	2451.0	2428.0
Crystal size/mm ³	0.06 × 0.04 × 0.02	0.08 × 0.06 × 0.04	0.06 × 0.04 × 0.02
Radiation	Mo Kα (λ = 0.71073)	Mo Kα (λ = 0.71073)	Mo Kα (λ = 0.71073)

20 range for data collection/°	4.14 to 54.04	3.842 to 53.896	3.78 to 54.548
Index ranges	-16 ≤ h ≤ 16, -25 ≤ k ≤ 24, -27 ≤ l ≤ 27	-16 ≤ h ≤ 16, -22 ≤ k ≤ 22, -29 ≤ l ≤ 28	-16 ≤ h ≤ 16, -23 ≤ k ≤ 23, -28 ≤ l ≤ 29
Reflections collected	69128	65213	71129
Independent reflections	11834 [$R_{int} = 0.0891$, $R_{sigma} = 0.0520$]	11541 [R _{int} = 0.1151, R _{sigma} = 0.1490]	11909 [R _{int} = 0.1276, R _{sigma} = 0.1725]
Data/restraints/parameters	11834/0/550	11541/0/524	11909/0/559
Goodness-of-fit on F ²	1.061	1.015	0.951
Final R indexes [I>=2σ (I)]	R ₁ = 0.0825, wR ₂ = 0.2123	R ₁ = 0.1072, wR2 = 0.2608	R ₁ = 0.0798, wR ₂ = 0.1931
Final R indexes [all data]	R ₁ = 0.1108, wR ₂ = 0.2383	R ₁ = 0.2624, wR2 = 0.3614	R ₁ = 0.2427, wR ₂ = 0.2652
Largest diff. peak/hole / e Å ⁻	4.70/-3.64	2.12/-0.80	0.79/-0.71

Table 4.5 Selected bond lengths (Å) and bond angle (deg) parameters of 4.1

Sn2-O13	2.082(5)	Sn3-07	2.067(7)
Sn2-O5	2.057(6)	Sn3-O6	2.151(7)
Sn2-O11	2.068(6)	Sn3-O9	2.116(11)
Sn2-O10	2.128(6)	Sn3-O28	2.067(7)
Sn2-O14	2.147(6)	Co1-O12	1.945(7)
Sn2-C15	2.145(9)	Co1-O2	1.924(6)
Sn2-O13	2.082(5)	Co1-O3	1.923(6)
Sn1-O13	2.079(6)	Co1-N1	2.054(8)
Sn1-O4	2.049(7)	O12-Co1-N1	103.7(3)
Sn1-08	2.084(7)	O2-Co1- O12	113.8(3)
Sn1-O14	2.150(7)	O2-Co1-N1	98.8(3)
Sn1-O9	2.159(7)	O3-Co1-O12	116.7(3)
Sn1-O27	2.139(12)	O3-Co1-O2	119.7(3)

Sn3-O13	2.059(5)	O3-Co1-N1	99.2(3)
Sn3-O10	2.177(6)		

 $\textbf{Table 4.6} \ \ \textbf{Selected bond lengths (Å) and bond angle (deg) parameters of 4.2}$

Sn3-O5	2.079(5)	O5-Sn2-C10	172.6(4)
Sn3-O9	2.059(6)	O10-Sn2-O5	85.6(2)
Sn3-06	2.070(6)	O10-Sn2-O12	93.5(2)
Sn3-O2	2.130(6)	O10-Sn2-O8	86.5(2)
Sn3-08	2.145(6)	O10-Sn2-O3	160.5(2)
Sn3-C14	2.140(9)	O10-Sn2-C10	101.2(4)
Sn2-O5	2.075(5)	O12-Sn2-O8	162.5(2)
Sn2-O10	2.051(6)	O12-Sn2-O3	87.0(3)
Sn2-O12	2.087(6)	O12-Sn2-C10	95.7(4)
Sn2-08	2.150(6)	O8-Sn2-O3	87.2(3)
Sn2-O3	2.153(7)	C10-Sn2-O8	101.5(4)
Sn2-C10	2.138(11)	O6-Sn3-C14	97.3(3)
Sn1-05	2.060(5)	O2-Sn3-O8	87.3(3)
Sn1-O2	2.176(6)	O2-Sn3-C14	98.7(3)
Sn1-04	2.076(6)	C14-Sn3-O8	99.1(3)
Sn1-O1	2.074(6)	O5-Sn2-O12	86.7(2)
Sn1-O3	2.150(7)	O5-Sn2-O8	75.8(2)
Sn1-C6	2.114(11)	O5-Sn2-O3	75.0(2)
Zn1-O11	1.946(6)	O9-Sn3-O2	162.3(2)
Zn1-07	1.922(6)	O9-Sn3-O8	87.0(2)
Zn1-O13	1.926(6)	O9-Sn3-C14	98.7(3)
Zn1-N1	2.046(8)	O6-Sn3-O5	87.4(2)
O5-Sn3-O2	75.9(2)	O6-Sn3-O2	86.8(2)
O5-Sn3-O8	75.8(2)	O6-Sn3-O8	163.2(2)
O5-Sn3-C14	172.7(3)	O9-Sn3-O6	93.9(2)

O9-Sn3-O5	86.4(2)	

Table 4.7 Selected bond lengths (Å) and bond angle (deg) parameters of 4.3

Dy1-021 2.244(6) O21-Dy1-N1 86.3(3) Dy1-012 2.219(7) O12-Dy1-O21 166.9(3) Dy1-03 2.209(7) O12-Dy1-O5 94.9(3) Dy1-O5 2.242(8) O12-Dy1-O4 96.4(3) Dy1-O4 2.221(8) O12-Dy1-N1 81.3(3) Dy1-N1 2.448(11) O3-Dy1-O21 85.1(3) Sn3-Sn1 3.2978(14) O3-Dy1-O21 85.1(3) Sn3-O13 2.043(7) O3-Dy1-O12 90.2(3) Sn3-O14 2.056(7) O3-Dy1-O5 166.6(3) Sn3-O14 2.074(8) O3-Dy1-O4 95.3(3) Sn3-O11 2.074(8) O3-Dy1-N1 87.8(4) Sn3-O16 2.159(9) O5-Dy1-N1 87.2(3) Sn3-O10 2.148(10) O5-Dy1-N1 80.8(4) Sn1-O13 2.059(7) O4-Dy1-O21 96.2(3) Sn1-O15 2.049(8) O4-Dy1-O5 96.4(3) Sn1-O16 2.149(9) O4-Dy1-N1 176.2(3) Sn1-O8 2.138(10) O13-Sn3	
Dy1-O3 2.209(7) O12-Dy1-O5 94.9(3) Dy1-O5 2.242(8) O12-Dy1-O4 96.4(3) Dy1-O4 2.221(8) O12-Dy1-N1 81.3(3) Dy1-N1 2.448(11) O3-Dy1-O21 85.1(3) Sn3-Sn1 3.2978(14) O3-Dy1-O12 90.2(3) Sn3-O13 2.043(7) O3-Dy1-O5 166.6(3) Sn3-O14 2.056(7) O3-Dy1-O4 95.3(3) Sn3-O11 2.074(8) O3-Dy1-N1 87.8(4) Sn3-O16 2.159(9) O5-Dy1-N1 87.2(3) Sn3-O10 2.148(10) O5-Dy1-N1 80.8(4) Sn1-O13 2.059(7) O4-Dy1-O21 96.2(3) Sn1-O15 2.049(8) O4-Dy1-O5 96.4(3) Sn1-O16 2.149(9) O4-Dy1-N1 176.2(3) Sn1-O8 2.138(10) O13-Sn3-Sn1 36.7(2) Sn1-C4 2.18(3) O13-Sn3-O14 87.3(3)	
Dy1-O5 2.242(8) O12-Dy1-O4 96.4(3) Dy1-O4 2.221(8) O12-Dy1-N1 81.3(3) Dy1-N1 2.448(11) O3-Dy1-O21 85.1(3) Sn3-Sn1 3.2978(14) O3-Dy1-O12 90.2(3) Sn3-O13 2.043(7) O3-Dy1-O5 166.6(3) Sn3-O14 2.056(7) O3-Dy1-O4 95.3(3) Sn3-O11 2.074(8) O3-Dy1-N1 87.8(4) Sn3-O16 2.159(9) O5-Dy1-O21 87.2(3) Sn3-O10 2.148(10) O5-Dy1-N1 80.8(4) Sn1-O13 2.059(7) O4-Dy1-O21 96.2(3) Sn1-O15 2.049(8) O4-Dy1-O5 96.4(3) Sn1-O16 2.149(9) O4-Dy1-N1 176.2(3) Sn1-O8 2.138(10) O13-Sn3-Sn1 36.7(2) Sn1-C4 2.18(3) O13-Sn3-O14 87.3(3)	
Dy1-O4 2.221(8) O12-Dy1-N1 81.3(3) Dy1-N1 2.448(11) O3-Dy1-O21 85.1(3) Sn3-Sn1 3.2978(14) O3-Dy1-O12 90.2(3) Sn3-O13 2.043(7) O3-Dy1-O5 166.6(3) Sn3-O14 2.056(7) O3-Dy1-O4 95.3(3) Sn3-O11 2.074(8) O3-Dy1-N1 87.8(4) Sn3-O16 2.159(9) O5-Dy1-O21 87.2(3) Sn3-O10 2.148(10) O5-Dy1-N1 80.8(4) Sn1-O13 2.059(7) O4-Dy1-O21 96.2(3) Sn1-O15 2.049(8) O4-Dy1-O5 96.4(3) Sn1-O16 2.149(9) O4-Dy1-N1 176.2(3) Sn1-O8 2.138(10) O13-Sn3-Sn1 36.7(2) Sn1-C4 2.18(3) O13-Sn3-O14 87.3(3)	
Dy1-N1 2.448(11) O3-Dy1-O21 85.1(3) Sn3-Sn1 3.2978(14) O3-Dy1-O12 90.2(3) Sn3-O13 2.043(7) O3-Dy1-O5 166.6(3) Sn3-O14 2.056(7) O3-Dy1-O4 95.3(3) Sn3-O11 2.074(8) O3-Dy1-N1 87.8(4) Sn3-O16 2.159(9) O5-Dy1-O21 87.2(3) Sn3-O10 2.148(10) O5-Dy1-N1 80.8(4) Sn1-O13 2.059(7) O4-Dy1-O21 96.2(3) Sn1-O15 2.049(8) O4-Dy1-O5 96.4(3) Sn1-O16 2.149(9) O4-Dy1-N1 176.2(3) Sn1-O8 2.138(10) O13-Sn3-Sn1 36.7(2) Sn1-C4 2.18(3) O13-Sn3-O14 87.3(3)	
Sn3-Sn1 3.2978(14) O3-Dy1-O12 90.2(3) Sn3-O13 2.043(7) O3-Dy1-O5 166.6(3) Sn3-O14 2.056(7) O3-Dy1-O4 95.3(3) Sn3-O11 2.074(8) O3-Dy1-N1 87.8(4) Sn3-O16 2.159(9) O5-Dy1-O21 87.2(3) Sn3-O10 2.148(10) O5-Dy1-N1 80.8(4) Sn1-O13 2.059(7) O4-Dy1-O21 96.2(3) Sn1-O15 2.049(8) O4-Dy1-O5 96.4(3) Sn1-O16 2.149(9) O4-Dy1-N1 176.2(3) Sn1-O8 2.138(10) O13-Sn3-Sn1 36.7(2) Sn1-C4 2.18(3) O13-Sn3-O14 87.3(3)	
Sn3-O13 2.043(7) O3-Dy1-O5 166.6(3) Sn3-O14 2.056(7) O3-Dy1-O4 95.3(3) Sn3-O11 2.074(8) O3-Dy1-N1 87.8(4) Sn3-O16 2.159(9) O5-Dy1-O21 87.2(3) Sn3-O10 2.148(10) O5-Dy1-N1 80.8(4) Sn1-O13 2.059(7) O4-Dy1-O21 96.2(3) Sn1-O15 2.049(8) O4-Dy1-O5 96.4(3) Sn1-O16 2.149(9) O4-Dy1-N1 176.2(3) Sn1-O8 2.138(10) O13-Sn3-Sn1 36.7(2) Sn1-C4 2.18(3) O13-Sn3-O14 87.3(3)	
Sn3-O14 2.056(7) O3-Dy1-O4 95.3(3) Sn3-O11 2.074(8) O3-Dy1-N1 87.8(4) Sn3-O16 2.159(9) O5-Dy1-O21 87.2(3) Sn3-O10 2.148(10) O5-Dy1-N1 80.8(4) Sn1-O13 2.059(7) O4-Dy1-O21 96.2(3) Sn1-O15 2.049(8) O4-Dy1-O5 96.4(3) Sn1-O16 2.149(9) O4-Dy1-N1 176.2(3) Sn1-O8 2.138(10) O13-Sn3-Sn1 36.7(2) Sn1-C4 2.18(3) O13-Sn3-O14 87.3(3)	
Sn3-O11 2.074(8) O3-Dy1-N1 87.8(4) Sn3-O16 2.159(9) O5-Dy1-O21 87.2(3) Sn3-O10 2.148(10) O5-Dy1-N1 80.8(4) Sn1-O13 2.059(7) O4-Dy1-O21 96.2(3) Sn1-O15 2.049(8) O4-Dy1-O5 96.4(3) Sn1-O16 2.149(9) O4-Dy1-N1 176.2(3) Sn1-O8 2.138(10) O13-Sn3-Sn1 36.7(2) Sn1-C4 2.18(3) O13-Sn3-O14 87.3(3)	
Sn3-O16 2.159(9) O5-Dy1-O21 87.2(3) Sn3-O10 2.148(10) O5-Dy1-N1 80.8(4) Sn1-O13 2.059(7) O4-Dy1-O21 96.2(3) Sn1-O15 2.049(8) O4-Dy1-O5 96.4(3) Sn1-O16 2.149(9) O4-Dy1-N1 176.2(3) Sn1-O8 2.138(10) O13-Sn3-Sn1 36.7(2) Sn1-C4 2.18(3) O13-Sn3-O14 87.3(3)	
Sn3-O10 2.148(10) O5-Dy1-N1 80.8(4) Sn1-O13 2.059(7) O4-Dy1-O21 96.2(3) Sn1-O15 2.049(8) O4-Dy1-O5 96.4(3) Sn1-O16 2.149(9) O4-Dy1-N1 176.2(3) Sn1-O8 2.138(10) O13-Sn3-Sn1 36.7(2) Sn1-C4 2.18(3) O13-Sn3-O14 87.3(3)	
Sn1-O13 2.059(7) O4-Dy1-O21 96.2(3) Sn1-O15 2.049(8) O4-Dy1-O5 96.4(3) Sn1-O16 2.149(9) O4-Dy1-N1 176.2(3) Sn1-O8 2.138(10) O13-Sn3-Sn1 36.7(2) Sn1-C4 2.18(3) O13-Sn3-O14 87.3(3)	
Sn1-O15 2.049(8) O4-Dy1-O5 96.4(3) Sn1-O16 2.149(9) O4-Dy1-N1 176.2(3) Sn1-O8 2.138(10) O13-Sn3-Sn1 36.7(2) Sn1-C4 2.18(3) O13-Sn3-O14 87.3(3)	
Sn1-O16 2.149(9) O4-Dy1-N1 176.2(3) Sn1-O8 2.138(10) O13-Sn3-Sn1 36.7(2) Sn1-C4 2.18(3) O13-Sn3-O14 87.3(3)	
Sn1-O8 2.138(10) O13-Sn3-Sn1 36.7(2) Sn1-C4 2.18(3) O13-Sn3-O14 87.3(3)	
Sn1-C4 2.18(3) 013-Sn3-O14 87.3(3)	
Sn1-O7 2.043(10) O13-Sn3-O11 85.9(3)	
Sn2-O13 2.043(7) O13-Sn3-O16 75.2(3)	
Sn2-O6 2.052(10) O13-Sn3-O10 74.7(4)	
Sn2-O9 2.089(9) O14-Sn3-Sn1 78.7(2)	
Sn2-O10 2.142(11) O14-Sn3-O11 93.8(3)	
Sn2-O8 2.119(10) O14-Sn3-O16 87.4(3)	
Sn2-C1 2.22(3) O14-Sn3-O10 161.9(4)	
Dy1-O21 2.244(6) O11-Sn3-Sn1 121.8(2)	
Dy1-O12 2.219(7) O11-Sn3-O16 161.0(3)	
Dy1-O3 2.209(7) O11-Sn3-O10 86.7(4)	
Dy1-O5 2.242(8) O16-Sn3-Sn1 39.9(2)	
Dy1-O4 2.221(8) O10-Sn3-Sn1 85.6(3)	
Dy1-N1 2.448(11) O10-Sn3-O16 86.3(4)	

Table 4.8 Selected bond lengths (Å) and bond angle (deg) parameters of 4.4

		[,
Er1091	2.244(13)	O13-Sn3-Sn1	36.7(2)
Er1010	2.245(14)	O13-Sn3-O14	87.3(3)
Er1011	2.199(13)	O13-Sn3-O11	85.9(3)
Er1012	2.227(14)	O13-Sn3-O16	75.2(3)
Er1014	2.224(13)	O13-Sn3-O10	74.7(4)
Er1N1	2.45(2)	O14-Sn3-Sn1	78.7(2)
Sn2Sn4	3.283(3)	O14-Sn3-O11	93.8(3)
Sn3-Sn1	3.2978(14)	O14-Sn3-O16	87.4(3)
Sn3-O13	2.043(7)	O14-Sn3-O10	161.9(4)

Sn3-O14	2.056(7)	O11-Sn3-Sn1	121.8(2)
Sn3-O11	2.074(8)	O11-Sn3-O16	161.0(3)
Sn3-O16	2.159(9)	O11-Sn3-O10	86.7(4)
Sn3-O10	2.148(10)	O16-Sn3-Sn1	39.9(2)
Sn1-O13	2.059(7)	O10-Sn3-Sn1	85.6(3)
Sn1-O15	2.049(8)	O10-Sn3-O16	86.3(4)
Sn1-O16	2.149(9)	O13-Sn3-Sn1	36.7(2)
Sn1-08	2.138(10)	O2-Er-1O-9 ¹	164.6(5)
Sn1-C4	2.18(3)	02-Er-102	89.8(5)
Sn1-07	2.043(10)	02-Er-103	94.2(5)
Sn2-O13	2.043(7)	02-Er-104	97.9(5)
Sn2-O6	2.052(10)	O2-Er-1N1	78.7(6)
Sn2-O9	2.089(9)	03-Er-109 ¹	88.5(5)
Sn2-O10	2.142(11)	03-Er-105	169.5(5)

Table 4.9 Selected bond lengths (Å) and bond angle (deg) parameters of 4.5

Gd1-O3	2.240(6)	O2-Gd1-O3	94.1(3)
Gd1-O2	2.289(7)	O1-Gd1-O3	165.8(3)
Gd1-O1	2.265(7)	O1-Gd1-O2	89.3(3)
Gd1-O61	2.262(8)	O6 ¹ -Gd1-O3	87.4(3)
Gd1-O4	2.222(9)	O6 ¹ -Gd-O2	166.0(3)
Gd1-N1	2.486(11)	O6 ¹ -Gd1-O1	86.0(3)
Sn2-Sn3	3.2922(13)	O4-Gd1-O3	98.4(3)
Sn2-O14	2.048(7)	O4-Gd1-O2	94.8(3)
Sn2-O10	2.084(8)	04-Gd1-O1	95.1(3)
Sn2-O12	2.087(9)	O4-Gd1-O6 ¹	98.7(3)
Sn2-O16	2.139(10)	N1-Gd1-O3	78.6(3)
Sn2-O15	2.139(10)	N1Gd1-O2	81.6(3)
Sn2-C30	2.155(14)	N1-Gd1-O1	88.3(3)
Sn3-O14	2.037(8)	N1-Gd1-O6 ¹	85.0(3)
Sn3-O9	2.077(9)	N1-Gd1-O4	175.1(3)
Sn3-07	2.064(8)	O2-Gd1-O3	94.1(3)
Sn3-O16	2.152(9)	01-Gd1-O3	165.8(3)
Sn3-O17	2.181(10)	O1-Gd1-O2	89.3(3)
Sn2-Sn3	3.2922(13)	O61-Gd1-O3	87.4(3)
Sn2-O14	2.048(7)	O61-Gd-O2	166.0(3)
Sn2-O10	2.084(8)	O61-Gd1-O1	86.0(3)
Sn2-O12	2.087(9)	O4-Gd1-O3	98.4(3)
Sn2-O16	2.139(10)	O4-Gd1-O2	94.8(3)
Sn2-O15	2.139(10)	O4-Gd1-O1	95.1(3)
Sn2-C30	2.155(14)	O4-Gd1-O6 ¹	98.7(3)
Sn3-O14	2.037(8)	N1-Gd1-O3	78.6(3)
Sn3-O9	2.077(9)	N1Gd1-O2	81.6(3)
Sn3-07	2.064(8)	N1-Gd1-O1	88.3(3)
Sn3-O16	2.152(9)	N1-Gd1-O6 ¹	85.0(3)
Sn3-O17	2.181(10)	N1-Gd1-O4	175.1(3)
O9-Sn3-O14	85.6(3)	O16-Sn3-O14	75.1(3)
O7-Sn3-Sn2	123.0(2)	O16-Sn3-O9	88.4(3)

07-Sn3-O14	87.2(3)	O16-Sn3-O7	162.2(3)
07-Sn3-O9	92.0(3)	017-Sn1-O14	75.2(3)
O16-Sn3-Sn2	39.7(2)	O17-Sn1-O8	86.8(4)
O17-Sn1-O13	161.3(4)	C15-Sn1-O15	99.7(6)
O17-Sn1-O15	87.8(4)	C15-Sn1-O17	100.4(9)
C15-Sn1-O14	173.1(7)		
C15-Sn1-O8	97.0(6)		
C15-Sn1-O13	97.9(9)		

Table 4.10 Selected bond lengths (\mathring{A}) and bond angle (deg) parameters of 4.6

Y1-01 Y1-01 2.223(8) Sn3-06 2.098(10) Y1-02 2.173(10) Sn3-C9 2.175(15) Y1-03 2.217(9) Sn3-O9 2.149(11) Y1-N1 2.474(12) O14-Y1-O1 89.4(3) Y1-017 2.245(8) O14-Y1-O3 165.9(3) Sn1-Sn2 3.2670(16) O14-Y1-N1 86.3(4) Sn1-O11 2.086(8) O1-Y1-N1 80.8(4) Sn1-O7 2.088(9) O1-Y1-O17 165.6(3) Sn1-O10 2.136(10) O2-Y1-O14 98.3(3) Sn1-O13 2.139(10) O2-Y1-O1 96.9(3) Sn1-C16 2.15(2) O2-Y1-O3 94.4(3) Sn2-O15 2.097(9) O2-Y1-N1 174.8(4) Sn1-Sn2 3.2670(16) O2-Y1-O17 97.0(3) Sn2-O8 2.057(9) O3-Y1-O1 95.1(3) Sn2-O8 2.057(9) O3-Y1-O1 95.1(3) Sn2-O9 2.147(10) O3-Y1-O17 87.5(3) Sn2-O9 2.147(10) O3-Y1-O17 87.5(3) Sn2-O13 2.178(16) O11-Sn1-Sn2 278.7(2) Sn3-O4 2.020(10) O11-Sn1-O1 98.4(6) O15-Sn2-Sn1 79.6(3) O9-Sn2-C13 98.4(6) O15-Sn2-C13 99.6(6) C13-Sn2-C13 98.4(6) O15-Sn2-C13 99.6(6) C13-Sn2-C13 98.4(6) O15-Sn2-C13 99.6(6) C13-Sn2-C13 98.4(6) O15-Sn2-C13 99.6(6) C13-Sn2-C13 98.4(6) O8-Sn2-C13 70.5(3) O8-Sn2-C13 98.4(6) O8-Sn2-C13 70.5(3) O8-Sn2-C13 98.4(6) O8-Sn2-C13 70.5(3) O8-Sn2-C13 98.4(6) O8-Sn2-C13 70.5(4) O8-Sn2-C13 70.5(4) O8-Sn2-C13 70.5(4) O8-Sn2-C13 70.5(4) O8-Sn2-C13 70.5(4) O8-Sn2-C13 70.5(4) O8-Sn2-C03 87.0(4) O5-Sn2-O9 90.5(4) O4-Sn3-O8 87.3(3) O5-Sn2-O9 90.5(4) O4-Sn3-O10 162.0(4)	Y1-O14	2.104/0\	C=2 00	2.140/11\
Y1-O2 2.173(10) Sn3-C9 2.175(15) Y1-O3 2.217(9) Sn3-O9 2.149(11) Y1-N1 2.474(12) O14-Y1-O1 89.4(3) Y1-O17 2.245(8) O14-Y1-O3 165.9(3) Sn1-Sn2 3.2670(16) O14-Y1-N1 86.3(4) Sn1-O11 2.086(8) O1-Y1-O17 ¹ 85.0(3) Sn1-O8 2.054(8) O1-Y1-O17 ¹ 85.0(3) Sn1-O7 2.088(9) O1-Y1-O17 ¹ 80.8(4) Sn1-O10 2.136(10) O2-Y1-O14 98.3(3) Sn1-O13 2.139(10) O2-Y1-O14 98.3(3) Sn1-O13 2.139(10) O2-Y1-O3 94.4(3) Sn2-O15 2.097(9) O2-Y1-O3 94.4(3) Sn1-Sn2 3.2670(16) O2-Y1-O17 ¹ 97.0(3) Sn2-O8 2.057(9) O3-Y1-O17 97.0(3) Sn2-O9 2.147(10) O3-Y1-O17 87.5(3) Sn2-O13 2.174(10) O17-Y1-N1 85.6(4) Sn3-O4 2.051(8) O11-Sn1-O13<		2.194(8)	Sn3-09	2.149(11)
Y1-O3 2.217(9) Sn3-O9 2.149(11) Y1-N1 2.474(12) O14-Y1-O1 89.4(3) Y1-O17 2.245(8) O14-Y1-O3 165.9(3) Sn1-Sn2 3.2670(16) O14-Y1-N1 86.3(4) Sn1-O11 2.086(8) O14-Y1-O17 ¹ 85.0(3) Sn1-O8 2.054(8) O1-Y1-O17 ¹ 165.6(3) Sn1-O7 2.088(9) O1-Y1-O17 ¹ 165.6(3) Sn1-O10 2.136(10) O2-Y1-O14 98.3(3) Sn1-O13 2.139(10) O2-Y1-O14 98.3(3) Sn1-C16 2.15(2) O2-Y1-O3 94.4(3) Sn2-O15 2.097(9) O2-Y1-O1 96.9(3) Sn1-Sn2 3.2670(16) O2-Y1-O17 97.0(3) Sn2-O8 2.057(9) O3-Y1-O1 95.1(3) Sn2-O9 2.147(10) O3-Y1-O17 87.5(3) Sn2-O13 2.174(10) O17-Y1-N1 85.6(4) Sn2-O13 2.174(10) O17-Y1-N1 85.6(4) Sn2-O13 2.174(10) O17-Sn1-O1		· · ·		. ,
Y1-N1 2.474(12) O14-Y1-O1 89.4(3) Y1-O17 2.245(8) O14-Y1-O3 165.9(3) Sn1-Sn2 3.2670(16) O14-Y1-N1 86.3(4) Sn1-O11 2.086(8) O14-Y1-O17¹ 85.0(3) Sn1-O8 2.054(8) O1-Y1-N1 80.8(4) Sn1-O7 2.088(9) O1-Y1-O17¹ 165.6(3) Sn1-O10 2.136(10) O2-Y1-O14 98.3(3) Sn1-O13 2.139(10) O2-Y1-O1 96.9(3) Sn1-C16 2.15(2) O2-Y1-O3 94.4(3) Sn2-O15 2.097(9) O2-Y1-O17 97.0(3) Sn2-O15 2.097(9) O2-Y1-O17¹ 97.0(3) Sn2-O8 2.057(9) O3-Y1-O17¹ 97.0(3) Sn2-O8 2.057(9) O3-Y1-O1 95.1(3) Sn2-O9 2.147(10) O3-Y1-O17¹ 87.5(3) Sn2-O13 2.174(10) O17¹-Y1-N1 85.6(4) Sn2-O13 2.178(16) O11-Sn1-Sn2 278.7(2) Sn3-O8 2.051(8) O11-Sn1-O13 <th></th> <th>• • •</th> <th></th> <th></th>		• • •		
Y1-O17 2.245(8) O14-Y1-O3 165.9(3) Sn1-Sn2 3.2670(16) O14-Y1-N1 86.3(4) Sn1-O11 2.086(8) O14-Y1-O17¹ 85.0(3) Sn1-O8 2.054(8) O1-Y1-N1 80.8(4) Sn1-O7 2.088(9) O1-Y1-O17¹ 165.6(3) Sn1-O10 2.136(10) O2-Y1-O14 98.3(3) Sn1-O13 2.139(10) O2-Y1-O1 96.9(3) Sn1-C16 2.15(2) O2-Y1-O3 94.4(3) Sn2-O15 2.097(9) O2-Y1-N1 174.8(4) Sn1-Sn2 3.2670(16) O2-Y1-O17¹ 97.0(3) Sn2-O8 2.057(9) O3-Y1-O1 95.1(3) Sn2-O5 2.055(9) O3-Y1-O1 95.1(3) Sn2-O5 2.055(9) O3-Y1-O17¹ 87.5(3) Sn2-O13 2.174(10) O17¹-Y1-N1 85.6(4) Sn2-C13 2.178(16) O11-Sn1-Sn2 278.7(2) Sn3-O8 2.051(8) O11-Sn1-O1 86.5(3) Sn3-O10 2.174(10) O11-Sn1-C16<		· · ·		. ,
Sn1-Sn2 3.2670(16) O14-Y1-N1 86.3(4) Sn1-O11 2.086(8) O14-Y1O-17¹ 85.0(3) Sn1-O8 2.054(8) O1-Y1-N1 80.8(4) Sn1-O7 2.088(9) O1-Y1-O17¹ 165.6(3) Sn1-O10 2.136(10) O2-Y1-O14 98.3(3) Sn1-O13 2.139(10) O2-Y1-O1 96.9(3) Sn1-C16 2.15(2) O2-Y1-O3 94.4(3) Sn2-O15 2.097(9) O2-Y1-N1 174.8(4) Sn1-Sn2 3.2670(16) O2-Y1-O17¹ 97.0(3) Sn2-O8 2.057(9) O3-Y1-O1 95.1(3) Sn2-O8 2.057(9) O3-Y1-N1 81.3(4) Sn2-O9 2.147(10) O3-Y1-O17¹ 87.5(3) Sn2-O13 2.174(10) O17²-Y1-N1 85.6(4) Sn2-O13 2.178(16) O11-Sn1-Sn2 278.7(2) Sn3-O8 2.051(8) O11-Sn1-O13 86.5(3) Sn3-O4 2.020(10) O11-Sn1-O13 86.5(3) Sn3-O10 2.174(10) O11-Sn1-		• • •		
Sn1-011 2.086(8) 014-Y10-17¹ 85.0(3) Sn1-08 2.054(8) 01-Y1-N1 80.8(4) Sn1-07 2.088(9) 01-Y1-O17¹ 165.6(3) Sn1-010 2.136(10) 02-Y1-O14 98.3(3) Sn1-013 2.139(10) 02-Y1-O1 96.9(3) Sn1-C16 2.15(2) 02-Y1-O3 94.4(3) Sn2-O15 2.097(9) 02-Y1-N1 174.8(4) Sn1-Sn2 3.2670(16) 02-Y1-O17¹ 97.0(3) Sn2-O8 2.057(9) 03-Y1-O1 95.1(3) Sn2-O8 2.055(9) 03-Y1-N1 81.3(4) Sn2-O9 2.147(10) 03-Y1-O17¹ 87.5(3) Sn2-O13 2.174(10) 017-Sn1-Sn2 278.7(2) Sn3-O8 2.051(8) 011-Sn1-Sn2 278.7(2) Sn3-O8 2.051(8) 011-Sn1-O13 86.5(3) Sn3-O4 2.020(10) 011-Sn1-O13 86.5(3) Sn3-O3 2.174(10) 011-Sn1-O13 86.5(3) Sn3-O4 2.056(3) 09-Sn2-C13		· · ·		
Sn1-O8 2.054(8) O1-Y1-N1 80.8(4) Sn1-O7 2.088(9) O1-Y1-O17¹ 165.6(3) Sn1-O10 2.136(10) O2-Y1-O14 98.3(3) Sn1-O13 2.139(10) O2-Y1-O1 96.9(3) Sn1-C16 2.15(2) O2-Y1-O3 94.4(3) Sn2-O15 2.097(9) O2-Y1-N1 174.8(4) Sn1-Sn2 3.2670(16) O2-Y1-O17¹ 97.0(3) Sn2-O8 2.057(9) O3-Y1-O1 95.1(3) Sn2-O8 2.055(9) O3-Y1-N1 81.3(4) Sn2-O9 2.147(10) O3-Y1-O17¹ 87.5(3) Sn2-O13 2.174(10) O17²-Y1-N1 85.6(4) Sn2-O13 2.178(16) O11-Sn1-Sn2 278.7(2) Sn3-O8 2.051(8) O11-Sn1-O7 94.7(3) Sn3-O4 2.020(10) O11-Sn1-O13 86.5(3) Sn3-O10 2.174(10) O11-Sn1-C16 99.1(6) O15-Sn2-Sn1 79.6(3) O9-Sn2-C13 98.4(6) O15-Sn2-O13 87.4(4) O13-		-		
Sn1-O7 2.088(9) O1-Y1-O17¹ 165.6(3) Sn1-O10 2.136(10) O2-Y1-O14 98.3(3) Sn1-O13 2.139(10) O2-Y1-O1 96.9(3) Sn1-C16 2.15(2) O2-Y1-O3 94.4(3) Sn2-O15 2.097(9) O2-Y1-N1 174.8(4) Sn1-Sn2 3.2670(16) O2-Y1-O17¹ 97.0(3) Sn2-O8 2.057(9) O3-Y1-O1 95.1(3) Sn2-O8 2.055(9) O3-Y1-O1 95.1(3) Sn2-O5 2.055(9) O3-Y1-N1 81.3(4) Sn2-O9 2.147(10) O3-Y1-O17¹ 87.5(3) Sn2-O13 2.174(10) O11-Sn1-Sn2 278.7(2) Sn3-O8 2.051(8) O11-Sn1-O7 94.7(3) Sn3-O4 2.020(10) O11-Sn1-O13 86.5(3) Sn3-O10 2.174(10) O11-Sn1-C16 99.1(6) O15-Sn2-Sn1 79.6(3) O9-Sn2-C13 98.4(6) O15-Sn2-O13 87.4(4) O13-Sn2-Sn1 40.4(2) O15-Sn2-C13 99.6(6) C				, ,
Sn1-O10 2.136(10) O2-Y1-O14 98.3(3) Sn1-O13 2.139(10) O2-Y1-O1 96.9(3) Sn1-C16 2.15(2) O2-Y1-O3 94.4(3) Sn2-O15 2.097(9) O2-Y1-O1 174.8(4) Sn1-Sn2 3.2670(16) O2-Y1-O17¹ 97.0(3) Sn2-O8 2.057(9) O3-Y1-O1 95.1(3) Sn2-O5 2.055(9) O3-Y1-O1 95.1(3) Sn2-O5 2.055(9) O3-Y1-O1 95.1(3) Sn2-O9 2.147(10) O3-Y1-O17¹ 87.5(3) Sn2-O13 2.174(10) O17¹-Y1-N1 85.6(4) Sn2-O13 2.178(16) O11-Sn1-Sn2 278.7(2) Sn3-O8 2.051(8) O11-Sn1-O7 94.7(3) Sn3-O8 2.051(8) O11-Sn1-O13 86.5(3) Sn3-O4 2.020(10) O11-Sn1-O13 86.5(3) Sn3-O10 2.174(10) O11-Sn1-C16 99.1(6) O15-Sn2-Sn1 79.6(3) O9-Sn2-C13 98.4(6) O15-Sn2-O13 87.4(4) O13-				
Sn1-O13 2.139(10) O2-Y1-O1 96.9(3) Sn1-C16 2.15(2) O2-Y1-O3 94.4(3) Sn2-O15 2.097(9) O2-Y1-N1 174.8(4) Sn1-Sn2 3.2670(16) O2-Y1-O17¹ 97.0(3) Sn2-O8 2.057(9) O3-Y1-O1 95.1(3) Sn2-O8 2.055(9) O3-Y1-N1 81.3(4) Sn2-O5 2.055(9) O3-Y1-O17¹ 87.5(3) Sn2-O9 2.147(10) O3-Y1-O17¹ 87.5(3) Sn2-O13 2.174(10) O17¹-Y1-N1 85.6(4) Sn2-O13 2.178(16) O11-Sn1-Sn2 278.7(2) Sn3-O8 2.051(8) O11-Sn1-O7 94.7(3) Sn3-O4 2.020(10) O11-Sn1-O13 86.5(3) Sn3-O4 2.020(10) O11-Sn1-O13 86.5(3) Sn3-O10 2.174(10) O11-Sn1-C16 99.1(6) O15-Sn2-Sn1 79.6(3) O9-Sn2-C13 98.4(6) O15-Sn2-O9 161.7(4) O13-Sn2-Sn1 40.4(2) O15-Sn2-O15 88.1(3) <				
Sn1-C16 2.15(2) O2-Y1-O3 94.4(3) Sn2-O15 2.097(9) O2-Y1-N1 174.8(4) Sn1-Sn2 3.2670(16) O2-Y1-O17¹ 97.0(3) Sn2-O8 2.057(9) O3-Y1-O1 95.1(3) Sn2-O5 2.055(9) O3-Y1-O17¹ 81.3(4) Sn2-O9 2.147(10) O3-Y1-O17¹ 87.5(3) Sn2-O13 2.174(10) O17¹-Y1-N1 85.6(4) Sn2-C13 2.178(16) O11-Sn1-Sn2 278.7(2) Sn3-O8 2.051(8) O11-Sn1-O7 94.7(3) Sn3-O4 2.020(10) O11-Sn1-O13 86.5(3) Sn3-O10 2.174(10) O11-Sn1-C16 99.1(6) O15-Sn2-Sn1 79.6(3) O9-Sn2-C13 98.4(6) O15-Sn2-O9 161.7(4) O13-Sn2-Sn1 40.4(2) O15-Sn2-O13 87.4(4) O13-Sn2-C13 101.2(6) O8-Sn2-Sn1 37.4(2) O9-Sn2-C13 98.4(6) O8-Sn2-O15 88.1(3) O13-Sn2-Sn1 40.4(2) O8-Sn2-O3 73.8(4) <th></th> <th>• • •</th> <th></th> <th></th>		• • •		
Sn2-O15 2.097(9) O2-Y1-N1 174.8(4) Sn1-Sn2 3.2670(16) O2-Y1-O17¹ 97.0(3) Sn2-O8 2.057(9) O3-Y1-O1 95.1(3) Sn2-O5 2.055(9) O3-Y1-N1 81.3(4) Sn2-O9 2.147(10) O3-Y1-O17¹ 87.5(3) Sn2-O13 2.174(10) O17¹-Y1-N1 85.6(4) Sn2-C13 2.178(16) O11-Sn1-Sn2 278.7(2) Sn3-O8 2.051(8) O11-Sn1-O7 94.7(3) Sn3-O4 2.020(10) O11-Sn1-O13 86.5(3) Sn3-O10 2.174(10) O11-Sn1-C16 99.1(6) O15-Sn2-Sn1 79.6(3) O9-Sn2-C13 98.4(6) O15-Sn2-O9 161.7(4) O13-Sn2-Sn1 40.4(2) O15-Sn2-O13 87.4(4) O13-Sn2-C13 101.2(6) O8-Sn2-Sn1 37.4(2) O9-Sn2-C13 98.4(6) O8-Sn2-O15 88.1(3) O13-Sn2-Sn1 40.4(2) O8-Sn2-O3 73.8(4) O13-Sn2-Sn1 40.4(2) O8-Sn2-O13 76.5(3)				` '
Sn1-Sn2 3.2670(16) O2-Y1-O17¹ 97.0(3) Sn2-O8 2.057(9) O3-Y1-O1 95.1(3) Sn2-O5 2.055(9) O3-Y1-N1 81.3(4) Sn2-O9 2.147(10) O3-Y1-O17¹ 87.5(3) Sn2-O13 2.174(10) O17¹-Y1-N1 85.6(4) Sn2-C13 2.178(16) O11-Sn1-Sn2 278.7(2) Sn3-O8 2.051(8) O11-Sn1-O7 94.7(3) Sn3-O4 2.020(10) O11-Sn1-O13 86.5(3) Sn3-O10 2.174(10) O11-Sn1-C16 99.1(6) O15-Sn2-Sn1 79.6(3) O9-Sn2-C13 98.4(6) O15-Sn2-Sn1 79.6(3) O9-Sn2-C13 98.4(6) O15-Sn2-O9 87.4(4) O13-Sn2-Sn1 40.4(2) O15-Sn2-C13 99.6(6) C13-Sn2-Sn1 141.5(6) O8-Sn2-O15 88.1(3) O13-Sn2-Sn1 40.4(2) O8-Sn2-O15 88.1(3) O13-Sn2-Sn1 40.4(2) O8-Sn2-O13 76.5(3) C13-Sn2-Sn1 141.5(6) O8-Sn2-C13 1				
Sn2-O8 2.057(9) O3-Y1-O1 95.1(3) Sn2-O5 2.055(9) O3-Y1-N1 81.3(4) Sn2-O9 2.147(10) O3-Y1-O17¹ 87.5(3) Sn2-O13 2.174(10) O17¹-Y1-N1 85.6(4) Sn2-C13 2.178(16) O11-Sn1-Sn2 278.7(2) Sn3-O8 2.051(8) O11-Sn1-O7 94.7(3) Sn3-O4 2.020(10) O11-Sn1-O13 86.5(3) Sn3-O10 2.174(10) O11-Sn1-C16 99.1(6) O15-Sn2-Sn1 79.6(3) O9-Sn2-C13 98.4(6) O15-Sn2-O9 161.7(4) O13-Sn2-Sn1 40.4(2) O15-Sn2-O13 87.4(4) O13-Sn2-Sn1 101.2(6) O8-Sn2-C13 99.6(6) C13-Sn2-Sn1 141.5(6) O8-Sn2-O15 88.1(3) O13-Sn2-C13 98.4(6) O8-Sn2-O15 88.1(3) O13-Sn2-Sn1 40.4(2) O8-Sn2-O13 76.5(3) C13-Sn2-Sn1 141.5(6) O8-Sn2-C13 171.9(6) O9-Sn2-C13 98.4(6) O5-Sn2-Sn1 <t< th=""><th></th><th>· · ·</th><th></th><th></th></t<>		· · ·		
Sn2-O5 2.055(9) O3-Y1-N1 81.3(4) Sn2-O9 2.147(10) O3-Y1-O17¹ 87.5(3) Sn2-O13 2.174(10) O17¹-Y1-N1 85.6(4) Sn2-C13 2.178(16) O11-Sn1-Sn2 278.7(2) Sn3-O8 2.051(8) O11-Sn1-O7 94.7(3) Sn3-O4 2.020(10) O11-Sn1-O13 86.5(3) Sn3-O10 2.174(10) O11-Sn1-C16 99.1(6) O15-Sn2-Sn1 79.6(3) O9-Sn2-C13 98.4(6) O15-Sn2-O9 161.7(4) O13-Sn2-Sn1 40.4(2) O15-Sn2-O13 87.4(4) O13-Sn2-C13 101.2(6) O15-Sn2-C13 99.6(6) C13-Sn2-Sn1 141.5(6) O8-Sn2-Sn1 37.4(2) O9-Sn2-C13 98.4(6) O8-Sn2-O15 88.1(3) O13-Sn2-Sn1 40.4(2) O8-Sn2-O13 76.5(3) C13-Sn2-Sn1 141.5(6) O8-Sn2-C13 171.9(6) O9-Sn2-C13 98.4(6) O5-Sn2-Sn1 120.6(3) O8-Sn3-O10 74.7(4) O5-Sn2-O8		· · · · · · · · · · · · · · · · · · ·		
Sn2-O9 2.147(10) O3-Y1-O17¹ 87.5(3) Sn2-O13 2.174(10) O17¹-Y1-N1 85.6(4) Sn2-C13 2.178(16) O11-Sn1-Sn2 278.7(2) Sn3-O8 2.051(8) O11-Sn1-O7 94.7(3) Sn3-O4 2.020(10) O11-Sn1-O13 86.5(3) Sn3-O10 2.174(10) O11-Sn1-C16 99.1(6) O15-Sn2-Sn1 79.6(3) O9-Sn2-C13 98.4(6) O15-Sn2-O9 161.7(4) O13-Sn2-Sn1 40.4(2) O15-Sn2-O13 87.4(4) O13-Sn2-C13 101.2(6) O15-Sn2-C13 99.6(6) C13-Sn2-Sn1 141.5(6) O8-Sn2-Sn1 37.4(2) O9-Sn2-C13 98.4(6) O8-Sn2-O15 88.1(3) O13-Sn2-Sn1 40.4(2) O8-Sn2-O9 73.8(4) O13-Sn2-C13 101.2(6) O8-Sn2-O13 76.5(3) C13-Sn2-Sn1 141.5(6) O8-Sn2-C13 171.9(6) O9-Sn2-C13 98.4(6) O5-Sn2-O15 89.8(3) O8-Sn3-O9 73.9(4) O5-Sn2-O8		· · ·		, ,
Sn2-O13 2.174(10) O17¹-Y1-N1 85.6(4) Sn2-C13 2.178(16) O11-Sn1-Sn2 278.7(2) Sn3-O8 2.051(8) O11-Sn1-O7 94.7(3) Sn3-O4 2.020(10) O11-Sn1-O13 86.5(3) Sn3-O10 2.174(10) O11-Sn1-C16 99.1(6) O15-Sn2-Sn1 79.6(3) O9-Sn2-C13 98.4(6) O15-Sn2-O9 161.7(4) O13-Sn2-Sn1 40.4(2) O15-Sn2-O13 87.4(4) O13-Sn2-C13 101.2(6) O15-Sn2-C13 99.6(6) C13-Sn2-Sn1 141.5(6) O8-Sn2-Sn1 37.4(2) O9-Sn2-C13 98.4(6) O8-Sn2-O15 88.1(3) O13-Sn2-Sn1 40.4(2) O8-Sn2-O9 73.8(4) O13-Sn2-Sn1 141.5(6) O8-Sn2-O13 76.5(3) C13-Sn2-Sn1 141.5(6) O8-Sn2-C13 171.9(6) O9-Sn2-C13 98.4(6) O5-Sn2-Sn1 120.6(3) O8-Sn3-O10 74.7(4) O5-Sn2-O8 84.5(3) O8-Sn3-O6 87.0(4) O5-Sn2-O9		· , ,		
Sn2-C13 2.178(16) O11-Sn1-Sn2 278.7(2) Sn3-O8 2.051(8) O11-Sn1-O7 94.7(3) Sn3-O4 2.020(10) O11-Sn1-O13 86.5(3) Sn3-O10 2.174(10) O11-Sn1-C16 99.1(6) O15-Sn2-Sn1 79.6(3) O9-Sn2-C13 98.4(6) O15-Sn2-O9 161.7(4) O13-Sn2-Sn1 40.4(2) O15-Sn2-O13 87.4(4) O13-Sn2-C13 101.2(6) O8-Sn2-C13 99.6(6) C13-Sn2-Sn1 141.5(6) O8-Sn2-Sn1 37.4(2) O9-Sn2-C13 98.4(6) O8-Sn2-O15 88.1(3) O13-Sn2-Sn1 40.4(2) O8-Sn2-O9 73.8(4) O13-Sn2-Sn1 40.4(2) O8-Sn2-O13 76.5(3) C13-Sn2-Sn1 141.5(6) O8-Sn2-C13 171.9(6) O9-Sn2-C13 98.4(6) O5-Sn2-Sn1 120.6(3) O8-Sn3-O10 74.7(4) O5-Sn2-O8 84.5(3) O8-Sn3-O6 87.0(4) O5-Sn2-O9 90.5(4) O4-Sn3-O8 87.3(3)		, ,		
Sn3-O8 2.051(8) O11-Sn1-O7 94.7(3) Sn3-O4 2.020(10) O11-Sn1-O13 86.5(3) Sn3-O10 2.174(10) O11-Sn1-C16 99.1(6) O15-Sn2-Sn1 79.6(3) O9-Sn2-C13 98.4(6) O15-Sn2-O9 161.7(4) O13-Sn2-Sn1 40.4(2) O15-Sn2-O13 87.4(4) O13-Sn2-C13 101.2(6) O15-Sn2-C13 99.6(6) C13-Sn2-Sn1 141.5(6) O8-Sn2-Sn1 37.4(2) O9-Sn2-C13 98.4(6) O8-Sn2-O15 88.1(3) O13-Sn2-Sn1 40.4(2) O8-Sn2-O9 73.8(4) O13-Sn2-C13 101.2(6) O8-Sn2-O13 76.5(3) C13-Sn2-Sn1 141.5(6) O8-Sn2-C13 171.9(6) O9-Sn2-C13 98.4(6) O5-Sn2-Sn1 120.6(3) O8-Sn3-O10 74.7(4) O5-Sn2-O15 89.8(3) O8-Sn3-O9 73.9(4) O5-Sn2-O8 84.5(3) O8-Sn3-O6 87.0(4) O5-Sn2-O9 90.5(4) O4-Sn3-O8 87.3(3)				
Sn3-O4 2.020(10) O11-Sn1-O13 86.5(3) Sn3-O10 2.174(10) O11-Sn1-C16 99.1(6) O15-Sn2-Sn1 79.6(3) O9-Sn2-C13 98.4(6) O15-Sn2-O9 161.7(4) O13-Sn2-Sn1 40.4(2) O15-Sn2-O13 87.4(4) O13-Sn2-C13 101.2(6) O15-Sn2-C13 99.6(6) C13-Sn2-Sn1 141.5(6) O8-Sn2-Sn1 37.4(2) O9-Sn2-C13 98.4(6) O8-Sn2-O15 88.1(3) O13-Sn2-Sn1 40.4(2) O8-Sn2-O9 73.8(4) O13-Sn2-C13 101.2(6) O8-Sn2-O13 76.5(3) C13-Sn2-Sn1 141.5(6) O8-Sn2-C13 171.9(6) O9-Sn2-C13 98.4(6) O5-Sn2-Sn1 120.6(3) O8-Sn3-O10 74.7(4) O5-Sn2-O15 89.8(3) O8-Sn3-O9 73.9(4) O5-Sn2-O8 84.5(3) O8-Sn3-O6 87.0(4) O5-Sn2-O9 90.5(4) O4-Sn3-O8 87.3(3)	Sn2-C13	· · · · · · · · · · · · · · · · · · ·		
Sn3-O10 2.174(10) O11-Sn1-C16 99.1(6) O15-Sn2-Sn1 79.6(3) O9-Sn2-C13 98.4(6) O15-Sn2-O9 161.7(4) O13-Sn2-Sn1 40.4(2) O15-Sn2-O13 87.4(4) O13-Sn2-C13 101.2(6) O15-Sn2-C13 99.6(6) C13-Sn2-Sn1 141.5(6) O8-Sn2-Sn1 37.4(2) O9-Sn2-C13 98.4(6) O8-Sn2-O15 88.1(3) O13-Sn2-Sn1 40.4(2) O8-Sn2-O9 73.8(4) O13-Sn2-C13 101.2(6) O8-Sn2-O13 76.5(3) C13-Sn2-Sn1 141.5(6) O8-Sn2-C13 171.9(6) O9-Sn2-C13 98.4(6) O5-Sn2-Sn1 120.6(3) O8-Sn3-O10 74.7(4) O5-Sn2-O15 89.8(3) O8-Sn3-O9 73.9(4) O5-Sn2-O8 84.5(3) O8-Sn3-O6 87.0(4) O5-Sn2-O9 90.5(4) O4-Sn3-O8 87.3(3)				
O15-Sn2-Sn1 79.6(3) O9-Sn2-C13 98.4(6) O15-Sn2-O9 161.7(4) O13-Sn2-Sn1 40.4(2) O15-Sn2-O13 87.4(4) O13-Sn2-C13 101.2(6) O15-Sn2-C13 99.6(6) C13-Sn2-Sn1 141.5(6) O8-Sn2-Sn1 37.4(2) O9-Sn2-C13 98.4(6) O8-Sn2-O15 88.1(3) O13-Sn2-Sn1 40.4(2) O8-Sn2-O9 73.8(4) O13-Sn2-C13 101.2(6) O8-Sn2-O13 76.5(3) C13-Sn2-Sn1 141.5(6) O8-Sn2-C13 171.9(6) O9-Sn2-C13 98.4(6) O5-Sn2-Sn1 120.6(3) O8-Sn3-O10 74.7(4) O5-Sn2-O15 89.8(3) O8-Sn3-O9 73.9(4) O5-Sn2-O8 84.5(3) O8-Sn3-O6 87.0(4) O5-Sn2-O9 90.5(4) O4-Sn3-O8 87.3(3)	Sn3-O4		O11-Sn1-O13	` '
O15-Sn2-O9 161.7(4) O13-Sn2-Sn1 40.4(2) O15-Sn2-O13 87.4(4) O13-Sn2-C13 101.2(6) O15-Sn2-C13 99.6(6) C13-Sn2-Sn1 141.5(6) O8-Sn2-Sn1 37.4(2) O9-Sn2-C13 98.4(6) O8-Sn2-O15 88.1(3) O13-Sn2-Sn1 40.4(2) O8-Sn2-O9 73.8(4) O13-Sn2-C13 101.2(6) O8-Sn2-O13 76.5(3) C13-Sn2-Sn1 141.5(6) O8-Sn2-C13 171.9(6) O9-Sn2-C13 98.4(6) O5-Sn2-Sn1 120.6(3) O8-Sn3-O10 74.7(4) O5-Sn2-O15 89.8(3) O8-Sn3-O9 73.9(4) O5-Sn2-O8 84.5(3) O8-Sn3-O6 87.0(4) O5-Sn2-O9 90.5(4) O4-Sn3-O8 87.3(3)	Sn3-O10	2.174(10)		99.1(6)
O15-Sn2-O13 87.4(4) O13-Sn2-C13 101.2(6) O15-Sn2-C13 99.6(6) C13-Sn2-Sn1 141.5(6) O8-Sn2-Sn1 37.4(2) O9-Sn2-C13 98.4(6) O8-Sn2-O15 88.1(3) O13-Sn2-Sn1 40.4(2) O8-Sn2-O9 73.8(4) O13-Sn2-C13 101.2(6) O8-Sn2-O13 76.5(3) C13-Sn2-Sn1 141.5(6) O8-Sn2-C13 171.9(6) O9-Sn2-C13 98.4(6) O5-Sn2-Sn1 120.6(3) O8-Sn3-O10 74.7(4) O5-Sn2-O15 89.8(3) O8-Sn3-O9 73.9(4) O5-Sn2-O8 84.5(3) O8-Sn3-O6 87.0(4) O5-Sn2-O9 90.5(4) O4-Sn3-O8 87.3(3)	O15-Sn2-Sn1	. ,	O9-Sn2-C13	. ,
O15-Sn2-C13 99.6(6) C13-Sn2-Sn1 141.5(6) O8-Sn2-Sn1 37.4(2) O9-Sn2-C13 98.4(6) O8-Sn2-O15 88.1(3) O13-Sn2-Sn1 40.4(2) O8-Sn2-O9 73.8(4) O13-Sn2-C13 101.2(6) O8-Sn2-O13 76.5(3) C13-Sn2-Sn1 141.5(6) O8-Sn2-C13 171.9(6) O9-Sn2-C13 98.4(6) O5-Sn2-Sn1 120.6(3) O8-Sn3-O10 74.7(4) O5-Sn2-O15 89.8(3) O8-Sn3-O9 73.9(4) O5-Sn2-O8 84.5(3) O8-Sn3-O6 87.0(4) O5-Sn2-O9 90.5(4) O4-Sn3-O8 87.3(3)	O15-Sn2-O9	161.7(4)	O13-Sn2-Sn1	40.4(2)
O8-Sn2-Sn1 37.4(2) O9-Sn2-C13 98.4(6) O8-Sn2-O15 88.1(3) O13-Sn2-Sn1 40.4(2) O8-Sn2-O9 73.8(4) O13-Sn2-C13 101.2(6) O8-Sn2-O13 76.5(3) C13-Sn2-Sn1 141.5(6) O8-Sn2-C13 171.9(6) O9-Sn2-C13 98.4(6) O5-Sn2-Sn1 120.6(3) O8-Sn3-O10 74.7(4) O5-Sn2-O15 89.8(3) O8-Sn3-O9 73.9(4) O5-Sn2-O8 84.5(3) O8-Sn3-O6 87.0(4) O5-Sn2-O9 90.5(4) O4-Sn3-O8 87.3(3)	O15-Sn2-O13	<u> </u>	O13-Sn2-C13	
O8-Sn2-O15 88.1(3) O13-Sn2-Sn1 40.4(2) O8-Sn2-O9 73.8(4) O13-Sn2-C13 101.2(6) O8-Sn2-O13 76.5(3) C13-Sn2-Sn1 141.5(6) O8-Sn2-C13 171.9(6) O9-Sn2-C13 98.4(6) O5-Sn2-Sn1 120.6(3) O8-Sn3-O10 74.7(4) O5-Sn2-O15 89.8(3) O8-Sn3-O9 73.9(4) O5-Sn2-O8 84.5(3) O8-Sn3-O6 87.0(4) O5-Sn2-O9 90.5(4) O4-Sn3-O8 87.3(3)	O15-Sn2-C13	99.6(6)	C13-Sn2-Sn1	141.5(6)
O8-Sn2-O9 73.8(4) O13-Sn2-C13 101.2(6) O8-Sn2-O13 76.5(3) C13-Sn2-Sn1 141.5(6) O8-Sn2-C13 171.9(6) O9-Sn2-C13 98.4(6) O5-Sn2-Sn1 120.6(3) O8-Sn3-O10 74.7(4) O5-Sn2-O15 89.8(3) O8-Sn3-O9 73.9(4) O5-Sn2-O8 84.5(3) O8-Sn3-O6 87.0(4) O5-Sn2-O9 90.5(4) O4-Sn3-O8 87.3(3)	O8-Sn2-Sn1	<u> </u>	O9-Sn2-C13	98.4(6)
O8-Sn2-O13 76.5(3) C13-Sn2-Sn1 141.5(6) O8-Sn2-C13 171.9(6) O9-Sn2-C13 98.4(6) O5-Sn2-Sn1 120.6(3) O8-Sn3-O10 74.7(4) O5-Sn2-O15 89.8(3) O8-Sn3-O9 73.9(4) O5-Sn2-O8 84.5(3) O8-Sn3-O6 87.0(4) O5-Sn2-O9 90.5(4) O4-Sn3-O8 87.3(3)	O8-Sn2-O15	88.1(3)	O13-Sn2-Sn1	40.4(2)
O8-Sn2-C13 171.9(6) O9-Sn2-C13 98.4(6) O5-Sn2-Sn1 120.6(3) O8-Sn3-O10 74.7(4) O5-Sn2-O15 89.8(3) O8-Sn3-O9 73.9(4) O5-Sn2-O8 84.5(3) O8-Sn3-O6 87.0(4) O5-Sn2-O9 90.5(4) O4-Sn3-O8 87.3(3)	O8-Sn2-O9	73.8(4)	O13-Sn2-C13	101.2(6)
O5-Sn2-Sn1 120.6(3) O8-Sn3-O10 74.7(4) O5-Sn2-O15 89.8(3) O8-Sn3-O9 73.9(4) O5-Sn2-O8 84.5(3) O8-Sn3-O6 87.0(4) O5-Sn2-O9 90.5(4) O4-Sn3-O8 87.3(3)	O8-Sn2-O13	76.5(3)	C13-Sn2-Sn1	141.5(6)
O5-Sn2-O15 89.8(3) O8-Sn3-O9 73.9(4) O5-Sn2-O8 84.5(3) O8-Sn3-O6 87.0(4) O5-Sn2-O9 90.5(4) O4-Sn3-O8 87.3(3)	O8-Sn2-C13	171.9(6)	O9-Sn2-C13	98.4(6)
O5-Sn2-O8 84.5(3) O8-Sn3-O6 87.0(4) O5-Sn2-O9 90.5(4) O4-Sn3-O8 87.3(3)	O5-Sn2-Sn1	120.6(3)	O8-Sn3-O10	74.7(4)
O5-Sn2-O9 90.5(4) O4-Sn3-O8 87.3(3)	O5-Sn2-O15	89.8(3)	O8-Sn3-O9	73.9(4)
	O5-Sn2-O8	84.5(3)	O8-Sn3-O6	87.0(4)
O5-Sn2-O13 160.9(4) O4-Sn3-O10 162.0(4)	O5-Sn2-O9	90.5(4)	O4-Sn3-O8	87.3(3)
	O5-Sn2-O13	160.9(4)	O4-Sn3-O10	162.0(4)

O5-Sn2-C13	97.9(6)	O4-Sn3-O6	90.8(4)
O9-Sn2-Sn1	84.5(3)	O4-Sn3-C9	98.2(7)
O9-Sn2-O13	86.4(4)	O9-Sn3-O10	85.4(4)
O11-Sn1-C16	278.7(2)	O8-Sn2-O13	76.5(3)
O8-Sn1-Sn2	94.7(3)	O8-Sn2-C13	171.9(6)
O8-Sn1-O11	86.5(3)	O9-Sn2-C13	98.4(6)
08-Sn1-07	99.1(6)	O13-Sn2-Sn1	40.4(2)
O8-Sn1-O10	37.4(3)	O13-Sn2-C13	101.2(6)
O8-Sn1-O13	87.7(3)	O9-Sn3-C9	102.7(6)
O8-Sn1-C16	84.8(3)	O6-Sn3-O10	89.9(4)
O7-Sn1-Sn2	75.5(4)	O6-Sn3-O9	160.8(4)
O7-Sn1-O10	77.3(4)	O8-Sn3-O10	74.7(4)
07-Sn1-O13	173.0(6)	O8-Sn3-O9	73.9(4)
O7-Sn1-C16	121.5(2)	08-Sn3-06	87.0(4)
O10-Sn1-Sn2	86.0(4)	O9-Sn3-C9	102.7(6)

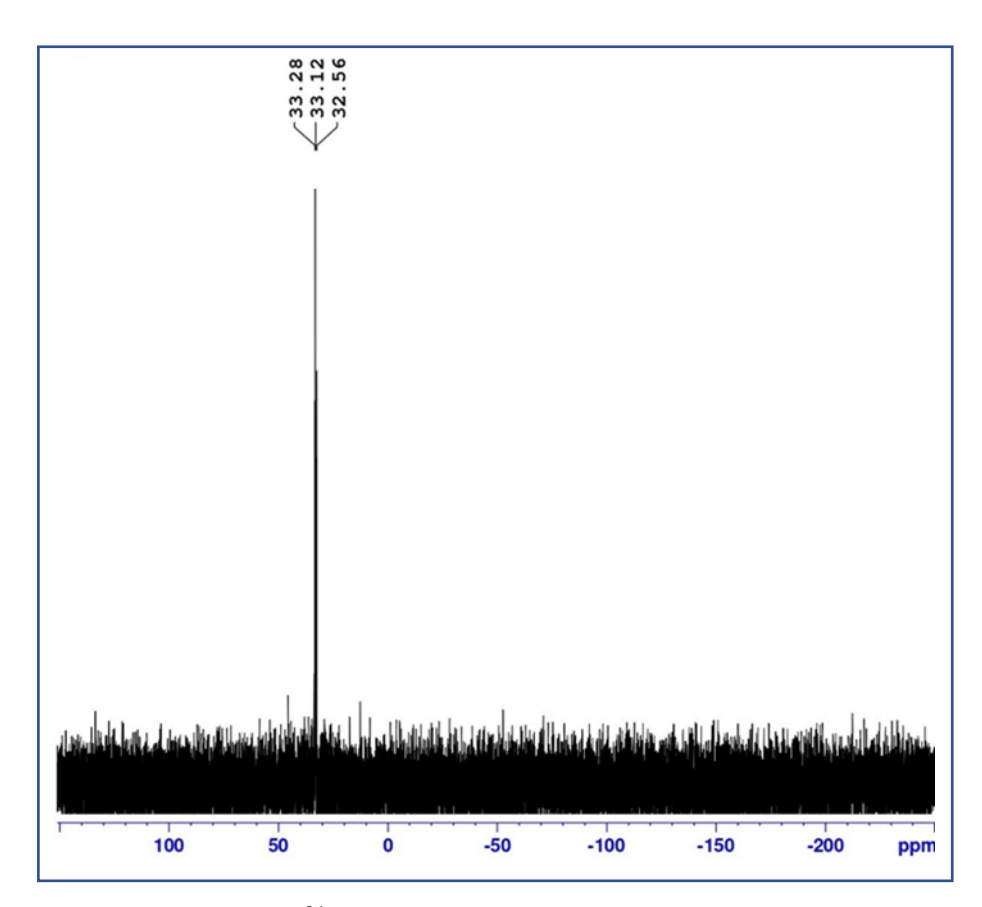


Fig 4.5 31 p NMR spectra for compound 4.2

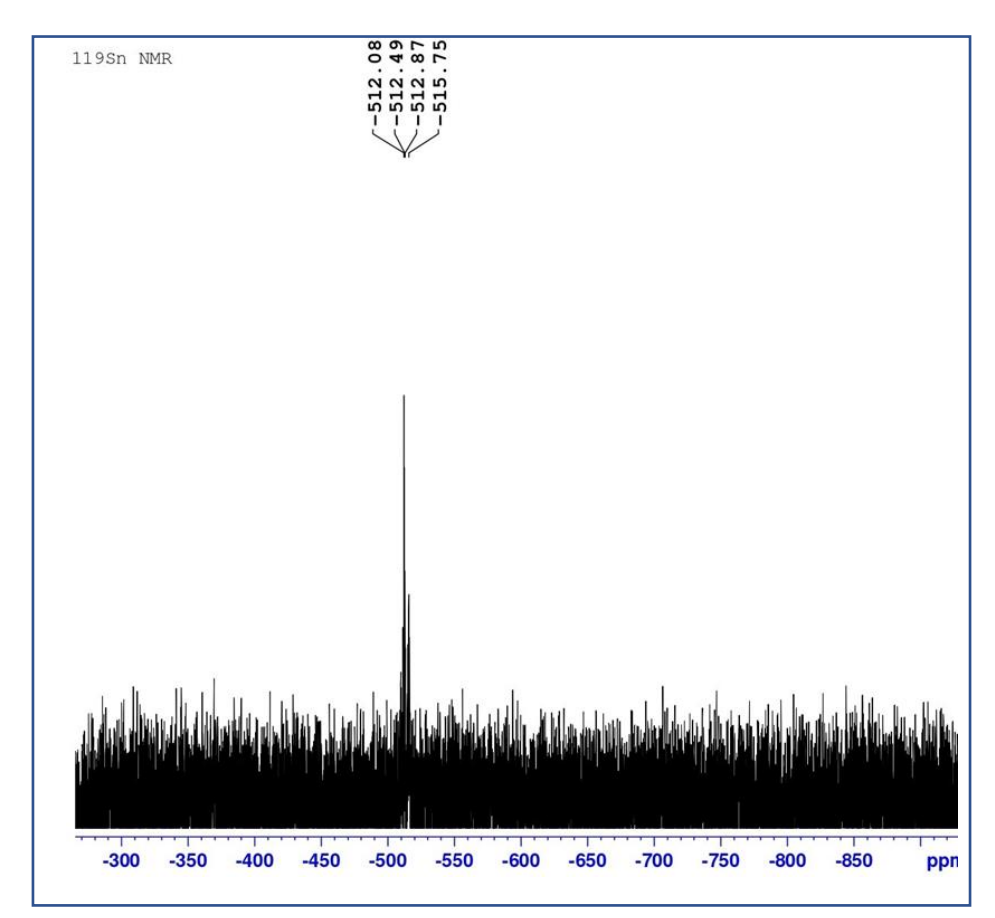


Fig 4.6 119 Sn NMR for compound 4.2

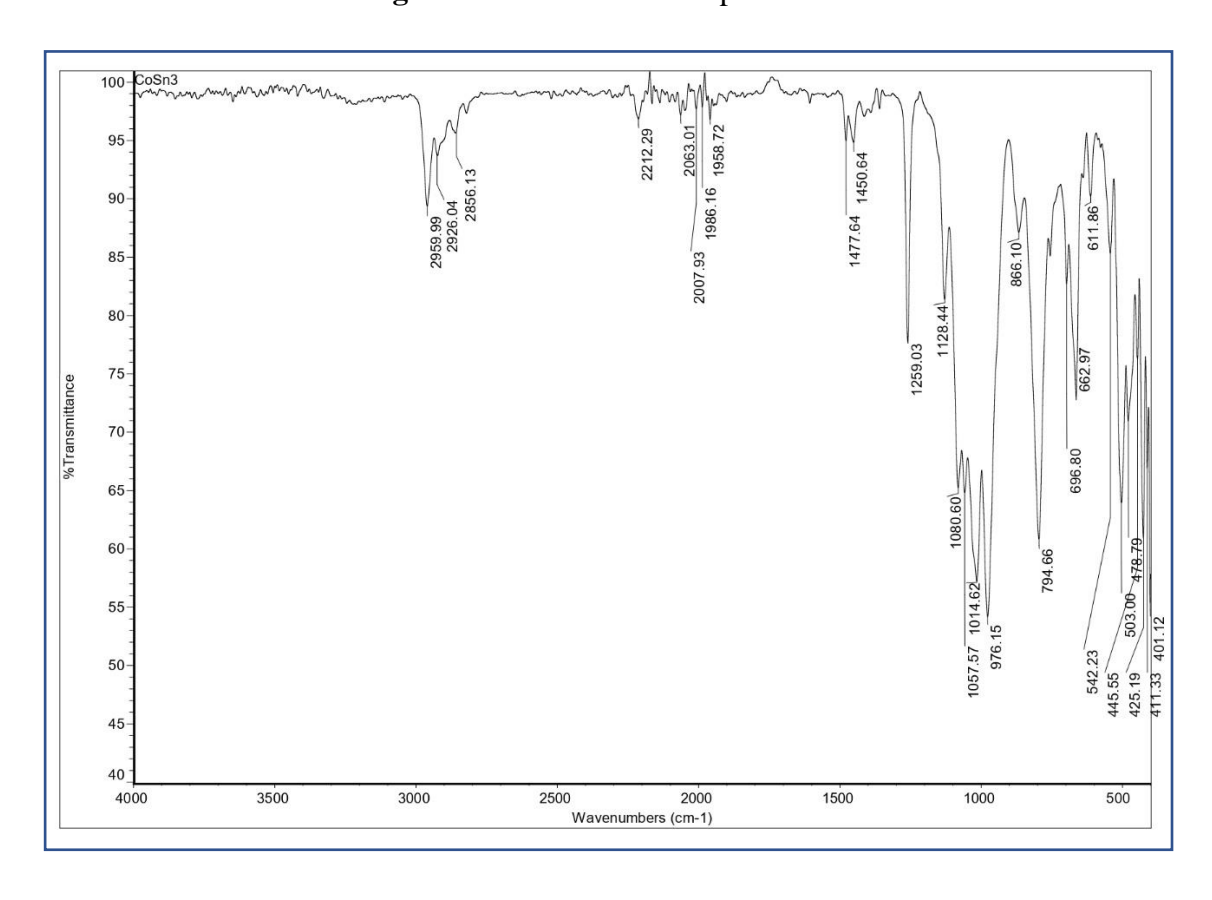


Fig 4.7 IR spectrum of 4.1

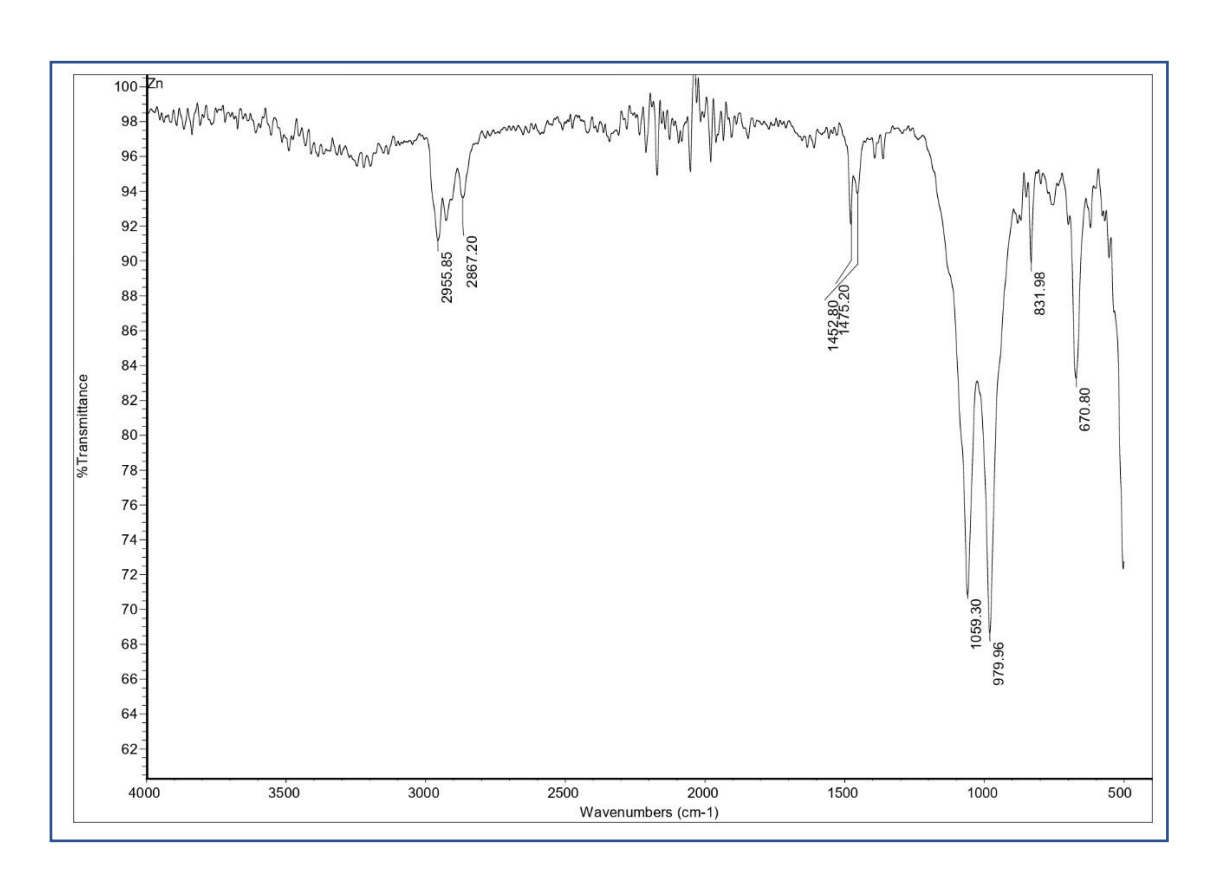


Fig 4.8 IR spectrum of 4.2

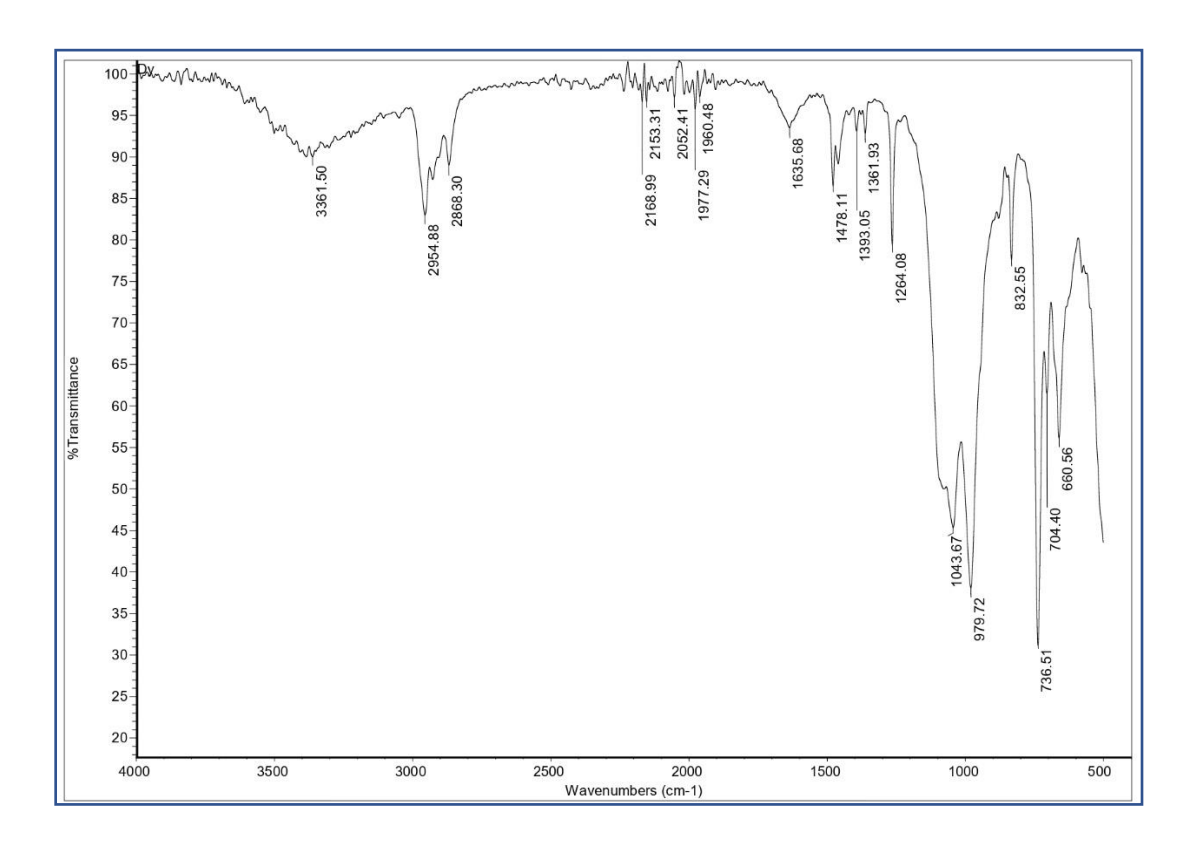


Fig 4.9 IR spectrum of 4.3

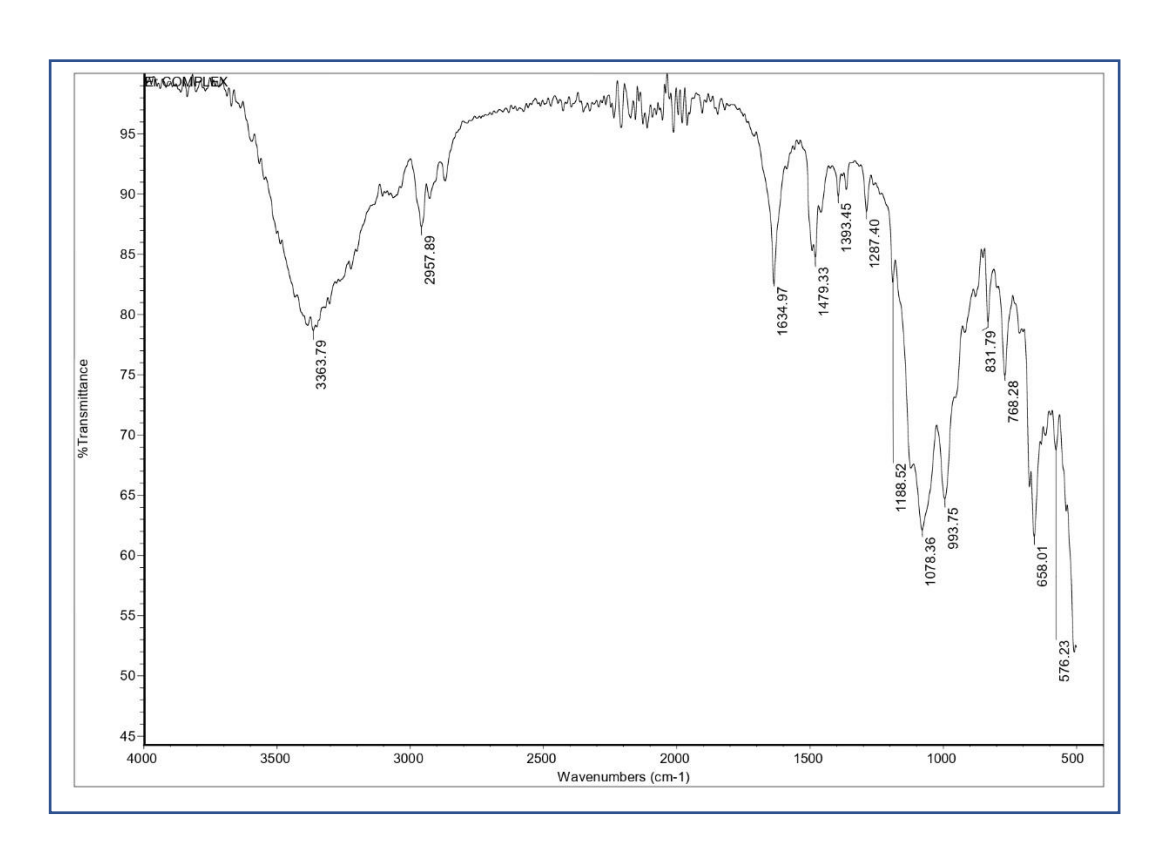


Fig 4.10 IR spectrum of 4.4

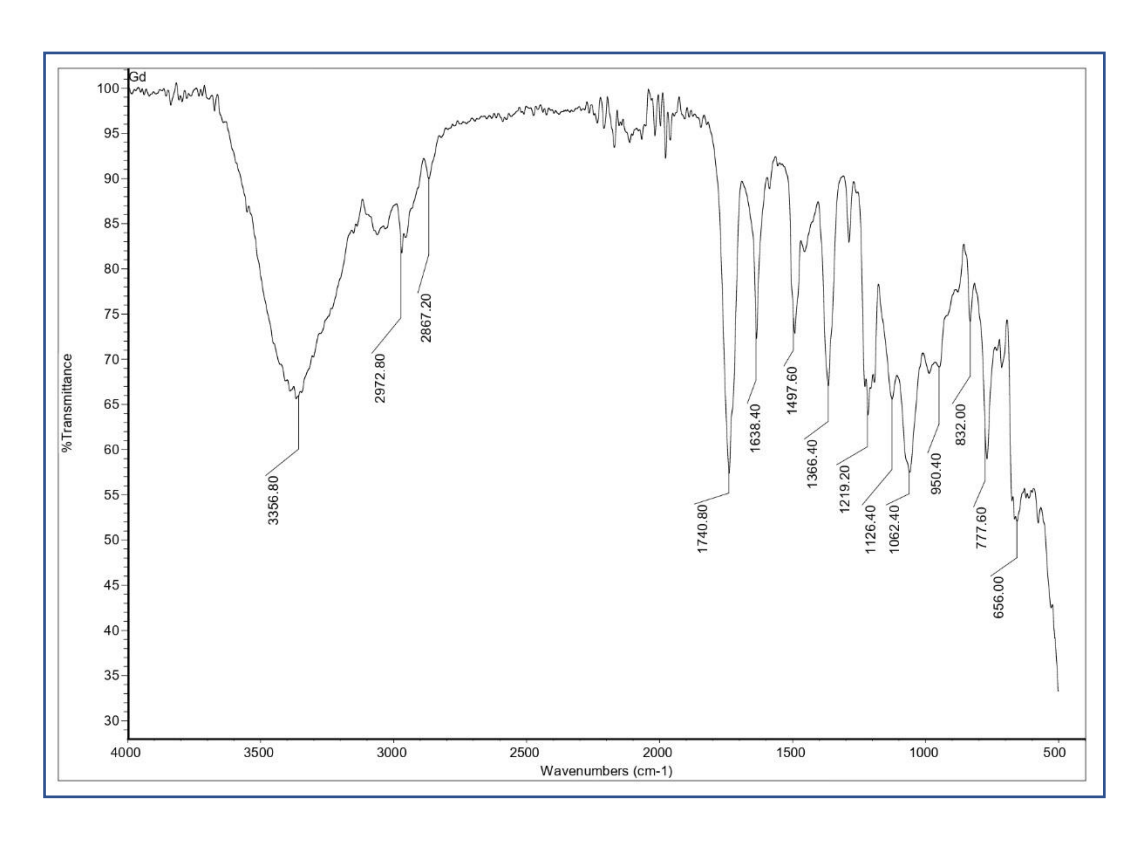


Fig 4.11 IR spectrum of 4.5

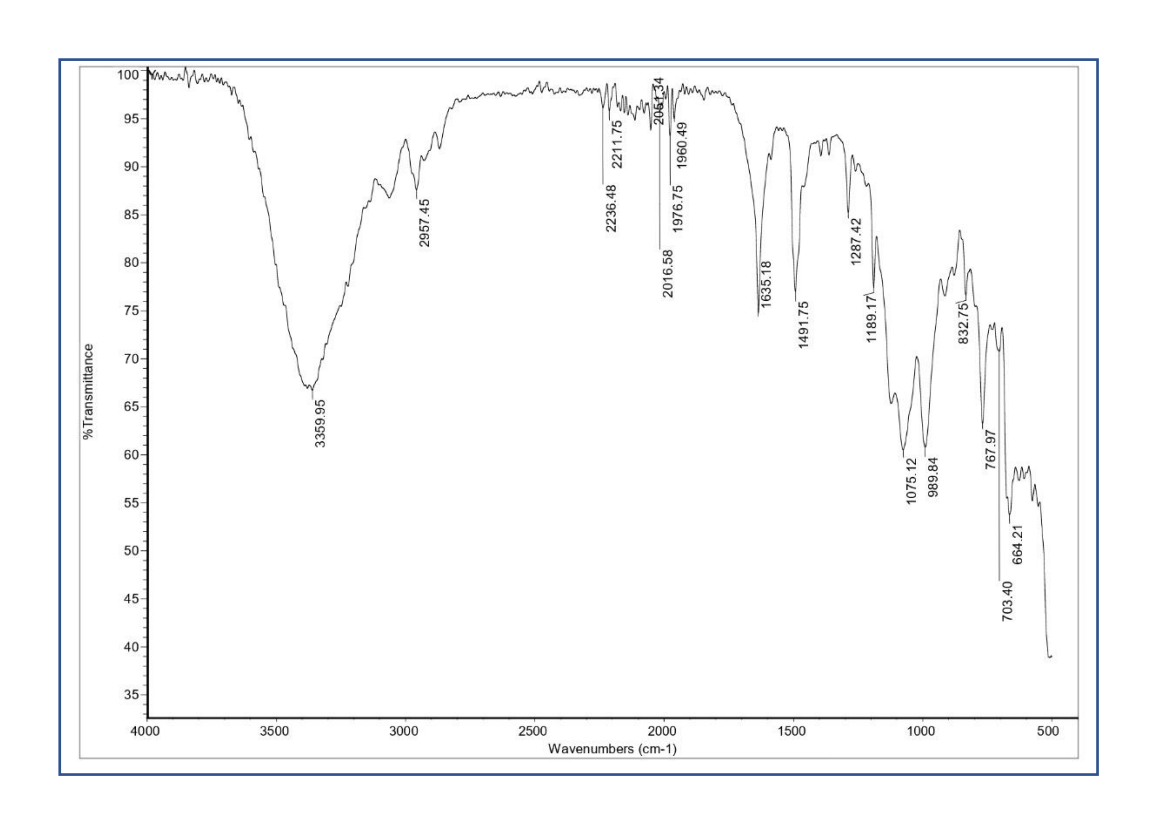


Fig 4.12 IR spectrum of 4.6

Table 4.3(A) Shape calculation for compound 4.1 for Co

Sl.no	Geometry	Cshm value for Co
1	Square (D4h)	33.003
2	Tetrahedron (Td)	1.131
3	Seesaw (C2v)	7.288
4	Vacant trigonal bipyramid (C3v)	0.846

Table 4.3(B) Shape calculation for compound 4.1 for Sn

Sl.no	Geometry	Cshm value for Co
1	Hexagon (D6h)	32.973
2	Pentagonal pyramid (C5v)	28.416
3	Octahedron (Oh)	0.677

4	Trigonal prism (D3h)	14.881
5	Johnson pentagonal pyramid J2 (C5v)	31.460

Table 4.4(A) Shape calculation for compound 4.3 for Sn $\,$

Sl.no	Geometry	Cshm value for Co
1	Hexagon (D6h)	32.973
2	Pentagonal pyramid (C5v)	28.416
3	Octahedron (Oh)	0.677
4	Trigonal prism (D3h)	14.881
5	Johnson pentagonal pyramid J2 (C5v)	31.460

Table 4.4(B) Shape calculation for compound 4.3 for Dy

Sl.no	Geometry	Cshm value for Co
1	Hexagon (D6h)	32.973
2	Pentagonal pyramid (C5v)	28.416
3	Octahedron (Oh)	0.677
4	Trigonal prism (D3h)	14.881
5	Johnson pentagonal pyramid J2 (C5v)	31.460

EDAX analysis of compound 4.1-4.6

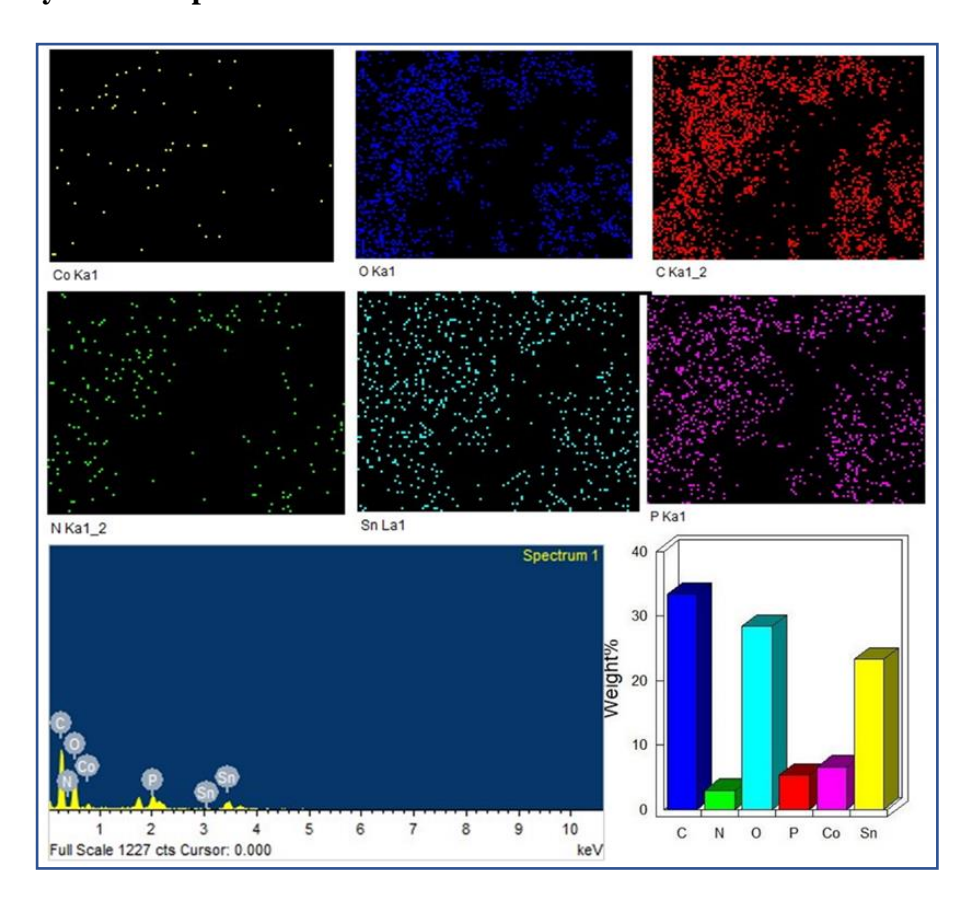


Fig 4.13 EDAX of compound 4.1

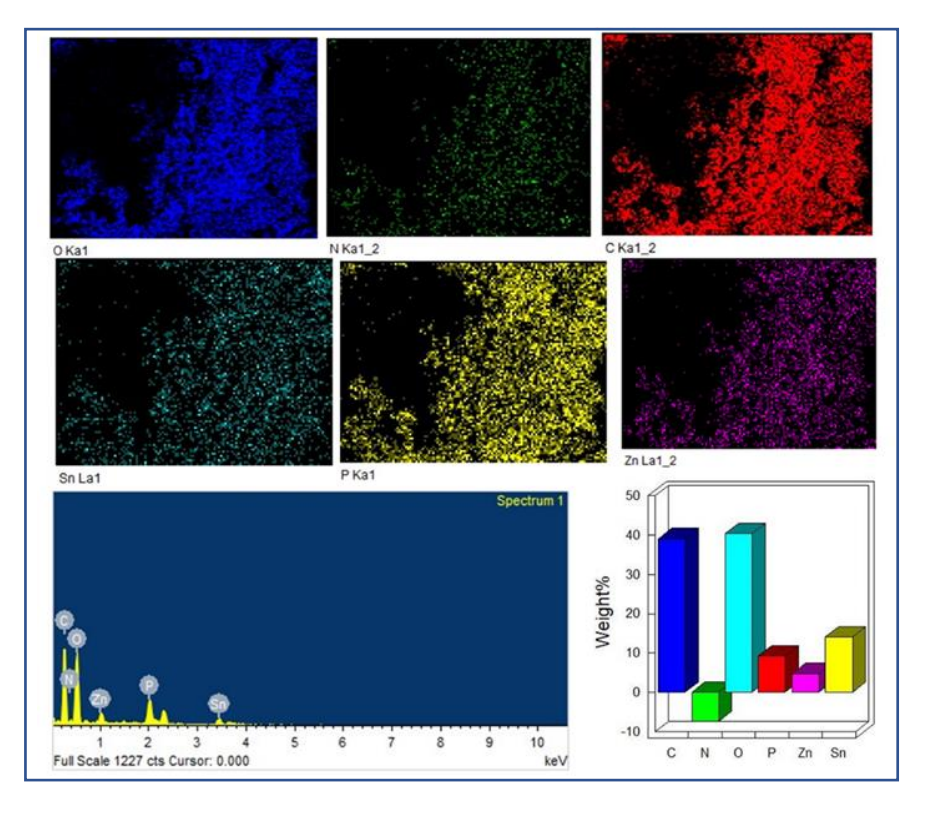


Fig 4.14 EDAX of compound 4.2

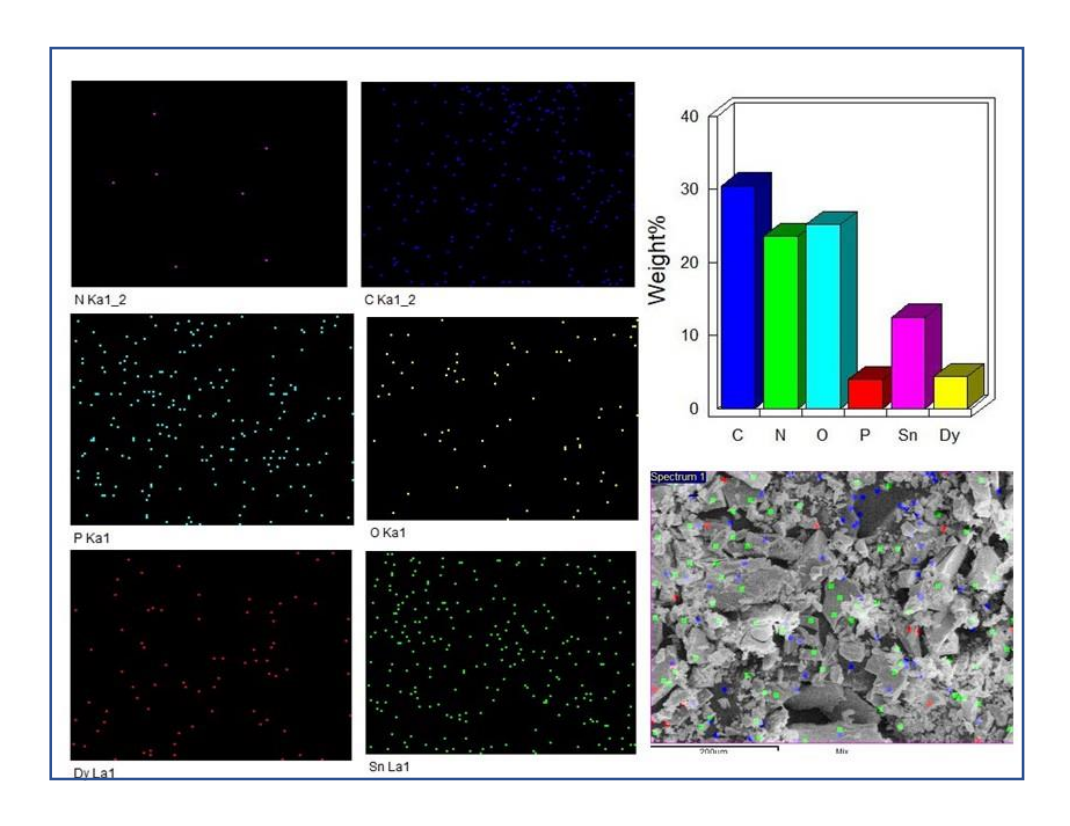


Fig 4.15 EDAX of compound 4.3

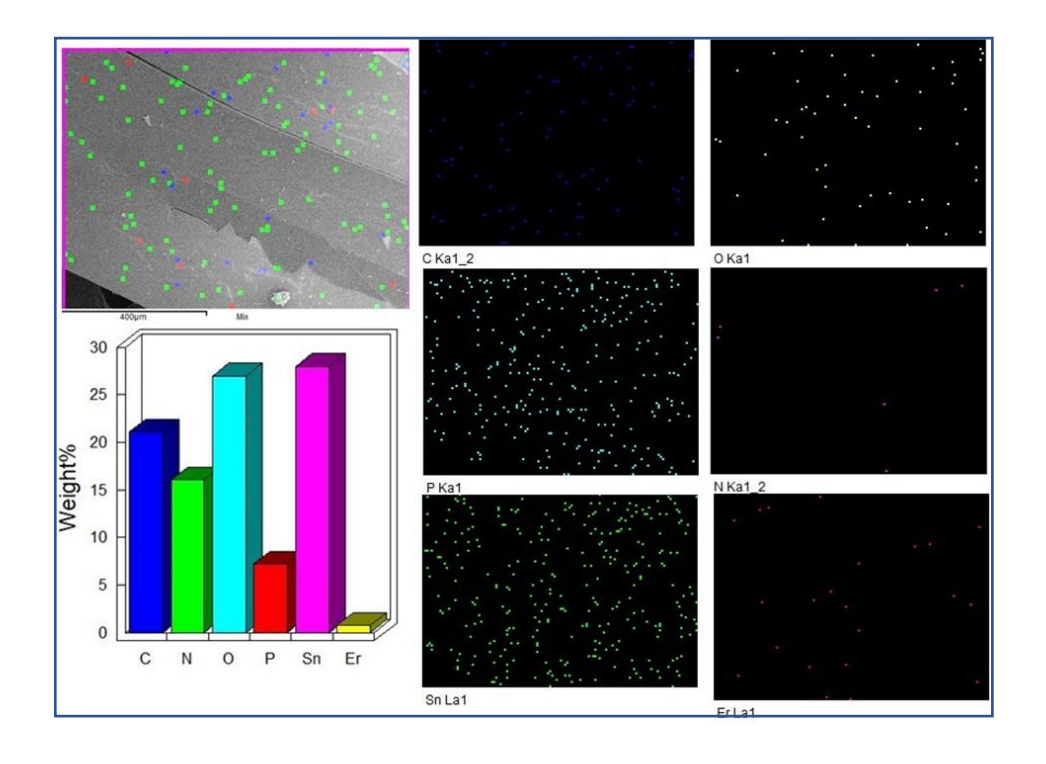


Fig 4.16 EDAX of compound 4.4

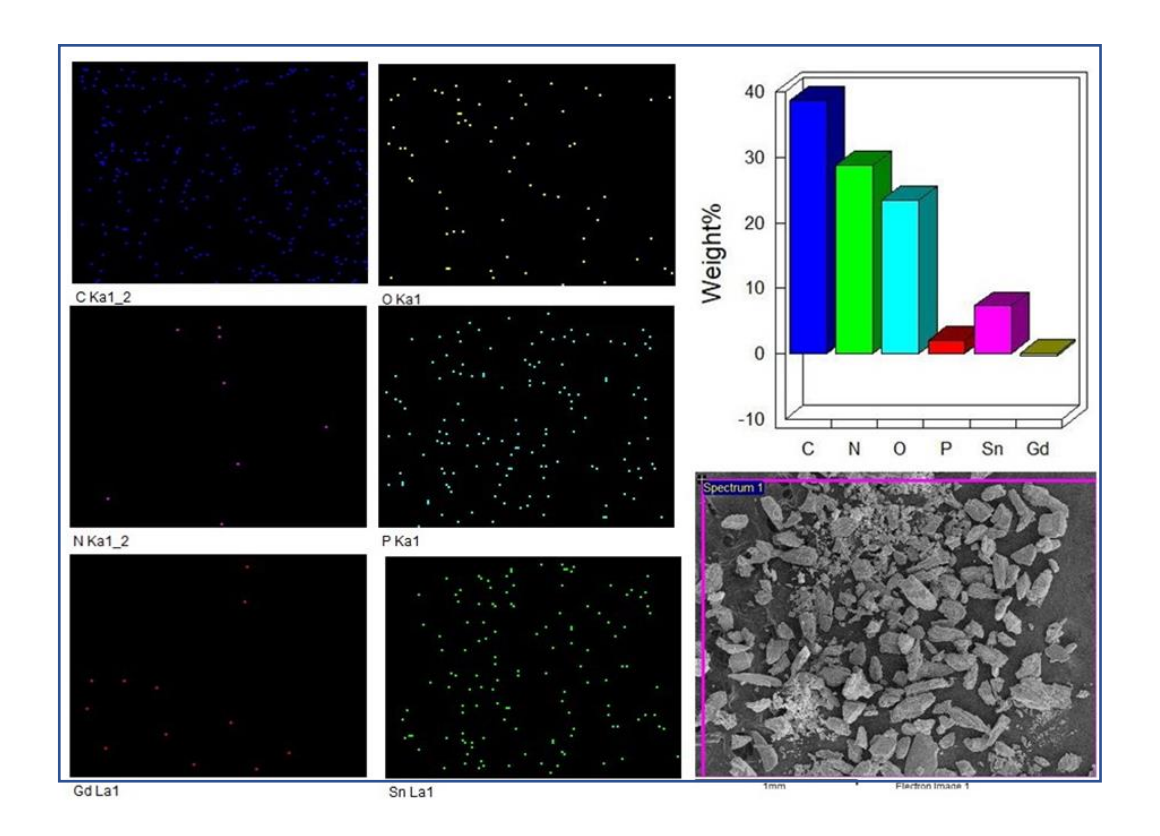


Fig 4.17 EDAX of compound 4.5

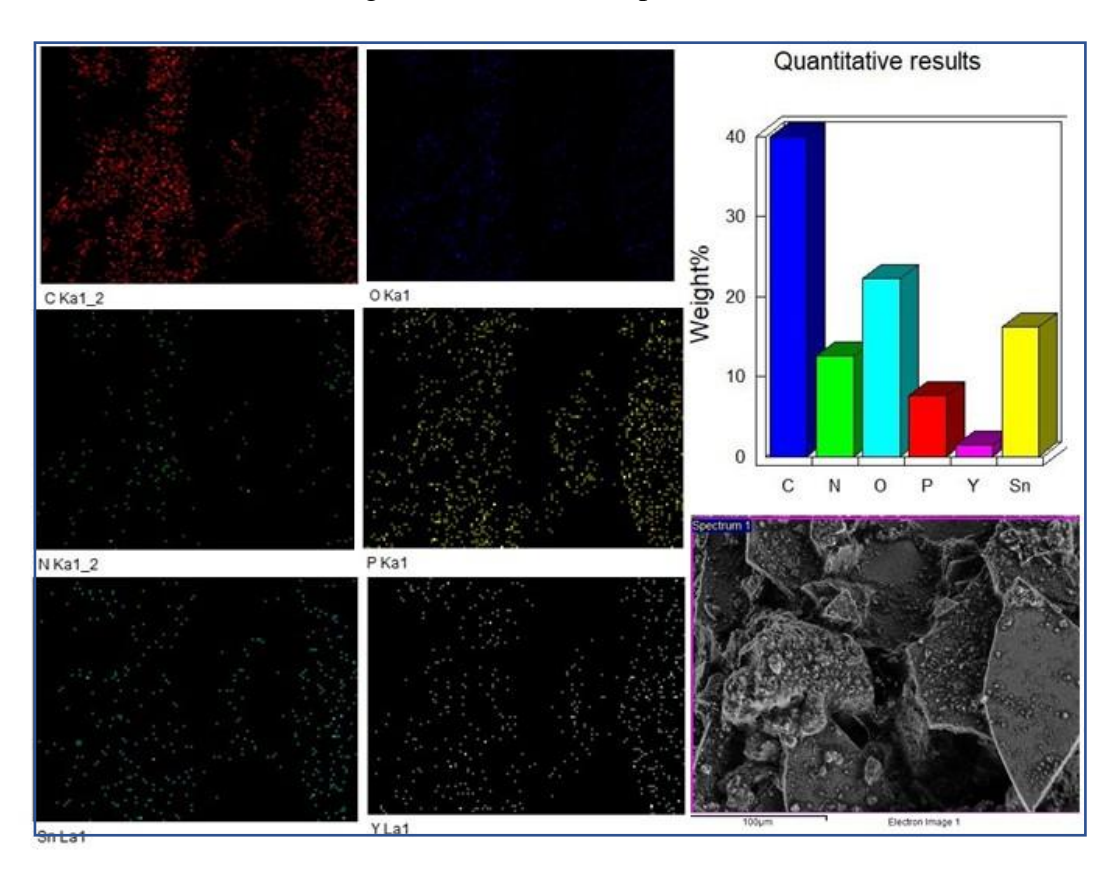


Fig 4.18 EDAX of compound 4.6

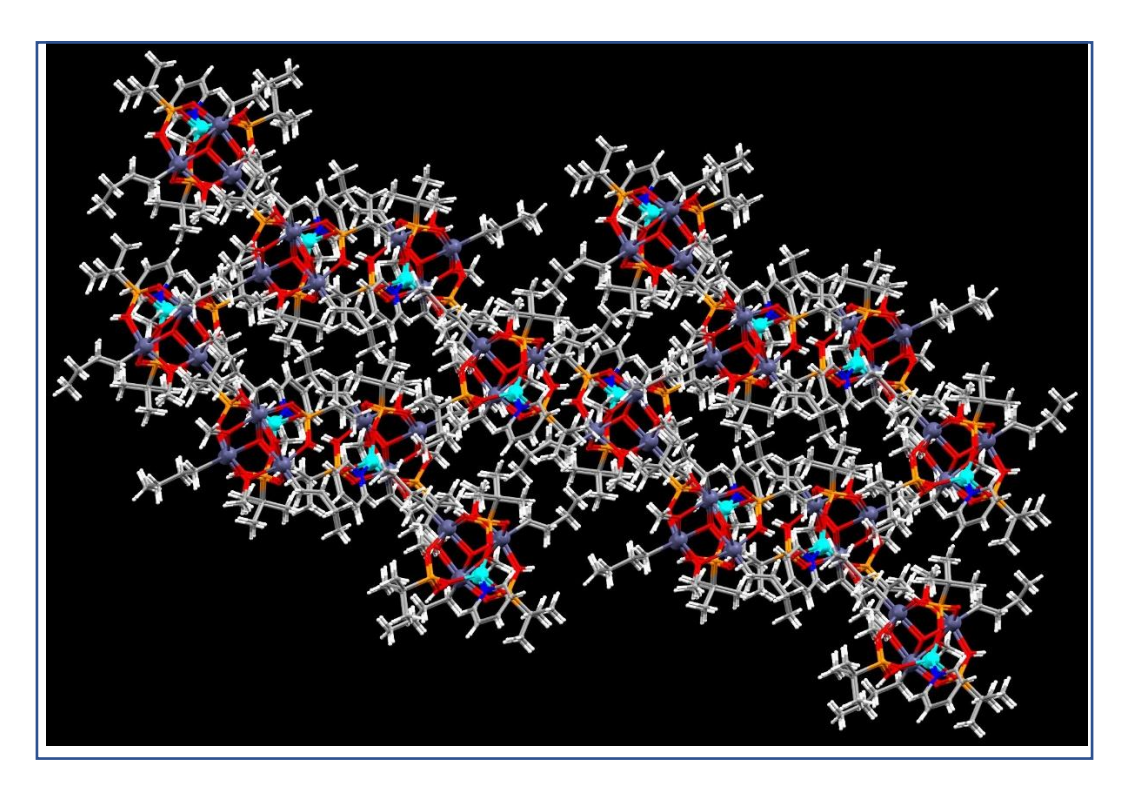


Fig 4.19 Packing diagram array of 4.1

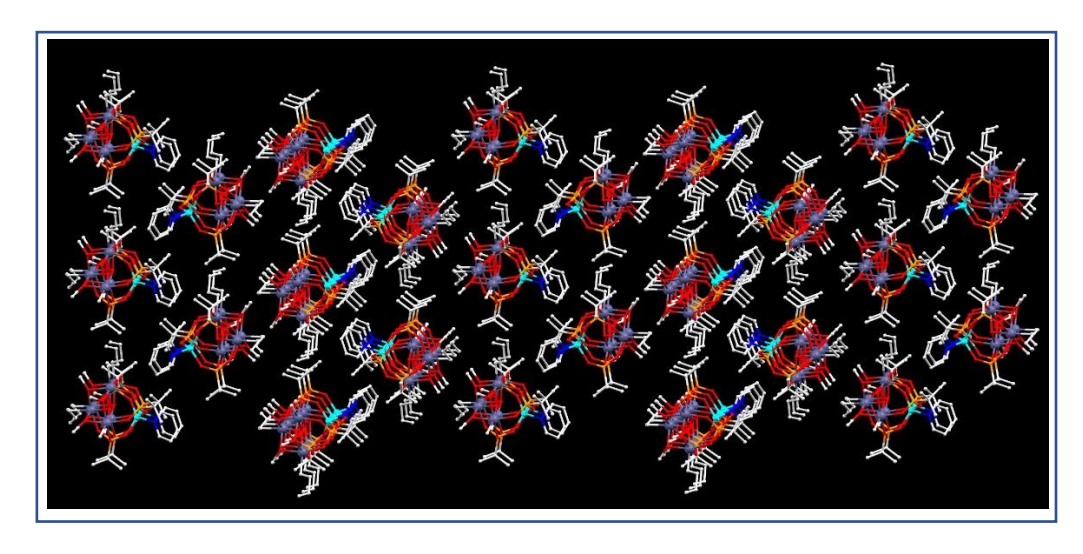


Fig 4.20 Packing diagram array of 4.2

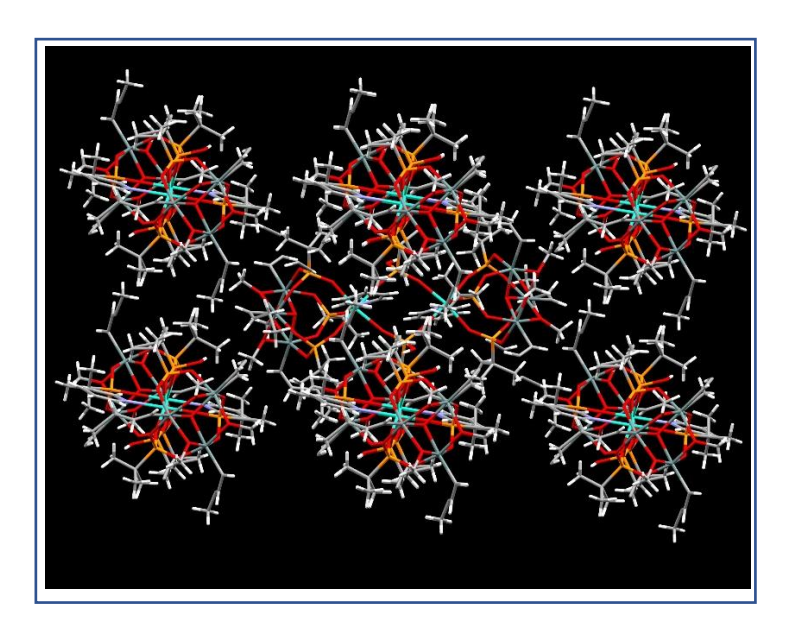


Fig 4.21 Packing diagram array of 4.3

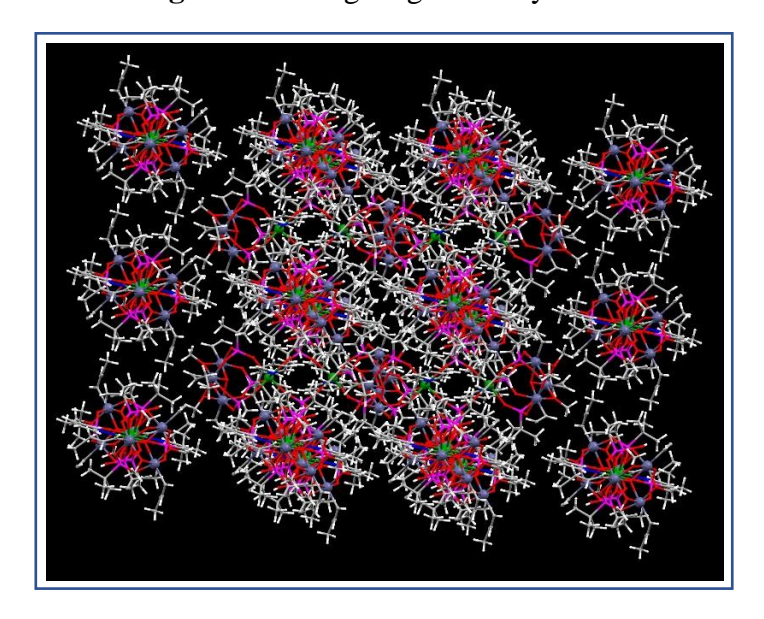


Fig 4.22 Packing diagram array of 4.4

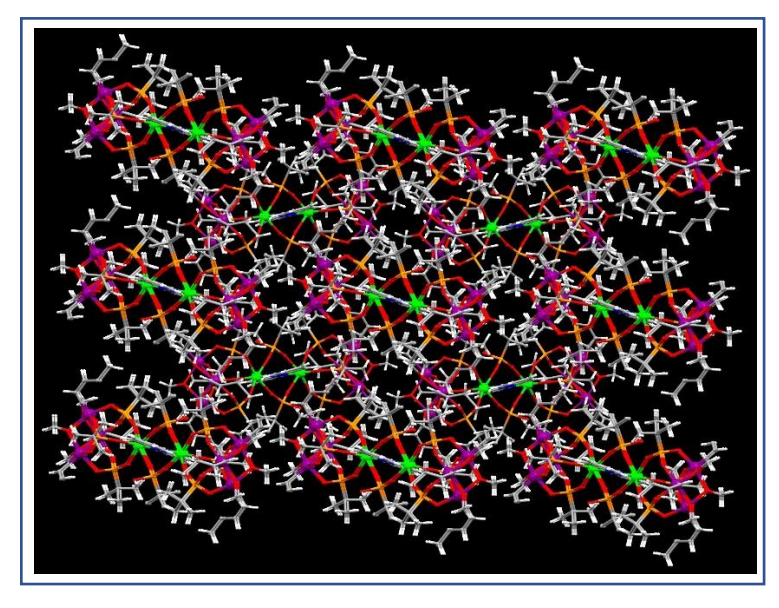


Fig 4.23 Packing diagram array of 4.5

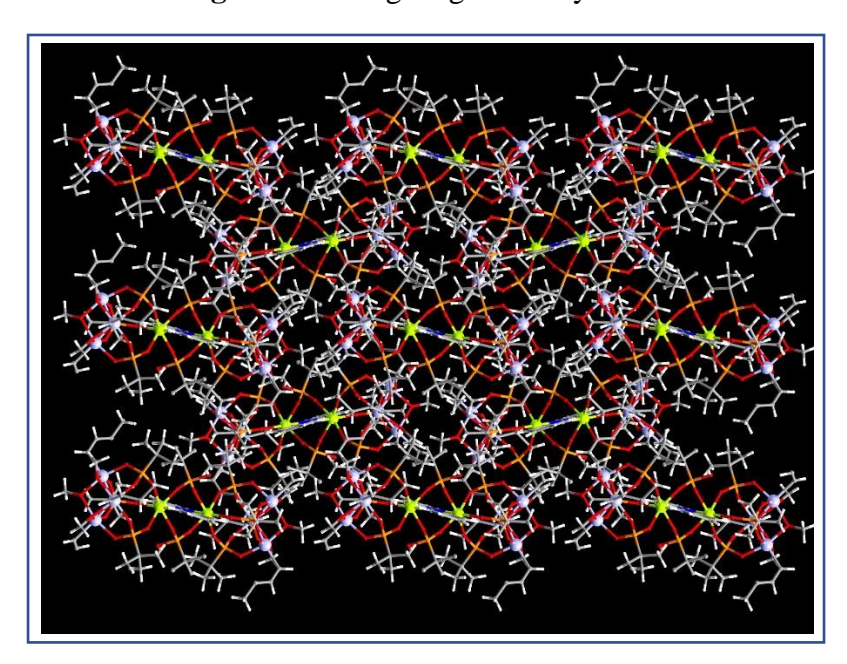


Fig 4.24 Packing diagram array of 4.6

FUTURE SCOPE OF THE THESIS

This thesis demonstrates the synthesis, structural characterization, and catalytic studies of Lanthanum oxo clusters and in other half of the thesis it deals with 3d / 4f molecular architectures resulting from the pro-ligand approach.

Chapter 2: The reaction of modified Schiff base ligands with coligand in presence of excess base with hydrated lanthanide metal salts results hexanuclear Ln6 cluster. The cluster encapsulates aerial CO₂ as carbonate anions and in application to the Ln6 cluster it catalyses the cyclo addition reaction of epoxides in presence of CO₂ and TBAB. This study paves the way for catalysis of terminal alkynes to do the carboxylation in presence lanthanum oxo clusters. This work can be extended further for carboxylation of different substituted aromatic aliphatic alkynes in presence of our synthesized Lanthanum oxo cluster by using cesium carbonate as cocatalyst further followed by acidification with 1M. HCl with pH value 1.

Chapter 3: In this chapter we have activated less reactive sulphur based small molecules in presence of our synthesized LOC. Novel small molecules have been synthesized, it has also been activated tosylaziridines and thiols to form beta hydroxy sulphides. This work can be extended to activate other small chalcogenides and form unique series of complexes. This chalcogenide activations can be carried out by passing H₂S gas and by reacting with sulphur powder in solid state medium and CS₂ as a liquid.

Chapter 4: Novel mixed valent 3*d- main group* and 4*f*-main group proligand based clusters have been synthesized with organo phosphonate organo stannoxane proligands with hydrated transition metal precursors and hydrated lanthanide salts in solovothermal condition in presence of medium and the magnetic studies are being carried out. This work can be further extended by playing with varying different types of basic mediums. As earlier reported works solid state band gap studies can be carried out along with further electro catalytic studies.

List of Publications

1.Lutetium oxo clusters utilizing mixed ligand System: Isolation of a rare Lu₄ oxo cluster in a tetrahedral architecture.

Ananda Kumar Jami, **Smruti Prangya Behera**, Suman Mondal, Viswanathan Baskar, *Inorg. Chem. Commun.* **2022**, 143, 109784.

2. In Situ Assembled Polynuclear Zinc Oxo Clusters Using Modified Schiff Bases as Ligands.

Suman Mondal, **Smruti Prangya Behera**, Mohammed Alamgir, and Viswanathan Baskar, *ACS Omega* **2022**, 7, 1, 1090–1099.

3. Activation of Small Molecules via Lewis acidic La₆Oxo Cluster.

Smruti Prangya Behera, Renuka Pradhan, Upakarasamy Lourderaj, Viswanathan Baskar.

Inorg. Chem. (Manuscript ID: ic-2023-04411z). (Communicated).

Poster and Oral Presentations / Workshops

- 1. Attended a workshop and conference entitled "Indo-French School and Conference on the Magnetism of Molecular Systems" held at the Indian Institute of Science, Bangalore on November 26-30, 2018.
- 2. Attended conference entitled "Spins in Molecular system: Experiment, Theory and Applications" conference held at Indian Institute of Science, Bangalore on December 2-4, 2019.
- 3. Presented a poster entitled "Organoantimony Oxo clusters led to novel 3d, 4f molecular Aggregates" in "Spins in Molecular system: Experiment, Theory and Applications" conference held at Indian Institute of Science, Bangalore on December 2-4, 2019.
- 4. Attended conference entitled 'Modern Trends in Inorganic Chemistry' conference held at the Indian Institute of Technology, Guwahati on December 11-14, 2019.
- 5. Presented poster entitled "Reactivity of N-O donor ligands with diamagnetic 4f ions" in "Chemfest-2022" held at the University of Hyderabad, India, on April 22-23, 2022.
- 6. Attended a webinar entitled "Rigaku School for Practical Crystallography" from July 6-17th, 2020.
- 7. Presented poster entitled "Synthesis and characterization of Lu based oxo clusters" in 'Modern Trends in Inorganic Chemistry" conference held at "Department of Chemistry, Institute of Science, Banaras Hindu University", India, on December 15-17, 2023.
- 8. Delivered an oral talk and presented a poster entitled "Lanthanide cluster for CO₂ conversion & CO₂ terms".

Small molecule Activation by Lanthanide Oxo Clusters and Proligand Approach Towards Assembling Heterometallic Architectures

by Smruti Prangya Behera

Submission date: 08-Jan-2024 03:14PM (UTC+0530)

Submission ID: 2267838441

File name: Smruti_Prangya_Behera.docx (98.67K)

Word count: 12990 Character count: 75356

Small molecule Activation by Lanthanide Oxo Clusters and Proligand Approach Towards Assembling Heterometallic Architectures

ORIG	INALITY REPORT			
SIMI	% LARITY INDEX	1% INTERNET SOURCES	4% PUBLICATIONS	4% STUDENT PAPERS
PRIMA	ARY SOURCES			
1	Submitt Hyderak Student Pape		of Hyderabad	3%
2	Min Fen	g Huang, Qingxi g, Zhiping Zheng atalytic Applicati sters", Magneto	g. "Recent Adv ons of Lantha	vances \ \ \ \ \ \ \ \ \ \ \ \ \ \ \ \ \ \ \
3	diamono Internet Source	d.kist.re.kr		<1%
4	Khodaba opening alcohols	allah-Mehrjardi, ikhsh Niknam. " of epoxides: tre synthesis", Jour l Society, 2018	Nucleophilic r ends in β-subs	ring- stituted
5	Suman M	Kumar Jami, Sm Iondal, Viswana n oxo clusters u	ithan Baskar.	ligand

System: Isolation of a rare Lu4 oxo cluster in a tetrahedral architecture", Inorganic Chemistry Communications, 2022

Publication

6	Lina M. Aguirre-Díaz, Natalia Snejko, Marta
0	Iglesias, Félix Sánchez, Enrique Gutiérrez-
	Puebla, M. Ángeles Monge. "Efficient Rare-
	Earth-Based Coordination Polymers as Green
	Photocatalysts for the Synthesis of Imines at
	Room Temperature", Inorganic Chemistry,
	2018

Publication

7	os.zhdk.cloud.switch.ch
	Internet Source

<1%

Sandeep K. Gupta, Stuart K. Langley, Kamna Sharma, Keith S. Murray, Ramaswamy Murugavel. "Pentanuclear Lanthanide Monoorganophosphates: Synthesis, Structure, and Magnetism", Inorganic Chemistry, 2017

<1%

Emil Roduner. "Understanding catalysis", Chem. Soc. Rev., 2014

<1%

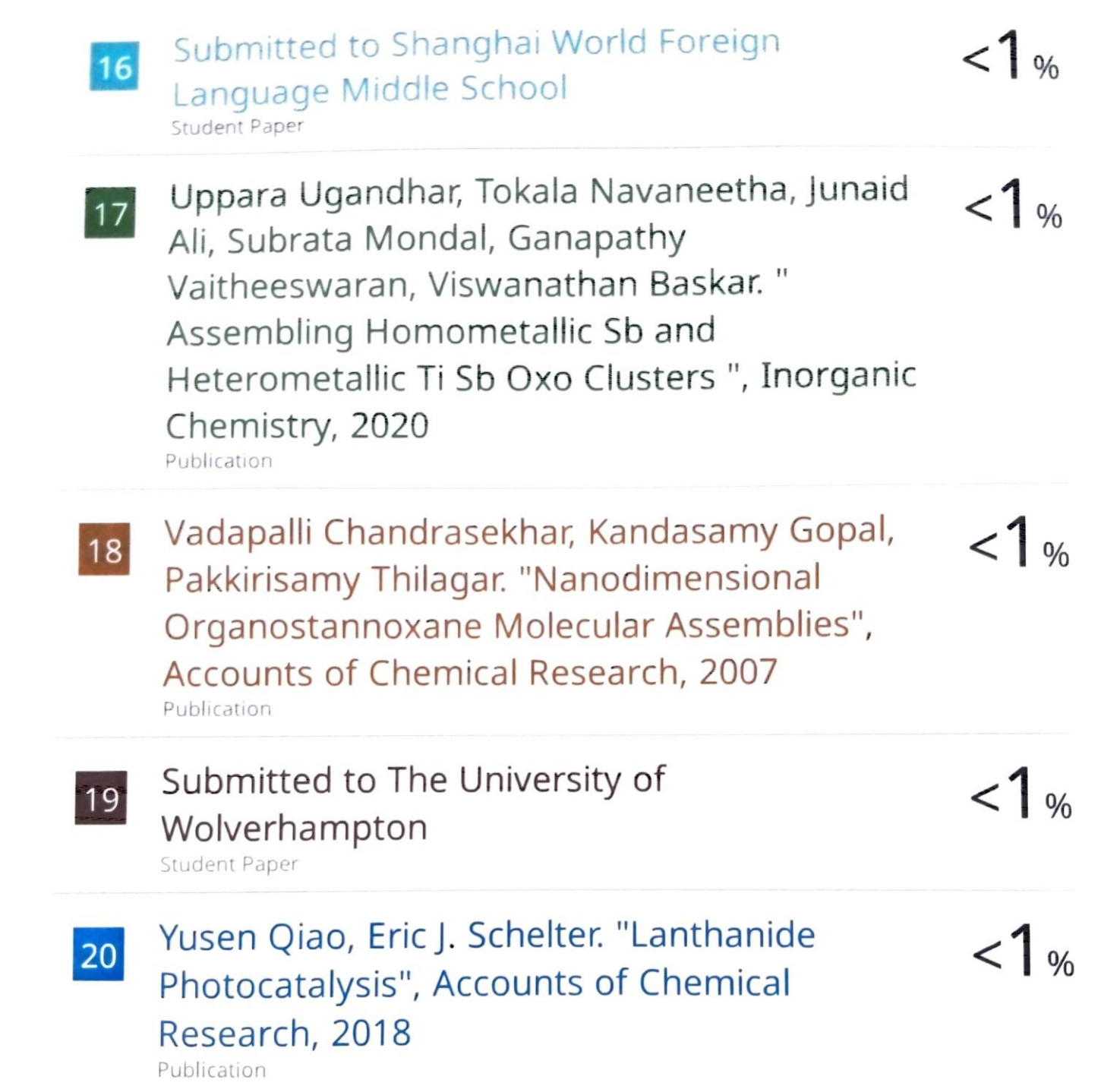
Publication

R. Sessoli, D. Gatteschi, A. Caneschi, M. A. Novak. "Magnetic bistability in a metal-ion cluster", Nature, 1993

<1%

Publication

11	Debraj Saha, Rupam Sen, Tanmoy Maity, Subratanath Koner. "Anchoring of Palladium onto Surface of Porous Metal-Organic Framework through Post-Synthesis Modification and Studies on Suzuki and Stille Coupling Reactions under Heterogeneous Condition", Langmuir, 2013	<1%
12	Hidemi Nagao, Syusuke Yamanaka, Masamichi Nishino, Yasunori Yoshioka, Kizashi Yamaguchi. "Theoretical studies on the magnetic quantum tunneling rates in Mn clusters by the path integral method", Chemical Physics Letters, 1999	<1%
13	www.amrita.edu Internet Source	<1%
14	core-cms.prod.aop.cambridge.org	<1%
15	Naoto Ishikawa, Miki Sugita, Tadahiko Ishikawa, Shin-ya Koshihara, Youkoh Kaizu. "Lanthanide Double-Decker Complexes Functioning as Magnets at the Single- Molecular Level", Journal of the American Chemical Society, 2003	<1%



Exclude quotes On Exclude bibliography On

Exclude matches

< 14 words